CHARACTERISATION OF THE TRANSCRIPTOMIC AND PROTEOMIC PROFILE OF ASTROCYTES IN MULTIPLE SCLEROSIS

By

Rachel Waller

Submitted for the degree of Doctor of Philosophy (PhD)

Sheffield Institute for Translational Neuroscience
University of Sheffield

January 2014

Volume I

For Joan Ann Waller

Forever in my thoughts. This is for you.

ACKNOWLEDGEMENTS

First and foremost I would like to acknowledge my significant academic supervisory team; Dr. Julie Simpson, Prof. Stephen Wharton, Prof. Paul Ince, Dr. Paul Heath, Dr. Simona Francese, Prof. Nicola Woodroofe and Prof. Basil Sharrack for their scientific and at times personal guidance, support and patience throughout my PhD.

My utmost gratitude goes to Julie for her continuous help, support and reassurance throughout. I am grateful to Julie for her natural ability to calm me and keep me sane with her thoughtful and encouraging words, having the knack of saying the right thing at the right time to me. But most of all I am thankful to Julie for her belief in me when at times I found it hard to.

I will be eternally grateful to Nicola, you have inspired me to get where I am today. Thank you for the countless conversations over many a glass of wine, and most of all for giving me a chance from the beginning.

Thank you to Biogen Idec for funding my PhD and importantly to all the donors and their families at the UK MS Society Tissue Bank. Thank you for deciding to donate your tissue to scientific research, without you this work would not have been possible.

Thanks to all my work colleagues and friends both at Sheffield University and Sheffield Hallam University, for your never ending support and always being there for me to moan at and conspire with! A special thanks to Natalie and Ruth for your excellent lab assistance and Dr. Laura Cole for your understanding and patience.

I will forever be grateful to Paul, my rock throughout. You have been by my side during this long journey and have always believed in me and encouraged me, helping me to realise and fulfil my ambitions and dreams. You've shared with me my ultimate lows always being there to pick me up, and we've laughed out loud together through the highs. I will be eternally grateful for your down to earth attitude towards life, words of wisdom and witty sense of humour, you've kept me grounded and I love you for all these things.

Finally a huge thank you to my long suffering parents and sister, Rebecca. You have ALWAYS encouraged me to be the best I can be. No dream is out of reach 'as long as you've tried your hardest that's the best you can do' (Waller *et al* 1988-present). Well, thanks to your love and support, the endless cups of tea, lemon barley and ginger biscuits (for the nerves!) I've tried my hardest and I've done it!

Every accomplishment in life starts with a decision to try...

ABSTRACT

Multiple sclerosis (MS) is a chronic, neuroinflammatory demyelinating disease of the central nervous system (CNS). Typical white matter lesions (WML) in MS are surrounded by areas of non-demyelinated normal appearing white matter (NAWM) with complex subtle pathology, including blood brain barrier (BBB) dysfunction, axonal damage and glial activation. Astrocytes, the most abundant cell type within the CNS, are known to support neuronal function, maintain homeostasis within the CNS and regulate neurotransmission. Yet conversely, can promote an inflammatory response, inhibit myelin repair and support the production of autoreactive T cells in MS. This thesis aimed to investigate the transcriptomic and proteomic profile of astrocytes in MS NAWM to determine whether specific astroglial changes exist, which may contribute/prevent disease progression in MS.

Initial data presented in this thesis demonstrated a change in astrocyte phenotype within different pathological regions of the CNS in MS, as observed by the distinct immunoprofile of a variety of known astrocyte markers. Being able to isolate cell types from human tissue is fundamental in beginning to define a particular cell's role in disease pathogenesis. An immuno-laser capture microdissection (LCM) method was developed to enable the isolation of glial cells from human post mortem (PM) CNS tissue. In the current study glial fibrillary acidic protein (GFAP) positive astrocytes were isolated from MS NAWM and control WM via immuno-LCM and microarray analysis completed to compare their transcriptome. Significantly differentially expressed genes were associated with the immune response, cell signaling, cytoskeletal changes and regulation of homeostasis which relate to the distinct roles of astrocytes. Interestingly, from the top 20 significant differentially upregulated genes, six of them were related to the regulation of iron homeostasis and oxidative stress, including *metallothionein I-II (MT-I+II), ferritin light chain (FTL)* and *transferrin (TF).* Subsequent transcriptomic and proteomic investigations were carried out on candidate genes using polymerase chain reaction, immunohistochemistry, western blotting and mass spectrometry to investigate the neuroprotective role of astrocytes in regulating iron homeostasis and oxidative stress in MS NAWM.

Evidence presented in this thesis demonstrates the importance of astrocytes in the pathogenesis of MS. The results indicate that further investigations into the protective roles of astrocytes in regulating iron and oxidative stress in MS NAWM are warranted.

TABLE OF CONTENTS

LIST OF FIGURES

Chapter 1

Chapter 2

Chapter 3

Chapter 4

Chapter 5

LIST OF TABLES

Chapter 2

Chapter 3

Chapter 4

Chapter 5

ABBREVIATIONS

ABC-HRP	Horseradish peroxidase-conjugated avidin-biotin complex
ACN	Acetonitrile
AD	Alzheimer's disease
ADAM	A disintegrin and metalloprotease domain
ADE	Acoustic droplet ejection
AJ	Adherin junctions
ALDH1L1	Aldehyde dehydrogenase 1L1
ALS	Amyotrophic lateral sclerosis
AMPA	a-amino-3-hydroxy-5-methyl-4-isoxazolepropionic acid
APC	Antigen presenting cells
aRNA	Antisense-ribonucleic acid
AT-EAE	Adaptive transfer experimental autoimmune encephalomyelitis
ATP	Adenosine triphosphate
ATP2B1	ATPase, Ca^{2+} transporting, plasma membrane 1
βA	Beta actin
BAK	BCL2 antagonist killer
BBB	Blood brain barrier
BCL2	B-cell lymphoma 2
BDNF	Brain-derived neurotrophic factor
bp	Base pairs
BSA	Bovine serum albumin
BVEC	Blood vessel endothelial cells
CAL	Chronic active lesions
cDNA	Complementary deoxyribonucleic acid
CFA	Complete Freund's adjuvant
CHCA	α-Cyano-4-hydroxycinnamic acid
CI	Chemical ionisation
CIS	Clinically isolated syndrome
CIRBP	Cold inducible RNA binding protein
CNS	Central nervous system
CO	Control
COX-I	Cytochrome C oxidase-I
COX-2	Cyclooxygenase-2
Cp	Ceruloplasmin
CSF	Cerebrospinal fluid
Ct	Cycle threshold
CTGF	Connective tissue growth factor
CXCL	Chemokine CXC ligand
CXCR	Chemokine CXC receptor
Da	Dalton
DAB	3, 3'-diaminobenzidine
DAMPs	Damage-associated molecular patterns
DAVID	Database for Annotation Visualisation and Integrated Discovery
DC	Dendritic cells
DCTB	Trans-2-(3-(4-tert-Butylphenyl)-2methyl-2-propenylidene) malononitrile
DEPC	Diethylpyrocarbonate
DFO	Desferrioxamine
DHB	2,5-dihydroxybenzoic acid
dH_2O	Distilled water

DIT	Dithranol
DMT1	Divalent metal transporter 1
DNA	Deoxyribonucleic acid
dNTP	Deoxyribonucleotide triphosphate
dsDNA	Double stranded deoxyribonucleic acid
DYNC1LI2	Dynein, cytoplasmic 1, light intermediate chain 2
DYNC2LI1	Dynein, cytoplasmic 2, light intermediate chain 1
DZ	Dizygotic
EA	Early active
EAAT1/2	Excitatory amino acid transporter 1/2
EAE	Experimental autoimmune encephalomyelitis
EBV	Epstein-Barr virus
EC	Endothelial cells
ECM	Extracellular matrix
EDSS	Expanded disability status scale
EDTA	Ethylenediaminetetraacetic acid
EI	Electron ionisation
EGCG	Epigallocatechin gallate
ESI	Electrospray ionisation
FA	Ferulic acid
Fe^{2+}	Ferrous iron
Fe^{3+}	Ferric iron
FFPE	Formalin fixed, paraffin embedded
FGF-1/2	Fibroblast growth factor-1/2
FPT	Ferroportin
FT	Ferritin
FTL	Ferritin light chain
FTLD	Frontotemporal lobar degeneration
FU	Fluorescence units
GAPDH	Glyceraldehyde-3-phosphate dehydrogenase
GCOS	Gene chip operating software
GEO	Gene expression omnibus
GFAP	Glial fibrillary acidic protein
GLT-1	Glutamate transporter-1
GLAST	Glutamate aspartate transporter
GM	Grey matter
GML	Grey matter lesion**s**
GS	Glutamine synthetase
GWAS	Genome wide association studies
HA	Hyaluronan
H&E	Haematoxylin and eosin
HIF-1α	Hypoxia-inducible factor 1-alpha
HK	Housekeeping
HLA	Human leukocyte antigen
HNSCC	Squamous cell carcinoma of the head and neck
HPA	Hydroxypicolinic acid
H_2O_2	Hydrogen peroxide
IA	Inactive
IAA	Trans-3-indoleacrylic acid
ICAM-1	Intercellular Adhesion Molecule-1
IFITM 1/2	Interferon induced transmembrane protein 1/2
IFNβ	Interferon beta

IFNγ	Interferon gamma
Ig	Immunoglobulin
IHC	Immunohistochemistry
IL	Interleukin
IR	Infra-red
IRE	Iron-responsive element
IRP	Iron-regulatory proteins
IVT	*In vitro* transcription
JAK/STAT	Janus kinase/STAT
kDa	Kilodalton
KEGG	Kyoto Encyclopedia of Genes and Genomes
KHz	Kilohertz
KIF1C	Kinesin family member 1C
KO	Knock-out
kV	Kilovolts
LA	Late active
LCM	Laser capture microdissection
LC-MS/MS	Liquid chromatography-tandem mass spectrometry
LFA-1	Leukocyte-associated antigen-1
LFB	Luxol fast blue
Ltf	Lactotransferrin
MALDI-MS	Matrix assisted laser desorption ionisation mass spectrometry
MAP	Microtubule-associated protein
MAPK	Mitogen-activated protein kinase
MAPKAPK2	Mitogen-activated protein kinase-activated protein kinase 2
MBP	Myelin basic protein
mg	milligram
Mg	Microglia
MHC	Major Histocompatibility complex
miRNA	Micro ribonucleic acid
ml	millilitre
MM	Mastermix
M/M	Monocyte/macrophage
MMPs	Metalloproteinases
MND	Motor neuron disease
MOG	Myelin oligodendrocyte glycoprotein
MRI	Magnetic resonance imaging
mRNA	Messenger ribonucleic acid
MRS	Magnetic resonance spectroscopy
MS	Multiple sclerosis
MS/MS	Tandem mass spectrometry
MSI	Mass spectrometry imaging
MSP	Mass spectrometry profiling
MSSS	Multiple sclerosis severity score
MT	Metallothionein
MTR	Magnetization transfer ratio
MZ	Monozygotic
m/z	mass-to-charge ratio
N/A	Not applicable
n/a	Not available
NAA	N-acetyl-aspartate
NAGM	Normal appearing grey matter

NAWM	Normal appearing white mater
NCM	Nitrocellulose membrane
Nd:YAG	Neodymium-doped:yttrium aluminum garnet
Nd:YVO_4	Neodymium-doped:yttrium vanadate
NF	Neurofilaments
NFkB	Nuclear factor kappa-light-chain-enhancer of activated B cells
NFL	Neurofilament light
ng	Nanogram
NH_4HCO_3	Ammonium bicarbonate
nm	Nanometre
nM	Nanomolar
NMDA	N-methyl-D-aspartate
NO	Nitric oxide
NOS	Nitric oxide synthese
NP	Neuronal progenitors
NSAIDs	Non-steroidal anti-inflammatory drugs
NTC	Non-template control
NTKR2	Neurotrophic tyrosine kinase receptor, type 2
NTP	Nucleoside triphosphate
N_2	Nitrogen
OcGlc	Octyl-α/β-glucoside
OCB	Oligoclonal bands
$OH^{\bullet}$	Hydroxyl radical
OH-	Hydroxyl anion
OLG	Oligodendrocyte
o/n	Overnight
OP	Osteopontin
OPCs	Oligodendrocyte precursor cells
O_2^-	Superoxide anion
PA	Pilocytic astrocytoma
PBMC	Peripheral blood mononuclear cells
PCR	Polymerase chain reaction
PD	Parkinson's disease
PDCD5	Programmed cell death 5
pg	Picogram
PIAS1	Protein inhibitor of the activated signal transducer and activator of transcription (STAT) 1
PIMP2	Peripheral myelin protein 2
PLP	Proteolipid protein
PM	Post mortem
PMCA1/2	Plasma-membrane Ca^{2+}-ATPase 1/2
PMF	Peptide mass fingerprinting
PMI	Post mortem interval
PPMS	Primary progressive multiple sclerosis
PPWM	Periplaque white matter
PRMS	Progressive relapsing multiple sclerosis
psi	Pounds per square inch
PTGS2	Prostaglandin-endoperoxide synthase 2
PTP4A2	Protein tyrosine phosphatase 4A2
PVC	Perivascular cuffs
Q	Quadrupole
qPCR	quantitative real-time polymerase chain reaction

Q-TOF	Quadrupole-time of flight
RAGE	Receptor for advanced end glycation products
RawQ	Raw noise
rf	Radio frequency
RIN	RNA integrity number
RNA	Ribonucleic acid
ROCK	Rho Kinase
ROI	Regions of interest
ROS	Reactive oxygen species
RP	Ribosomal protein
rpm	Revolutions per minute
RRMS	Relapse remitting multiple sclerosis
RT	Room temperature
RT-PCR	Reverse transcriptase-polymerase chain reaction
s	Seconds
SA	Sinapinic acid
SAPE	Streptavidin phycoerythrin
SBTB	Sheffield Brain Tissue Bank
SDS-PAGE	Sodium dodecyl sulphate polyacrylamide gel electrophoresis
Shh	Sonic hedgehog
SOD	superoxide dismutase
SPMS	Secondary progressive multiple sclerosis
STAT	signal transducer and activator of transcription
TBS	Tris-buffered saline
TBS-T	Tris-buffered saline-Tween20
TC	Cytotoxic T cell
TF	Transferrin
TFA	Trifluoroacetic acid
TFR	Transferrin receptor
TGF-β1/3	Transforming growth factor, beta 1/3
Th	T-helper
THAP	Trihydroxyacetophenone
THBS4	Thrombospondin-4
Tim2	T cell mucin domain containing receptor-2
TJ	Tight junctions
TLR	Toll like receptor
Tm	Melting temperature
TM	Tuberculous meningitis
TMEV	Theiler's murine encephalomyelitis virus
TNFα	Tumour necrosis factor alpha
TNFβ1	Tumour necrosis factor beta 1
TOF	Time-of-flight
Tregs	Regulatory T cells
TrkB	Tropomyosin receptor kinase B
TSC	Tri-sodium citrate
TUB	Beta tubulin
UTR	Untranslated region
UV	Ultraviolet
V	Volts
VCAM-1	Vascular cell adhesion molecule-1
VEGF	Vascular endothelial growth factor
VEZF1	Vascular endothelial zinc finger-1

VLA-4	Very late antigen-4
VWM	Vanishing matter disease
v/v	volume to volume
WB	Western blotting
WM	White matter
WML	White matter lesions
WT	Wild-type
µg	microgram
µm	micrometer
µM	micromolar
$^{+}$	Positive
$^{-}$	Negative
$^{+ve}$	Positive control
$^{-ve}$	Negative control
σ	Sigma
γ	Gamma
δ	Delta
1º	Primary antibody
2º	Secondary antibody
2D-DIGE	Two-Dimensional Differential Gel Electrophoresis

CHAPTER 1

AN INTRODUCTION TO MULTIPLE SCLEROSIS

1.1 Multiple Sclerosis (MS)

Multiple Sclerosis (MS) is traditionally regarded as an inflammatory, demyelinating disease affecting both the brain and spinal cord of the central nervous system (CNS). Demyelination of axons and the formation of inflammatory lesions (plaques) leads to the disruption of nerve conduction within the CNS typically associated with the symptoms displayed by the patient (Compston & Coles 2008).

MS is a complex disease displaying several pathological features including demyelination, inflammation, axonal/neuronal damage, gliosis, oxidative stress, excitotoxicity, changes in the immune system and blood brain barrier (BBB) dysfunction (Stables *et al* 2010). The disease mainly affects the white matter (WM) in the CNS but recent pathological and magnetic resonance imaging (MRI) studies have also shown significant cortical involvement (Barnett *et al* 2009b). In the majority of patients, MS is characterised by a variety of symptoms depending on the anatomical location of the demyelinated lesions; these can include visual impairment, limb weakness, sensory disturbance, balance and postural problems, sphincter dysfunction, cognitive impairments, pain and fatigue (Milo & Kahana 2010).

More recently there has been recognition that MS is more than an inflammatory condition with the involvement of neurodegenerative processes. The degenerative component of the disease is commonly unresponsive to immunosuppressant therapy, with neurodegeneration driving the progressive neurological impairment associated with the disease (Hauser & Oksenberg 2006).

The exact aetiology of MS is unknown, but most probably involves the interplay between both environmental and genetic factors. The disease is more predominant in particular races and geographical locations (Milo & Kahana 2010) and is generally more prominent in females (in a 3:1 ratio) indicative of possible hormonal involvement in its pathogenesis (Barnett *et al* 2009a, Dunn & Steinman 2013). Typically, MS presents in adults between 20-50 years of age, with a general peak onset age of 30 years old (Compston 2006), with the disease said to affect 2.5 million people worldwide (Antel *et al* 2012).

1.2 Clinical features and disease course in MS

MS presents with a range of symptoms that depend on lesion location in the CNS. For example, optic neuritis, a classical symptom of MS occurs when lesions reside on the optic nerve. Other symptoms can include numbness, muscle weakness, fatigue, speech

impairment, cognitive disturbances, bladder and bowel disruptions and ataxia (Shivane & Chakrabarty 2007). A definitive diagnosis of MS is given when one or more of these symptoms occurs on more than one occasion, in separate incidents known as a clinically isolated syndrome (CIS) (Stables *et al* 2010) which cannot be justified by any other CNS disorder. As well, diagnosis can also be supported by laboratory testing including the sampling of cerebrospinal fluid (CSF) for the presence of oligoclonal bands (OCB) recognising an immune reaction within the brain and the use of MRI for lesion identification (Baranzini *et al* 2009).

The disease course of MS can be characterised into separate clinical subtypes (Figure 1.1). Primarily in most early cases, around 80% of patients present with relapse-remitting MS (RRMS), characterised by sudden acute attacks followed by complete or partial recovery (Antel *et al* 2012, Compston & Coles 2008) thought to be as a result of inflammatory demyelinating lesions. Around 50-60% of patients who present with RRMS subsequently develop secondary-progressive MS (SPMS), where neurological disability occurs more frequently and for longer periods of time without or between relapses. A general progression and worsening of symptoms (Antel *et al* 2012) as a result of widespread WM atrophy and cortical demyelination is apparent in patients with SPMS (Kremenchutzky *et al* 2006).

Around 10-15% of patients present with primary progressive MS (PPMS), where neurological disability steadily develops over time from disease onset, without distinct relapses or improvement of symptoms (Antel *et al* 2012). Generally patients will present with PPMS 10 years later than patients presenting with RRMS with little evidence of BBB disruption or presence of inflammatory, actively demyelinating lesions within the WM. Instead, inflammation in progressive MS is more diffuse and present behind an intact BBB, said to be compartmentalised inflammation proving challenging for study and investigation (Farrell 2013, Reynolds *et al* 2011). Patients who display constant disease progression with distinct disease relapses with or without full recovery are classified as having progressive-relapsing MS (PRMS) (Sobel & Moore 2008). MS can be classified as benign where patients present with little or no neurological impairment over a period of 15 years from disease onset. In contrast, malignant MS involves a short, rapid disease course with huge neurological impairment leading to patient death in a short period of time (Sobel & Moore 2008).

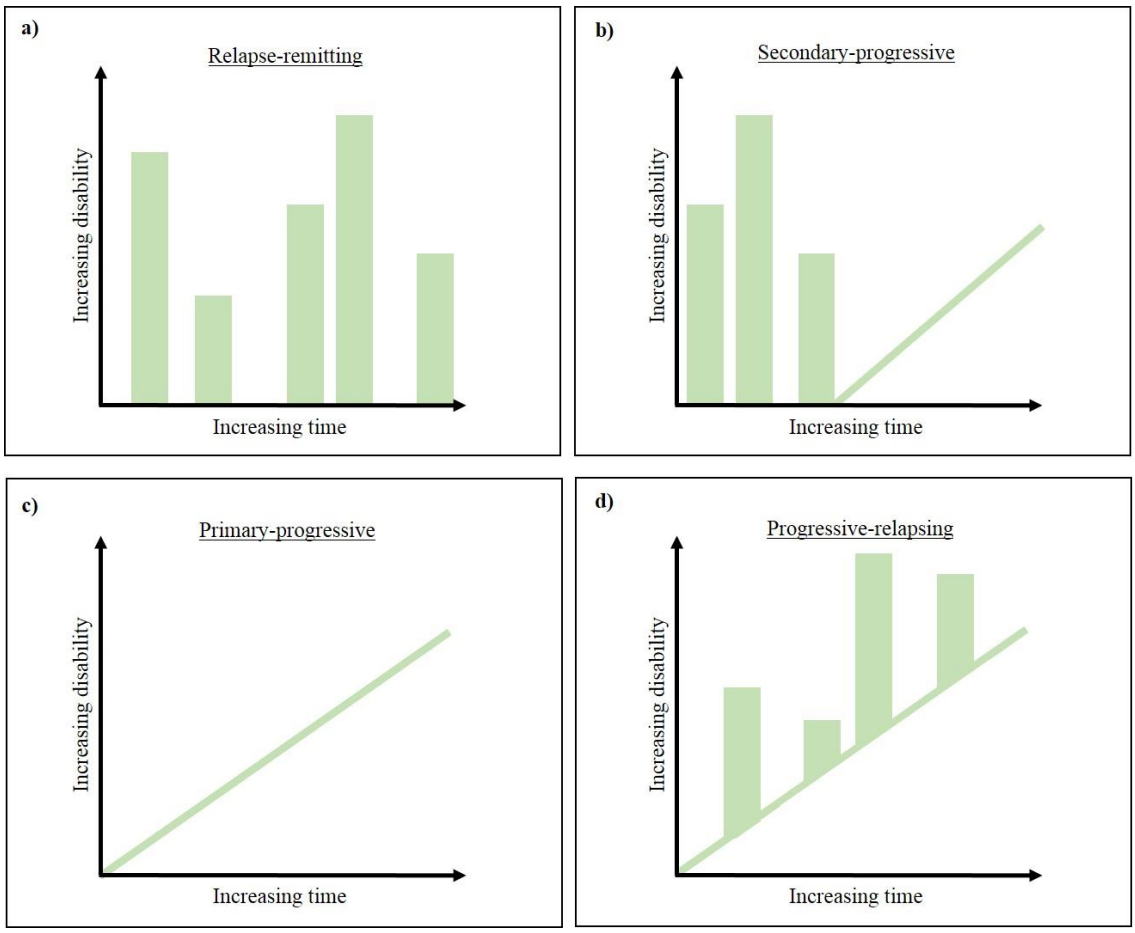

Figure 1.1 A summary of the clinical classification of MS subtypes

Around 80% of patients will present with relapse-remitting (RRMS) with periods of varying neurological impairment (relapse) interspersed with periods of stability (remission) (a). Around half of patients with RRMS will go onto secondary-progressive MS (SPMS) where the periods of remission are shorter and the disease takes on a more progressive phenotype with little improvement in symptoms (b). Around 10-20% of patients will present with primary-progressive MS (PPMS) where the patients experience neurological decline and progression of disease from onset, with very little improvement (c). A small proportion of patients may present with progressive-relapsing MS (PRMS). In comparison to PPMS, a PRMS patient will experience periods of relapses over a general progression of disease, with minor improvements between relapses (d). Figure adapted from Zuvich *et al* 2009.

1.3 Pathological hallmarks of MS – lesion type

The affected areas of CNS tissue in MS are known as white matter lesions (WML) or plaques which are usually centred around several vessels (Shivane & Chakrabarty 2007). Pathological features of MS lesions include: BBB leakage, demyelination, oligodendrocyte (OLG) damage, axonal damage and loss, glial scar formation and the presence of inflammatory infiltrates that mainly consist of lymphocytes and macrophages (Sospedra & Martin 2005). There are several different types of lesion that differ based on the stage and subtype of the patient's MS, as well as the age and location of the lesion within the CNS (Lassmann 2011). The classical active MS lesion contains activated macrophages, containing myelin debris as a result of the demyelinating process (Lassmann 2011). The typical active lesion can be sub divided into different types;

Acute MS plaque – referred to as the early active (EA) lesion, contain an even distribution of macrophages throughout the whole lesion, with the same stage of digested myelin products (Lassmann 2011).

Chronic active MS plaque – referred to as the late active (LA) lesion, contain macrophages at the lesion edge with early stages of myelin product digestion, while macrophages containing more degraded myelin products are found in the lesion core, or have already been removed from the lesion centre (Lassmann 2011).

Due to the nature of MS as a disease, lesion classification is quite difficult to fully define. There have been various attempts to classify lesion types in studies by Lucchinetti *et al* 2000 who defined lesions based on aggressiveness, ranging from slowly developing to rapidly developing severe chronic lesions. While Bruck *et al* 1995 classified the initial stages of MS lesions as containing macrophages with the earliest stages of myelin digestion, failing to appreciate that the uptake of myelin into macrophages follows a period of myelin destruction. As well, it is known that the typical chronic MS lesion is divided into various subtypes involving a complicated set of molecular mechanisms involved in tissue destruction and repair (Lassmann 2011). In addition to WML, demyelination also occurs in the cerebral cortex and grey matter (GM), these GM lesions (GML) are associated with neuronal loss in the absence of inflammation, complement deposition and BBB breakdown, yet are probably driven by meningeal inflammatory infiltrates (Choi *et al* 2012, Gardner *et al* 2013, Popescu & Lucchinetti 2012). GML accumulation has been suggested as a factor in the transition

from RRMS to SPMS in patients (Stadelmann 2011). The pathology behind these types of lesion is relatively unknown and most probably reflects an immune response to the sparse myelin present in the region or to neuronal antigens (Weissert 2013).

1.4 MS normal appearing white matter

Adjacent to WML in MS is the area of tissue known as the normal appearing white matter tissue (NAWM). Despite its name, there is increasing evidence that NAWM is abnormal with regards to several biochemical and histological features (Lund *et al* 2013). The cause and pathological mechanisms affecting NAWM remain unclear, but have been suggested to be a result of diffuse factors dependent on the macroscopic pathology within the tissue, or the result of discrete lesions beyond the sensitivity of current imaging instrumentation, or as a result of damage to axons within the lesions (Mistry *et al* 2011). However, these explanations fail to account for the NAWM abnormalities present in PPMS patients, which do not typically display inflammatory lesions to the same extent as in patients with SPMS. Evidence that cytokines can induce the typical symptoms of MS, without the presence of inflammatory lesions, along with the upregulation of pro- and anti-inflammatory cytokines in MS NAWM may account for these subtle differences (Mistry *et al* 2011, Zeis *et al* 2008). Evidence of NAWM abnormalities have been obtained from various histological and neuroimaging data. An increased level of gliosis, microglial activation, BBB breakdown, cellular infiltration, reduced myelin density, and axonal loss have been observed (Allen & McKeown 1979, Allen *et al* 2001, Kutzelnigg *et al* 2005, Lund *et al* 2013). Neuroimaging studies have shown NAWM alterations, using proton-magnetic resonance spectroscopy (MRS), N-acetyl-aspartate (NAA) levels in MS NAWM were reduced in comparison to healthy controls (Aboul-Enein *et al* 2010, Sarchielli *et al* 1999). NAA is a specific marker of functional neurons, therefore lower levels of NAA in the NAWM indicate a reduction in axonal density. A decrease in axonal density in NAWM brain tissue was confirmed also by a reduced magnetization transfer ratio (MTR) in the area, which reflects the transfer of magnetization between protons in macromolecules and in the surrounding water (Davies *et al* 2005, Filippi *et al* 1998). Consequently, MS NAWM has shown to be both structurally and functionally different from neurological control tissue. As well from MTR studies, around 50% of new WML in MS have shown to develop in the NAWM (Allen *et al* 2001). It is in these areas of NAWM where pre-lesional changes occur, which have been termed pre-active lesions, where the tissue is primed with clusters of activated microglia in the absence of active demyelination or lymphocyte infiltration in

the first instance (van der Valk & Amor 2009). In the majority of these pre-active lesions, the initial pathology resolves and only a small number progress into demyelinating WML associated with MS (van der Valk & Amor 2009, van Noort *et al* 2011). Investigations into the cellular phenotype and interactions in NAWM will ultimately help gain a better understanding of MS pathology.

1.5 Proposed mechanisms underlying the aetiology of MS

Understanding the aetiology of MS is a hugely debatable topic, and a definitive answer is unknown. The disease is believed to occur due to an interplay between both genetic and environmental factors in certain predisposed individuals. There are a number of theories as to the cause of MS which will be discussed.

1.5.1 Influence of genetics on MS

A genetic susceptibility to MS is clear, with initial work conducted on familial aggregation identifying a genetic link with human leukocyte antigen (HLA) class I antigens (Jersild *et al* 1972, Naito *et al* 1972). Across the many MS genome wide association studies (GWAS) carried out to date, in the Caucasian population, the strongest genetic association with MS has been linked with HLA-DR2 (HLA-DRB1*15) (Ramagopalan *et al* 2009). Other HLA alleles have been reported to be associated with MS, yet due to the complexity of the major histocompatibility complex **(**MHC) and the disease itself having specific variants and associations it is continuingly challenging to identify specific genetic associations (Fernando *et al* 2008, Ramagopalan *et al* 2009). It has been shown that a higher susceptibility of disease is apparent in first, second and third degree relatives of people with MS, compared with the general population (Sadovnick *et al* 1988). Also, MS twin studies have shown a 25-30% concordance level in monozygotic (MZ) twins compared to 2-5% in dizygotic (DZ) twins (Hawkes & Macgregor 2009). Consequently, due to the relatively low concordance level in MZ twins, additional factors other than purely genetics must be apparent in the pathogenesis of the disease (Handel *et al* 2010b, Sadovnick 2013). Despite a known increase incidence of MS in females compared to males, no genetic link to the X chromosome has been defined (International Multiple Sclerosis Genetics *et al* 2011), suggesting that sex hormones may exert an active role in disease pathogenesis (Correale *et al* 2013).

1.5.2 Environmental factors associated with MS

A number of environmental factors have been proposed as risks for developing MS, including bacterial and viral infections (Handel *et al* 2010a), vitamin D deficiency (Nessler & Bruck 2010), smoking (Hedstrom *et al* 2013, Ramagopalan *et al* 2013) and obesity (Hedstrom *et al* 2012, Munger 2013). Evidence has shown these factors to be population and geographical based rather than intra-familial (Sadovnick 2013). Such examples of infectious pathogens proposed as being involved in the development/exacerbation of MS include the bacteria, *Mycoplasma pneumoniae* and *Chlamydia pneumoniae*, along with viruses including the herpes virus and Epstein-Barr virus (EBV). Viral involvement in the disease has been proposed as being a major contributor in MS due to the increased number of $CD8^+$ (positive) cytotoxic T cells observed within MS lesions, which function to clear viral infections (Babbe *et al* 2000). The way in which infectious agents could lead to an increase in MS susceptibility is through molecular mimicry, epitope spreading and bystander activation. Superantigens are proteins produced by bacteria (or viruses) that potently activate $CD4^+$ T cells, inducing a rapid increase in cellular proliferation and cytokine production, most probably involved in MS. Staphylococcal enterotoxins were identified as superantigens capable of reactivating autoreactive T cells in asymptomatic experimental autoimmune encephalomyelitis (EAE), the animal model of MS, suggesting a role of bacteria and superantigens in the development and progression of MS (Brocke *et al* 1993, Schiffenbauer *et al* 1993). In a lot of examples however, as with EBV, the mechanisms responsible for these bacterial/viral agents in increasing disease susceptibility and possible development are unclear (Tselis 2012). Exposure to EBV has been suggested to increase the risk of developing MS especially if an individual contracts the virus as a young adult. However, children who contract EBV infection have a reduced risk of developing MS later in life (Milo & Kahana 2010).

Vitamin D has been shown to have immunomodulatory actions on T and B cells, with a limited vitamin D exposure in early life shown to increase an individual's risk of developing MS (Goldacre *et al* 2004). The first study on MS patients with regard to vitamin D and its association with the disease identified an increased release of the cytokine tumour necrosis factor beta 1 (TNFβ1), responsible for inhibiting T cells, in patients treated with vitamin D (Mahon *et al* 2003). Complementary studies have identified the anti-inflammatory and neuroprotective properties of vitamin D (Ascherio *et al* 2010, Correale *et al* 2009, Pierrot-Deseilligny 2009). Conversely low levels of

Vitamin D3 were shown to increase MS risk, severity and progression (Ascherio *et al* 2010).

Both the duration and intensity of smoking have been shown to be associated with an increased risk of developing MS. However, contrary to many other environmental factors where an individual's exposure to these factors at a specific age increases their risk of developing MS, smoking does not follow this trend (Hedstrom *et al* 2013). The mechanism by which smoking increases an individual's risk of developing MS is suggested to occur initially in the lung. In response to smoking, oxidative stress and inflammatory responses occur in the cells of the lung. As well, post-translational modifications may affect certain proteins and their antigenicity (Hedstrom *et al* 2013). Within the immune system of MS animal models including their innate immunity, B and T cells have shown to be affected by exposure to smoking (Fusby *et al* 2010). Therefore, the possibility that autoimmunity occurs against proteins modified in the lung that cross-react with CNS proteins is evident (Odoardi *et al* 2012). As well, the presence of memory T cells in the lung could potentially be a factor linked to autoimmunity in MS. Memory T cells may rapidly proliferate and migrate into the CNS contributing to the initiation of MS (Odoardi *et al* 2012).

Obesity in late adolescence/early adulthood has been shown to increase the risk of developing MS, with one study showing a 40% increased risk of developing MS in obese late adolescent individuals (Munger *et al* 2009). Another study identified that obese individuals at the age of 20 had a two-fold increased risk of developing MS (Hedstrom *et al* 2012). The link between being obese in earlier life and an increased risk of developing MS later in life is unknown. Yet studies have identified low levels of vitamin D in the blood of obese people, and therefore the risk may in part be related to the vitamin D pathway (Wortsman *et al* 2000). Alternatively, an increased release of adipokines, such as leptin from surplus adipose tissue in obese individuals as shown to alter the immune system, promoting inflammatory T cell responses (Lord *et al* 1998) and decreasing regulatory T cells (De Rosa *et al* 2007). Supporting this theory in relation to MS, leptin deficient mice have shown to be protected against EAE (Matarese *et al* 2001a, Matarese *et al* 2001b).

1.6 Proposed pathophysiology of MS – an inflammatory or degenerative disease?

MS lesions are characterised histopathologically by inflammation, demyelination, partial remyelination, damage to axons and gliosis (Kuhlmann *et al* 2009). The MS lesion is proposed to develop through the breakdown of immune tolerance and passage of immune cells across the BBB. Destructive effects follow such as the release of toxic oxygen species, and cytokines that lead to an inflammatory response, demyelination and neurodegenerative processes typical of MS (Sospedra & Martin 2005).

MS has generally been considered a T cell mediated autoimmune disease, where T cells recognise myelin peptides and induce tissue damage by activating macrophages and microglia leading to demyelination resulting in inefficient nerve signal conduction throughout the nervous network (Lassmann 1999). Over time it is believed that neurodegeneration becomes independent of the inflammatory response continuing on into the progressive stage of the disease (Trapp & Nave 2008).

In contrast to the generally accepted autoimmunity aetiology of MS is the concept that MS disease progression and neurodegeneration work independently from the neuroinflammatory component of the disease (Stys *et al* 2012). This mechanism favours an unidentified degenerative factor possibly targeting the oligodendrocyte, whether this be a virus or other foreign agent is still to be determined. As a result, demyelination occurs which over time initiates an immunological response, which is associated with the varying degree of inflammatory activity represented in the relapse and remitting clinical phenotype of the disease, while neurodegeneration progressively occurs in the background resulting in increasing disability (Stys *et al* 2012). Supporting this alternative view on MS pathogenesis is the knowledge that the neuroinflammatory component of the disease can be controlled to an extent by the currently available therapy, while neurodegeneration continues regardless (Stys *et al* 2012).

It is clear that inflammation and degeneration are constant contributors to MS pathogenesis yet the initiating factor has eluded researchers. At present the majority of research on MS has focussed on the immunological influence on MS lesions and potential mechanism of disease which has led to the currently accepted concept that MS is an autoimmune disease. Supporting this are the numerous studies that have discovered known pathology, mechanisms, and therapeutics for the early relapsing disease course. Currently available clinical data and the known genetic associations of

MS also support the autoimmune hypothesis. Yet despite many years of research there is still no definite cause of MS, nor has there been any definitive CNS autoantigen identified (Chaudhuri 2013). As well, very limited therapy for the progressive stage of the disease has been developed, which is arguably the most disabling element of the disease. More importantly, no cure for the disease has been discovered. These are all questions that ultimately indicate that further work addressing the pathogenesis of the disease is needed (Bar-Or 2008, Chaudhuri 2013, Stys *et al* 2012).

1.6.1 The blood brain barrier (BBB)

The BBB is a term used to describe a set of discrete properties of blood vessels in the CNS that regulate the movement of molecules, ions and cells between the blood and CNS tissue (Abbott *et al* 2010, Begley 2003). In the brain and spinal cord the BBB is comprised of specialised endothelial cells (EC) that line the walls of blood capillaries held together by tight junctions (TJ) and adherens junctions (AJ) (Begley 2003). This lining of endothelium surrounding blood capillaries is closely associated with pericyte cells enclosed in the basal lamina, an extracellular matrix (ECM), composed of collagen, laminins, and heparin (Luissint *et al* 2012). The extended processes of astrocytes ensheath the blood vessels, as well as directly contacting neurons and axons. Also, perivascular macrophages are held in close proximity to this neurovascular unit providing an immune surveillance to the vessels. These cells help to support BBB maintenance and function (Abbott *et al* 2010, Abbott *et al* 2006), (Figure 1.2). The major role of the BBB is to act as a physical barrier to diffusion, but also as a transport barrier and metabolic barrier (Begley 2003) to maintain homeostasis throughout the CNS. As a physical barrier to diffusion, the TJ proteins between the EC of the BBB prevents the passive diffusion of solutes from the blood into the brain (Begley 2003). As a transport barrier, the BBB mediates the passage of nutrients, oxygen, vitamins, proteins and peptides to the CNS (Bundgaard & Abbott 2008). Functioning as a metabolic barrier, the BBB also limits the entry of toxins, pathogens and immune cells into the CNS tissue, while aiding in the removal of toxic metabolites from the CNS (Abbott *et al* 2010).

1.6.2 BBB dysfunction in MS

An intact BBB is vital in the physiology of the CNS and evidence has shown that BBB dysfunction contributes to lesion formation and expansion in MS (McQuaid *et al* 2009). The BBB can be affected in two ways by dysfunction and/or activation.

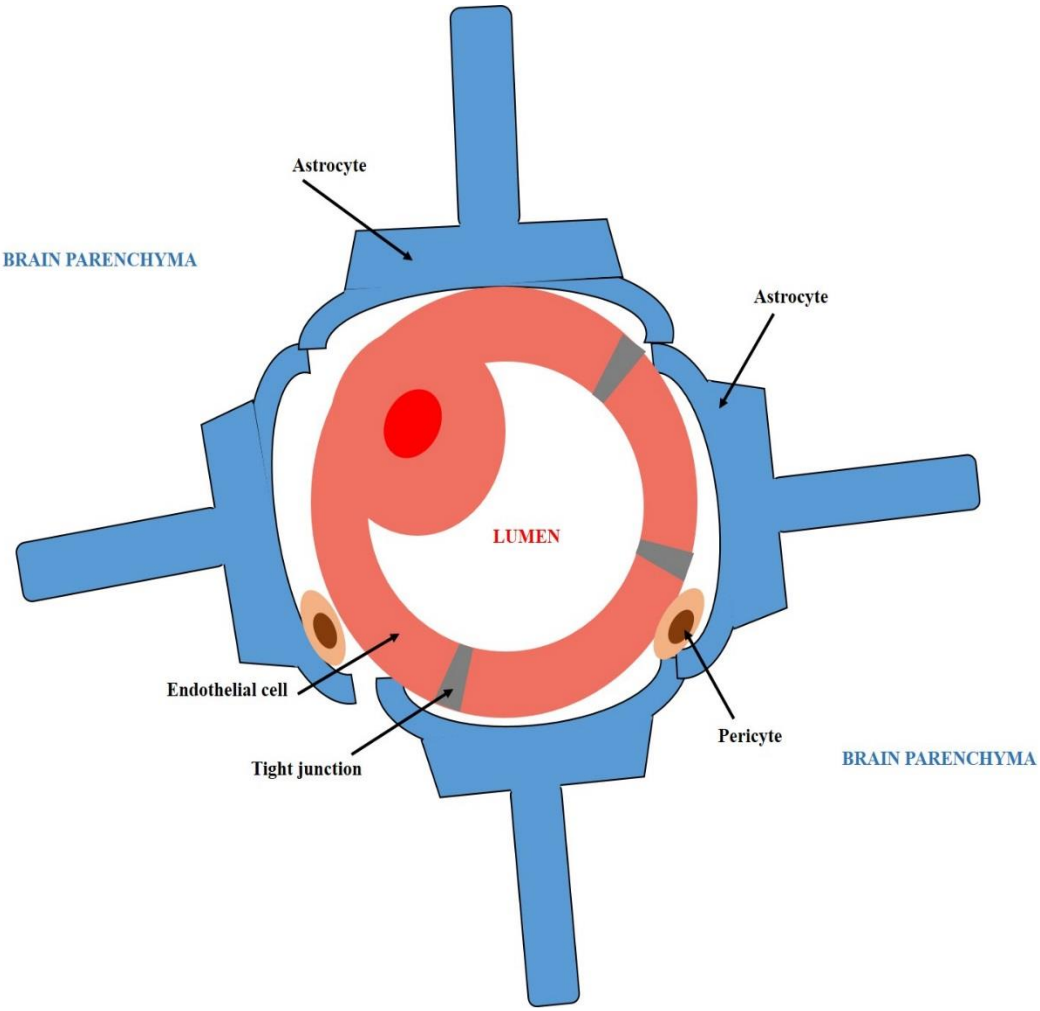

Figure 1.2 The major cellular components of the BBB

Endothelial cells (EC) form a capillary tube in which blood can flow, the cells fold on themselves and adhere to one and other through the formation of tight junctions (TJ). Pericytes are found adhered to the abluminal side of the EC that is surrounded by extracellular matrix (ECM), with astrocyte end feet ensheathing the whole blood vessels. Figure adapted from Abbott *et al* 2010.

Dysfunctional changes to the BBB exist in neuroinflammatory conditions as seen in MS when defective TJ and AJ allow the passage of molecules normally excluded from the CNS (Persidsky *et al* 2006). Alterations in the BBB are believed to be an early pathological event in MS, preceding lesion formation (Larochelle *et al* 2011) that can be identified through histology at post mortem and also through MRI both at post-mortem and during life (Alvarez *et al* 2011a). It is proposed that peripheral immune cells and antigen presenting cells (APC) enter the CNS through the altered BBB leading to demyelination, along with the infiltration of autoreactive T cells that causes oedema, axonal loss and gliosis (Klegeris & McGeer 2005). Activated cells of the BBB including EC, astrocytes and pericytes release an array of cytokines and chemokines that aid in the recruitment and survival of immune cells entering the CNS (Alvarez *et al* 2011a). There are many proposed causes of BBB breakdown in MS including the involvement of vascular endothelial growth factors (VEFGs), matrix metalloproteinases (MMPs), cytokines and reactive oxygen species (ROS) (Daneman 2012, Minagar & Alexander 2003). The release of inflammatory agents can directly affect the permeability of the BBB. For example, tumour necrosis factor alpha (TNFα) released by EC weaken the AJ between the tightly connected EC of the BBB due to a loss of VE-cadherin (Wojciak-Stothard *et al* 1998). Expression of interleukin (IL)-1β by infiltrating macrophages has been shown to induce the expression of MMP-9, an enzyme responsible for the cleavage of the TJ proteins occludin, ZO-1 and claudin 5, destabilising the BBB further (Lleo *et al* 2007, Yang *et al* 2007). BBB permeability in MS is also seen as an advantage in promoting self-repair, allowing the movement of anti-inflammatory T helper (Th)2 cells and regulatory T cells (Tregs) into the CNS to reduce inflammation (Larochelle *et al* 2011). Yet prolonged BBB breakdown can lead to oedema, and increase in brain volume due to the movement of water into the brain causing an altered cellular architecture, myelin degradation, astrocyte activation and neuronal dysfunction (Daneman 2012). Whether BBB breakdown is a consequence of a primary pathological event in MS is continuously questioned (Correale & Villa 2007).

1.6.3 Inflammation in MS – the autoimmune hypothesis.

MS has long since been regarded as an inflammatory disorder of the brain and spinal cord, with a complex autoimmune association. Immune cell involvement in MS pathogenesis has been suggested from many animal studies showing the involvement of both Th17 and Th1 cells (Gilgun-Sherki *et al* 2005). T cells can be divided into $CD4^+$ Th cells or $CD8^+$ cytotoxic T cells (TC), with Th cells further divided into Th1, Th2, Th17 and Tregs, distinguished based on the cytokines they produce and their effector

functions. Th1 cells release an array of proinflammatory cytokine such as TNFα and interferon gamma (IFNγ), designed to eliminate pathogens but also heighten the autoimmune responses in the body (Bar-Or 2008). Th2 cells release cytokines designed to support antibody production by B cells (Haider *et al* 2011). In comparison, during inflammation the physiologically low number of TC cells in the CNS is increased providing direct killing of cells through release of perforin and granzymes (Gravano & Hoyer 2013).

In MS, autoreactive T cells in the periphery become activated as a result of the interaction with chemoattractant factors displayed on the surface of EC, which support the cells passage across the BBB into the CNS (McFarland & Martin 2007). These autoreactive T cells once in the CNS become re-activated when in contact with specific CNS APCs, causing cellular proliferation and secretion of an array of cytokines and chemokines (Bar-Or 2008). In turn this stimulates the recruitment and activation of microglia and astrocytes along with other immune cells, releasing a further array of cytokines and chemokines, causing OLG damage and demyelination resulting in the typical neurological symptoms associated with MS (Bar-Or 2008). The process by which T cells become autoreactive is hugely debated and has been proposed as being the result of molecular mimicry. In molecular mimicry an external environmental antigen resembling a self-antigen, thought to be a myelin protein, is presented to the T cells together with MHC on the surface of APCs in the periphery (Sospedra & Martin 2005). Once in the CNS, autoreactive T cells become reactivated by myelinated axons presented to infiltrated immune cells by CNS APCs. Myelin basic protein (MBP) positive $CD4^+$ T cells (predominantly Th1 cells) are initiators of MS, however it is predominantly the $CD8^+$ T cells that reside in the inflammatory MS lesions (Neumann *et al* 2002, Shivane & Chakrabarty 2007). Activated T cells express molecules including very late antigen-4 (VLA-4) and leukocyte-associated antigen-1 (LFA-1), that bind to adhesion molecules present on EC such as vascular cell adhesion molecule-1 (VCAM-1) and intercellular adhesion molecule-1 (ICAM-1), to facilitate their traffic across the BBB (Bar-Or 2008).

In MS, the sites of inflammation within the brain are dominated by $CD8^+$ T cells resulting in lesion formation throughout the CNS (Compston & Coles 2008). In contrast, research on the EAE model of MS identified the primary stage of disease inflammation occurs through the Th17 lymphocyte subtypes, that secrete IL-17 under IL-23 control. The release of IL-17 can disrupt the BBB allowing Th17 cells and other

immune cells to infiltrate into the CNS. The precise activity of the inflammatory response in MS in unknown and most probably involves a complex interplay between genetic and environmental factors (Gilgun-Sherki *et al* 2005). An individual's different disease stage and subtype may determine whether Th17 or Th1 cell lineage is the main driver of pathology. As well, these individual differences may also play a hand in the different cell type involved in disease pathogenesis, with the Th lineage initiating disease and possibly other immune cells, such as the $CD8^+$ CT cells continuing the detrimental effects (Gilgun-Sherki *et al* 2005).

In a similar way autoreactive T cells are considered to develop, increasing evidence is implementing the role of B cells and the production of CNS directed autoantibodies in MS pathogenesis (Bar-Or 2008). Specifically associated with MS, antibodies are produced by B cells stimulated by particular cytokines including Il-4, Il-6 and Il-10 (Barun & Bar-Or 2012). These antibodies participate in demyelination through the formation of immune complexes which activate complement, or partake in antibody dependent cell cytotoxicity (Barun & Bar-Or 2012). B cells can also act as APC involved in the activation of T cells in MS (Barun & Bar-Or 2012). Over 95% of patients with established MS have increased levels of soluble clonal IgG, known as OCB in their CSF (Walsh *et al* 1985), yet deciphering the target antigen of B cell immunity in MS is contradictory. There is evidence to support myelin peptides and EBV antigens as targets for OCB antibodies (Cepok *et al* 2005, O'Connor *et al* 2005). However, whether autoantibodies produced in MS contribute to disease pathogenesis, or are generated as a result of tissue injury associated with the disease is not fully understood (Bar-Or 2008).

1.6.4 Neurodegeneration in MS

Disease progression in MS is associated with the accumulation of axon degeneration in an acute inflammatory setting (Trapp *et al* 1998), and demyelination of axons is a key factor in this (Dutta *et al* 2006, Trapp & Nave 2008). For example, a partially demyelinated axon cannot conduct nerve signals effectively explaining the symptoms of fatigue (Compston & Coles 2008). Axonal damage occurs early in the disease alongside inflammatory demyelination and continues throughout the disease. Within the progressive phase of the disease, the accumulation of neurodegeneration accounts for permanent disability in MS, generally in the absence of new inflammatory demyelinating lesions (Frischer *et al* 2009, Kuhlmann *et al* 2002). Ultimately, the driving force behind permanent neurodegeneration must be caused by additional factors

to infiltrating immune cells and inflammation (Trapp & Nave 2008). A number of theories have been put forward as to alternative/additional causes of neurodegeneration in MS, involving mitochondrial injury, oxidative damage and glutamate excitotoxicity as key factors.

1.6.4.1 Mitochondrial damage in MS lesions

Determining a specific factor that could drive neurodegeneration in all MS patients has been a continuing area of research. An autoimmune attack of myelin epitopes present in OLG and on myelinated axons is a naïve view and rarely seen in MS lesions. Only in aggressive forms of MS are $CD8^+$ CT cells shown to be infiltrating MS lesions and exhibiting toxic effects on OLG and axons (Neumann *et al* 2002). Similarly, the observation of autoantibodies towards myelin proteins have only been seen in a subset of MS patients, generally children with MS (Brilot *et al* 2009). Therefore the proposed immune response mounted against myelin in MS may only account for a subset of patients. Instead, an alternative mechanism for tissue injury in all MS lesions must be apparent and has been linked to mitochondrial dysfunction in cells (Lassmann & van Horssen 2011). Mitochondria partake in a number of roles crucial to cell survival, primarily the organelle produces adenosine triphosphate (ATP) as a source of cellular energy, while also being involved in maintaining ion homeostasis and cellular apoptosis. Alterations in mitochondria have been associated with MS pathogenesis, identified by immunohistochemistry (IHC), gene expression microarray studies, biochemical studies and electron microscopy (Mahad *et al* 2008, Mahad *et al* 2009, Su *et al* 2013, Su *et al* 2009, van Horssen *et al* 2012). In acute lesions these changes include a loss of cytochrome C oxidase-I (COX-I) and complex IV immunoreactivity, components of the mitochondria respiratory chain (Mahad *et al* 2008). In contrast, mitochondria levels and activity in inactive (IA) lesions is increased to meet the energy demands of demyelinated axons (Mahad *et al* 2009). In relation to MS pathogenesis, disturbances in mitochondria can lead to proapoptotic events, which has been linked to OLG damage and demyelination associated with the disease (Veto *et al* 2010). Ineffective mitochondria in oligodendrocyte precursor cells (OPCs) can cause impaired cell differentiation, therefore affecting remyelination in areas of demyelination (Ziabreva *et al* 2010). Consequently, neuronal mitochondrial dysfunction in MS can lead to neuronal energy failure contributing to neurodegeneration (Lassmann & van Horssen 2011).

1.6.4.2 Oxidative damage in MS lesions

Damage to mitochondria in OLGs and other cells in the CNS can be accounted for by oxidative stress. Neuroinflammation is a major instigator of oxidative stress in MS through two possible mechanisms; the production of ROS by activated glia cells including microglia and astrocytes, and also through the activation of cyclooxygenases and lipoxygenase pathways involved in the production of prostaglandins and conversion of polyunsaturated fatty acids respectively (Ortiz et al 2013). As well oxidative stress can occur when the production of oxidants exceeds the antioxidant capacity of cells, or when a cell's defence system against oxidative species becomes impaired (Ortiz et al 2013). ROS and nitric oxide (NO) can damage lipids, proteins and nucleic acids leading to cell death. In MS it has been suggested that the diffuse inflammatory activity and prolonged disease duration is associated with increasing levels of ROS and NO, leading to mitochondria damage within CNS cells compared to controls (Campbell *et al* 2012). ROS are mainly derived from activated microglia and macrophages which promotes demyelination and axonal damage (Haider *et al* 2011). It has been shown that oxidative damage in MS in is an early event in the disease and is implicated in active MS lesion development (Lassmann & van Horssen 2011). Another source of ROS comes from iron or related divalent cations that can cause the formation of highly reactive hydroxyl ($OH^{\bullet}$) radicals through the Fenton reaction (Jomova & Valko 2011). Consequently, the accumulation of oxidative damage within MS lesions can contribute to additional demyelination and neurodegeneration, which can feedback to produce further oxidative species. In MS lesions as a result of mitochondrial dysfunction there is an increase in pro apoptotic events, leading to OLG degeneration. These cells are a major source of iron, therefore increasing iron levels within the CNS and ultimately increasing oxidative species (Lassmann & van Horssen 2011, Williams *et al* 2012). In the same way, activated macrophages remove myelin debris and excess iron in MS lesions, leading to additional oxidative burst and ROS production by these cells. At the same time, defective mitochondria in cells residing in the MS lesion, leads to proapoptotic action of these cells, supplementing a second wave of oxidative species and iron release into the lesion. Consequently, the continued cycles of oxidative damage within a lesion centre increases tissue damage and neurodegeneration associated with the progression of the disease, irrespective of the presence of inflammation.

1.6.4.3 Glutamate excitotoxicity in MS lesions

In MS lesions an increase in glutamate is common due to the activation of microglial and macrophages, along with a reduction in glutamate transporter expression by cells

such as astrocytes in the lesions that leads to excitotoxicity (Su *et al* 2009). Glutamate excitotoxicity leads to a disruption of ion channels and impairment of Ca^{2+} homeostasis resulting in an increased influx of Ca^{2+} into the cell. Increased levels of Ca^{2+} leads to mitochondrial dysfunction, but also causes the release of several enzymes that disrupt cellular DNA, cytoskeleton and cellular membrane promoting apoptosis (Su *et al* 2009), all factors that can lead to neurodegeneration in MS.

1.7 Animal models of MS

Studying the pathological basis of MS in patients is challenging due to the difficulty in accessing CNS tissue throughout the course of the disease. Therefore, a number of animal models of CNS demyelination have been developed, which enable the pathology of disease to be interrogated and aid the identification of potential diagnostic and therapeutic targets. These models include chemically induced [cuprizone (van der Star *et al* 2012) and ethidium bromide (Guazzo 2005)], and viral-induced [murine hepatitis virus (Bergmann *et al* 2006) and Theiler's virus (Mecha *et al* 2013)] models of demyelination. In addition, zebrafish can provide a model system for investigating remyelination mechanisms *in vivo* (Buckley *et al* 2008, Buckley *et al* 2010) but can also be used as a demyelinating model, through the ablation of oligodendrocytes (Chung *et al* 2013). However, the most widely used animal model for CNS demyelination is EAE, a term used to describe multiple models of CNS autoimmunity that can mimic a wide range of MS traits (Baker *et al* 2011, Mecha *et al* 2013). First discovered when monkeys were immunised with rabbit brain extract, the disease presents with paralysis and is pathologically associated with perivascular infiltration and demyelination of the brain and spinal cord (Rivers *et al* 1933). Since these initial experiments, EAE has been induced in many species including non-human primates (Haanstra *et al* 2013), and guinea pigs (Aritake *et al* 2010) but the majority of research to date has primarily investigated EAE in mice and rats. There is no single EAE model that mimics all aspects of MS, however the course of this autoimmune, inflammatory, demyelinating disease has proven to reflect several aspects of the human disease. Variation is dependent on a number of aspects including the age, sex and genetic background of the animal, through to the antigenic substance used and the way it is administrated into the animal (deLuca *et al* 2010) resulting in models that mimic RRMS (McRae *et al* 1992), SPMS (Hampton *et al* 2008) and PPMS (Tsunoda *et al* 2000).

1.7.1 Induction of experimental autoimmune encephalomyelitis (EAE)

EAE can be induced in animals via two methods: active or passive induction. Active EAE is induced in susceptible animals by immunisation with animal CNS tissue or myelin proteins, such as MBP, myelin oligodendrocyte glycoprotein (MOG) or proteolipid protein (PLP) (Constantinescu *et al* 2011). After 9-12 days disease onset occurs with various pathological and symptomatic behaviour consistent with relapse-remitting or chronic progressive CNS inflammation (Constantinescu *et al* 2011). In contrast, passive EAE, or adoptive transfer EAE (AT-EAE), is induced when pathogenic, myelin-specific $CD4^+$ T cells from actively induced EAE animals are transferred by active immunisation. Specific alterations of T cells can occur prior to AT by the use of specific cytokines to prime the cells, or by labelling T cells prior to transfer to enable the cells' activity, localisation, and interactions with other cell types to be determined (Constantinescu *et al* 2011). EAE models include the traditional RR disease course model where $PLP^{139-151}$ antigen is administered into SJL/J mice (Tuohy *et al* 1989). A more chronic relapsing disease course is induced in Biozzi AB/H (antibody high) using spinal cord homogenate in adjuvant (Baker *et al* 1990), while mimicking PPMS C57BL6/J mice are immunised with MOG^{35-55} (Sayed *et al* 2011).

1.7.2 Autoimmune hypothesis of EAE

AT-EAE, mediated by myelin-specific T cells, infers the strong association of MS with MHC class II alleles (Simmons *et al* 2013). Myelin specific activated Th1 cells, Th17 cells and autoantibodies enter the CNS across a disrupted the BBB. Within the CNS the T cells interact with infiltrating APC that present MHC class II antigen to them, resulting in inflammation, myelin breakdown and axonal damage (Figure 1.3).

To date, the identity of the Th cells which are critical for EAE induction is still unknown and highly debated. The majority of the literature claims the Th1 subset of cells are the main pathogenic cell type in both EAE and MS (Fletcher *et al* 2010). However, the critical involvement of an alternative Th17 cell was proposed when researchers identified IL23, rather than the Th1 promoting cytokine IL12 essential to initiate EAE (Becher *et al* 2002, Cua *et al* 2003). It has been proposed that the overall phenotype of disease is associated with the T cell lineage used to induce EAE, with a more clinically severe phenotype being associated with Th17 cell-induced EAE compared to Th1 cell induced EAE (Jager *et al* 2009, Langrish *et al* 2005). The T cell lineage administered also has a direct effect on the clinical symptoms, initially both Th1 and Th17 cells induce the classical EAE with ascending tail and limb paralysis,

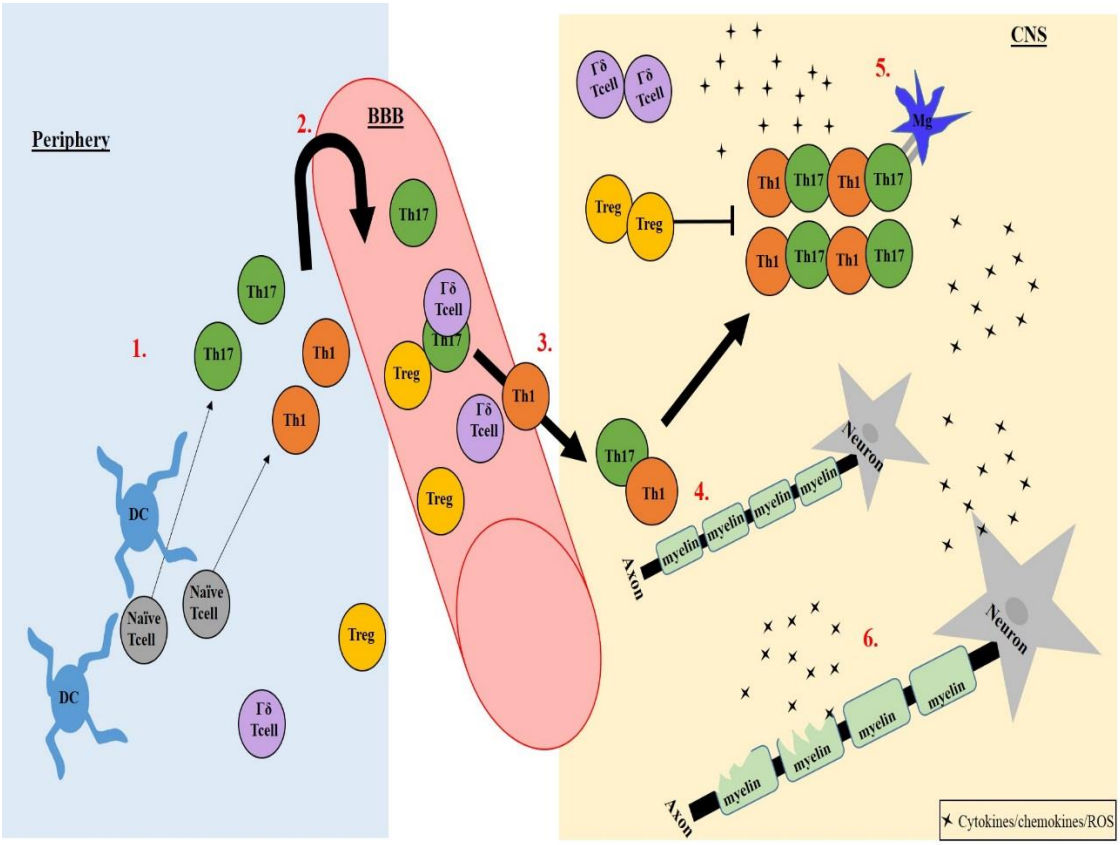

Figure 1.3 The pathophysiology of classical EAE induction

In EAE the animals are immunised with a myelin antigen in complete Freund's adjuvant (CFA). Antigen presenting cells (APC), the dendritic cells (DC) become activated by CFA presenting the administered myelin antigen to naïve $CD4^+$ T cells supporting their differentiation into Th1 and Th17 T cells (1). The activated myelin specific T cells enter the bloodstream and cross the BBB (2), which leads to further infiltration of additional cells including gamma delta (γδ) T cells, regulatory T cells (Tregs), as well as other inflammatory cells (3). On entering the CNS, the primed T cells recognise the innate myelin protein present in the myelin sheath surrounding axons, causing the reactivation of the T cells by local APC (4). The reactivated T cells undergo clonal expansion and release cytokines and chemokines that attract additional inflammatory cells and activate resident microglia. Additional cytotoxic mediators including a variety of cytokines, chemokines, reactive oxygen species (ROS) (5) are released leading to the breakdown of myelin surrounding axons (6), and ultimately neuronal damage. Figure adapted from Fletcher *et al* 2010.

however Th17 cells also develop additional symptoms including ataxia and rolling (Domingues *et al* 2010).

A number of factors can affect the pathophysiology of EAE models including the animal species or strain used, along with the type of immunisation peptide or subclass of Th cells administered (Simmons *et al* 2013). Variations of these factors determines the specific disease course of the model whether this be acute, chronic progressive or relapsing remitting (Steinman 1999). Clearly, no overall model displays every aspect of MS, however these animal models have helped to define certain immunologically processes in MS and supported the development of key therapeutics including Copaxone, Mitoxantrone and Natalizumab (Rosenling et al 2011).

1.7.3 Translation of EAE to MS; the pros and cons

There are clear distinctions in the innate and adaptive immune systems between rodents and man (Mestas & Hughes 2004), therefore caution must be taken when translating potential pathology mechanisms from the EAE model to MS (Baker *et al* 2011). The activation of both Th1 and Th17 cells in EAE requires specific classes of cytokines, however it is unclear as to what extent MS is driven by $CD4^+$ and MHC class II^+ cells, especially as MHC class I $CD8^+$ T cells are more dominant in MS lesions (Lassmann & Ransohoff 2004). Several EAE models lack the involvement of the brain, with inflammation mainly presenting in the spinal cord of the animal leading to paralysis (Simmons *et al* 2013). This lack of pathological similarity infers differences in the pathological mechanisms between EAE and MS, which has been proposed as being the reason for the increased number of drug failures in clinical trials, which had successfully been used in treatment for EAE models (Sriram & Steiner 2005). Another limitation to the EAE model is the artificial administration of myelin specific protein to initiate disease, which does not mimic the spontaneity of MS (Mecha *et al* 2013) and therefore does not reflect important disease initiator mechanisms. Furthermore, animal models are restricted in environmental exposures, which may affect the way in which the animal's immune system is primed. Many animals used in EAE models are raised in specific pathogen free conditions, in laboratories not comparable to a human environment (Adams *et al* 2003). Despite the limitations of the animal model EAE, it remains the main focus of MS research, with successful drug treatments derived from its study. However in order to establish more clinical, pathological relevant processes associated with MS, results from multiple EAE studies should be combined (Rosenling *et al* 2011). As well, new enhanced EAE models need to be developed using species

more closely resembling humans, with a similar genetic make-up and mature immune system with more environmental exposures, such as the marmoset (Kap *et al* 2010).

1.8 Glial Cells in MS

Several processes and various cell types contribute to the pathology of MS (Sobel & Moore 2008). Glial cells form the supportive and protective network of the CNS, surrounding neurons and axons, glial cells do not conduct electrical impulses but are capable of extensive signaling in response to specific stimuli, such as inflammation (Sobel & Moore 2008). There are three main types of glial cells; oligodendrocytes are involved in the production of the myelin surrounding axons. Microglia act as macrophages and form the basis of the CNS immune system. Astrocytes support neuronal metabolism, maintenance of the extracellular environment and transmission of nerve signals (Figure 1.4), (Sobel & Moore 2008).

1.8.1 Oligodendrocytes in MS

OLG are primarily involved in the production of myelin that surrounds axons in the brain. These cells help provide nutritional support to axons and are critical for axon function and survival (Funfschilling *et al* 2012). Myelin acts as a protective, insulating layer and accelerates neural conduction along axons. OLG produce myelin in segments along axons, which are separated by myelin free areas known as nodes of Ranvier where sodium and potassium channels are located. Nerve impulses pass from one node of Ranvier to another, therefore accelerating nerve conduction across the myelinated axon (Dupree *et al* 1999). A single mature OLG in the CNS is capable of generating myelin for upto 40 axons (Brodel 2010). Diseases affecting OLG, such as in MS, lead to a loss of myelin in addition to axonal loss (Brodel 2010).

1.8.2 Microglia in MS

Microglia make upto 20% of the total glia in the brain and are the resident macrophages of the CNS (Brodel 2010, de Pablos *et al* 2013). The cells have a role in development, plasticity and immune surveillance (Jack *et al* 2005), exhibiting several macrophage like actions in the brain, reinforcing its major role as the resident immunosurveillance cell of the CNS. The cells are relatively evenly distributed throughout the CNS (Brodel 2010), but in injury or response to CNS insult the number of microglia with phagocytic capabilities increases (Brodel 2010). Microglia can be defined by their activation state, the typical ramified morphology of a microglia is characteristic of a resting cell. Many fine processes extend from ramified microglia constantly sampling the environment,

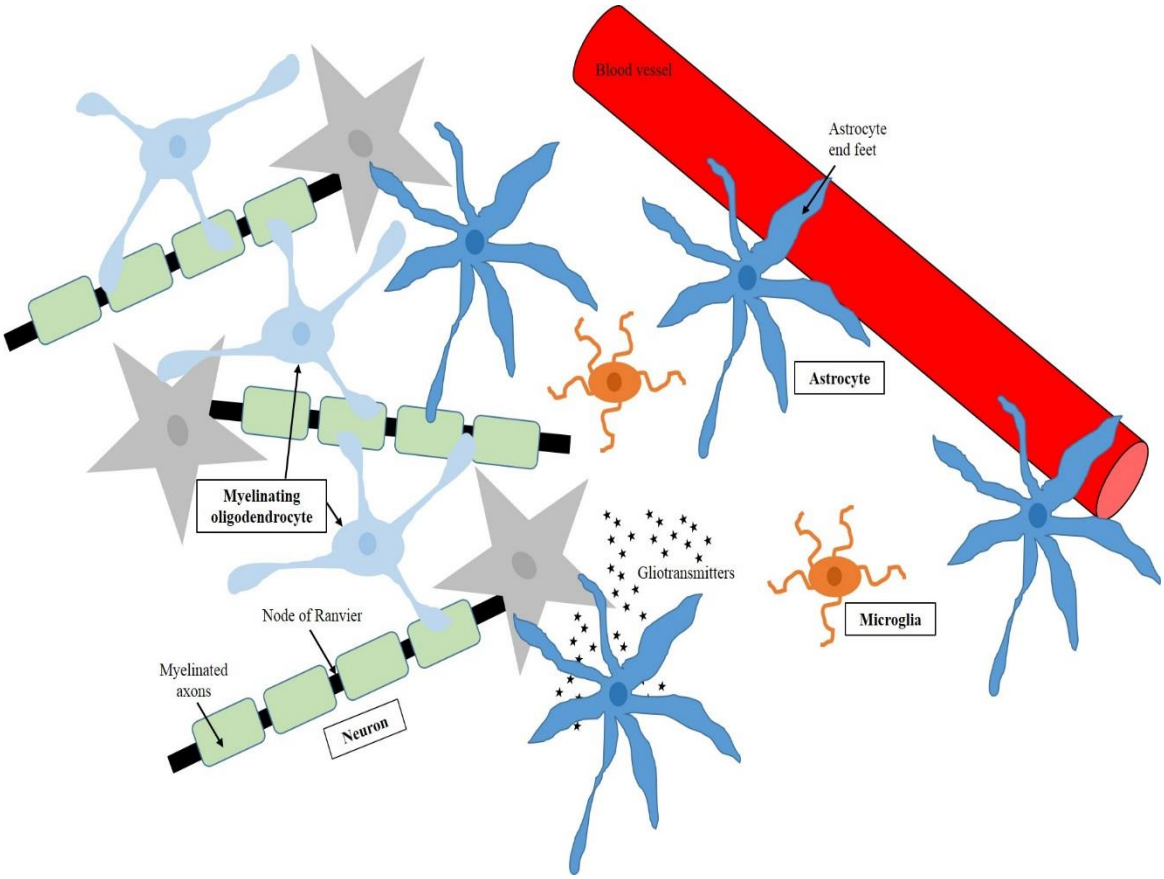

Figure 1.4 Brain structures involved in multiple sclerosis

The blood capillaries in the brain are surrounded by microglia/macrophages that act as the immunosurveillance cell in the CNS. Astrocytes ensheath blood vessels and align with axons releasing an array of neuromodulatory molecules into the CNS supporting neurotransmission. Oligodendrocyte (OLG) myelinate axons and increase axonal stability, also releasing soluble factors that induce sodium channel reorganisation to allow for powerful conduction of nerve impulse across the axons. Figure adapted from Miller 2012.

ensuring the cell is ready to respond in case of any insult (Nimmerjahn *et al* 2005). In comparison, microglial cells under insult are enlarged and spherical in shape, lacking processes and are termed amoeboid cells. These activated microglia have shown to express an increase in MHC class II molecules, having the ability to activate lymphocytes in an immune response. In a positive manner, activated microglia can release neurotrophins that support neurons, also activated cells can eliminate neurotoxins and ROS through their expression of superoxide dismutase (SOD) and other catalases, along with the removal of dying cells and cellular debris (Stables *et al* 2010, Wang *et al* 2004). However, persistent microglial activation, as in MS, has shown to be detrimental affecting the permeability of the BBB promoting further infiltration of immune cells into the CNS (Stables *et al* 2010). As well, microglia can release an array of chemokines, and cytokines upon activation, deciphering whether the cell is being protective or damaging in relation to neurodegeneration is highly debatable and possibly depends on the manner in which the microglia were activated (Boche *et al* 2013).

1.8.3 Astrocytes in MS

Initially, astrocytes were believed to solely function in a structural role within the CNS (Sofroniew & Vinters 2010). Yet with more research, astrocytes are increasingly being implicated as having a fundamental role in many neurological diseases, whether that role is protective or harmful is a continuing debate. In MS, astrocytes exhibit opposing roles and are known to enhance immune responses, prevent myelin repair, and aid in inflammation. On the contrary, astrocytes can serve in protecting against the disease and support remyelination by limiting CNS inflammation, supporting OLG action and axonal preservation by uptake of excess glutamate (Marz *et al* 1999, Mason *et al* 2001, Moore *et al* 2011, Yi & Hazell 2006). The impact of astrocytes on the pathogenesis of MS is most probably dependent on a number of factors including: the stage of disease, the environment surrounding the lesion, along with the interactions made with other cell types that may affect their state of activation (Nair *et al* 2008).

1.8.3.1 Astrocytes and the BBB in MS

Astrocytes are a fundamental cell of the BBB forming the glial limitans, and have been suggested to play a role in both its function and dysfunction in MS. Factors released by astrocytes have shown to have beneficial effects on the BBB. For example, astrocytes have been shown to secrete sonic hedgehog (Shh), a glycoprotein that acts on EC receptors which has shown to induce and maintain BBB function limiting the passage of immune cells into the CNS (Alvarez *et al* 2011b). Levels of Shh were increased in

activated astrocytes *in vitro*, also supported by corresponding human studies Shh immunoreactivity in MS lesional tissue was increased identifying astrocyte involvement in facilitating BBB repair in demyelinated WML (Alvarez *et al* 2011b). Alternatively astrocytes may promote a loss of BBB integrity as in response to increased levels of IL-1 expressed in MS lesions, astrocytes have been shown to increase their expression of both transcription factor hypoxia-inducible factor 1 (HIF-1), and it's target vascular endothelial growth factor (VEGF-A) (Argaw *et al* 2006). VEGF-A binds with its EC receptor promoting a downregulation of TJ proteins claudin-5 and occludin, causing an overall loss of BBB integrity allowing for immune cell infiltration across the disrupted BBB and MS lesion development (Argaw *et al* 2012, Argaw *et al* 2009).

1.8.3.2 Astrocytes and their role in preventing myelin repair in MS

Astrocytes can inhibit OPC maturation through the release of fibroblast growth factor-2 (FGF-2), a trophic factor that is required for survival and proliferation of progenitor cells. However, FGF-2 prevents the development of mature OLG needed for remyelination to occur. FGF-2 is predominantly produced by astrocytes upon myelin injury and has been shown to produce elevated levels of OPCs around demyelinated regions (Messersmith *et al* 2000). However, intravenously administered FGF-2 in rats has been shown to result in patchy myelinated axons, demonstrating the potential negative effect that FGF-2 released by astrocytes may have on remyelination (Goddard *et al* 1999). Recent studies have shown MS patients to have elevated CSF levels of FGF-2 compared to control patients, with even higher levels being observed in relapse patients compared to those patients in remission (Sarchielli *et al* 2008). Hyaluronan (HA) is another molecule believed to prevent maturation of OPCs, and is found throughout the CNS WM (Sherman *et al* 2002). HA binds to its receptor CD44 on astrocytes in control WM and on astrocytes, T cells and OPCs in MS WM tissue altering their function (Williams *et al* 2007).

1.8.3.3 Reactive astrocytes associated with inflammation and gliotic scar formation

Hypertrophic astrocytes are abundant in early MS lesions compared with the glial scarring evident in later chronic active and IA lesions. Severe astrogliosis results in a higher expression of glial fibrillary acidic protein (GFAP), increased astrocyte proliferation and secretion of proinflammatory cytokines (Eng & Ghirnikar 1994). Severely activated astrocytes are associated with gliotic scar formation, where a physical border of hypertrophic astrocytes separates an area of CNS damage from non-diseased tissue (Fitch & Silver 2008) resulting in changes in the ECM that prevents

remyelination. Along with the physical barrier presented by the gliotic scar, remyelination is restricted due to the increased release of proinflammatory cytokines, and toxic products as a result of tissue damage and the presence of immune cells (Nash *et al* 2011a). In contrast, the gliotic scar can be protective preventing further spread of damage across the CNS tissue (Miljkovic *et al* 2011), indicating the astrocyte's dual role in MS, probably dependent on the location and extent of pathology present within the brain.

1.8.3.4 Astrocytes and the immune system

Astrocytes are known to attract T cells via the release of chemokines, and support the production of autoreactive T cells (Stuve *et al* 2002) through the release of cytokines (Constantinescu *et al* 2005), MMPs (Crocker *et al* 2006, Larsen *et al* 2003) and additional chemokines contributing to MS pathogenesis. Astrocytes can act as immune cells, with increasing evidence of the cells contribution to both the adaptive and innate immune responses in the CNS (Nair *et al* 2008). Directly, astrocytes have shown to be capable of acting as APC, with astrocytes *in vitro* having shown to express MHC class I and II (Wong *et al* 1984). Following treatment with IFNγ, astrocytes have shown to increase their expression of costimulatory molecules CD80 (B7-1) and CD86 (B7-2) which interact with CD28 expressed on T cells contributing to their activation (Wong *et al* 1984). Astrocytes treated with IFNγ are able to activate both classes of $CD4^+$ and $CD8^+$ T cells (Nikcevich *et al* 1997, Tan *et al* 1998).

Supporting the role of astrocytes involvement in the immune response, *in vitro* astrocytes expressing MS associated MHC-Class II HLA-DR2 and HLA-DR4 led to the combined pro- and anti-inflammatory cytokine release in MOG-specific T cells (Kort *et al* 2006). In contrast, a predominant stimulation and differentiation of Th2 cells over Th1 cells has been associated with astrocyte interactions *in vitro* (Aloisi *et al* 1999, Aloisi *et al* 1998). Consequently, in a chronic inflammatory environment as seen in MS/EAE where Th1 cells predominate the CNS, astrocytes may act as an APC to drive the recruitment and differentiation of an increased number of Th2 cells supporting an anti-inflammatory effect in areas of chronic inflammation.

In vivo studies deciphering the involvement of astrocytes in the immune response in the CNS are inconclusive; Sprague-Dawley rats treated intrathecally with IFNγ led to the increased expression of MHC class II on astrocyte's cell membrane and proximal processes as identified by IHC, suggesting the cells capability of acting as APC in inflammatory disease (Vass & Lassmann 1990). However, another study concluded that

astrocytes do not express the costimulatory molecules required to act as APC ruling out their involvement in EAE development (Cross & Ku 2000). Clearly, the role of astrocytes in the immune system is not fully distinguished and is worth further investigation in particular in relation to a neuroinflammatory setting.

1.8.3.5 Astrocyte cytokine actions in MS pathology

Astrocyte cytokine production is believed to contribute to inflammation in MS, astrocytes produce IL-12 and IL-23, which help initiate both Th1 and Th17 T cells thought to play a role in the demyelinating disease (Constantinescu *et al*. 2005). Other cytokines released by astrocytes include IL-1, IL-6, TNFα and IL-10, depending on the inflammatory environment these cytokines can drive and determine the immune response. The most prominent cytokine to be released from astrocytes is TNFα, levels of which are increased in the CSF of MS patients (Tsukada *et al* 1991). *In vitro*, TNFα has been shown to increase OLG and myelin damage (Selmaj and Rain 1988) and the extent of demyelination in MS patients directly correlates with their levels of TNFα (Bitsch *et al* 2000). TNFα has been shown to prevent the differentiation of OPCs in local MS lesional sites preventing OLG maturation and therefore inhibiting remyelination (Cammer 2000). Not only do astrocytes produce proinflammatory factors during tissue damage, studies have shown that astrocytes promote anti-inflammatory effects on other cell types such as microglia, a key contributor to CNS inflammation (Sofroniew 2009).

In vitro studies have demonstrated that astrocytes promote both a pro- and anti-inflammatory cytokine network (Nair *et al* 2008). For example, not only are the production of proinflammatory cytokines induced through the activation of astrocyte toll like receptors (TLR), but the expression of TLR3 by a specific subtype of adult human astrocytes *in vitro*, has led to the production of anti-inflammatory cytokines IL-9, IL-10 and IL-11. As well, TLR3 expression led to the downregulation of IL-12 and IL-23 (Bsibsi *et al* 2006), however this theory has yet to be tested *in vivo.*

1.8.3.6 Astrocyte derived chemokines in MS pathology

Immune mediated demyelination in MS is thought to be associated significantly with astrocyte chemokine production, such as chemokine C-X-C ligand (CXCL)9 and 10 and chemokine ligands (CCL)3 and 5. CXCL10 is expressed on the processes of astrocytes, in particular those in close proximity to blood vessels. This chemokine is chemotactic for Th1 T cells which may provide the driving force behind the infiltration of lymphocytes across the BBB in MS (Nair *et al* 2008). Close to the edge of lesions,

chemokines CXCL12 and CCL2 are expressed by astrocytes which help to recruit macrophages and microglia as well as lymphocytes to the lesion (Calderon *et al* 2006, Tanuma *et al* 2006, Van Der Voorn *et al* 1999). Studies conducted *in vitro* on human astrocytes have shown that cytokines IL-1β, TNFα and IFNγ normally expressed *in vivo* during the inflammatory response, help promote chemokine production, which supports the theory that astrocytes are involved in the activation of T cell infiltration associated with MS (Barna *et al* 1994, Calderon *et al* 2006, Salmaggi *et al* 2002).

There is conflicting evidence for the role of secreted cytokines and chemokines from astrocytes in MS. For instance the chemokine CXCL10, secreted by activated astrocytes, shares its chemokine CXC receptor (CXCR)3 with CXCL9 and CXCL11, and because OLG express CXCR3 this may be the target for CXCL10 secreted by astrocytes, hindering OLG maturation and axonal wrapping (Nash *et al* 2011a). However on the contrary a viral model of MS showed that neutralising antibodies to CXCL10 led to a reduction in disease progression and suppressed ongoing demyelination (Liu *et al* 2001), suggesting opposing roles of CXCL10 secreted by astrocytes in CNS pathologies (Nash *et al* 2011a). Other positive actions of chemokines secreted from astrocytes in MS is evidence that CXCL1 and it's receptor CXCR2 have been shown to aid in OLG maturation and axon remyelination (Padovani-Claudio *et al* 2006).

1.9 Overall aims of this thesis

Astrocytes perform many essential functions in the CNS and are known to be both protective and detrimental in their action. The role of astrocytes in MS is most probably associated with their location within the brain and the extent of pathology present. Therefore, the overall hypothesis of this thesis is that specific astroglial changes exist in MS NAWM compared to control WM that are contributing to the overall WM pathology in MS. In order to elucidate the exact role of astrocytes in the pathogenesis of the disease astrocytes in MS NAWM, areas of WM absent in apparent pathology were analysed, to determine whether specific genes are expressed and proteomic astroglial changes exist, which either support lesion development and disease progression or inhibit tissue damage, lesion expansion and disease development. To establish an understanding of the behaviour and functions of astrocytes in MS the project aims will be addressed by the following objectives;

1. To perform a detailed characterisation of the astrocyte phenotype in MS by immunohistologically investigating a panel of known astrocyte markers.
2. To develop a method to isolate glial cells from post mortem (PM) CNS tissue using immuno-laser capture microdissection (LCM)
3. To use microarray technology to identify transcriptomic differences in MS NAWM astrocytes compared to control WM astrocytes to distinguish the role of astrocytes in MS NAWM.
4. To apply additional quantitative real-time polymerase chain reaction (qPCR), IHC, western blotting (WB) and matrix assisted laser desorption ionisation-mass spectrometry (MALDI-MS) experiments to explore the potential role of astrocytes MS.

CHAPTER 2

HISTOLOGICAL CHARACTERISATION OF THE ASTROCYTE PHENOTYPE IN THE WHITE MATTER IN MULTIPLE SCLEROSIS

2.1 Introduction

Astrogliosis is a poorly understood event within the CNS and occurs when astrocytes undergo varying molecular and morphological changes in response to CNS insult. The activation state of astrocytes is directly related to the degree of CNS injury and can range from mild subtle molecular changes to extreme astrocyte hypertrophy, proliferation and scar formation (Figure 2.1). A recent paper suggests that a change in astrocyte phenotype, rather than astrocyte proliferation, accounts for the apparently increased number of astrocytes detected in Alzheimer's disease (AD) (Serrano-Pozo *et al* 2013a). It is known that reactive astrocytes respond differently to particular signaling events, leading to a loss or gain of function. Consequently this highlights the dual role of astrocytes as a potential supportive and/or toxic influence in the surrounding CNS environment. Histologically, astrogliosis is characterised by a dense increase in the protein GFAP, an intermediate filament protein, currently the most commonly used marker for astrocytes. Molecularly, astrogliosis can be identified by changes in the cells' gene expression profile, with evidence of an increase in nuclear factor kappa-light-chain-enhancer of activated B cells (NFkB) resulting in changes in synaptic signaling and in immune responses (Brambilla *et al* 2005) and upregulation of signal transducer and activator of transcription (STAT)3 responsible for changes in cell growth and apoptosis (Herrmann *et al* 2008).

An overall account of the extent of astrocyte activation, proliferation, change in morphology and function in MS pathogenesis is still missing from the literature. Many histological studies on astrocytes have been carried out, yet the precise role of astrocytes is still unknown. Astrocytes are a heterogeneous population of cells, therefore characterising them is challenging due to a lack of appropriate markers. There are anatomical distinctions between astrocyte 'types' such as fibrous and protoplasmic astrocytes, which reside in the white and grey matter respectively (Sofroniew & Vinters 2010, Swanson *et al* 2004). These cells also have distinct gene expression profiles, highlighting the diversity of these astrocyte cell populations. Undoubtedly the capabilities of these cells to activate and proliferate, their anatomical location and the molecules they express, for example whether pro- or anti-inflammatory, are all factors that play a vital role in understanding the function of astrocytes in neurological disease. With the increasing number of astrocyte markers being proposed, most recently aldehyde dehydrogenase L 1 (ALDH1L1) (Cahoy *et al* 2008), this current

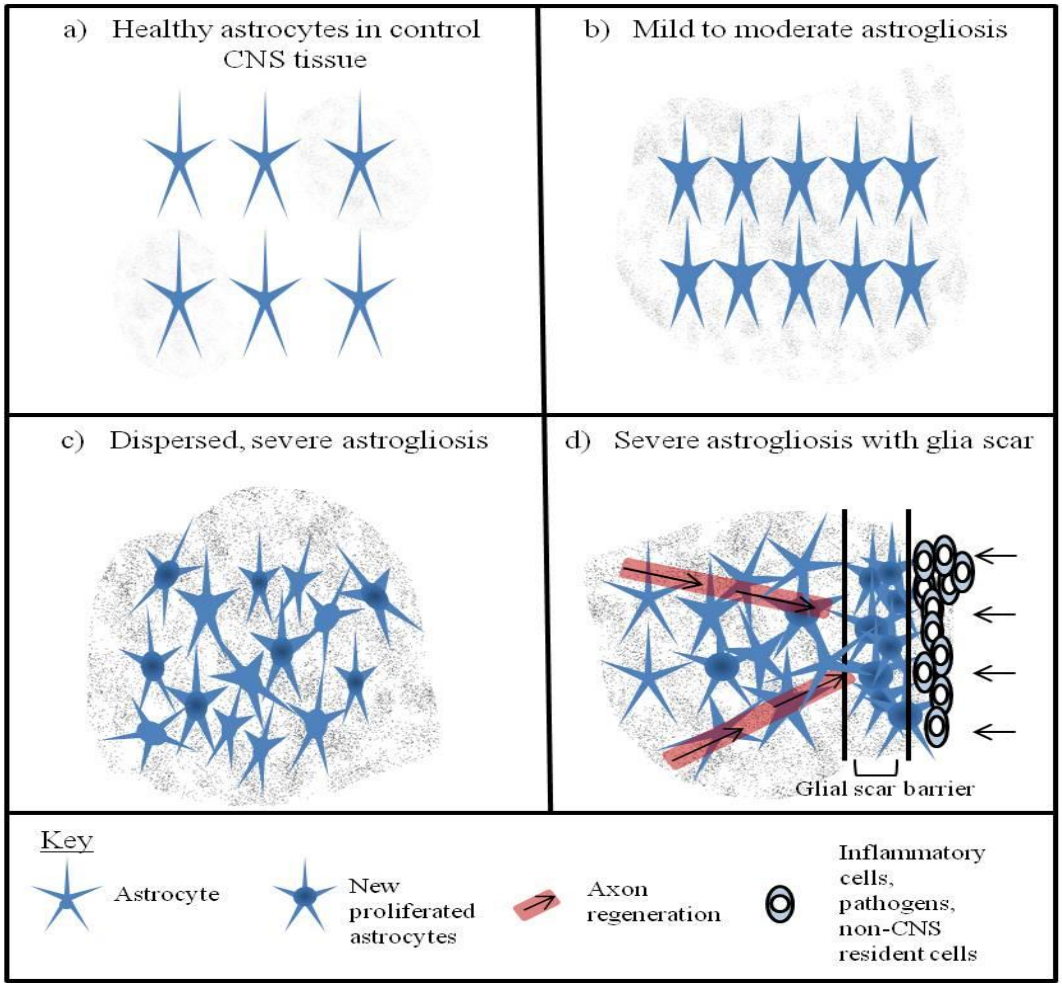

Figure 2.1 Astrogliosis

Astrocytes in normal healthy control CNS tissue, each individual astrocyte has its own domain (a). Mild to moderate astrogliosis is identified by astrocytes becoming hypertrophic with changes in their molecular and functional roles. This type of astrogliosis occurs due to either low level local trauma or in response to some drastic trauma in distant tissue; such as infection or inflammation. The majority of these astrocytes are $GFAP^{+}$, however very little proliferation occurs and the astrocytes are still conserved in their own domains (b). A dispersed spread of severe astrogliosis occurs in areas of lesions, infections or in response to neurodegenerative initiators. These cells are hypertrophic, proliferative and have changes in their molecular and functional activity. The cells no longer reside in their own domain causing chaotic tissue architecture (c). Severe astrogliosis occurs after prolonged insult/inflammation, the densely packed astrocytes form a gliotic scar barrier between the inflamed area and healthier tissue, the processes of these astrocytes overlap and act as barriers to inflammatory cells and other pathogenic agents as well as preventing the regeneration of axons in areas of demyelination (d). Figure adapted from Sofroniew & Vinters 2010.

study was designed to carry out a detailed characterisation of all current candidate astrocyte markers in MS. Astrocytes are the most abundant cell type in the CNS contributing more than 90% of the total number of cells in the human brain (He & Sun 2007). Due to their role in CNS surveillance and maintaining homeostasis, astrocytes respond to any alterations in brain pH as a result of agonal states, inflammation as a result of trauma, infection or autoimmunity. Astrocyte hypertrophy is a result of an increase in cytoskeletal proteins including GFAP (Ridet *et al* 1997). GFAP was first isolated from old, established demyelinated MS plaques, and was associated with the cytoplasm of reactive astrocytes, as detected by IHC (Eng & Ghirnikar 1994) and was identified as an early marker of astrogliosis (O'Callaghan & Sriram 2005). When GFAP is knocked down in mice, astrocytes become unstable, leading to their inability to regulate the BBB effectively (Liedtke *et al* 1996). Prolonged GFAP knockdown has shown to lead to other neurological deficits including poor CNS vascularisation (Liedtke *et al* 1996) and an increased sensitivity to traumatic injury (Li *et al* 2008b). Immunohistochemical staining of GFAP labels the cell body and immediate processes of astrocytes, which is regarded as the typical astrocyte stellate morphology in neuropathology (Nedergaard *et al* 2003).

Alongside GFAP, S100B previously known as S100-beta calcium binding protein, is highly expressed in the brain, mainly by astrocytes (Nair *et al* 2008). However, the expression of S100B within the CNS is not restricted to astrocytes and is also associated with a number of other cell types including oligodendrocytes, hippocampal neurons and EC (Steiner *et al* 2007). Also, within the periphery, S100B is expressed by Müller cells in the retina (Kondo *et al* 1984), T cells (Takahashi *et al* 1987), chondrocytes and bone marrow cells (Donato 2001). S100B has many roles including: maintaining calcium homeostasis (Donato *et al* 2009, Xiong *et al* 2000), regulating cellular structure and proliferation (Donato *et al* 2009, Goncalves *et al* 2008), and inhibiting the phosphorylation of presynaptic proteins (Heizmann *et al* 2002, Rothermundt *et al* 2003). Within the CNS, S100B is located in the nucleus and cytoplasm of astrocytes, complementing the pattern of immunoreactivity displayed by GFAP.

Astrocytes play a key role in regulating synaptic transmission through the expression of a number of glutamate transporters and receptors. Within the CNS, astrocytes regulate levels of the major excitatory neurotransmitter, glutamate, in a sodium and potassium coupled process, sodium is required for glutamate binding and potassium for transport into the cell (Danbolt 2001). Approximately 80% of the total uptake of glutamate by

astrocytes is by two specific transporters, namely excitatory amino acid transporter 1 (EAAT1) and EAAT2 (Rothstein *et al* 1996), both of which are routinely used as immunohistological markers of astrocytes. Glutamate is vital for neuronal function and neurotransmission, however too much extracellular glutamate, as a result of pathological changes within the brain can result in glutamate excitotoxicity which is detrimental for both neurons (Wang & Michaelis 2010) and other glial cells including oligodendrocytes (Matute *et al* 1997, McDonald *et al* 1998) leading to dysfunction and degeneration (Lau & Tymianski 2010). Astrocytes express EAAT1 [rodent analog: glutamate aspartate transporter (GLAST)] and EAAT2 [rodent analog: glutamate transporter-1 (GLT-1)] in areas that are close to the sites of glutamate release by neurons, and have the ability to react to increasing levels of glutamate by redistributing their transporters for optimum uptake of excess glutamate within the CNS (Shin *et al* 2009).

Glutamine synthetase (GS), the enzyme involved in transforming excitotoxic glutamate into glutamine, was initially proposed to be solely expressed by astrocytes, however further studies identified the expression of the GS protein by Müller cells of the retina (Derouiche & Rauen 1995, Prada *et al* 1998), as well as oligodendrocytes (Werner *et al* 2001).

The expression of GS is highly regulated and mediated by a number of mediators such as insulin, thyroid hormone, corticosteroid hormone (Grenier *et al* 2005, Juurlink *et al* 1981, Koyama *et al* 1997, Patel *et al* 1989). Within astrocytes the GS enzyme is located within the cytoplasm (Coulter & Eid 2012). The activity of GS has been shown to decrease in the presence of ADP suggesting this reduction in enzymatic activity is a result of energy deprivation in the cells (Yamamoto *et al* 1987).

ALDH1L1 association with the CNS, in particular with astrocytes, was first identified in adult rat studies by IHC (Neymeyer *et al* 1997), however the role of ALDH1L1 and its link with neurodegenerative diseases is largely unknown. ALDH1L1 plays a role in cell division and growth, participating as a folate enzyme aiding in the conversion of 10-formyltetrahydrofolate to tetrahydrofolate (Krupenko 2009). ALDH1L1 is associated with highly branched astrocyte processes and cell bodies (Cahoy *et al* 2008).

CD44 is a cell surface glycoprotein that serves as a receptor for HA and an adhesion molecule mediating cell-cell and cell-matrix interactions (Lesley *et al* 1993, Ponta *et al* 2003). In comparison to GFAP, where the immunoreactivity of astrocytes is restricted

mainly to the cell body and immediate proximal cell processes, CD44 is expressed on the cell surface, and it's immunostaining pattern is therefore more extensive, running along the fine, delicate processes of astrocytes (Akiyama *et al* 1993). CD44 is present in the human WM from birth and expression in the cortex occurs from around 60 years of age (Cruz *et al* 1985). CD44 expression is not restricted to astrocytes and is highly expressed on antigen activated T cells, suggesting a role in controlling lymphocyte trafficking to sites of inflammation (Bradley & Watson 1996, Brennan *et al* 1999, Brocke *et al* 1999, Budd *et al* 1987). Despite CD44 being found in astrocytes of normal and diseased brains (Zeltner *et al* 2007), there is very little recent research into its role in neurological disease.

The aim of this study was to characterise the astrocyte phenotype in MS by immunohistologically investigating the expression of all currently known astrocyte markers, namely GFAP, S100B, EAAT1, EAAT2, GS, ALDH1L1 and CD44, in a range of MS WM lesion types in comparison to control WM. Both qualitative and quantitative assessment of the immunoreactivity of each marker across the different MS lesion types classified according to (Lassmann 2011b) was performed. Specific differences of the astrocyte phenotype within the lesion centre, immediate lesional edge and NAWM compared to control WM were determined, reflecting a possible change in astrocyte function in MS. Furthermore, the selection of the most suitable astrocyte marker for use in LCM of astrocytes from NAWM and control tissue was determined.

2.2 Aims and objectives of the study

The aims of this study were to:

- Characterise the astrocyte phenotype in MS by immunohistologically investigating the expression of a panel of astrocyte markers in MS tissue compared to control tissue.
- Provide a qualitative description of the staining pattern of each astrocyte marker within different lesion types in MS compared to control tissue.
- Provide a quantative analysis of the immunoreactivity of each astrocyte marker within the lesion centre of different lesion types in MS, the perilesional edge, and the NAWM/ control WM.
- To identify the most suitable marker for LCM in the isolation of astrocytes from NAWM and control PM tissue for further studies.

2.3 Material and methods

2.3.1 Suppliers

Abcam, 330 Cambridge Science Park, Cambridge, CB4 0FL, UK; **DAKO UK Ltd.**, Cambridge House, St Thomas Place, Ely, Cambridgeshire CB7 4EX; **Fisher Scientific Inc.**, Bishop Meadow Road, Loughborough, Leicestershire, LE11 5RG, UK; **Leica Microsystems Ltd.**, Davy Avenue, Knowhill, Milton Keynes, MK5 8LB Buckinghamshire, UK; **Millipore Ltd.**, Suite 3&5, Building 6, Croxley Green Business Park, Watford, WD18 8YH, UK; **Olympus,** KeyMed House, Stock Road, Southend-on-Sea, SS2 5QH, UK: **Vector laboratories Ltd.**, 3 Accent Park, Bakewell Road, Orton Southgate, Peterborough, PE2 6XS.

2.3.2 Case selection

All human PM CNS tissue was obtained from the UK MS Society Tissue Bank (MREC/02/2/39, Appendix I). Tissue was donated from MS patients and control patients with no neurological disease, who had provided informed consent. The role of the MS Tissue Bank is to supply tissue to MS researchers, with the aim of developing and enhancing research and knowledge about the disease. Preparation of tissue blocks used throughout this project was completed at the MS Tissue Bank (Appendix II). The brain was either fixed in formalin to provide formalin fixed, paraffin embedded (FFPE) material or directly cut into blocks and snap frozen (Appendix II). For this study FFPE sections (5μm) from 12 MS cases (3 separate brain regions) and 12 control cases (2 separate brain regions) were provided, as detailed in Appendix III. Prior to carrying out the astrocyte phenotype study, all samples were histologically characterised into relevant lesion type based on published criteria (Lassmann 2011b).

2.3.3 Neuropathological assessment of samples

Tissue sections were histologically stained with haematoxylin and eosin (H&E) and Luxol fast blue (LFB) and IHC was carried out for CD68. H&E was used to assess the inflammatory state of the case and overall tissue structure. LFB was used to determine the extent of demyelination, and CD68, a lysosomal marker, used to identify the presence of phagocytic microglia (Zotova *et al* 2011).

2.3.4 Haematoxylin and Eosin (H&E) stain

H&E staining is commonly used to assess the histological architecture of tissue (Bancroft & Gamble, 2008). The basic haematoxylin dye stains basophilic tissue components by reacting with the acidic components of cell nuclei and ribosomes,

displaying a blue/purple colour (Bancroft & Gamble, 2008). In contrast, the acidic eosin stains acidophilic cytoplasmic components of the cell pink/red such as the connective tissue, collagen and cytoplasm (Bancroft & Gamble, 2008).

FFPE sections (5µm) were dewaxed in xylene (Fisher Scientific, UK), rehydrated in a graded series of ethanol [100%, 100%, 95%, 70% (Fisher Scientific, UK)] for 5 minutes in each. All sections were immersed in filtered Harris's haematoxylin (Leica, UK) for 2 minutes at room temperature (RT). Sections were quickly rinsed with tap water and differentiated in acid/alcohol (Appendix IV) for approximately 30 seconds and placed into Scott's tap water (Appendix IV) for 10-15 seconds before being rinsed in tap water and placed in eosin (Leica, UK) for 5 minutes at RT. The sections were quickly washed in tap water and dehydrated through graded alcohols [70%, 95%, 100%, 100% (Fisher Scientific, UK)] for 30-60 seconds in each. Sections were cleared in xylene (Fisher Scientific, UK) for 5 minutes, before being mounted using DPX mountant media (Leica, UK) and glass cover slips (Fisher Scientific, UK).

2.3.5 Luxol Fast Blue (LFB) stain

LFB enables the visualisation of myelinated axons within brain tissue, any areas of demyelination are identified by loss of LFB stain. The staining works via an acid-base reaction with the base of the lipoprotein in myelin replacing the base of the dye and causing a colour change (Bancroft & Gamble, 2008).

FFPE sections (5µm) were dewaxed in xylene (Fisher Scientific, UK), rehydrated in graded decreasing concentrations of ethanol [100%, 100%, 95%, 70% (Fisher Scientific, UK) for 5 minutes in each]. All sections were placed in LFB solution (Appendix IV) for 2 hours at 60°C. Any excess stain was removed in 95% ethanol (Fisher Scientific, UK) and the sections rinsed in distilled water (dH_2O). Sections were differentiated in lithium carbonate (Appendix IV) for 30 seconds until the cortex and WM were clearly defined. The sections were cleared in xylene (Fisher Scientific, UK) for 5 minutes before being mounted using DPX mountant media (Leica, UK) and glass cover slips (Fisher Scientific, UK).

2.3.6 Immunohistochemistry - background to the technique

Antibodies are routinely used to visualise the cellular localisation of proteins (antigens) of interest in cells, tissues or biological fluids. This detection of antigens using specific antibodies in tissue is known as IHC, the technique used in this study was the standard horseradish peroxidase-conjugated avidin-biotin complex (ABC-HRP) IHC technique

(Vectastain Elite kit; Vector Laboratories UK) with 3, 3'-diaminobenzidine (DAB) (Vector Laboratories UK) as substrate (Figure 2.2).

Prior to antibody application the tissue was fixed, permeabilised and if necessary blocked. Fixation preserves the cellular structures within the tissue as well as preserving the antigen of interest. An example of a common fixative is formalin to preserve the tissue structure, or the use of acetone/ethanol to remove lipids, dehydrate cells and precipitate out antigens. However, cross linking fixatives such as formalin can prevent the binding of some antibodies to their specific antigen, and therefore often require antigen retrieval prior to IHC (refer to sections 2.3.6.2 and 2.3.6.3).

2.3.6.1 Blocking endogenous peroxidase activity

All sections were dewaxed in xylene (5 minutes in Xylene 1 and 2 [Fisher Scientific]) and rehydrated in a graded series of ethanol (100%, 100%, 95%, 70% [Fisher Scientific, UK]) for 5 minutes in each. Many cells, including red blood cells, contain endogenous peroxidase, which must be saturated prior to IHC. Without saturation, the endogenous peroxidase would react with the DAB substrate during the IHC and lead to non-specific staining of the tissue section. Therefore prior to antigen retrieval and after dewaxing and rehydrating, sections were placed in 3% hydrogen peroxide (Fisher Scientific, UK) in methanol (Fisher Scientific, UK) for 20 minutes to prevent any endogenous peroxidase activity.

2.3.6.2 Tri-sodium citrate (TSC) antigen retrieval

Sections in a plastic slide rack, were placed into tri-sodium citrate (TSC) solution pH6.5 (Appendix IV), and heated in a microwave on full power (800W) for 10 minutes and rinsed in tap water until cool.

2.3.6.3 Ethylenediaminetetraacetic acid (EDTA) antigen retrieval

Sections were placed into specifically designed plastic pressure cooker slide holders with 200 mL 1mM EDTA pH8.0 (Appendix IV). The sections were placed in the pressure cooker surrounded by 500 mL d.H_2O and run at 125°C, 20 psi, for 30 secs.

2.3.7 CD68 immunohistochemistry

FFPE sections (5µm) were dewaxed, rehydrated, blocked for endogenous peroxidase activity (section 2.3.6.1) and antigen retrieval carried out by microwaving in TSC pH6.5 (section 2.3.6.2). Sections were cooled in running water and subjected to IHC following the standard ABC-HRP technique using a mouse Vectastain Elite kit (Vector Laboratories, UK) with DAB (Vector Laboratories, UK) as substrate.

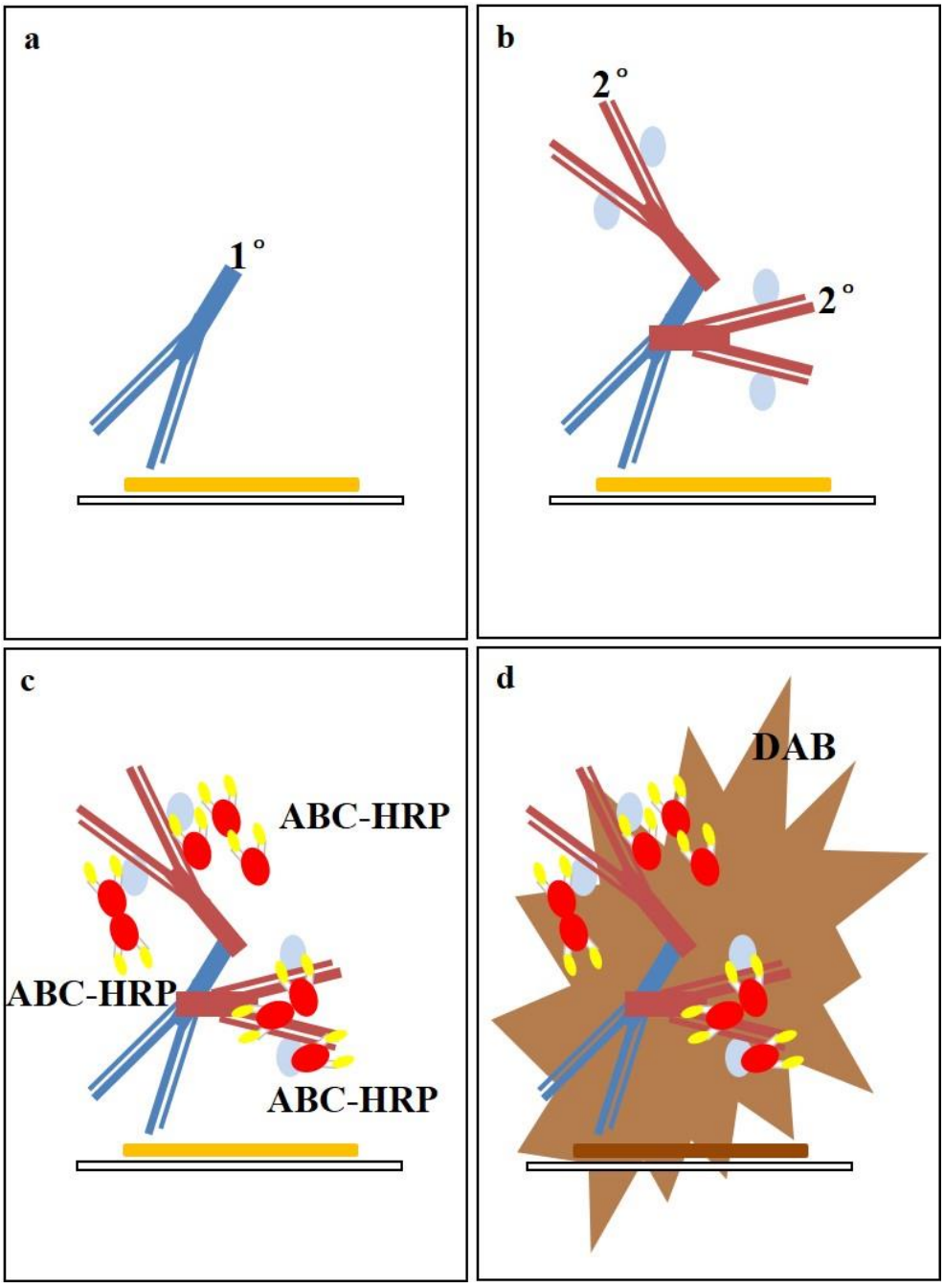

Figure 2.2 Overview of immunohistochemistry

The primary unlabelled antibody binds with high affinity to the specific antigen of interest (a) The species specific biotinylated secondary antibody binds to the primary antibody (b). ABC-HRP is applied which irreversibly binds with high affinity to the biotinylated secondary antibody through avidin (c) the HRP substrate DAB is added and produces a brown insoluble reaction product which can be visualised (d).

Key: 1°: primary antibody, 2°: secondary antibody, ABC-HRP: avidin/biotin horseradish pereoxidase complex, DAB: substrate.

Sections were blocked in 1.5% normal horse serum (150µl in 10 ml Tris-buffered saline [TBS]) for 30 minutes and the serum removed from the sections. Mouse monoclonal anti-human CD68 antibody (Dako, UK) was applied to the sections at 1:100 dilution in 1.5% horse serum and incubated for 60 minutes at RT. For negative controls, the primary antibody was omitted from a section in each IHC run, or the section was incubated with an isotype control at the same protein concentration as the primary antibody. All sections were washed in 2 x 5 minute washes in TBS. 0.5% biotinylated secondary antibody (50µl in 1.5% horse serum) was applied to all sections and incubated for 30 minutes at RT. Sections were washed in 2 x 5 minute washes in TBS prior to the addition of the ABC-HRP reagent (100µl 'A' reagent, 100µl 'B' reagent' in 10 ml TBS, prepared at least 30 minutes prior to use), and left to incubate for 30 minutes. A final 2 x 5 minute wash step with TBS followed. Antibody staining was visualised by incubating sections for 5 minutes with the substrate DAB (Vector Laboratories, UK) (100µl buffer, 200µl DAB, 100µl hydrogen peroxide in 5 ml dH_2O), the enzyme reaction was quenched by washing the slides with dH_2O. Sections were counterstained using Harris's haematoxylin (Leica, UK) (5-10 seconds) before being dehydrated through graded alcohols [70%, 95%, 100%, 100% (Fisher Scientific, UK)] for 30-60 seconds each and cleared in xylene (Fisher Scientific, UK) for 5 minutes. Sections were mounted using DPX mounting media (Leica, UK) and glass cover slips (Fisher Scientific, UK) and viewed using an Olympus microscope (BX61) (Olympus, UK).

2.3.8 Astrocyte marker immunohistochemistry

IHC was carried out on all cases (Appendix III) following the standard ABC-HRP technique (Vectastain Elite kit; Vector Laboratories UK) with DAB (Vector Laboratories UK) as substrate. Rabbit or mouse immunoglobulin (Ig) ABC elite kits (Vector laboratories, UK) were used depending on the species of primary antibody (Table 2.1).The antigen retrieval method required for each antibody is indicated in Table 2.1. Control staining was carried out on additional sections with the omission of the primary antibody, or inclusion of an appropriate isotype control (Table 2.1).

Primary antibody target	Species	Clonality	Isotype	Supplier	Dilution	Antigen retrieval method	Role
Glial Fibrillary Acidic Protein **(GFAP)**	Rabbit	Polyclonal	IgG	DAKO, UK	**1:1000**	TSC, pH 6.5 / microwave	Main intermediate filament in reactive astrocytes
S100	Rabbit	Polyclonal	IgG	DAKO, UK	**1:4000**	TSC, pH 6.5 / microwave	Intercellular signalling molecule for calcium
Excitatory Amino Acid Transporter 1 **(EAAT1)**	Mouse	Monoclonal	IgG2a	Leica Microsystems, UK	**1:20**	EDTA, pH 8.0 / Pressure cooker	Regulates levels of neurotransmitter glutamate
Excitatory Amino Acid Transporter 2 **(EAAT2)**	Mouse	Monoclonal	IgG2a	Leica Microsystems, UK	**1:20**	EDTA, pH 8.0 / Pressure cooker	Main regulator of extracellular glutamate
Glutamate Synthetase **(GS)**	Mouse	Monoclonal	IgG2a	DAKO, UK	**1:1000**	TSC, pH 6.5 / microwave	A catalyst enzyme for the conversion of glutamic acid to glutamine
Aldehyde dehydrogenase 1 **(ALDH1L1)**	Rabbit	Polyclonal	IgG	Abcam, UK	**1:50**	TSC, pH 6.5 / microwave	Responsible for formate oxidation
(CD44) Phagocytic Glycoprotein-1	Mouse	Monoclonal	IgG	DAKO, UK	**1:20** **1:50** **1:100**	TSC, pH6.5/ microwave + EDTA, pH 8.0/ pressure cooker	A cell surface glycoprotein that serves as a receptor for hyaluronic acid
Rabbit IgG Isotype control	Rabbit	-	IgG	Vector,UK	GFAP **1:1000** S100B **1:4000** ALDH1L1 **1:50**	TSC, pH 6.5 / microwave	Isotype control
Mouse IgG2a Isotype control	Mouse	-	IgG2a	Vector, UK	EAAT1 **1:20** EAAT2 **1:20** GS **1:1000**	EDTA, pH 8.0 / Pressure cooker TSC, pH 6.5 / microwave	Isotype control
Mouse IgG Isotype control	Mouse	-	IgG	Vector, UK	CD44 **1:100**	TSC, pH6.5/ microwave + EDTA, pH 8.0/ pressure cooker	Isotype control

Table 2.1 Antibody source, specificity, antigen retrieval method and role of antigen
Astrocyte candidate markers were used to qualitatively and quantitatively assess the phenotype of astrocytes in PM CNS tissue. (All dilutions were made in the appropriate blocking serum).

Key: EDTA: Ethylenediaminetetraacetic acid, Ig: Immunoglobulin, TSC: tri-sodium citrate.

2.3.9 Immunohistochemistry (IHC)

For ALDH1L1, GFAP and S100B IHC sections were incubated with 1.5% goat serum for 30min at RT, whilst for EAAT1, EAAT2, GS and CD44 IHC sections were incubated with 1.5% horse serum. Blocking sections prevented non-specific binding of the primary and secondary antibodies. CD44 antibody was initially optimised by selecting a range of dilutions based on the manufacturer's recommendations, while all the other primary antibodies were used at previously published concentrations, (Simpson *et al* 2010). Table 2.1 provides a summary of the primary antibodies used in this study, each primary antibody was prepared in blocking solution and sections were tapped to remove excess blocking solution prior to the addition of ~100µl primary antibody to each section. The sections were left to incubate for 1 hour at RT before being washed with TBS (2 x 5 minute washes). Biotinylated species-specific secondary antibody was prepared, by adding 150 µl goat/horse serum in 10 ml TBS and then adding 50 µl of biotinylated secondary antibody. Secondary antibody (100 µl/section) was left to incubate at RT for 30 minutes prior to being washed with TBS (2 x 5 minute washes). The ABC reagent was prepared by adding 100 µl reagent A and reagent B to 5 ml TBS at least 30 minutes prior to use. ABC reagent was added to the sections and left to incubate at RT for 30 minutes, prior to washing with TBS (2 x 5 minute washes). DAB substrate (Vector Laboratories, UK) was prepared by adding 100 µl hydrogen peroxide 200 µl DAB and 100 µl buffer to 5 ml dH_2O. DAB was added to the sections (100 µl/section) and left for 5 minutes and the reaction was stopped by washing the sections in water. Sections were counterstained in Harris's haematoxylin (Leica, UK) for 30 seconds, rinsed in tap water until the water ran clear, dehydrated in a series of graded alcohols (Fisher Scientific, UK) and mounted using DPX (Leica, UK) and glass coverslips (Fisher Scientific, UK). For internal controls, the primary antibody was omitted to ensure the absence of non-specific binding from the secondary antibody.

2.3.10 Image analysis

All IHC and histology was examined using the BX61 Olympus microscope and CellR image software system (Olympus, UK). Case identification and classification was determined by two independent observers (Rachel Waller and Dr. Julie Simpson) based on the published criteria by Lassmann 2011b. A qualitative description of the staining pattern of each antibody was noted across the different lesion types and control samples.

2.3.11 Quantitative analysis of astrocyte marker immunoreactivity

To provide a quantitative analysis of the different astrocyte markers, the analySIS^D software was used on captured images from all lesion types. Images were captured from 5 random fields within the three regions of interest (ROI), these being the lesion centre, the immediate lesion edge (periplaque white matter [PPWM]), NAWM/control WM at x20 magnification. In order to increase the number of cases investigated, data from both control WM and MS NAWM cases were pooled together as there was no difference in the data from each of the markers investigated between the two groups. Using analySIS^D software the total immunoreactive area of the field was determined per total area studied. For S100B a particle counting of greater than 300 pixels was used to eliminate any positive identification of the smaller positively stained oligodendrocytes, thereby only measuring the larger astrocytes. The average percentage area of immunopositive staining of each marker within the WM from all ROI was used for statistical analysis.

2.3.12 Statistical analysis

Statistical analysis of the expression of each astrocyte marker across control/NAWM and lesional groups was performed on PASW 18 (formerly SPSS) and overseen by Prof.. Stephen Wharton. Using a Kruskal-Wallis test the relationship between the different astrocyte markers and the lesion types were carried out. This identified, across the cohort, whether statistical relevance was present. This was followed by a pair wise Mann-Whitney U test to identify statistical differences in marker expression between the lesional groups and control/NAWM samples.

2.4 Results

2.4.1 CNS tissue classification

Initially 55 MS and control samples, [(12 MS cases, 3 brain regions) (10 CO cases, 2 brain regions*)] were assessed for evidence of inflammation, demyelination and the presence of amoeboid microglia to enable classification into lesion type (Lassmann 2011) (Table 2.2). The majority (33/36) of MS patient samples displayed some level of inflammation and lesional activity with only 3 samples identified as classical MS NAWM i.e., no inflammatory cell infiltration, no evidence of demyelination (as shown by positive LFB staining) and a regular distribution of resting ramified microglia (as shown by CD68 staining). Around one third (36%) of MS patient samples presented with multiple lesion types which varied considerably.

14 tissue blocks were classified as EA lesions, these lesion centres were highly attenuated with the region being hypercellular, as identified through H&E staining. There was a loss of LFB stain, which was patchy in some samples depending on the advancement of the lesion. EA lesion centres contained a dense distribution of $CD68^+$ microglia with a phagocytic phenotype presenting as large, swollen, amoeboid cells with retracted processes, in comparison to the surrounding NAWM where the $CD68^+$ cells were bipolar, ramified with extending processes (Figure 2.3).

26 MS patient samples contained one or more LA lesion, these lesion centres were highly attenuated and hypocellular, with the presence of PVC and inflammation. There was a complete loss of LFB in LA lesions with a clear demarcation of the lesion border. Within the lesion centre, few $CD68^+$ cells were present, and were ramified and bipolar in appearance. CD68 immunoreactivity was increased at the lesion border where a band of swollen, amoeboid microglia were identifiable, suggestive of a phagocytic phenotype at the area of ongoing demyelination (Figure 2.3).

5 MS patient samples presented with IA lesions, these lesions were again highly attenuated with thickening of blood vessels. There was a loss of myelin pallor and the lesion centre was hypocellular. Clear demyelination was evident by the complete loss of LFB staining, however there were very little $CD68^+$ microglia and no evidence of amoeboid microglia with a phagocytic phenotype, suggesting no ongoing demyelination in these IA lesions (Figure 2.3).

*For one of the control case only one brain region was analysed

Case	Lesion type	Total lesions	Case	Lesion type	Total lesions
MS200 (1)	1x EA	1	MS249 (1)	1x LA	1
MS200 (12)	1x EA	1	MS249 (12)	2x EA 1x LA	3
MS200 (21)	1x LA 2x EA	3	MS249 (13)	NAWM	0
MS235 (10)	NAWM	0	MS296 (1)	1x EA	1
MS235 (21)	1x EA 1x LA	2	MS296 (20)	1x LA	1
MS235 (22)	1x LA 1x IA	2	MS296 (22)	1x LA	1
MS237 (1)	1x EA	1	MS298 (9)	1x EA 1x LA	2
MS237 (12)	1x EA	1	MS298 (19)	2x LA	2
MS237 (21)	1x EA	1	MS298 (20)	2x IA	2
MS241 (9)	1x LA	1	MS300 (10)	1x EA 2x LA	3
MS241 (12)	1x LA	1	MS300 (12)	1x LA	1
MS241 (21)	1x LA	1	MS300 (23)	1x LA	1
MS242 (1)	NAWM	0	MS303 (12)	1x EA 4x LA	5
MS242 (11)	1x EA	1	MS303 (19)	1x LA	1
MS242 (12)	2x EA 1x LA	3	MS303 (20)	2x LA	2
MS245 (1)	1x LA	1	MS307 (12)	1x LA	1
MS245 (8)	1x LA 1x IA	2	MS307 (19)	1x IA	1
MS245 (12)	1x LA	1	MS307 (20)	3x LA	3

Table 2.2 Overall histological classification of MS samples

All samples were histologically characterised by two independent observers for full patient details see Appendix III.

Key: EA: Early active lesion (acute), LA: Late active lesion (chronic active), IA: Inactive lesion, NAWM: normal appearing white matter, (1): Superior frontal gyrus, (8): Thalamus + subthalamic, (9): Hippocampus anterior, (10): Temporal cortex, (11): Precentral gyrus - Motor cortex, (12): Primary visual cortex anterior, (13): Parietal lobule, (19): Optic chiasm, (20, 21, 22, 23): White matter lesion.

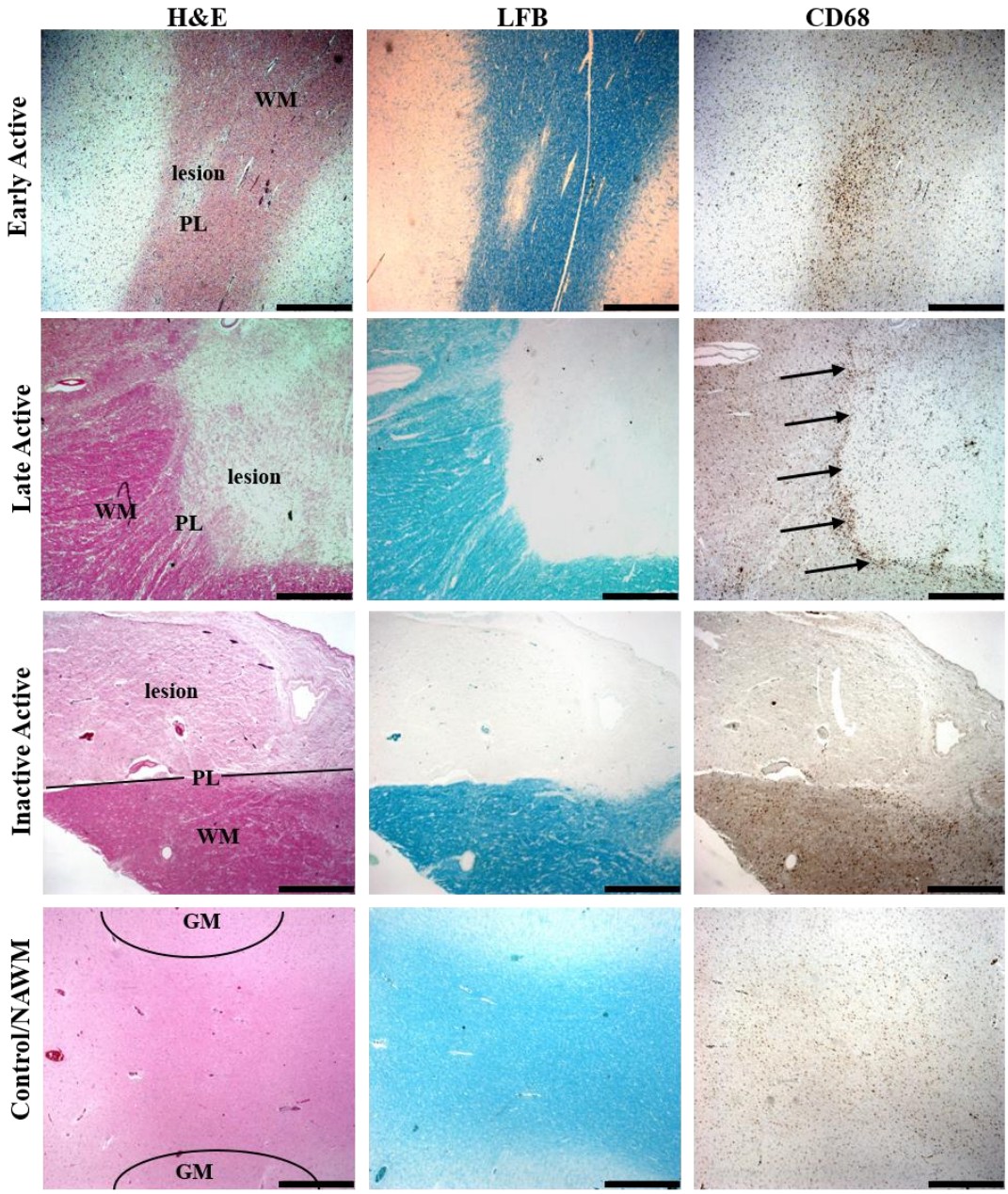

Figure 2.3 Tissue classification using H&E, LFB and CD68

EA lesions contained swollen, amoeboid phagocytic microglia with strong CD68 staining, in comparison to LA lesions that showed a hypercellular band of $CD68^+$ amoeboid microglia at the perilesional (PL) edge (black arrows) with very few $CD68^+$ cells within the lesion centre. Inactive (IA) lesions were highly attenuated, with complete loss of myelin and hypocellularity present in the lesion centre with no evidence of microglia activity. Control and NAWM were grouped together showing similar characteristics with no evidence of perivascular leukocyte accumulation, intact myelin and few $CD68^+$ microglia with a phagocytic phenotype. **Key:** GM: grey matter. *Scale bar represents 1000µm.*

All 19 control samples showed no evidence of inflammatory cell infiltration and contained a regular distribution of cell nuclei on H&E. There was no evidence of demyelination with a uniform distribution of LFB staining throughout the tissue, and a regular distribution of $CD68^+$ microglia with a resting ramified profile (Figure 2.3).

Similar to control WM, MS NAWM surrounding all lesions investigated showed no evidence of inflammation or PVC, the cell distribution was regular throughout the tissue with intact myelin shown by positive LFB staining. A regular distribution of $CD68^+$ microglia with a resting ramified appearance was apparent, with the occasional clustering of microglia.

2.4.2 Microglia phenotype – ramified versus amoeboid

Microglia are sensitive to environmental changes and respond to stress, trauma, infection (Boche *et al* 2013), therefore the phenotype of microglia provides an insight to each tissue sample, helping to classify the lesion type present in each case. $CD68^+$ microglia with a swollen, hypertrophic, amoeboid appearance accumulate in abundance within EA lesions and surrounding LA lesions, with retracted processes indicative of phagocytic microglia which play a key role in demyelination (Figure 2.4a). In contrast, control WM and NAWM contained a regular distribution of $CD68^+$ cells, displaying a more uniform, bipolar appearance with branched processes suggestive of resting microglia, which play a role in regulating and surveying the CNS in case of insult or trauma (Figure 2.4b). In some areas of NAWM, clusters of $CD68^+$ microglia were present (Figure 2.4c), which have been suggested to form preactive lesions in MS (van der Valk & Amor 2009, van Noort *et al* 2011).

2.4.3 Negative controls

To determine the level of background staining when carrying out IHC, negative and isotype controls were used. The omission of each primary astrocyte antibody and use of appropriate isotype control (at the same concentration as the primary antibody) was carried out on an additional NAWM section during each IHC run. No background staining from the secondary antibody was observed across all IHC controls (Figure 2.5).

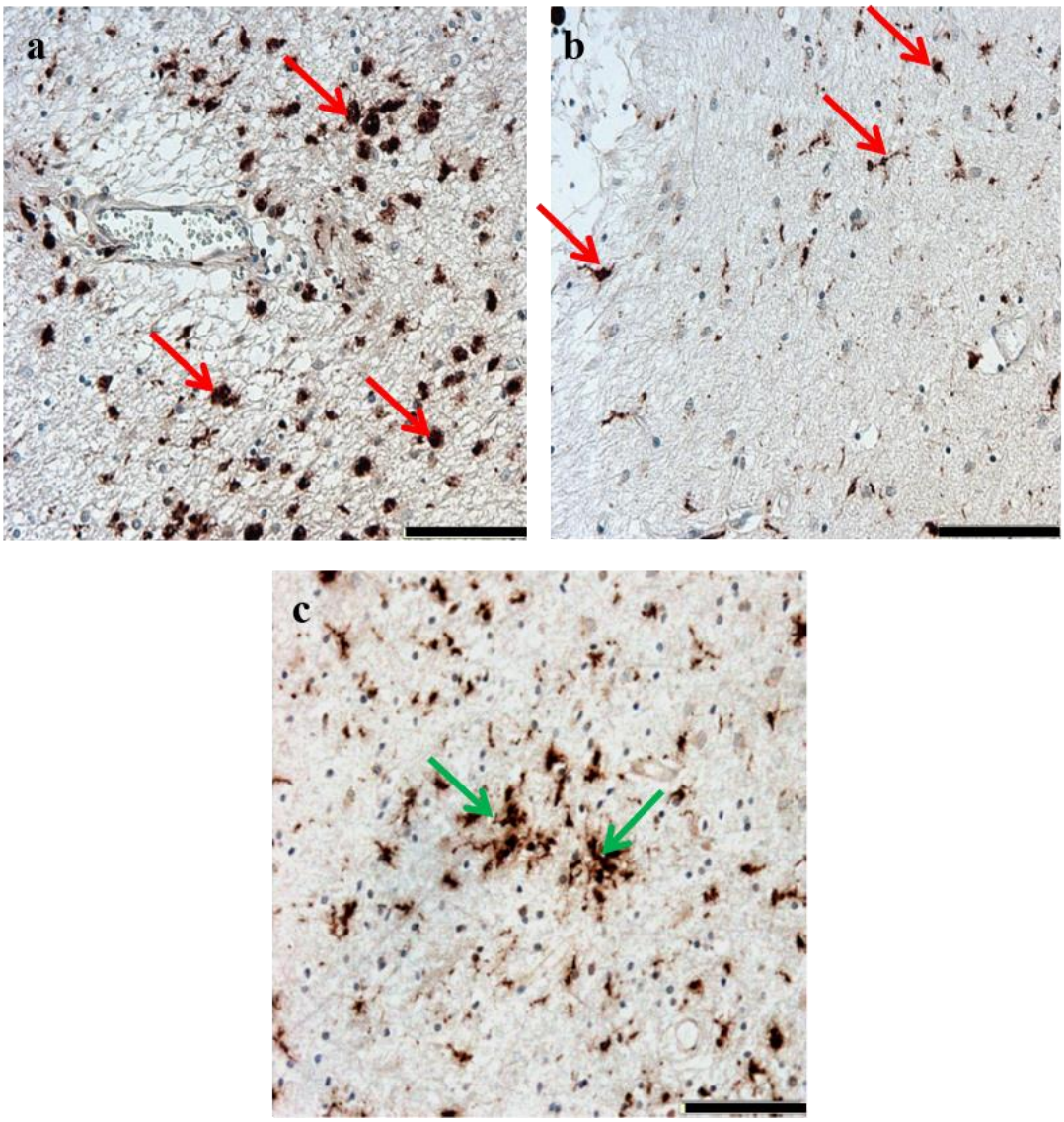

Figure 2.4 Patterns of CD68 immunoreactivity detected in the WM in MS CNS
The morphology of microglia, as determined by CD68 IHC, is indicative of the physiological state of the CNS of the patient. Microglia that take on a swollen, hypertrophic, amoeboid appearance with retracted processes are suggestive of phagocytic microglia (a, red arrows). In comparison, resting microglia appear bipolar and ramified with extending processes (b, red arrows). Within particular areas of NAWM the microglia appeared in clusters rather than a regular distribution (c, green arrow). *Scale bar represents 50µm.*

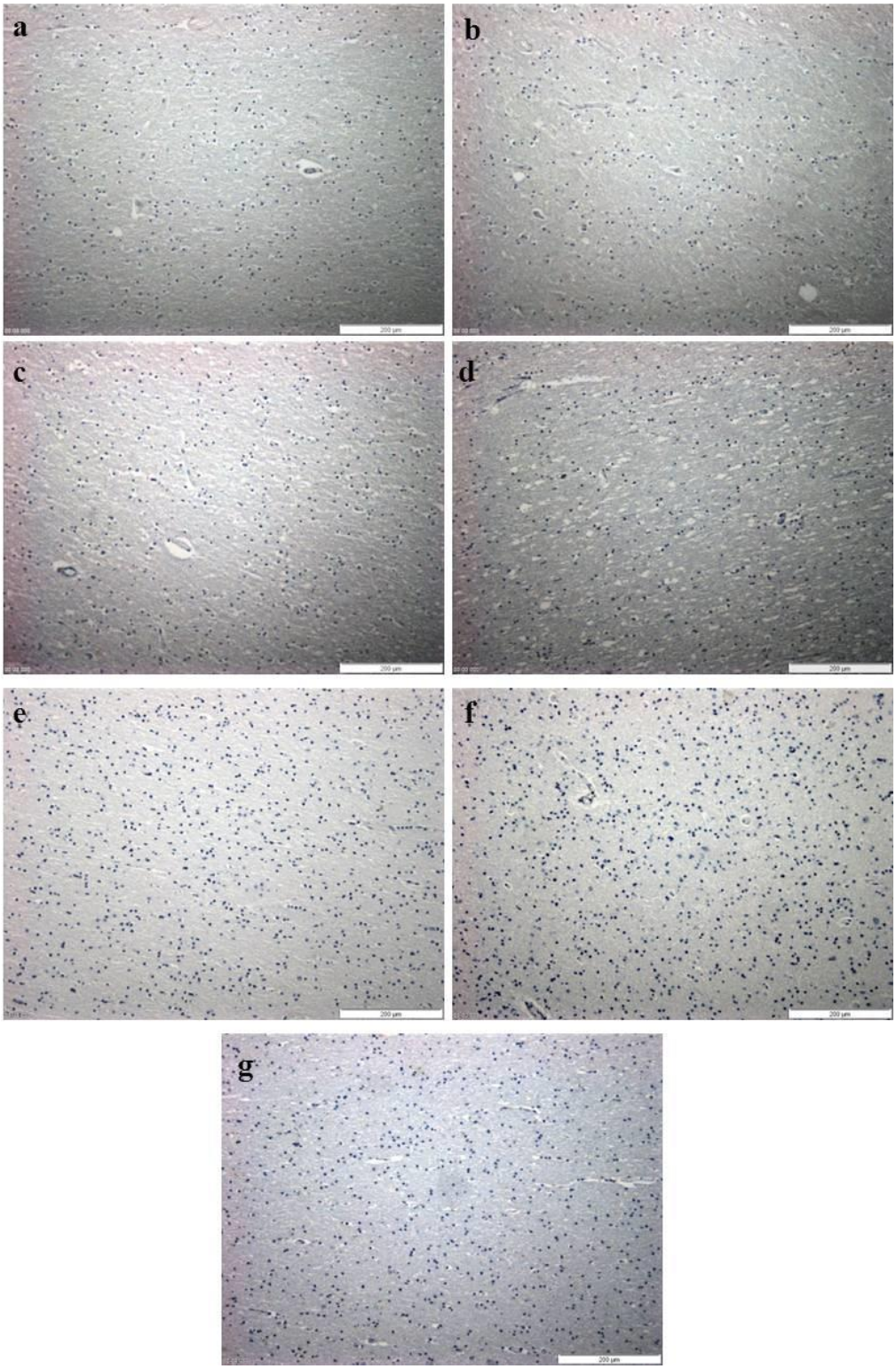

Figure 2.5 Negative controls

The omission of primary antibodies for GFAP (a), S100B (b) EAAT1 (c), EAAT2 (d), GS (e), ALDH1L1 (f), CD44 (g). Nuclei counterstained with haematoxylin. *Scale bar represents 200μm.*

2.4.4 Glial fibrillary acidic protein (GFAP) immunoreactivity increases within chronic active lesion centres

Dense GFAP immunoreactivity was a common feature of all lesion types (EA, LA, and IA lesions) with levels of GFAP significantly different across all groups (GFAP p=0.001, Kruskal-Wallis test). In a qualitative assessment, NAWM immediately surrounding MS lesions displayed an increase in GFAP immunoreactivity compared to control WM. There were clear differences in the size of astrocytes between MS samples regardless of lesion type, with some positively stained small stellate cells present in some samples, while others contained swollen and hypertrophic immunopositive cells. Overall there was a regular distribution of $GFAP^+$ astrocytes with a typical stellate morphology and extending processes in control/NAWM samples (Figure 2.6a, red arrows). An increase in immunoreactivity was present at the EC of blood vessels within all lesion types, yet individual cell types were hard to distinguish as a result of the dense gliosis present within lesion centres (Figure 2.6c). In some LA lesions immunopositive swollen, hypertrophic astrocytes were present at the lesion edge (Figure 2.6b, green arrows). Quantitatively all lesion types displayed a significant increase in GFAP immunoreactivity compared to control/NAWM cases (EA; p= 0.002, LA; p= 0.000, IA p= 0.023, Mann-Whitney U tests, Figure 2.7), confirming initial qualitative analysis. Mann-Whitney U tests between lesion types did not identify significant differences in GFAP expression (EA versus LA; p= 0.894, EA versus IA; p= 1.000, and LA versus IA; p= 0.945).

2.4.5 S100B immunoreactivity increases within chronic active lesion centres

S100B astrocyte immunoreactivity in the WM was primarily associated with the astrocyte cell body, with more typical stellate astrocyte profiles seen in the cortex. Overall a regular distribution of $S100B^+$ astrocytes was seen throughout the control/NAWM comprising of immunopositive cell body and immediate dense processes (Figure 2.8a, red arrows). The staining of delicate extended astrocyte processes was not as extensive with S100B as with GFAP. Also within the control/NAWM samples an intense staining of small spherical cells morphologically resembling oligodendrocytes was observed (Figure 2.8a, blue arrows). Some samples showed a punctate diffuse pattern of staining, however a qualitative increase in S100B immunoreactivity was visualised within the different lesion types, however individual cell profiles within the lesions were hard to determine due to gliosis (Figure 2.8c). The presence of $S100B^+$ hypertrophic, swollen astrocytes were seen at the lesion edge of some LA lesions. Overall the staining within the WM was higher than in the cortex

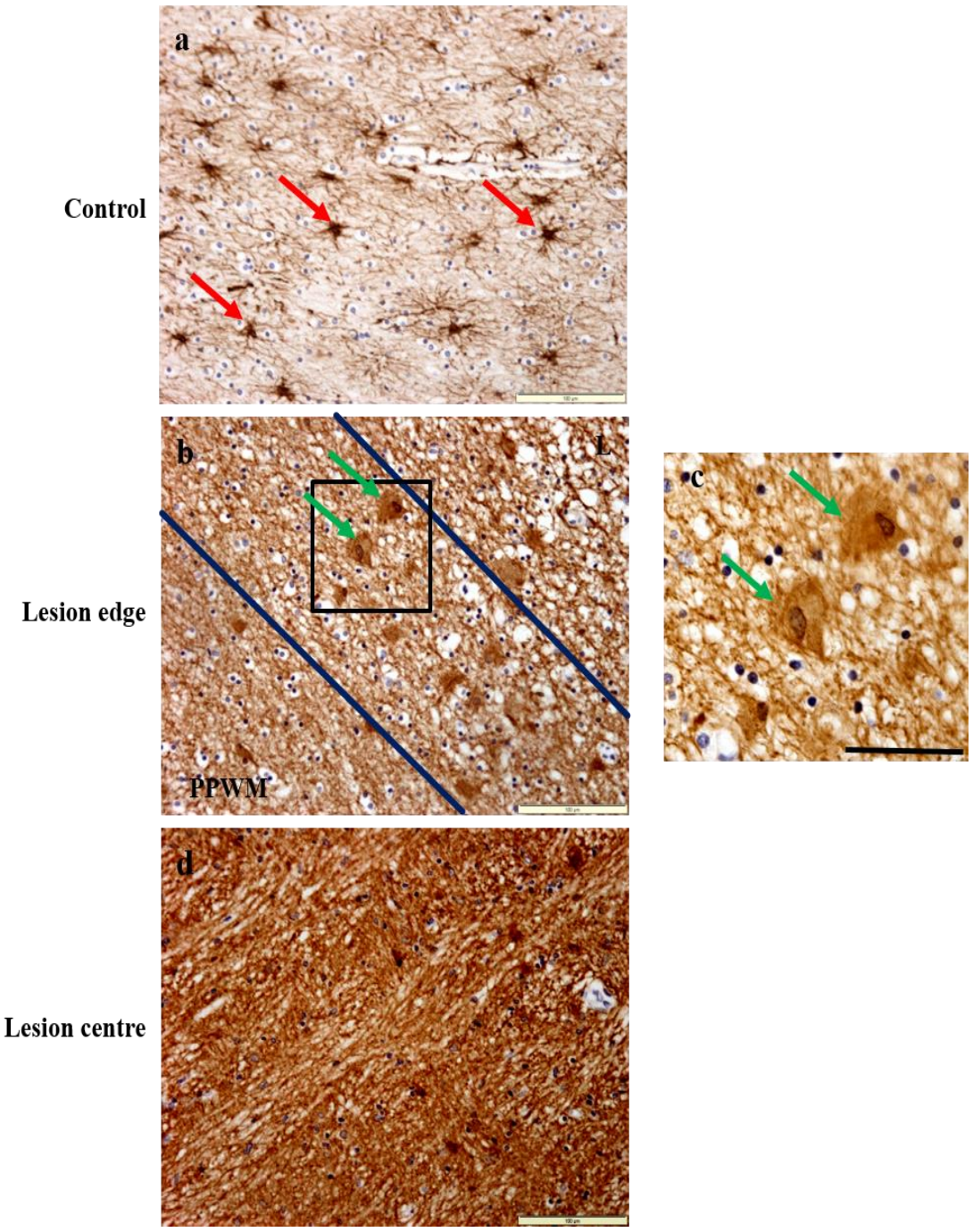

Figure 2.6 GFAP expression by IHC

The expression of GFAP (brown) within the control/NAWM identified individual stellate cells easily distinguishable (a, red arrows). At the lesion border a band of swollen hypertrophic $GFAP^{+}$ astrocytes were prominent (b&c, green arrows), leading into the lesion centre with a significant increase in staining (d), individual cells were no longer distinguishable in all 3 lesion types. Sections were counterstained with haematoxylin. *Scale bar represents 100µm (a,b,d) 50um (c).*

Key: PPWM: Periplaque White Matter, L: lesion, Blue lines represent lesion border.

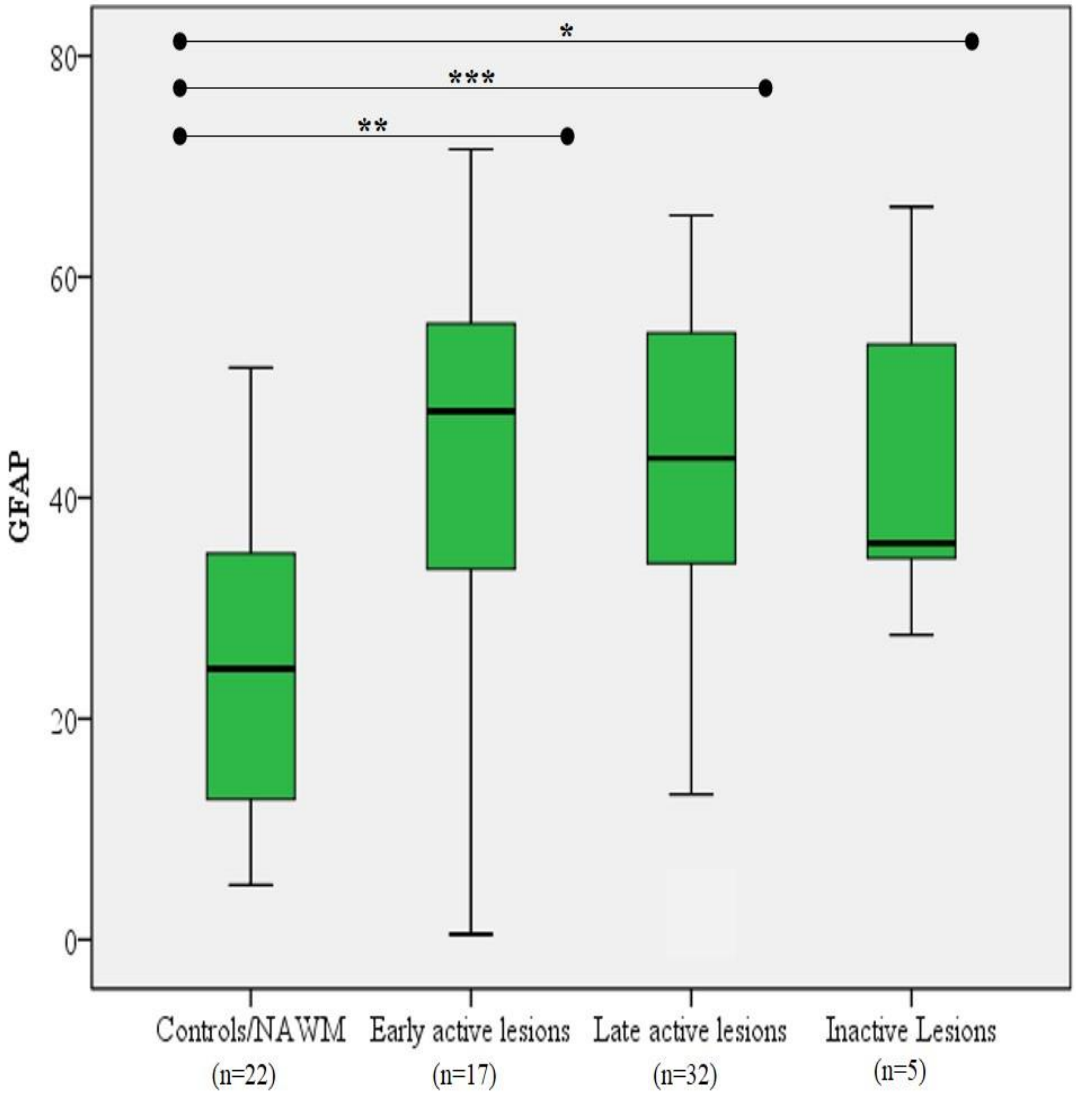

Figure 2.7 Comparison of GFAP immunoreactivity in neurological controls/NAWM samples and different MS lesion types

y-axis represents the overall percentage (%) area immunoreactivity of GFAP. GFAP expression was significantly increased in all lesion types in comparison to controls/NAWM samples of this study. Individual statistical differences between control/NAWM versus MS EA/ LA/ IA lesions are marked by asterisks. (*P<0.05, **P<0.01 ***P<0.001).

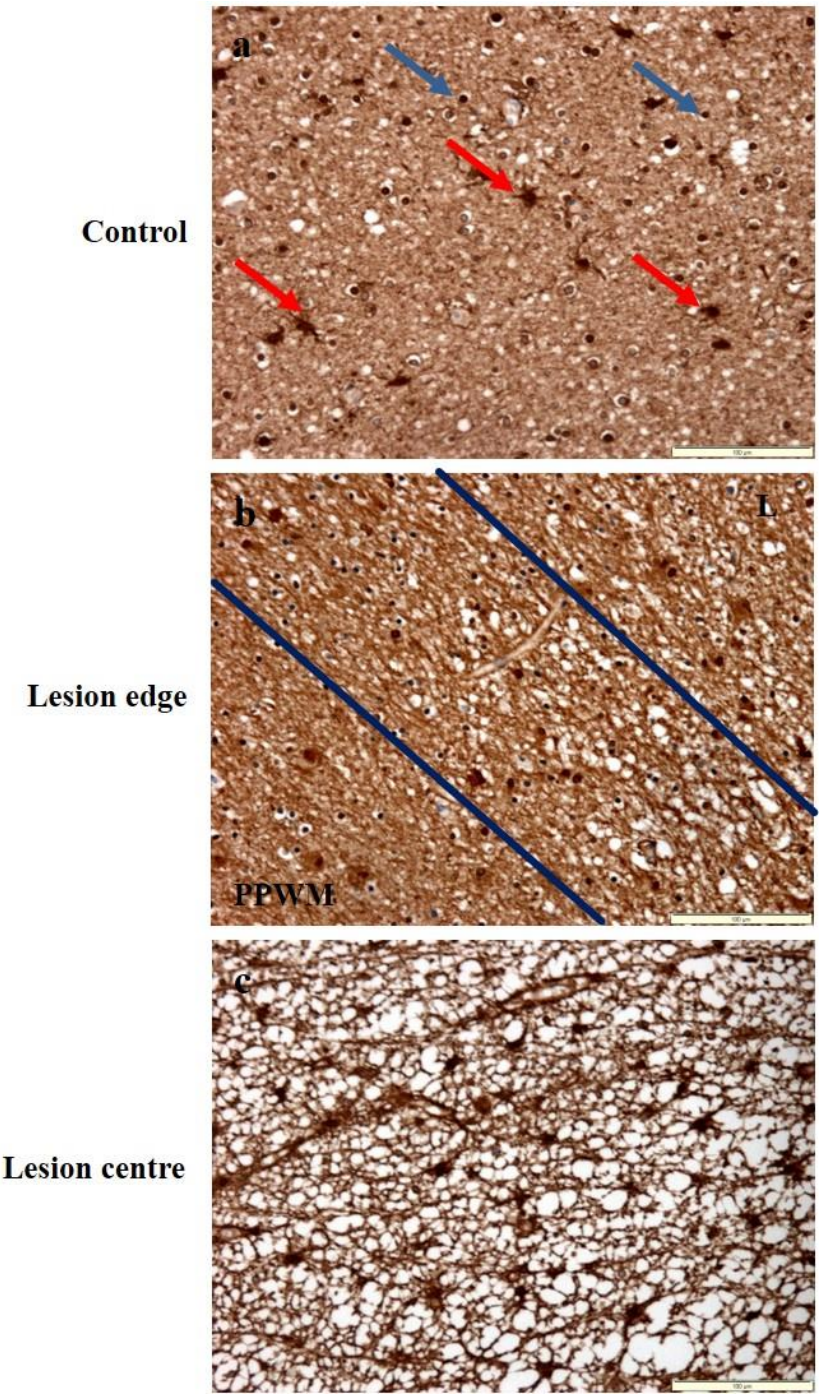

Figure 2.8 S100B expression by IHC

The expression of S100B (brown) within the control/NAWM identified dense cell body staining with immediate processes (a, red arrows) the presence of oligodendrocyte like staining was evident (a, blue arrows). The immunoreactivity was significantly increased within the lesion centre with individual cells hard to distinguish (c). Sections were counterstained with haematoxylin. *Scale bar represents 100µm.*

Key: PPWM: Periplaque White Matter, L: lesion, Blue lines represent lesion border.

where there appeared to be fewer S100B$^+$ cells. Levels of S100B were significantly different across all groups (S100B p=0.000, Kruskal-Wallis test). Quantitatively all lesion types displayed a significant increase in S100B immunoreactivity compared to control/NAWM cases (EA; p= 0.035, LA; p= 0.000, IA p= 0.033, Mann-Whitney U tests, Figure 2.9) confirming qualitative analysis. Mann-Whitney U tests between lesion types did not identify significant differences in S100B expression, (EA versus LA; p= 0.048*, EA versus IA; P=0.704, and LA versus IA; P=0.230).

* Not significant when the p-value is adjusted using the Bonferroni correction.

2.4.6 Excitatory amino acid transporter 1 (EAAT1) expression within chronic active lesion centres

EAAT1 protein expression displayed the most varied staining pattern amongst the seven different markers investigated. Overall the staining pattern varied greatly amongst the different MS/control samples and across the different lesion types. However, in general the immunoreactivity was restricted to the fine delicate processes of astrocytes in the NAWM and control samples. The extent of the astrocyte process extensions were clearly visible in the tissue (Figure 2.10a, red arrows). Qualitatively within the lesion centre a decrease in EAAT1 expression was observed across all three different lesion types (Figure 2.10c), however the quantitative findings suggesting an increase in EAAT1 immunoreactivity within all lesion centres investigated. However, these findings failed to reach statistical significance (EAAT1 p= 0.278, Figure 2.11a).

2.4.7 Excitatory amino acid transporter 2 (EAAT2) expression within chronic active lesion centres

EAAT2 immunoreactivity was restricted to the delicate astrocyte processes (Figure 2.12a, red arrows). Overall the staining was punctate and irregular throughout the different control WM and NAWM samples, with some control samples staining extensively (Figure 2.12a) while other samples were completely devoid of staining. However, in general a qualitative assessment of the pattern of staining showed a decrease in EAAT2 immunoreactivity within the different lesion types in comparison to control and NAWM (Figure 2.12c), however the quantitative findings suggesting an increase in EAAT2 immunoreactivity within the lesion centres investigated. However, these findings failed to reach statistical significance (EAAT2 p=0.311, refer to Figure 2.11b).

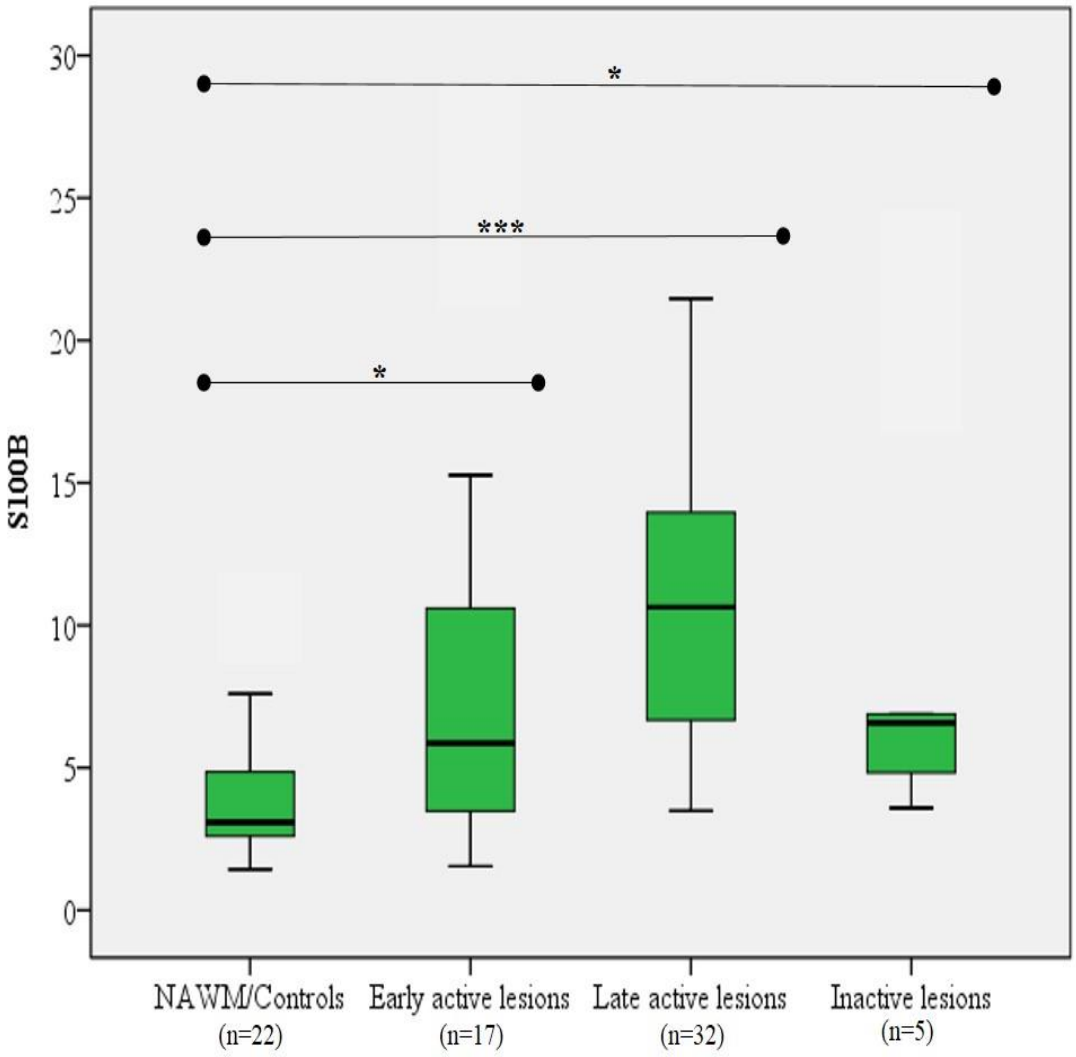

Figure 2.9 Comparison of S100B immunoreactivity in neurological controls/NAWM samples and different MS lesion types

y-axis represents the overall percentage (%) area immunoreactivity of S100B. S100B expression was significantly increased in all lesion types in comparison to controls/NAWM samples of this study. Statistical differences between control/NAWM versus MS EA/ LA/ IA lesions are marked by asterisks (*P<0.05, **P<0.01 ***P<0.001).

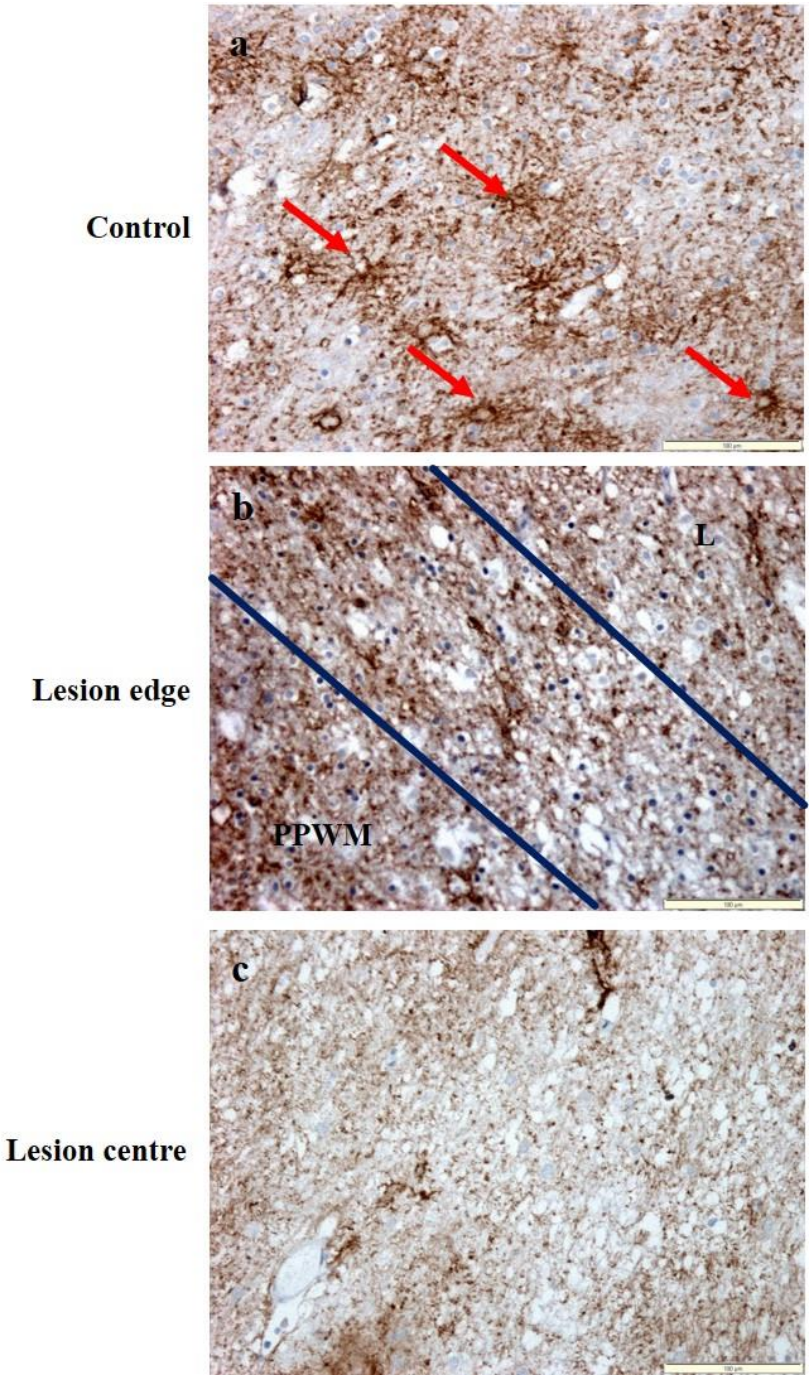

Figure 2.10 EAAT1 expression by IHC

A diffuse irregular pattern of EAAT1 staining was identified in control/NAWM labelling the astrocyte processes (a, red arrows) and at the lesion border (b). Qualitatively an overall decrease in EAAT1 expression was seen within the lesion centres (c). Sections were counterstained with haematoxylin. *Scale bar represents 100μm.*

Key: PPWM: Periplaque White Matter, L: lesion, Blue lines represent lesion border.

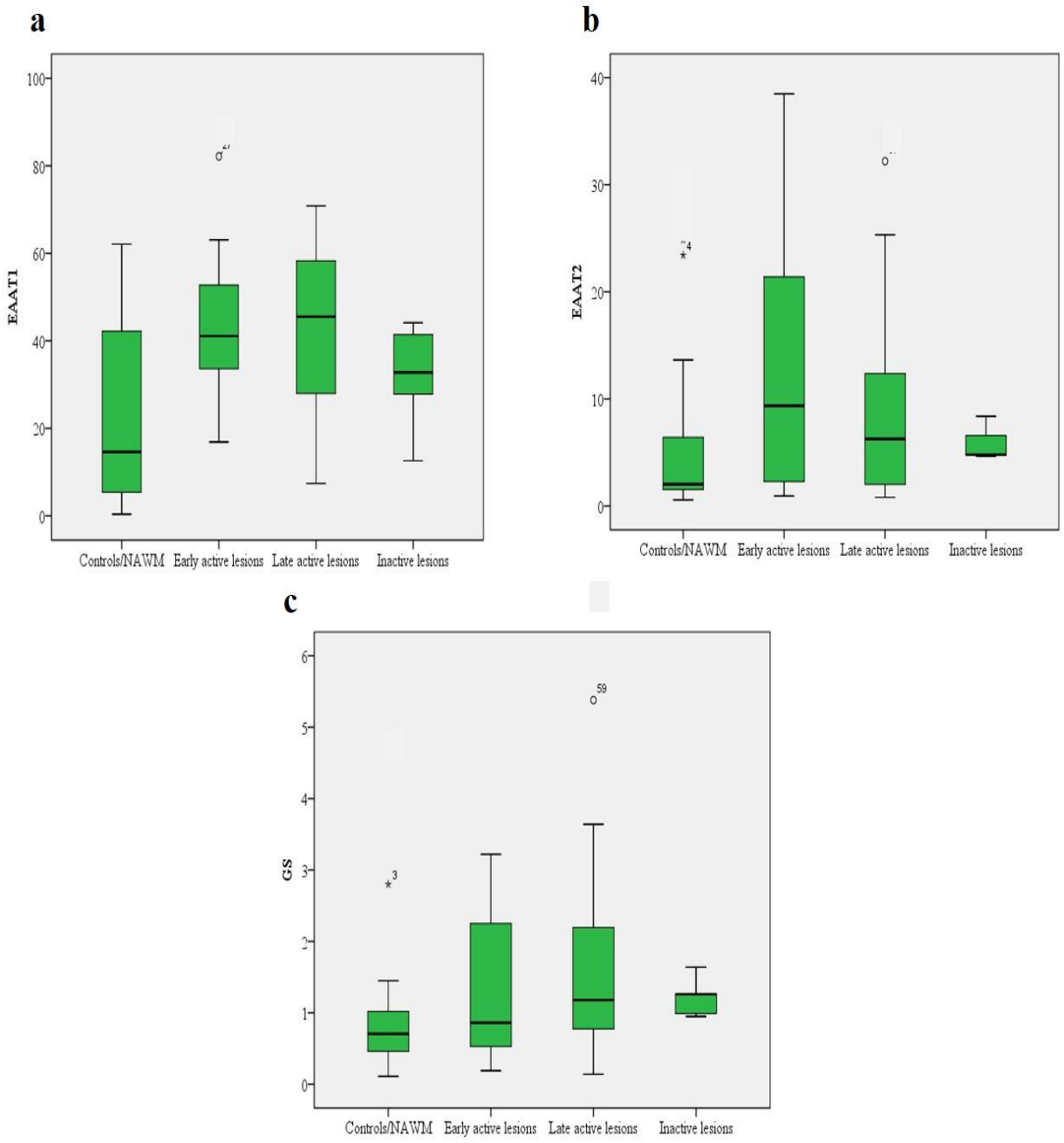

Figure 2.11 Comparison of EAAT1 (a), EAAT2 (b) and GS (c) immunoreactivity in neurological controls/NAWM samples and different MS lesion types

y-axis represents the overall percentage (%) area immunoreactivity of each antibody. Quantitatively a trend of increased reactivity of all three antibodies was observed in all lesion types in comparison to control/NAWM, yet no significance for any of the markers across the lesion types was observed.

Control/NAWM (n=22), Early active (n=17), Late active (n=32), Inactive (n=5).

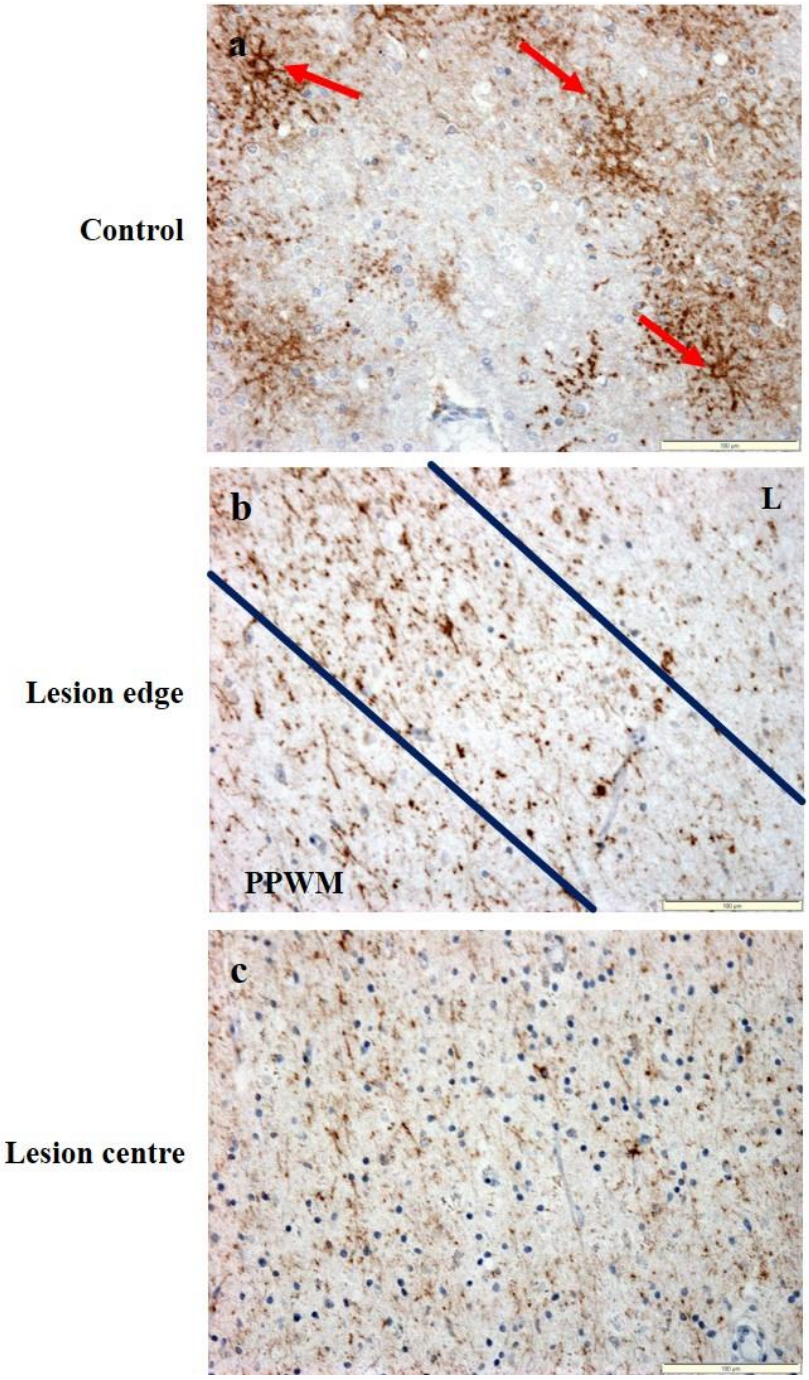

Figure 2.12 EAAT2 expression by IHC

A pitted, diffuse astrocyte process stain (brown) was presented in the control/NAWM with EAAT2 (a, red arrows). Qualitatively the expression of EAAT2 was reduced at the lesion edge (b) and within the lesion centre (c). Sections were counterstained with haematoxylin. *Scale bar represents 100μm.*

Key: PPWM: Periplaque White Matter, L: lesion, Blue lines represent lesion border.

2.4.8 Glutamine synthetase (GS) expression within chronic active lesion centre

GS immunoreactivity in astrocytes identified cells with a stellate morphology, and was predominantly restricted to the cell body and immediate processes, proving not as extensive as with GFAP labelling (Figure 2.13a, red arrows). GS immunoreactivity was not restricted to astrocytes as positive staining of the cytoplasm of small, spherical cells which morphologically resembled oligodendrocytes (Figure 2.13b, blue arrows) were also labelled. Within all lesion types investigated a qualitative assessment identified that GS immunoreactivity was reduced in lesion centres (Figure 2.13c), however the quantitative findings suggesting an increase in GS immunoreactivity within all lesion centres investigated compared to control/NAWM cases. However, these findings failed to reach statistical significance (GS p=0.068, refer to Figure 2.11c). At the border of some LA lesions was the presence of swollen, hypertrophic GS^+ astrocytes (Figure 2.13b, red arrows). The reactivity of GS appeared greater in the cortex than the WM.

2.4.9 Aldehyde dehydrogenase L 1 (ALDH1L1) is primarily associated with cortical tissue

The staining pattern displayed by ALDH1L1 immunoreactivity was of the astrocyte cell body and did not extend to the fine delicate extended astrocyte processes. ALDH1L1 also was expressed by small, spherical cells indicative of oligodendrocytes (Figure 2.14a, blue arrow). A more extensive staining pattern with this marker was seen in the cortex compared with the WM, where the immunoreactivity appeared to be dramatically reduced and in some samples absent (Figure 2.14b).

2.4.10 CD44 expression is not detectable in formalin fixed paraffin embedded (FFPE) tissue

Initial optimisation studies with the astrocyte marker CD44 within snap frozen tissue sections showed a clear distinct staining of WM astrocytes with the processes ensheathing blood vessels (Figure 2.15a). In comparison throughout the cortex CD44 immunoreactivity was reduced identifying this marker as a potential WM astrocyte marker. Despite a comprehensive range of antigen retrieval methods, this CD44 antibody failed to provide clear immunoreactivity in the FFPE material (Figure 2.15b). Overall the immunodetection of CD44 in the FFPE material failed to replicate the pattern of staining observed in the frozen material, therefore this antibody was not included in the overall assessment of the astrocyte phenotype in this study.

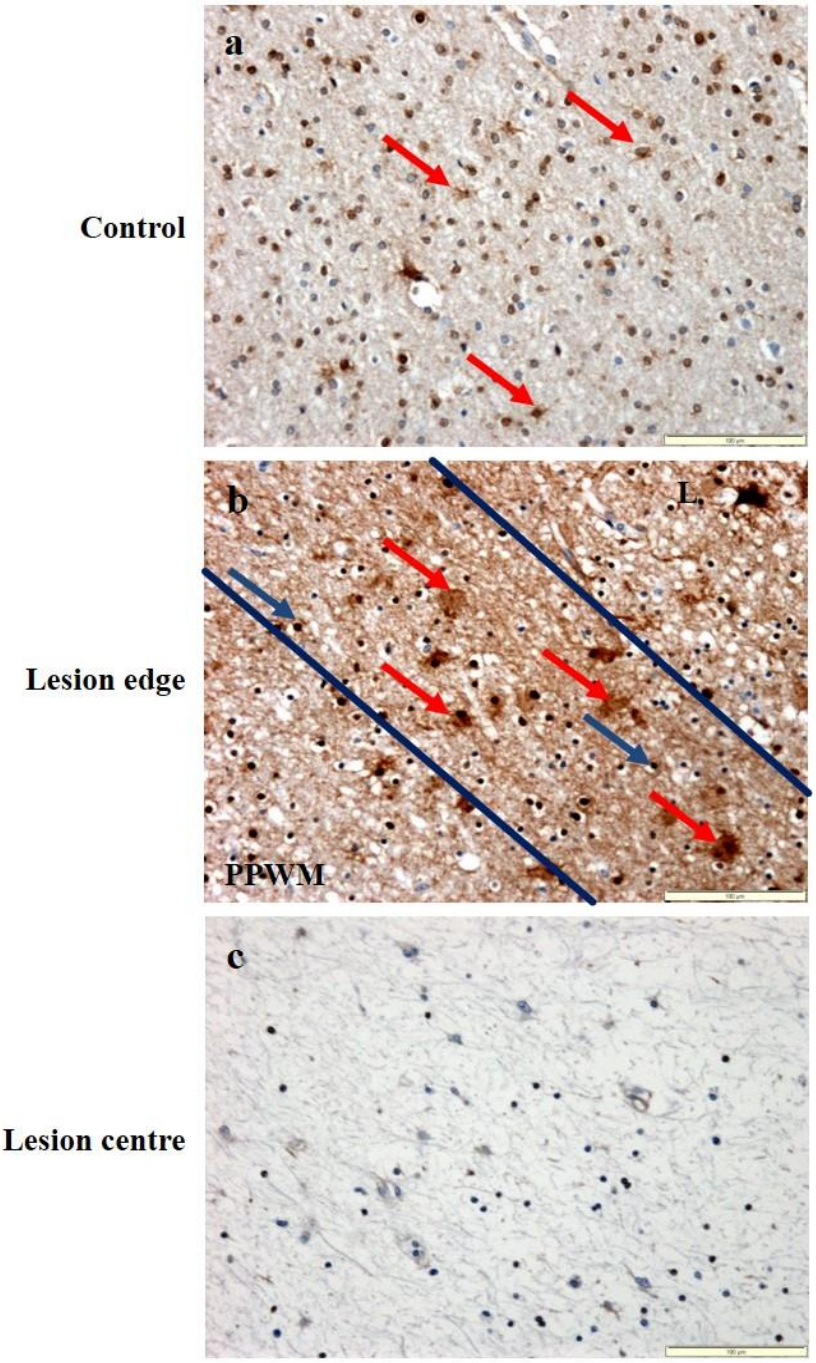

Figure 2.13 GS expression by IHC

The expression of GS (brown) within the control/NAWM identified small stellate cells (a, red arrows). In some samples at the lesion border a band of swollen GS positive astrocytes were prominent (b, red arrows). Also GS positive oligodendrocyte like cells were present (b, blue arrows). Qualitatatively GS protein expression was reduced within the lesion centre (c) in comparison to the lesion edge and control/NAWM. Sections were counterstained with haematoxylin. *Scale bar represents 100µm.*

Key: PPWM: Periplaque White Matter, L: lesion, Blue lines represent lesion border.

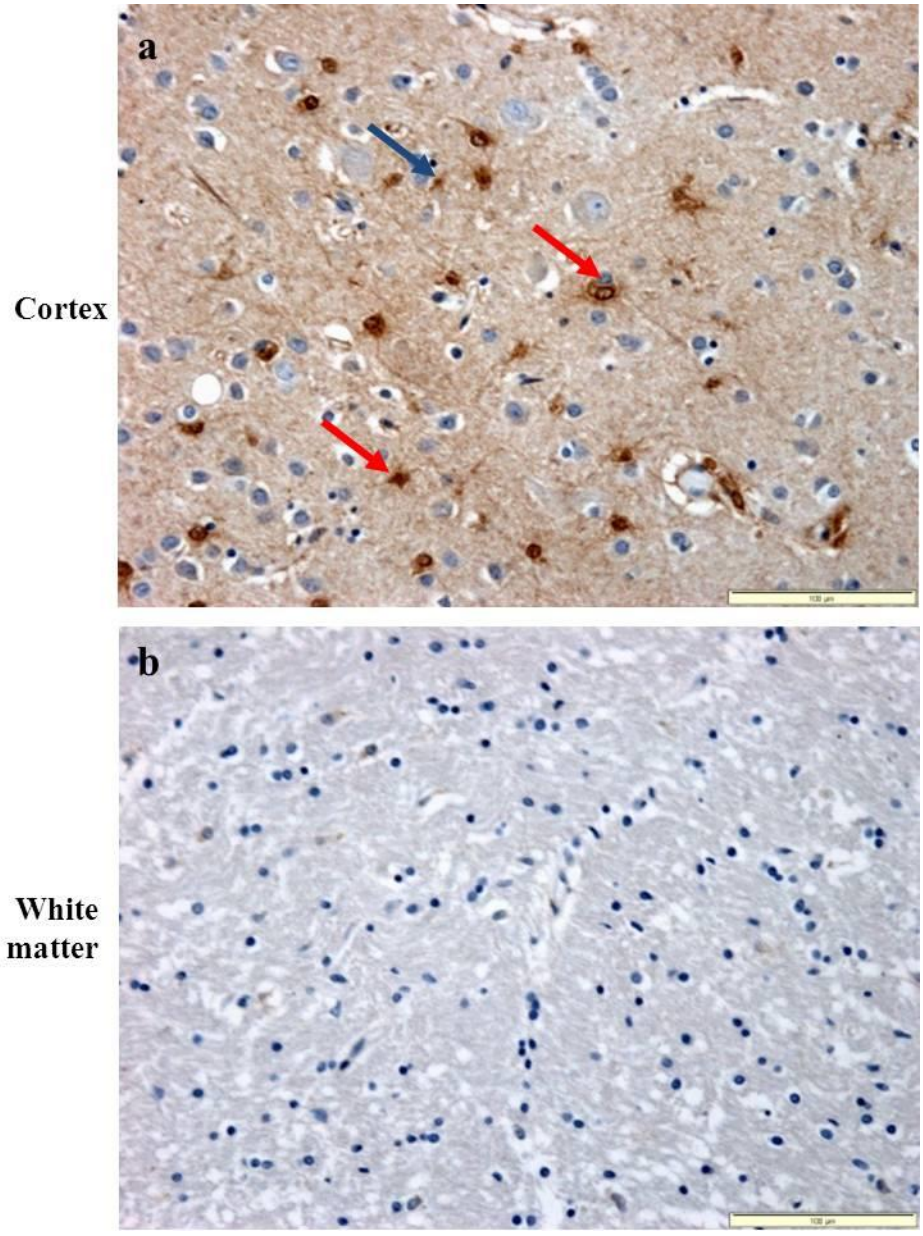

Figure 2.14 Higher expression of ALDH1L1 in cortex compared with white matter
Levels of ALDH1L1 were more abundant within the cortex (a) in comparison to white matter (b). Red arrows: astrocytes, blue arrow: possible oligodendrocytes. Sections were counterstained with haematoxylin. *Scale bar represents 100µm.*

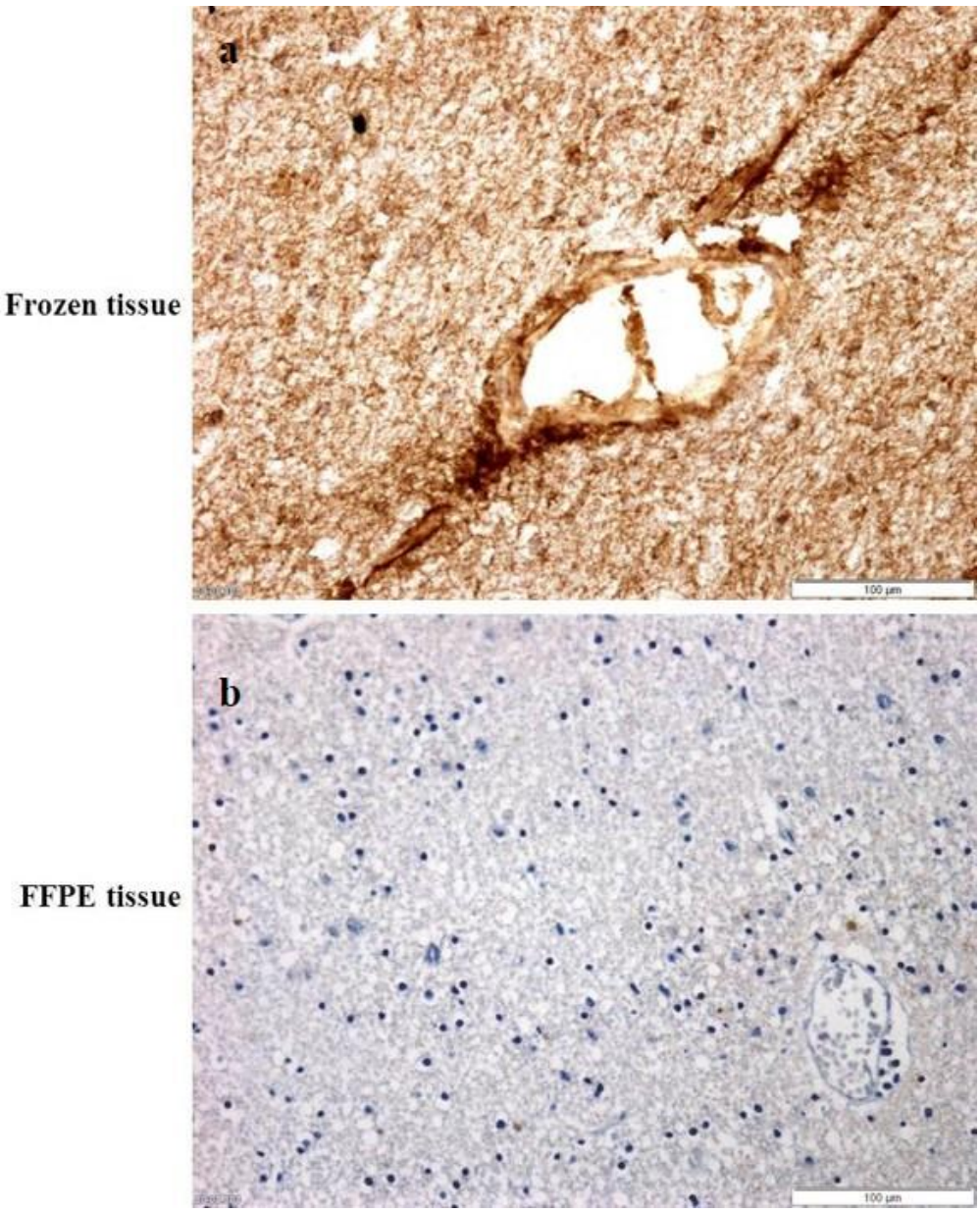

Figure 2.15 Comparison of CD44 expression in snap frozen and FFPE CNS tissue
The expression of CD44 (brown) on frozen issue was localised to the astrocyte end processes at blood vessels in the WM (a). CD44 staining of FFPE tissue failed to repeat the pattern of staining observed in the frozen material (b), despite a range of antigen retrieval methods. Sections were counterstained with haematoxylin. *Scale bar represents 100µm.*

2.5 Discussion

In this study the astrocyte phenotype was characterised in the WM from both MS and controls. Using a panel of seven currently recognised astrocyte markers, the pattern and extent of immunoreactivity within the lesion centre, perilesional edge and the surrounding NAWM was determined. Significantly more hypertrophic astrocytes, as indicated by a significant increase in GFAP and S100B immunoreactivity, were present in all lesion types in comparison to surrounding NAWM and control WM. In contrast, a dysregulation of glutamate in all MS lesion types compared to control WM and surrounding NAWM was identified by a non-significant increased expression of the glutamate transporters EAAT1 and EAAT2 along with an increase in the glutamate regulatory enzyme GS.

2.5.1 Increased expression of GFAP and S100β in MS lesions

With lesion progression and response to pathological injury, astrocytes become reactive and undergo astrogliosis with changes in their expression profile, overall morphology and function. In remyelinating and demyelinating lesions, astrocytes may act as either immune cells or supporting cells, expressing an array of cytokines/chemokines dependant on the stage of disease, their interactions with other cell types and changes in their surrounding environment (John *et al* 2002, Nair *et al* 2008). In the current study individual $GFAP^+$ cells were difficult to distinguish within MS lesions due to the prominent gliosis present. Within the LA lesion centres $GFAP^+$ astrocytic scar tissue were observed, supporting previous observations (Eng *et al* 1971, Fawcett & Asher 1999, Fitch & Silver 2008, Hibbits *et al* 2012, Holley *et al* 2003). A significant increase in GFAP immunoreactivity in MS lesions represents on-going fibrillary gliosis (Brosnan & Raine 2013). Large hypertrophic $GFAP^+$ astrocytes were prominent at the perilesional edge of a subset of LA lesions, which has previously been reported in MS /EAE lesions (Lavrnja *et al* 2012).

In response to injury/insult astrocytes undergo cellular hypertrophy and increase their expression of GFAP. However previous histological studies investigating GFAP expression in MS human brain tissue are surprisingly infrequent in comparison to animal/cell models or human CSF/serum studies. A 3-fold increase in GFAP expression in the cortex of MS patients compared to control samples has been observed, however this study failed to analyse GFAP levels in WM of MS patients, where most MS lesions are located (Petzold *et al* 2002). A small number of human MS PM studies have identified an increase in $GFAP^+$ astrocytes in areas of demyelination (Clarner *et al*

2012, Kipp *et al* 2011, Nishie *et al* 2004) supporting the findings from the current study, increasing the awareness that astrogliosis is a pathological hallmark MS.

A significant increase in CSF levels of GFAP has been reported from patients with SPMS, while levels of GFAP in RRMS patients were similar to control patients, suggesting that astrocytes have a role at the later stages of chronic demyelination (Linker *et al* 2009). GFAP levels are likely to correlate with the neurodegenerative processes of MS, and have been associated with the Expanded Disability Status Scale (EDSS) and the MS Severity Status (MSSS) (Axelsson *et al* 2011). An increase in CSF GFAP levels in SPMS supports the view that levels of GFAP positively correlate with neurodegeneration, which is more apparent in SPMS (Malmestrom *et al* 2003, Norgren *et al* 2004). However, other studies indicate neither CSF GFAP levels in MS patients significantly differ to control patients (Petzold *et al* 2002) nor correlate with the patient's EDSS (Madeddu *et al* 2013).

The current histological study investigated WM from SPMS, but future studies aimed at determining levels of GFAP in RRMS/PPMS patients could determine whether GFAP expression is significantly higher in those cases than control cases. However, obtaining such material for human studies is challenging as the majority of patients that present at PM have transferred into the SP phase of the disease, with a well-established disease phenotype.

There are a number of limitations to CSF studies when monitoring potential biomarkers of brain disease including GFAP. Foremost, CSF is not brain tissue and the protein profile from CSF may in part be influenced by other factors not relevant to the disease itself (Giovannoni 2006, Shiihara *et al* 2013) and with a general lack of CSF samples from healthy controls, comparison studies are problematic (Teunissen *et al* 2013). Also, standardised methods of CSF sample collection and processing between laboratories need to be applied to prevent variability in these types of study (Giovannoni 2006, Mattsson *et al* 2013). Analysis of CSF and serum samples for biomarkers is restricted by technology (Mattsson *et al* 2013), as many ELISA tests would be impractical in an emergency setting (Shiihara *et al* 2013), however developing mass spectrometry techniques may overcome this. Despite the limitations, CSF is the closest biological fluid to the pathology of the brain (Smolinska *et al* 2012) and by using this material disease development can be monitored throughout life, whereas histological evaluation of brain tissue is limited mainly to PM tissue.

Recent work on MS animal models have shown similar findings to the current study, with a regular distribution of $GFAP^+$ astrocytes observed in control mice, while over the course of MOG induced EAE, astrocytes become strongly $GFAP^+$ with a diffuse staining pattern indicative of a gliotic response (Linker *et al* 2009). An increase in GFAP expression has also been observed in other models of demyelination including EAE in rats and chronic relapsing EAE in mice (Lavrnja *et al* 2012, Norgren *et al* 2004, Petzold *et al* 2003a).

An increase in S100B, an established marker for astrocyte metabolism involved in intracellular and extracellular regulatory activities, has been linked to many neurodegenerative disorders including Parkinson's disease (PD) (Sathe *et al* 2012, Schaf *et al* 2005), amyotrophic lateral sclerosis (ALS) (Migheli *et al* 1999, Sussmuth *et al* 2010) and AD (Peskind *et al* 2001, Petzold *et al* 2003b). As astrocytes are increasingly recognised as more than just a supportive cell in the CNS, the increased astrocyte expression of S100B within MS lesions may indicate a fundamental important role of these cells in the pathogenesis of neurological disease. Elevated S100B levels are associated with activation of neurotoxic pathways triggering neuroinflammatory responses, including increased expression of receptor for advanced end glycation products (RAGE) ligand (Bianchi *et al* 2007). Also S100B induces the rise in ROS, cytochrome C release and activation of the caspase cascade (Bianchi *et al* 2007, Sen & Belli 2007). Elevated S100B encourages the release of proinflammatory cytokines from astrocytes, as well as being involved in apoptosis through the decreased expression of the anti-apoptotic protein B-cell lymphoma 2 (BCL2) (Rothermundt *et al* 2003), contributing to neurodegeneration (Hearst *et al* 2011).

Many studies on MS have identified an increase in S100B protein in the CSF/serum samples taken from patients (Bartosik-Psujek *et al* 2011, Rejdak *et al* 2007), which has been inferred as a marker of activated astrocytes (Rothermundt *et al* 2003, Sen & Belli 2007). These findings support our results of an increased trend in S100B expression in all MS lesions types (Bartosik-Psujek *et al* 2011, Michetti *et al* 1979, Missler *et al* 1997, Petzold *et al* 2004, Petzold *et al* 2002, Rejdak *et al* 2007). Despite the many studies supporting this theory it is worth noting that there is conflicting research that has failed to identify an increase in serum/plasma S100B in patients with either PPMS, RRMS or SPMS and consequently no correlation with disease activity (Koch *et al* 2007, Lim *et al* 2004). The trophic and toxic effects of S100B are mainly controlled by RAGE, a cell surface receptor found on neurons and microglia (Bianchi *et al* 2011,

Villarreal *et al* 2011) known to activate NF-kB and other proinflammatory responses such as the induction of TNFα and IL-6 expression (Basta *et al* 2002). The binding of S100B to RAGE initiates the activation of the inflammatory cascade, which may contribute to the inflammatory component of MS by chemoattracting $RAGE^+$ $CD4^+$ T cells (Yan *et al* 2003). Crucially the effect of extracellular S100B, whether trophic or neurotoxic, depends on its relative concentration, and also on the activation and expression of the ligand RAGE on corresponding cells (Sorci *et al* 2010). Under physiological conditions at low (nanomolar) levels S100B has been shown to be neuroprotective, protecting neurons from apoptosis, stimulating neurite growth enabling astrocyte proliferation and negatively controlling astrocytic/microglia response to harmful agents (Bianchi *et al* 2007, Sorci *et al* 2013). While at higher concentrations, (micromolar levels), S100B has shown to be cytotoxic displaying it's DAMP (damage-associated molecular pattern protein) effects (Donato 2001) and increasing intracellular NO production and calcium load causing RAGE dependant apoptosis and neuronal cell death (Bianchi *et al* 2011, Hu *et al* 1997, Iuvone *et al* 2007, Sorci *et al* 2013, Villarreal *et al* 2011).

Studies have shown that glial pathology precedes neuronal degeneration in MS inferring a potential role of S100B in disease mechanisms (Petzold *et al* 2003b). In contrast to our findings, where no significant differences between S100B expression in the different lesion types was found, a study identified a higher expression of S100B in the early lesions compared to the later lesions (Petzold *et al* 2002). As well, this study reported a higher expression of S100B in NAWM compared to control WM, which was not seen in the current study. This may be due to a number of factors including differences in IHC protocols used and the use of different antibodies, the effects of which are discussed later in this chapter. Furthermore, this study based their histological criteria using an older, alternative lesion classification method (Li *et al* 1993), claiming that astrocyte activation in early lesion development may return to normal despite continuing microglial activation in MS development. In contrast we report a significant increase in S100B expression in all lesion types investigated. The overall effect of an increase in S100B concentration could contribute to neurodegeneration, myelin degradation and inflammation associated with MS, as *in vitro* micromolar levels of S100B have been shown to induce NO secretion by microglia, and induce the down regulation of genes such as *BCL2* known to cause apoptosis of neuronal precursor cells (Wang *et al* 1999).

To date, there are limited neuropathological studies investigating the distribution of S100B at the cellular level in human CNS tissue from diseased cases, as much of the work has been conducted on cell lines or animal models of disease, as reviewed by (Steiner *et al* 2011). However a recent paper showed higher levels of S100B protein in PM substantia nigra of patients with PD compared with control tissue, concluding that S100B-associated neurodegeneration was mainly mediated by the RAGE/TNFα pathway (Sathe *et al* 2012). Future neuropathological studies of human CNS tissue should be carried out to elucidate the relationship between S100B and neurological disease and ultimately unravel the role of astrocytes in disease.

2.5.2 Increased expression of EAAT1, EAAT2 and GS in MS lesions

Glutamate is the primary excitatory neurotransmitter in the CNS and astrocytes play a role in moderating its synaptic transmission, through a number of glutamate transporters and receptors. Very little glutamate transverses the BBB, this is mainly due to the role of astrocytes, and their influence in the selectivity of substances that pass into and out of the CNS. Astrocytes regulate levels of glutamate by taking up the neurotransmitter from the synaptic cleft via the expression of multiple glutamate transporters. Glutamate is converted to glutamine via metabolising enzymes such as GS and released to neurons (Deitmer *et al* 2003). Within neurons, glutamine is converted back to glutamate via mitochondrial enzymes and transported to synaptic vesicles for release. The release of glutamate into the synaptic space enables excitatory neurotransmitter signals to be generated, the signal is terminated when astrocyte transporters such as the EAATs remove glutamate from the synaptic space. This cycle of events is referred to as the glutamate-glutamine cycle (Hertz 2004).

Previous studies have identified that around 80% of the total uptake of glutamate is through two specific transporters, EAAT1 and EAAT2 located primarily on astrocytes (Maragakis *et al* 2004a, Maragakis *et al* 2004b, Rothstein *et al* 1996), but also expressed by oligodendrocytes (Danbolt 2001, Werner *et al* 2001). Many reports have suggested a decrease in glutamate transporter expression and increased activation of glutamate receptors as being associated with glutamate excitotoxicity in MS (Danbolt 2001, Frigo *et al* 2012, Kostic *et al* 2012). Glutamate binds with glutamate receptors expressed on postsynaptic neurons including the a-amino-3-hydroxy-5-methyl-4-isoxazolepropionic acid (AMPA), N-methyl-D-aspartate (NMDA) and kainite receptors causing the initiation of signalling cascades (Stojanovic *et al* 2014). Yet in MS an increase in glutamate within the CNS occurs due to inflammatory mediator actions and

the release of glutamate from infiltrating cells (Stojanovic *et al* 2014). It has been proposed that glutamate excitotoxicity in MS is the result of decreased glutamate transporter action and therefore an impairment of excess glutamate uptake. This contributes to a surplus amount of glutamate available in the CNS that leads to the overstimulation of NMDA receptors (Stojanovic *et al* 2014). The beneficial effects of glutamate receptor antagonists used in EAE studies provides additional evidence to support the involvement of glutamate in MS pathology (Stojanovic *et al* 2014). Prolonged activation of glutamate receptors directly damages not only neurons but also oligodendrocytes (Matute 2006). As a result of an altered glutamatergic system, an impairment of calcium homeostasis, activation of nitric oxide synthase (NOS), generation of free radicals, programmed cell death and consequently progressive neurodegeneration could occur (Mehta *et al* 2013).

In this current study there was an increased level of EAAT1, EAAT2 and GS expression by astrocytes in MS lesion centres in comparison to the surrounding NAWM and control samples. However, these differences failed to reach statistical significance, most probably explaining the contradictory qualitative findings that suggested a reduced expression of EAAT1, EAAT2 and GS by astrocytes in MS lesion centres compared to the surrounding control/NAWM. A reduced expression in these key proteins supports existing literature, suggesting that in MS an impaired astrocyte glutamate regulation leads to glutamate excitotoxicity, a contributing factor in the development of MS (Frigo *et al* 2012, Kostic *et al* 2012).

Astrocytes express EAAT1 and EAAT2 in domains that are close to the sites of neuronal release of glutamate. Consequently astrocytes have the ability to react to increases in glutamate levels by redistributing their transporters for optimum uptake of excess glutamate within the CNS (Shin *et al* 2009). The expression of these particular transporters by astrocytes has been studied in different neurological diseases such as motor neuron disease (MND) (Honig *et al* 2000) AD (Scott *et al* 2011) and schizophrenia (Nanitsos *et al* 2005). In both MS and EAE, a reduction in EAAT1 and EAAT2 expression has been shown by IHC and WB (Olechowski *et al* 2010, Pampliega *et al* 2008, Vercellino *et al* 2007) contradicting the current IHC study. Research into memory impairment in MS patients also identified the decreased astrocyte expression of EAAT1 and EAAT2 by WB despite the presence of strong astrogliosis within the hippocampus (Dutta *et al* 2011). This study is also supported by the loss of EAAT2 staining in cortical MS lesions in areas of demyelination and inflammation, due to the

loss of astroglial expression rather than loss of astroglial cells which are relatively intact in lesions (Vercellino *et al* 2007). The decrease in both transporters EAAT1 and 2 could ultimately lead to an increase in extracellular levels of glutamate associated with glutamate excitotoxicity, a possible mechanism underlying MS pathogenesis.

However in contrast, oligodendrocytes have been shown to express the highest level of the glutamate transporters within the CNS, this expression was reduced within MS WM lesions centres, where oligodendrocytes had been depleted (Werner *et al* 2001). Carrying out dual labelling with EAAT1/2 and specific cell markers for astrocytes and oligodendrocytes, such as Olig-2, would clarify whether the expression is restricted to oligodendrocytes over astrocytes as previously described (Domercq *et al* 1999, Werner *et al* 2001). An obvious limitation to carrying out these proposed dual IHC studies is the lack of a specific antibody that only labels astrocytes and that labels all astrocyte populations. The EAAT1/2^{+} stellate cells, quantitatively assessed in the current study, morphologically resembled astrocytes and not smaller oligodendrocytes. The limitation with Werner's 2001 study is the patient cohort size. Only six patients were investigated, 3 patients had PPMS consisting of a variety of lesion types and 3 patients had SPMS all with silent lesions. Evidently this indicates the potential bias of the study, but also highlights possible differences in cellular expression of the transporters as a result of different disease courses of the patients.

EAAT2^{+} cells with the same morphology and distribution as GFAP^{+} cells have been reported in active and chronic active lesions (CAL) directly supporting the non-significant quantitative findings of the current study (Newcombe *et al* 2008). Likewise, the occasional EAAT1^{+} branched process bearing astrocyte was detected in control WM (Newcombe *et al* 2008) supporting current results. Similarly in agreement to the current study, an increase in EAAT1 messenger RNA (mRNA) and protein levels in the optic nerve from MS subjects correlated with an increased uptake of glutamate in these particular subjects (Vallejo-Illarramendi *et al* 2006). Overall these findings reinforce the potential differences in cellular and anatomical expression of the transporters between individuals.

In support of the regional differences in glutamate transporter expression, animal models of MS have shown GLAST to be distributed differently between regions of the rat brain, with a marked reduction seen in the cerebellum at peak EAE disease (Mitosek-Szewczyk *et al* 2008). As well, GLAST mRNA and protein levels were related inversely throughout the course of the disease (Mitosek-Szewczyk *et al* 2008).

In comparison, in transgenic mice GLAST was seen to be more highly expressed in the dentate gyrus, cerebellum and hippocampus, while GLT-1 expression was localised to the cortex, spinal cord and hippocampal grey matter (Regan *et al* 2007). Similar regional differences in glutamate transporter expression between the WM and cortical regions of cuprizone treat mice has been detected (Azami Tameh *et al* 2013). TNFα released by infiltrating T cells has shown to increase microglial release of TNFα resulting in a reduction of EAAT1 expression by astrocytes, leading to glutamate excitotoxicity in a rat EAE model (Korn *et al* 2005). Similarly within MS WM lesions TNFα, released by infiltrating T cells and by resident glial cells, could reduce EAAT1 expression leading to an impaired regulation of glutamate.

Opposing qualitative and quantitative findings of EAAT1/2 and GS immunoreactivity within the current study suggests that more cases are needed to be investigated in order to provide more corroborative and significant results. As highlighted throughout this thesis, investigating PM material represents a single snap shot of that individual's disease process. Investigating PM material provides no knowledge of how a particular lesion developed or would have developed if the patient had lived longer, which could provide the explanation for such varied and non-significant findings in the current study.

As well, variation between the different fields of vision or ROI applied for both the qualitative and quantitative assessment of each case could contribute to the large variation in findings. Differences in the sampling of IHC ROI for quantitative analysis has been identified in other studies (Dunstan *et al* 2011, Makkink-Nombrado *et al* 1995, Mikkelsen *et al* 2011), appearing to be the major cause of lack of reproducibility, which could also apply in the current study. Clearly a more strict sampling protocol of ROI is mandatory to obtain reproducible, quantitative IHC results. However, this poses a challenge when studying MS human subjects with varying lesion size, disease stage and individual differences. Consequently, a random selection of 5 ROI for quantitative measurement in this study may not have been a true representation of EAAT1/2 and GS expression in human subjects.

Clearly there are many studies investigating the role of glutamate transporters in MS pathology, however the overall findings are inconclusive. With MS being a heterogeneous disease with ever changing lesional activity, understanding the complex interplay between neurons and glia cells is crucial. A more systematic characterisation of astrocyte glutamate transporters and associated enzymes in relation to

neuropathology within the brain is needed. A greater understanding of their cellular expression, role in excitotoxicity, and effect on MS pathogenesis could potentially be used as a therapeutic target in prevention of disease progression.

2.5.3 GS expression in MS lesions plays a role in glutamate excitotoxicity

GS is the enzyme responsible for the conversion of glutamate and ammonia to glutamine in the glutamatergic system. The expression of GS is highly regulated and mediated by a number of substances such as insulin, thyroid hormone and corticosteroid hormone (Suarez *et al* 2002). GS is also expressed at various levels in different regions within the brain as identified in human MS and EAE animal studies (Castegna *et al* 2011, Hardin-Pouzet *et al* 1997, Werner *et al* 2001). The expression of GS in the brain is localised to areas where glutamate binding and clearance is essential to prevent excitotoxicity, such as glutamatergic nerve terminals (Eid *et al* 2013). GS is predominantly expressed by astrocytes at their proximal endfeet, and to a lesser degree by oligodendrocytes (Tansey *et al* 1991).

In this current study a non-significant increase in GS expression was identified in all lesion types in comparison to the surrounding NAWM and control WM, however a contrasting qualitative analysis representing a reduction in immunoreactivity within all lesion types. A band of hypertrophic GS^+ astrocytes were located at the perilesional edge of a number of LA lesion, as reported in previous studies (Newcombe *et al* 2008). This finding suggests that as perilesional astrocytes become reactive in response to increased levels of glutamate within the lesion centre, they increase GS expression in an attempt to prevent the spread of glutamate excitotoxicity and ultimately lesion spread. This accumulation of intracellular glutamate coupled to potassium uptake and accumulation of water could ultimately lead to cell death. Therefore the presence of amoeboid macrophages within EA lesions and surrounding LA lesions may not only be a result of on-going demyelination present in those areas but also due to cell death, including astrocyte death, as a result of increased levels of glutamate. In order to identify the distribution of glutamate within the MS CNS tissue further IHC with glutamate antibodies would help to clarify this. As well, additional work looking at possible apoptotic/cell damage markers associated with astrocytes would need to be carried out to confirm this hypothesis. Prolonged damage and death of astrocytes may lead to additional impairment of glutamate regulation exacerbating neuronal and glial cell damage (Newcombe *et al* 2008). Another implication of astrocyte swelling and oedema is the disruption of the BBB, which could lead to the infiltration of immune

cells and consequently immune responses associated with MS (Hardin-Pouzet *et al* 1997).

From previous human studies, the cellular localisation of GS in MS is of huge debate. In comparison to the current work, the presence of GS^+ hypertrophic microglia at the perilesional edge of active lesions has been identified (Werner *et al* 2001). As this current study was primarily focussed on characterising the astrocyte phenotype in MS, the presence of GS^+ microglia was not investigated. In previous studies, on normal WM, high level expression of GS was localised to $CNPase^+$ oligodendrocytes, yet in MS active lesions GS immunoreactivity was lost from oligodendrocytes and primarily associated with astrocytes and microglia (Werner *et al* 2001). This study concluded that an absence of glutamate metabolising enzymes from oligodendrocytes demonstrated the importance of this cell type in regulating glutamate homeostasis, however this study failed to appreciate the loss of oligodendrocytes in MS lesions (Werner *et al* 2001). In comparison GS has shown to be localised to microglia in control WM, and macrophage /astrocytes in active plaques (Newcombe *et al* 2008) which support our findings. These differences in cellular expression of GS may be explained by the variances in patient cohorts, as it is known that the course of MS is diverse between subjects. Also the different antibodies and IHC methodologies used between studies could account for the differences, as discussed later in this chapter.

In EAE models the severity of disease has been associated with a reduction in GS expression and elevation of glutamate. The loss of astrocyte GS function within the cortex of mice has been shown to result in glutamate excitotoxicity, identifying the possible pathophysiological process of glutamate excitoxicity occurring in the absence of inflammation or lesions (Castegna *et al* 2011). A potential therapeutic treatment, the anti-oxidant, fullerene ABS-75, was shown to rescue GS expression in the WM of mice with chronic progressive EAE (Basso *et al* 2008). This anti-oxidant reduced astrocyte expression of CCl2, a chemokine attractant for monocytes and leukocytes, but also the driver of inflammation, known to increase oxidative damage and add to the impairment of glutamate homeostasis by downregulating GS expression in glial cells (Basso *et al* 2008). Possibly this could account for the impaired glutamate regulation associated with MS.

In contrast to the current study findings, previous human PM studies have identified a reduction in GS expression in a range of neurological diseases, including AD (Boyd-

Kimball *et al* 2005, Butterfield *et al* 2006) and epilepsy (Eid *et al* 2004, Eid *et al* 2013). A uniform reduction in GS expression in the cortical regions of AD patients has been described, however this study failed to report WM expression (Robinson 2001). Similarly, reduced GS expression in the hippocampus of temporal lobe epilepsy patients has been shown (Eid *et al* 2004), but in this study the glutamate transporter levels remained constant (Eid *et al* 2004). The link between a reduced GS expression and increased IL-1 and TNFα associated inflammation and BBB disruptions in epilepsy, supports the MS studies that show inflammatory conditions reduces levels of glutamate transporters and GS (Hardin-Pouzet *et al* 1997, Korn *et al* 2005, Muscoli *et al* 2005). As well, decreased GS expression in the brain has been seen in neurodegenerative disorders involving iron mediated oxidative stress (Fernandes *et al* 2011). The reduction of GS expression in cultured astrocytes was not reliant on hydrogen peroxide (H_2O_2) alone but needed the presence of redox-active iron (Fernandes *et al* 2011). Iron induced oxidative stress and reduced GS expression has been documented in a number of neurological diseases including stroke (Carbonell & Rama 2007) AD (Barnham & Bush 2008, Bishop *et al* 2002), and PD (Barnham & Bush 2008).

Evidently from the existing literature and current qualitative analysis a reduction in not only GS but EAAT1/2 immunoreactivity within MS lesions contributes to an increased level of glutamate excitotoxicity. Therefore more confirmative experiments on increased patient numbers may elucidate more corroborative quantitative data.

2.5.4 ALDH1L1 expression in the cortex versus the white matter (WM)

Since its identification as an astrocyte marker (Neymeyer *et al* 1997), there are an increasing number of studies into ALDH1Ll and its possible function in the brain. Characterisation of the astrocyte, neuronal and oligodendrocyte transcriptome has shown an increased level of ALDH1L1 mRNA associated with astrocytes throughout the mouse/rat brain, in comparison to GFAP, which was predominantly expressed in the WM (Cahoy *et al* 2008). Complementary immunohistochemical staining further demonstrated an increased number of $ALDH1L1^+$ astrocytes compared to $GFAP^+$ astrocytes in rat tissue, with ALDH1L1 immunoreactivity associated with astrocyte cell bodies and extensive processes (Cahoy *et al* 2008). In contrast, while there was a considerable amount of ALDH1L1 immunoreactivity associated with astrocytes within the cortex, no immunoreactivity was detected within the WM in the current study. Furthermore, the immunoreactive staining profile in the cortex, detected astrocyte cell bodies and immediate processes rather than the extensive processes detected in the

Cahoy *et al* 2008 paper. A novel finding in this current study was the presence of ALDH1L1^{+} cells that morphologically resembled oligodendrocytes, conflicting with reports that ALDH1L1 is an astrocyte-specific cell marker (Anthony & Heintz 2007, Cahoy *et al* 2008, Neymeyer *et al* 1997). However this finding should be confirmed by dual labelling with ALDH1L1 and a specific cell marker for oligodendrocytes, such as OLIG-2.

To date, very few studies have examined ALDH1L1 expression in the human brain (Barley *et al* 2009, Rodriguez *et al* 2008b, Serrano-Pozo *et al* 2013a). ALDH1L1 protein is downregulated in certain forms of pilocytic astrocytomas (PAs) which are associated with aggressive histological features and with increased cellularity and necrosis. Looking at ALDH1L1 expression in the neural tube during CNS development showed increased ALDH1L1 expression correlated with a decrease in cellular proliferation (Anthony & Heintz 2007). These papers suggest that ALDH1L1 negatively regulates cellular proliferation, further supported by non-CNS studies which have also demonstrated that a decrease in ALDH1L1 expression is associated with increased cellular proliferation in prostate and lung cancer (Krupenko & Oleinik 2002).

Currently there is only one immunohistochemical study into ALDH1L1 expression in human neurodegenerative disease which concluded that ALDH1L1 was a constitutive astrocyte marker in the cortex of AD patients (Serrano-Pozo *et al* 2013a). However identification of ALDH1L1 as an astrocyte marker was based on findings of previously published animal work on ALDH1L1 (Cahoy *et al* 2008, Zamanian *et al* 2012). Reactive astrocytes were identified as GFAP^{+}/ALDH1L1^{+} cells while GFAP^{-} /ALDH1L1^{+} were identified as resting astrocytes, this research shows the heterogeneity of astrocytes and the need for a marker that labels all astrocytes regardless of their activation state (Serrano-Pozo *et al* 2013a). Across three neurological diseases including schizophrenia, major depression and bipolar disorder, ALDH1L1 was identified as an astrocyte-associated gene, correlating with GFAP expression which was also linked to patient age, while no age correlation was seen with ALDH1L1 gene expression (Barley *et al* 2009).

The majority of research on ALDH1L1 is from animal models (Anthony & Heintz 2007, Cahoy *et al* 2008, Dougherty *et al* 2012, Doyle *et al* 2008, Foo & Dougherty 2013, Neymeyer *et al* 1997, Pfrieger & Slezak 2012). The overall role and function of

ALDH1L1 is unknown in the brain and research into the expression of the enzyme throughout the brain has shown variable results. Within the CNS, ALDH1L1 has shown to completely label all astrocytes (Foo & Dougherty 2013), as shown in other studies (Barreto *et al* 2011, Cahoy *et al* 2008, Yang *et al* 2011) yet in contrast this current study and others detected localisation of the ALDH1L1 to astrocytes in the cortex in humans (Serrano-Pozo *et al* 2013a). A decrease in ALDH1L1 mRNA, protein and promoter activity in astrocytes isolated from the spinal cord of post natal ageing mice has been reported, yet a considerable increased ALDH1L1 expression was seen in reactive astrocytes in the diseased equivalent animals (Yang *et al* 2011). In contrast, a stroke mouse model found the expression of $ALDH1L1^{+}$ astrocytes remaining constant both pre- and post- stroke (Barreto *et al* 2011).

Evidently the expression of ALDH1L1 by astrocytes is associated with a number of factors including regional variation in the brain, disease and species specificity, and possibly by the age of subjects. All these factors must be studied further to gain a greater understanding of the role of ALDH1L1 in the brain and its usefulness as a potential marker of astrocytes in human studies.

2.5.5 CD44 detection in frozen tissue

When investigating the astrocytic expression of CD44, no staining was seen in the FFPE sections when using a range of antigen retrieval techniques combined with either manual or automated IHC methods. This was in contrast to the CD44 positive staining detected in frozen tissue, which labelled astrocytes in the WM, with processes which formed thick end feet on blood vessels, in line with a previous study (Akiyama *et al* 1993). Also in the study on frozen material, CD44 labelled astrocytes with the typical stellate morphology, in addition to astrocyte processes infiltrating into the cortex from the WM. The heterogeneity of the astrocyte phenotype and different pattern of astrocyte cell identification is especially apparent when using CD44 staining in frozen tissue samples.

CD44 is a receptor for osteopontin (OP) and HA amongst many other proteins and is implicated in inflammation associated with neuronal injury. CD44 has been suggested to play a role in CNS inflammation by recruiting inflammatory cells into the CNS (Brennan *et al* 1999, Brocke *et al* 1999) especially in diseases with BBB dysfunction (Matsumoto *et al* 2012). Expression of CD44 is also highly upregulated by glial cells in demyelinating conditions including EAE and MS (Back *et al* 2005, Girgrah *et al* 1991, Kim *et al* 2004) but also in other neurological conditions including AD (Akiyama *et al*

1993, Vogel *et al* 1992) tuberous sclerosis (Arai *et al* 2000), ALS (Matsumoto *et al* 2012) and gliomas (Hagel & Stavrou 1999, Zeltner *et al* 2007).

To date, there are very few studies investigating CD44 expression in human CNS material in relation to neurological disease. In vanishing white matter (VWM) disease the colocalisation of $CD44^+/GFAP^+$ astrocytes was identified in the WM and no other $CD44^+$ cell type was identified (Bugiani *et al* 2013). Snap frozen CNS tissue from MS patients was used as disease controls and the presence of $CD44^+/GFAP^+$ cells within and around chronically demyelinated MS lesions were supported by WB and qPCR analysis (Bugiani *et al* 2013). It has previously been shown that HA accumulates in regions of $CD44^+$ astrocytes in chronically demyelinated lesions in MS, increased HA prevents the maturation of OPC and therefore inhibits remyelination (Back *et al* 2005, Struve *et al* 2005). It is thought that HA is broken down into lower molecular weight units which block the maturation of OPC through the expression of toll-like receptor (TLR)2, a receptor for HA. In support of this concept, the over expression of TLR2 in MS tissue was seen in the (Bugiani *et al* 2013) study.

In contrast to the current study, in stroke patients the upregulation of CD44 was seen in snap frozen infarct tissue in both the cortex and WM, particularly associated with inflammatory cells (Al'Qteishat *et al* 2006). Also, negative CD44 expression was observed in control WM and weak expression in the cortex. The colocalisation of $CD44^+/GFAP^+$ astrocytes has been identified in brain tumours (Hagel & Stavrou 1999, Zeltner *et al* 2007) and CD44 expression correlated with tumour grading (Hagel & Stavrou 1999). It has been proposed that $CD44^+$ astrocytes located at the tumour border induce the production of increased levels of HA leading to increased extracellular space in which tumour cells can grow, divide and expand into. In relation to MS, an increased expression of $CD44^+$ astrocytes could lead to the accumulation of increased HA that disrupts the BBB facilitating the infiltration of immune cells leading to disease progression (Flynn *et al* 2013, Matsumoto *et al* 2012).

In vivo studies using EAE models of MS have shown that increasing levels of TNFα and IFNγ result in cell activation, inflammation and immune reactions within the CNS inducing the expression of CD44 in astrocytes (Haegel *et al* 1993). An increase in glial CD44 expression has been demonstrated at the border of WM lesions in a mouse EAE model (Haegel *et al* 1993), while increasing expression of CD44 by astrocytes in the WM is associated with disease progression in a rat EAE model (Kim *et al* 2004). The role of increased astrocytic expression of CD44 in the pathogenesis of EAE is unclear, it

has been suggested that CD44 expression by astrocytes regulates OP thereby contributing to repair (Kim *et al* 2004). The removal of CD44 has been shown to prevent the recruitment of leukocytes and inhibit the development of EAE (Brennan *et al* 1999, Brocke *et al* 1999, Guan *et al* 2011). In contrast, a deficiency in CD44 has shown to enhance EAE, possibly due to the accumulation of the CD44 ligand HA, leading to a more adhesive endothelial cell surface resulting in increased leukocyte extravasation (Flynn *et al* 2013). These studies demonstrate the confounding issues researching the role of CD44, including the use of different mouse/rat strains, inflammatory models and experimental approaches which make comparing these studies and relating them to human disease challenging (Flynn *et al* 2013).

2.5.6 Limitations of IHC on human PM CNS material.

There are a number of technical factors that contribute to the conflicting research findings from IHC studies, including the IHC methods followed, the tissue type used and the different antibodies applied. For example, there are differences between the IHC protocols used in the two studies investigating glutamate transporters (Werner *et al* 2001) and (Vercellino *et al* 2007). Firstly, frozen CNS tissue was used in the former study in comparison to FFPE CNS tissue in the latter study. The different types of tissue used involve the use of different fixative methods, acetone versus formalin which may affect the IHC outcome (Shi *et al* 2011). Secondly, FFPE tissue requires antigen retrieval that could alter the way in which antibodies recognise the antigen and therefore comparing results between studies is challenging (Engel & Moore 2011). Thirdly, different primary antibodies were used in two studies for example in the (Vercellino *et al* 2007) study, monoclonal anti-EAAT antibodies sourced from Novacastra were used as were in the current study, while the (Werner *et al* 2001) sourced polyclonal antibodies from Alpha Diagnostics, which are no longer in production. Similarly when using a polyclonal CD44 antiserum on frozen tissue the upregulation of CD44 was identified in WM lesions of MS patients (Girgrah *et al* 1991), despite many attempts to achieve staining with monoclonal CD44 antibodies on FFPE tissue (Girgrah *et al* 1991). These particular factors must be considered when reviewing the results from this current histological study. When using a monoclonal CD44 antibody (Dako, UK) immunoreactivity was only present in the frozen CNS samples over the FFPE CNS samples. Monoclonal antibodies only recognise one single epitope on the antigen in question, making them very specific. Consequently a limitation to this specificity is the vulnerability of FFPE tissue losing the single epitope as a result of chemical treatment during fixation or during antigen retrieval resulting in IHC failure (Lipman *et al* 2005).

Being able to source a polyclonal antibody recognising multiple epitopes of the antigen may be advantageous, yet care must be taken when interpreting positive staining as polyclonal antibodies have a tendency to cross react between proteins causing non-specific background staining (Lipman *et al* 2005). Also by using a combination of monoclonal antibodies in IHC may help improve results (Lipman *et al* 2005).

The 'gold standard' of IHC has been debated extensively in the literature (Arber 2002, Boenisch 2005, D'Amico *et al* 2009, Engel & Moore 2011, Shi *et al* 2008, Shi *et al* 2007, Shi *et al* 2011, Yamashita & Okada 2005). Aldehyde fixation has been a major explanation as to the failure of IHC in previous years. Yet the morphology, storage and surplus amount of archival FFPE tissue in hospital and research laboratories indicates that this source is more favourable over frozen tissue, which suffers from poor morphology affecting IHC outcome, and also requires specific storage conditions. Ultimately the fixation of the tissue used in this study and the particular antibodies employed (i.e. monoclonal anti-CD44, Dako, UK) may explain the poor IHC outcome. Alternative antigen retrieval methods such as the use of enzymatic antigen retrieval may need to be explored, or alternative polyclonal antibodies sourced.

Another limitation when comparing histological studies is not only the type of material used (frozen/FFPE) but the species investigated. As the majority of ALDH1L1 studies are on animal models care must be taken when comparing IHC findings between species, what is seen in the animal may not be apparent in the human.

Other factors to consider when interpreting current IHC findings is the possibility of astrocyte subtypes and differences in marker expression between anatomical locations investigated. Without further investigation into alternative brain regions and increased patient cohort size the current study is limited, which may otherwise provide more statistical relevant results rather than qualitative differences in the staining pattern for the glutamate transporters and enzymes. A limited patient cohort size has been a weakness in many human histological studies (Newcombe *et al* 2008, Vallejo-Illarramendi *et al* 2006, Vercellino *et al* 2007, Werner *et al* 2001). By broadening out the study to include different lesion types from different disease courses, in addition to increasing the number of control samples for comparison, a greater understanding of the astrocyte phenotype in MS pathogenesis could be revealed.

2.5.7 Conclusion

In conclusion, without a good pan astrocyte marker, detection of all astrocytes in the CNS remains challenging. The differences in astrocyte morphology and phenotype is demonstrated by each of the antibodies used in this study and suggests there are distinct astrocyte subpopulations. Deciphering the differences between these subclasses of astrocytes and their role in CNS physiology/pathology is fundamentally important. Furthermore, this study demonstrates that astrocytes are very sensitive to changes within the CNS and in MS are continuously changing and adapting to the demands of the disease. Future histological studies on a larger cohort of well-defined, classified MS CNS tissue from different disease courses would provide a further insight into the phenotype of astrocytes in the disease. Having access to biopsy samples at different stages of disease course, and not just at PM would allow a better understanding of the involvement of astrocytes in the development of the disease. Evidence provided from this study, as supported by previous work by others, suggests that astrocytes become hypertrophic with lesion progression and show a dysregulation of glutamate homeostasis within lesions. This study also highlights that currently GFAP is the best astrocyte marker at clearly identifying astrocytes within MS NAWM which will be used in proceeding work. Overall, the alteration of the astrocyte phenotype in MS suggests a change in the normal astrocyte function and potential role of this cell in disease pathogenesis.

CHAPTER 3

ISOLATION OF ENRICHED GLIAL CELL POPULATIONS FROM POST-MORTEM CENTRAL NERVOUS SYSTEM TISSUE

3.1 Introduction

Identifying transcriptomic changes within cells of the CNS from both control and disease cases may enhance our understanding of the underlying mechanisms of disease. Currently the majority of gene expression work in human subjects is carried out on whole tissue (Bossers *et al* 2009, Grunblatt *et al* 2007, Murray 2007, Wang *et al* 2006), or on individual cell lines or animal models of disease which, despite having many advantages, fail to fully replicate human disease processes (Jucker 2010). LCM allows the isolation of specific ROI, or an enriched cell population from human tissue (Emmert-Buck *et al* 1996). This technique has since been developed further by incorporating histochemistry (Chu *et al* 2009, Cunnea *et al* 2010, Greene *et al* 2010) and IHC to provide effective isolation of particular cells of interest from human PM tissue (Bi *et al* 2002, Fend *et al* 2000, Simpson *et al* 2011, Waller *et al* 2012).

Prior to LCM, the methods used to isolate cells or ROIs from heterogeneous tissue samples involved crude manual techniques including tissue dissection using scalpels or razor blades (Ren *et al* 1996), to more developed techniques including dissection needles (Beaty *et al* 1997, Going & Lamb 1996). However, there are a number of limitations with these manual methods of dissection including: contamination from other cell types or from the instrumentation employed (Burgemeister 2011). Other problems include the limited accuracy and precision, and the capability to effectively isolate specific cell-types from tissue, even under dissection microscopy.

Laser-assisted dissection methods were developed in the 1990s and enabled the isolation of cells or specific ROI in tissue proving to be faster, more reliable and an easier method to perform than manual dissection techniques. In general two methodologies were developed, the major difference between them being the laser employed (Emmert-Buck *et al* 1996, Schutze & Lahr 1998). One methodology uses an infra-red (IR) laser, which involves the placing of a cap with a thermoplastic film applied to the lower surface on top of a histological tissue section. Under microscopy the IR laser is guided over the ROI/cells and fired briefly causing the film to heat, melt and adhere to the ROI/cells (Figure 3.1). Upon removal of the cap from the tissue section, the ROI is removed leaving behind the remaining tissue (Emmert-Buck *et al* 1996). The film can then be transferred to buffers allowing for extraction of RNA/DNA or protein.

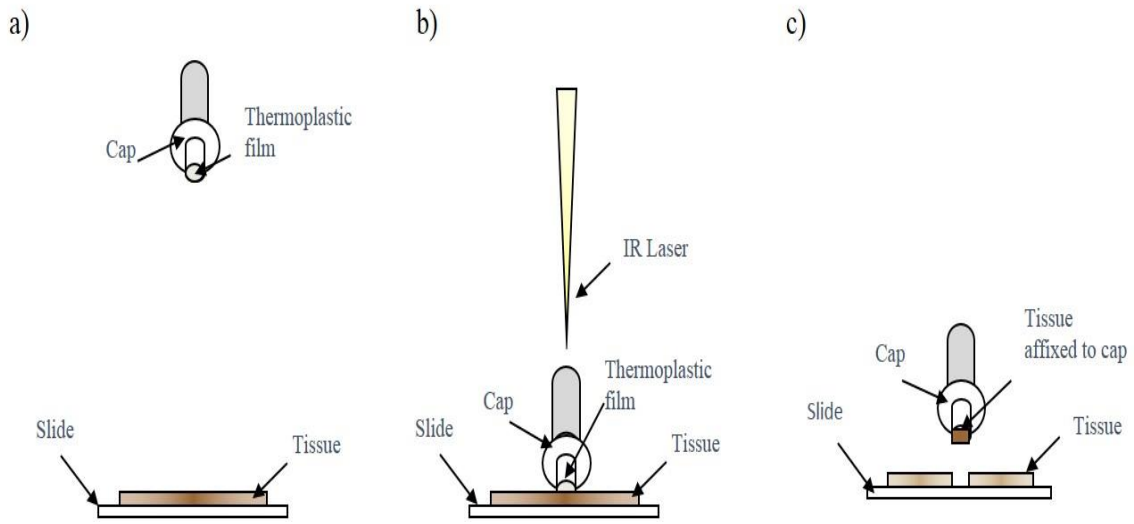

Figure 3.1 Overview of the laser capture microdissection procedure

A histological tissue section is collected onto an uncharged glass microscope slide (a). A film cap is lowered onto the tissue section and the infrared (IR) laser beam fired over the cells/ROI briefly heating and melting the thermoplastic film, causing the adherence to the cell/ROI (b). On lifting the cap from the tissue section, the isolated cells/ROI are also removed leaving behind the surrounding tissue (c).

In comparison, the alternative methodology developed used an ultra-violet (UV) laser to cut out cells or ROI and an increase of the laser power causes the transfer of isolated cells/tissue into a collection vessel (Schutze & Lahr 1998). The extraction of RNA, DNA and/or protein from the isolated cells enables specific gene/protein expression changes in diseased versus control samples to be determined.

Not all PM CNS tissue is suitable for LCM isolation of cells for gene expression analysis, as there are a number of factors that impact the RNA quality of the material and which must be considered when identifying suitable cases for LCM and subsequent transcriptomic studies. When carrying out LCM it has been reported that a general decline in sample RNA integrity number (RIN) occurs (Mazurek *et al* 2013, Waller *et al* 2012). The RIN is a numerical value ranging from 1-10, given to a biological sample as a measure of RNA quality based on the 28S/18S ribosomal peak ratio, with increasing degradation leading to a fall in ratio and decrease in the RIN (Figure 3.2). To ensure the gene expression data is comparable across different tissue samples, it is desirable that all cases have similar RINs prior to LCM (Strand *et al* 2007). However this statement has been contradicted, with one microarray study investigating PM CNS tissue showing reliable results over a range of RINs (RIN 1.0-8.5) (Trabzuni *et al* 2011). In general, the RIN is recognised as the numerical standard to assess RNA quality for genetic studies, yet its true relevance to downstream applications is continuously being questioned (Koppelkamm *et al* 2011, Stan *et al* 2006).

Microarray analysis enables the identification of genome wide transcriptional changes in diseased versus control samples of either human or animal disease models. The expression of thousands of mRNA transcripts from various disease/control samples can be quantified and comparisons made between their gene expression profiles. The basis underpinning the technique involves the hybridisation of sample mRNA molecules to single stranded complementary DNA (cDNA) probes, designed as oligonucleotide sequences which are adhered to a glass slide. The mRNA is labelled with a fluorescent tag and it's signal intensity is a measure of quantity of mRNA molecules that have hybridised to the probe, which is proportional to the amount of transcript in that particular sample (Courtney *et al* 2010).

To date, only 14 microarray gene expression studies have been completed on MS CNS brain tissue, 12 of which were reviewed by (Dutta & Trapp 2010) with two more recent studies using LCM to identify gene expression of particular areas within the MS brain including microdissected blood vessels (Cunnea *et al* 2010), and active MS

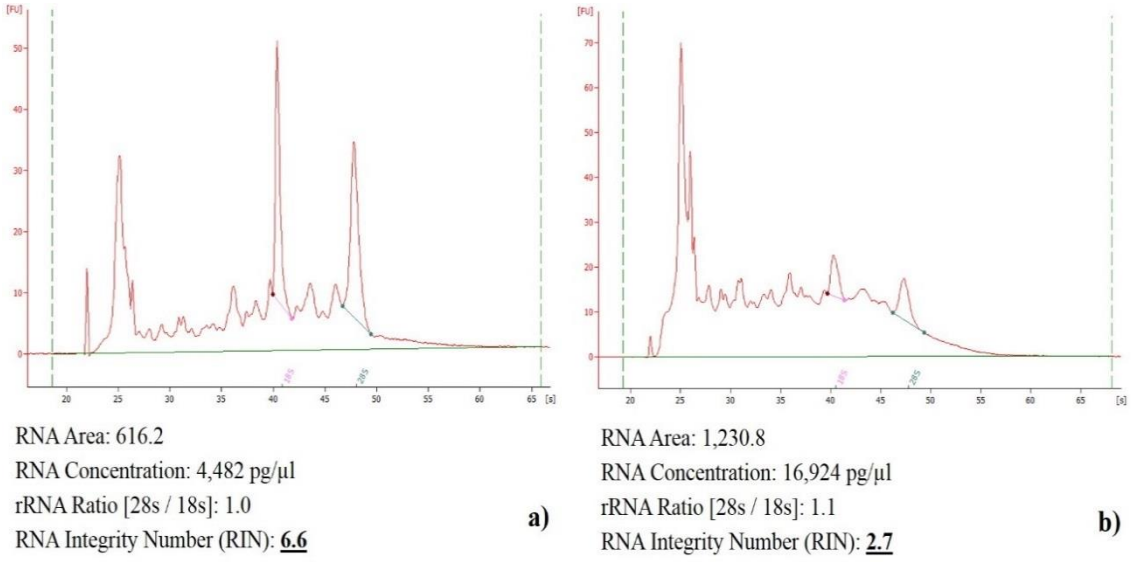

Figure 3.2 RNA integrity of PM CNS samples

The quality of each PM CNS sample was assessed on a 2100 bioanalyzer, an example of a suitable case for LCM with a RIN value of 6.6 (a). An example of a highly degraded PM CNS sample which would not be taken forward to LCM with a RIN value of 2.7 (b).

y-axis represents fluorescence units, (FU) and *x-axis* represents runtime in seconds, (s).

lesions (Mycko *et al* 2012). Using LCM to isolate particular cells of interest enables gene expression microarray, qPCR, and mass spectrometry experiments to be performed on an enriched cell population, in order to gain a better understanding of the transcriptomic and proteomic events in disease pathogenesis.

Ultimately the advantages of working with an enriched cell population is that it allows for a greater understanding of the role/function of that particular cell in a range of neurological conditions. When investigating a heterogeneous cell population (i.e. whole tissue samples) valuable data maybe masked and the association of potential pathogenic function to cell type lost. Therefore LCM aids the discovery of genes that could potentially indicate novel mechanisms that contribute to disease progression. Glial cells within the CNS are defined by their specific morphology and function and are comprised of 3 cell types; these include the most abundant cell type in the CNS, astrocytes, as well as oligodendrocytes and microglia. Glial cells provide essential neuronal support and their dysfunction can contribute to disease (Kettenmann & Verkhratsky 2008, Sobel & Moore 2008). Astrocytes provide neurotrophic support, maintain CNS homeostasis by regulating the extracellular environment, are components of the tripartite synapses involved in synapse function and plasticity, and participate in CNS immune responses (Fellin 2009, Jensen *et al* 2013, Perea *et al* 2009, Volterra & Meldolesi 2005). Oligodendrocytes primarily form the insulating myelin sheath that surrounds axons enabling efficient signal transduction in the CNS (Peferoen *et al* 2013, Sobel & Moore 2008). Microglia, which form around 10-20% of the total glial cell population within the CNS (Peferoen *et al* 2013), are the macrophages of the brain and spinal cord, forming the basis of the immune system of the CNS (Sobel & Moore 2008). Glia have been shown to contribute to a range of neurological disorders, including MS (Sriram 2011), AD (Naert & Rivest 2011, Serrano-Pozo *et al* 2013b, Verkhratsky *et al* 2010), PD (Fellner & Stefanova 2013, Halliday & Stevens 2011), MND (Lasiene & Yamanaka 2011), Huntington's disease (Hsiao & Chern 2010) and stroke (Thiel & Heiss 2011, Zhao & Rempe 2010). Also more recently glial cells have been proposed as having an involvement in neuropsychiatric diseases such as schizophrenia (Goudriaan *et al* 2013). As identified in many of these studies, glial cells contribute to and/or prevent disease pathogenesis, yet the understanding of each glial cells' specific role is continuously debated, therefore a better understanding of each cell specific roles in disease is fundamental.

This chapter describes the detailed methodology used to isolate an enriched population of each of these 3 glial cell types from PM CNS tissue, acknowledging the advantages and limitations of using PM CNS material in transcriptomic studies, along with combining rapid immunostaining of tissue sections with LCM. The study also verifies the enrichment of each glial cell population using reverse transcription-PCR (RT-PCR) and details the number of cells required to gain sufficient mRNA for downstream applications including microarray analysis.

3.2 Aims and objectives of the study

The aims of this study were to:

- To identify suitable PM CNS samples for LCM.
- To optimise an immuno-LCM method to isolate glial cells from frozen PM CNS tissue.
- To confirm cell enrichment using RT-PCR, and identify the number of cells needed to provide sufficient mRNA for downstream applications.
- To use the developed immuno-LCM to isolate enriched astrocyte populations from selected MS NAWM and control samples for the use in both transcriptomic and proteomic research.

3.3 Materials and Method

3.3.1 Suppliers

Abcam, 330 Cambridge Science Park, Cambridge, CB4 0FL, UK; **Agilent Technologies**, 610 Wharfedale Road, IQ Winnersh, Wokingham, Berkshire, RG41 5TP, UK; **DAKO UK Ltd.**, Cambridge House, St Thomas Place, Ely, Cambridgeshire CB7 4EX;Cambridge, UK; **Bioline Reagents Ltd.**, Unit 16 The Edge Business Centre, Humber Road, London, NW2 6EW, UK: **Cambridge Bioscience Ltd.**, Munro House, Trafalgar Way, Bar Hill, Cambridge, CB23 8SQ UK; **Eurofins MWG Operon**, Anzinger Str. 7a 85560 Ebersberg, Germany; **Fisher Scientific Inc.**, Bishop Meadow Road, Loughborough, Leicestershire, LE11 5RG, UK; **Leica Microsystems Ltd.**, Davy Avenue, Knowhill, Milton Keynes, MK5 8LB Buckinghamshire, UK; **Life Technologies Ltd.**, (Invitrogen, Arcturus) 3 Fountain Drive, Inchinnan Business Park, Paisley, PA4 9RF, UK; **Newmarket Scientific**, (Solis Biodyne) 9-10 Rosemary House Lanwades Business Park Kennett, Newmarket CB8 7PN, UK; **R&D Systems Europe Ltd.**, 19 Barton Lane, Abington Science Park, Abington, OX14 3NB, UK; **Sigma-Aldrich**, The Old Brickyard, New Road, Gillingham, Dorset, SP8 4XT, UK; **Syngene Europe office**, Sales, Service, Support, Manufacture, Beacon House, Nuffield Road, Cambridge, CB4 1TF; **Thermoscientific**, Stafford House, Boundary Way Hemel Hempstead, Hertfordshire HP2 7GE, UK; **Vector laboratories Ltd.**, 3 Accent Park, Bakewell Road, Orton Southgate, Peterborough, PE2 6XS, UK; **VWR International Ltd.** (Quanta Biosciences), Hunter Boulevard, Magna Park, Lutterworth, Leicestershire, LE17 4XN, UK.

3.3.2 Tissue source

All frozen tissue used in this study was obtained from the UK Multiple Sclerosis Society Tissue Bank and The Sheffield Brain Tissue Bank (SBTB), full ethical permission was obtained (Appendix I). Full clinical information and neuropathological assessment of each case is described in Appendix III. The RIN of each case was determined prior to and post LCM. All cases were from similar anatomical coronal brain slices and had a mean post mortem interval (PMI) time of 10 hours (range 5-18 hours).

3.3.3 Histological classification

Cases were histologically examined by H&E, LFB and CD68 IHC, refer to Appendix III for full details. If there was evidence of inflammation and/or demyelination, the

cases were eliminated from the study. 7µm sections were stained and classified following the protocols described in Chapter 2. As only frozen material was used, the sections did not require dewaxing or antigen retrieval, but were fixed in ice-cold acetone (Fisher Scientific, UK) for 10 minutes or 95% ethanol (Fisher Scientific, UK) for LFB, prior to staining.

3.3.4 Pre-LCM RNA integrity analysis

Snap-frozen tissue blocks of CNS material were selected for LCM based not just on their histological characteristics but also on their initial RNA quality. One section of each brain block (7 µm) was collected into a sterile 0.5 ml Eppendorf tube, and the RNA extracted using the standard Trizol method (Invitrogen, UK). Under sterile conditions 0.5 ml Trizol reagent (Invitrogen, UK) was added to each section of tissue and mixed until dissolved by pipetting. 0.1 ml chloroform (Fisher Scientific, UK) was added, vortexed to mix and left to stand at RT for 10 minutes. Each sample was centrifuged (Sigma centrifuges, UK) at 4°C, maximum speed (16,000g) for 15 minutes. The aqueous layer was transferred into a new sterile 1.5 ml Eppendorf tube where 250 µl isopropanol was added and left at RT for 5-10 minutes. The sample was centrifuged at 4°C, maximum speed (16,000g) for 10 minutes. The supernatant was discarded, the pellet washed with 1.0 ml ice-cold 75% ethanol (Fisher Scientific, UK) and mixed via vortexing. A final centrifugation step was carried out at 4°C, 8,000g for 5 minutes. Samples were left to air-dry before 25 µl of sterile d.H_2O was added to resuspend the pellet. To assess the quantity of RNA, the samples were analysed on a NanoDrop spectrophotometer (Thermoscientific, UK) and the quality of RNA checked on a bioanalyzer (Agilent, UK). Cases with RIN values of less than 4.0 were eliminated from further investigations. All RNA samples were stored at -80°C.

3.3.5 Sample preparation for LCM – rapid IHC

It was vital that all LCM was completed on freshly cut sections to prevent RNA degradation as a result of repeated freeze-thawing of samples (Boone *et al* 2013). Freshly cut, 7µm sections of each case were collected onto uncharged, sterile glass slides (Leica, UK) (6 sections per case) and warmed to RT for 30 seconds. The sections were fixed in ice-cold acetone (Fisher Scientific, UK) for 3 minutes and immunostained using the following modified rapid ABC staining method (Waller *et al* 2012). The protocol was carried out at RT, using sterile solutions made with diethylpyrocarbonate (DEPC)-treated water and under RNase-free conditions. Sections were blocked in the relevant normal 2% serum (Vectastain Elite kit; Vector Laboratories UK) (50 µl serum

Glial antibody	Isotype	Glial specificity	Dilution	Supplier
Glial fibrillary acidic protein (GFAP) (Reske-Nielsen et al., 1987)	Rabbit IgG	Astrocyte	1:50	Dako, UK
Oligodendrocyte-specific-protein (OSP) (Simard et al., 2010)	Rabbit IgG	Oligodendrocyte	1:25	Abcam, UK
CD68 (Aoki et al., 1999)	Mouse IgG1	Microglia	1:10	Dako, UK

Table 3.1 Glial specific primary antibodies

Antibodies used to identify specific cell populations in human PM CNS tissue for isolation by LCM.

in 2.5 ml TBS) for 3 minutes, incubated with a glial specific phenotype marker antibody (Table 3.1) diluted in blocking serum for 3 minutes, and rinsed briefly with TBS. Following a 3 minute incubation with 5% biotinylated secondary antibody (Vectastain Elite kit; Vector Laboratories UK) (50 µl secondary antibody in 1.0 ml blocking buffer), the sections were rinsed with TBS, incubated with 4% horseradish peroxidase conjugated ABC, (Vectastain Elite kit; Vector Laboratories UK) (50 µl drop A, 50 µl drop B in 2.5 ml TBS) prepared at least 30 minutes prior to use, for 3 minutes, and washed briefly with TBS. Antibody staining was visualised with DAB (Vector Laboratories, UK) for 3 minutes. The sections were dehydrated in a graded series of alcohol (Fisher Scientific, UK) (70%, 95%, 100%, 100% for 15 seconds each), cleared in xylene (Fisher Scientific) (15 seconds) and left to air dry at RT in an air flow hood for a minimum of 60 minutes prior to LCM.

3.3.6 Laser capture microdissection (LCM)

LCM was performed using the PixCell II laser-capture microdissection system (Arcturus Engineering, Mountain View, CA, USA) and CapSure Macro caps (Arcturus Engineering, Mountain View, CA). The air dried, immunostained section was overlaid with the CapSure cap, which consists of a thermoplastic film mounted on a transparent cap. A focussed infrared laser was fired through the cap causing the film to melt and adhere to the immunopositive cells (as demonstrated previously in Figure 3.1), and the number of cells captured was recorded. The LCM system was set to the following parameters: 7.5 µm spot size and ~40 mW power. Immunopositive cells were selected for capture using a 20× objective. After microdissection, the film was removed from the cap using sterile tweezers and transferred to a sterile 0.5 ml Eppendorf tube for RNA extraction.

3.3.7 RNA extraction

Total RNA was extracted from the isolated cells using the PicoPure RNA isolation kit (Arcturus BioScience, UK) (Figure 3.3), 50 µl extraction buffer was added to the film and the tube left to incubate at 42°C for 30 minutes. Meanwhile an RNA extraction column was conditioned for use by incubating with 250 µl conditioning buffer for 5 minutes, prior to a centrifugation step at 16,000g for 2 minutes, and the flowthrough discarded. Following the incubation step, 50 µl 70% ethanol was added to the sample and gently pipetted up and down to mix. The sample was transferred to the pre-conditioned column and centrifuged at 100g for 2 minutes to allow the RNA to become

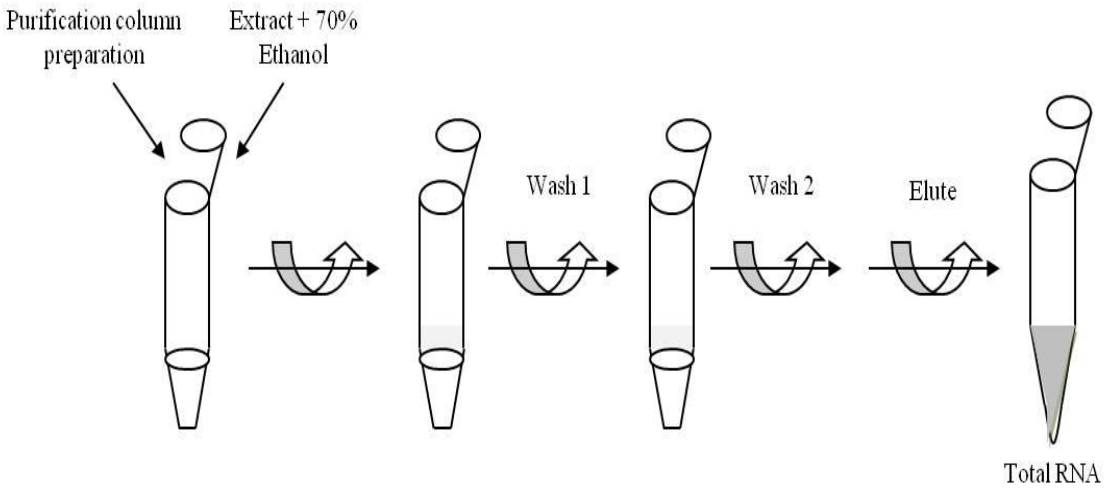

Figure 3.3 Overview of the PicoPure RNA extraction process from cells acquired using LCM

The process isolates total cellular RNA in a small volume of low ionic strength buffer by using RNA extraction/purification reagents and a purification column in a centrifugation step wise manner.

.

bound to the column followed by a faster spin at 16,000g for 1 minute, and the flow through discarded. 100 µl of wash buffer 1 was applied to the column which was then centrifuged at 8,000g for 1 minute. 100 µl of wash buffer 2 was applied and centrifuged as for buffer 1. A further 100 µl wash buffer 2 was added to the column and centrifuged at 16,000g for 2 minutes. The final step of the extraction involved placing the column into a fresh sterile 1.5 ml Eppendorf tube, 11 µl elution solution was added and the column left to incubate at RT for 1 minute to allow the release of the RNA from the column matrix prior to centrifugation at 1,000g for 1 minute, followed by a faster centrifugation at 16,000g for 2 minutes. The quantity and quality of the RNA were determined using a NanoDrop 1000 spectrophotometer (Thermoscientific, UK) and a 2100 Bioanalyzer, respectively (Agilent, UK). All RNA samples were stored under sterile conditions at −80°C for future analysis.

3.3.8 cDNA synthesis for RT-PCR

From each sample extract, RNA was synthesised to cDNA using qScript cDNA mix/supermix (Quanta, UK) which contains optimised concentrations of magnesium chloride ($MgCl_2$), deoxyribonucleotide triphosphates (dNTPs), recombinant RNase inhibitor protein, qScript reverse transcriptase, random primers, oligonucleotide (dT) primer and stabilisers. Following the manufacturer's protocol, in a sterile 0.2 ml Eppendorf tube, 2 µg RNA was added to 2 µl qScript and the volume adjusted to 10 µl with sterile d.H_2O. Samples were mixed thoroughly by gently vortexing and spun down to collect all liquid at the bottom of the tube. Samples were incubated at 25ºC for 5 minutes, 42ºC for 30 minutes, and the reaction stopped by heating to 85ºC for 5 minutes and the sample was then held at 4ºC. To check whether cDNA synthesis had been successful, RT-PCR was carried out using beta-actin (βA) forward and reverse primers (Table 3.2). PCR was performed using 50 ng cDNA, 5x Firepol green PCR mastermix (MM) (Solis Biodyne, UK) and optimised concentrations of forward and reverse primers in a total volume of 20 µl. To check for specificity, a no template control (NTC) was also run alongside the cDNA samples with d.H_2O replacing the cDNA. The PCR protocol consisted of denaturation at 95ºC for 10 minutes then 40 cycles of (95ºC for 15 seconds, 60ºC for 60 seconds) and finally 72ºC for 15 minutes.

3.3.9 RT-PCR optimisation and analysis: purity of glial cell capture

Confirmation of the isolation of enriched astrocyte, oligodendrocyte and microglia populations was performed by RT-PCR for GFAP (astrocyte), CD68 (microglia),

Gene	Primer sequence (5'-3')	Product size	Reference/source
βA	F:ATCCCCCAAAGTTCACAATG R:GTGGCTTTTAGGATGGCAAG	100bp	Sigma, UK
GFAP	F:GCAGAAGCTCCAGGATGAAAC R:TCCACATGGACCTGCTGTC	213bp	R&D Systems, UK
CD68	F:CGAGCATCATTCTTTCACCAGCT R:ATGAGAGGCAGCAAGATGGACC	135bp	Cambridge Bioscience, UK
OLIG2	F:CCCTGAGGCTTTTCGGAGCG R:GCGGCTGTTGATCTTAGACGC	474bp	Lin et al. (2005)
NFL	F:GGCTCTCAGTGTATTGGCTTCTGT R:AACCCAGCTCTAGTAAGCAGAAATG	84bp	Designed in house (Eurofins, Germany)

Table 3.2 Glial and control primer sequences

Details of glial and control primers tested in standard RT-PCR, including details of the primer sequences for the forward and reverse primers used, along with the expected product size and source of primers.

Key: F: forward, R: reverse, bp: base pairs.

OLIG-2 (oligodendrocyte) and NFL (neuron) (Waller *et al*, 2012). βA was used as a loading control and ran alongside the samples. Gene specific primers were sourced commercially or designed in house based on published sequences Primer-BLAST (basic local alignment search tool) software (*www*.ncbi.nlm.nih.gov/tools/primer-blast).

Optimisation of forward and reverse primer sets involved testing different concentrations of cDNA and primers, as well as different PCR programmes i.e. different annealing temperatures and cycle numbers. GFAP, CD68 and NFL PCR was performed following the programme described in section 3.3.8. For OLIG-2 an alternative PCR programme was used, following denaturation at 95ºC for 10 minutes the products were amplified (35 cycles at 95ºC for 60 seconds, 60ºC for 45 seconds and 72ºC for 60 seconds), followed by 72ºC for 15 minutes.

3.3.10 Agarose gel electrophoresis of PCR products

All PCR products were run on a 3% agarose gel to check that they were of the correct size. A 3% ethidium bromide stained agarose gel was prepared by adding 1.5 g agarose powder to 50 ml tris-acetate-EDTA (1x TAE) buffer (recipe, Appendix IV), the solution was heated in a microwave for ~2 minutes to dissolve the agarose. The solution was cooled slightly under a running tap, followed by the addition of 1 µl ethidium bromide (Sigma-Aldrich, UK) (from 10mg/ml stock concentration), and poured into a cassette, a gel comb was placed into the agarose solution and left to set for 45 minutes. Agarose gels were placed into an electrophoresis tank containing 1x TAE buffer. A DNA base pair marker, 2 µl DNA Hyperladder (V) (Bioline, UK) was loaded into the first well, with 10 µl RNA from astrocyte, oligodendrocyte, microglia and NTC samples loaded in consecutive wells. The gel was left to run at constant voltage (100V), for ~60 minutes and images captured using the GENi UV light imaging system (Syngene, UK).

3.4 Results

3.4.1 Case selection

A total of 15 tissue blocks were initially obtained for the study and based on the RIN assessment, 66% (10/15) of the tissue blocks had a RIN greater than 4.0. Histological evaluation identified 6 cases as having no evidence of inflammation or demyelination, these 6 blocks were taken forward for LCM of each of the 3 glial cell types (Table 3.3).

3.4.2 Immuno-LCM allows the isolation of specific glial cell populations

The use of the rapid IHC protocol allows for the detection of each glial cell type in human PM CNS tissue as shown in Figure 3.4. $GFAP^+$ astrocytes are recognised by their stellate appearance with immunoreactivity strongest in the cell's body and extending into the processes (Figure 3.4a, red arrows). OSP^+ oligodendrocytes are easily distinguished as small spherical cells with potent cell body immunoreactivity (Figure 3.4b, red arrows). $CD68^+$ resting microglia had a ramified, bipolar appearance with branched processes (Figure 3.4c, red arrows). Each cell type was isolated using LCM as shown in Figure 3.5 and the number of cells recorded to assess the quantity required to provide approximately 50ng of starting mRNA. Approximately 1000 astrocytes, 1500 oligodendrocytes and 1000 microglia were needed to achieve this. The RIN of each case post-LCM was assessed and an average 1.5 decrease in RIN was observed across the cases (range 1.1-1.8) as shown in Table 3.3. Each sample contained sufficient quality RNA for downstream studies, including RT-PCR.

3.4.3 Confirmation of cDNA synthesis from LCM-ed material

All experimental samples were checked on an agarose gel to confirm cDNA synthesis using βA primers. All samples showed a strong band at ~100 base pairs (bp) indicating the presence of βA RNA and confirming successful cDNA synthesis (Figure 3.6).

3.4.4 Isolation of enriched glial cell populations – confirmation by RT-PCR

RNA isolated from $GFAP^+$ cells had higher transcript levels of GFAP and lower levels of Olig-2 and CD68 transcript, confirming an enrichment of astrocytes using the rapid immuno-LCM method. Similarly with RNA extracted from OSP^+ cells, higher transcript levels of Olig-2 were observed with lower levels of GFAP and CD68 transcript confirming oligodendrocyte enrichment. RNA extracted from $CD68^+$ microglia provided a higher transcript level for CD68 and lower expression of the other two glial transcripts, confirming microglia enrichment (Figure 3.7).

Case	Age	Sex	pH	PMI	Pre-LCM RIN	Post-LCM RIN	Cause of death	H&E	LFB	CD68
1[a]	101	F	5.9	18	6.3	5.2	Urinary tract infection	Normal	Positive	Normal, resting ramified microglia
2[b]	77	F	6.6	9	5.2	3.5	Lung infection	Normal	Positive	Normal, resting ramified microglia
3[b]	78	F	7.2	5	5.1	3.5	Metastatic carcinoma	Normal	Positive	Mild reaction
4[b]	72	F	n/a	8	4.0	2.2	Bronchopneumonia	Normal	Positive	Normal, resting ramified microglia
5[b]	86	F	6.6	11	4.0	2.2	Bronchopneumonia	Normal	Positive	Mild reaction
6[b]	46	M	n/a	7	4.4	3.0	Bronchopneumonia	Normal	Positive	Mild reaction

Table 3.3 Details of cases used in the initial LCM study

All cases based on their histological characterisation did not contain any evidence of inflammation or demyelination and were comparable based on their RIN.

Key: n/a: data not available, [a]: case obtained from the Sheffield Brain Tissue Bank (SBTB), [b]: cases obtained from the MS Society Tissue Bank.

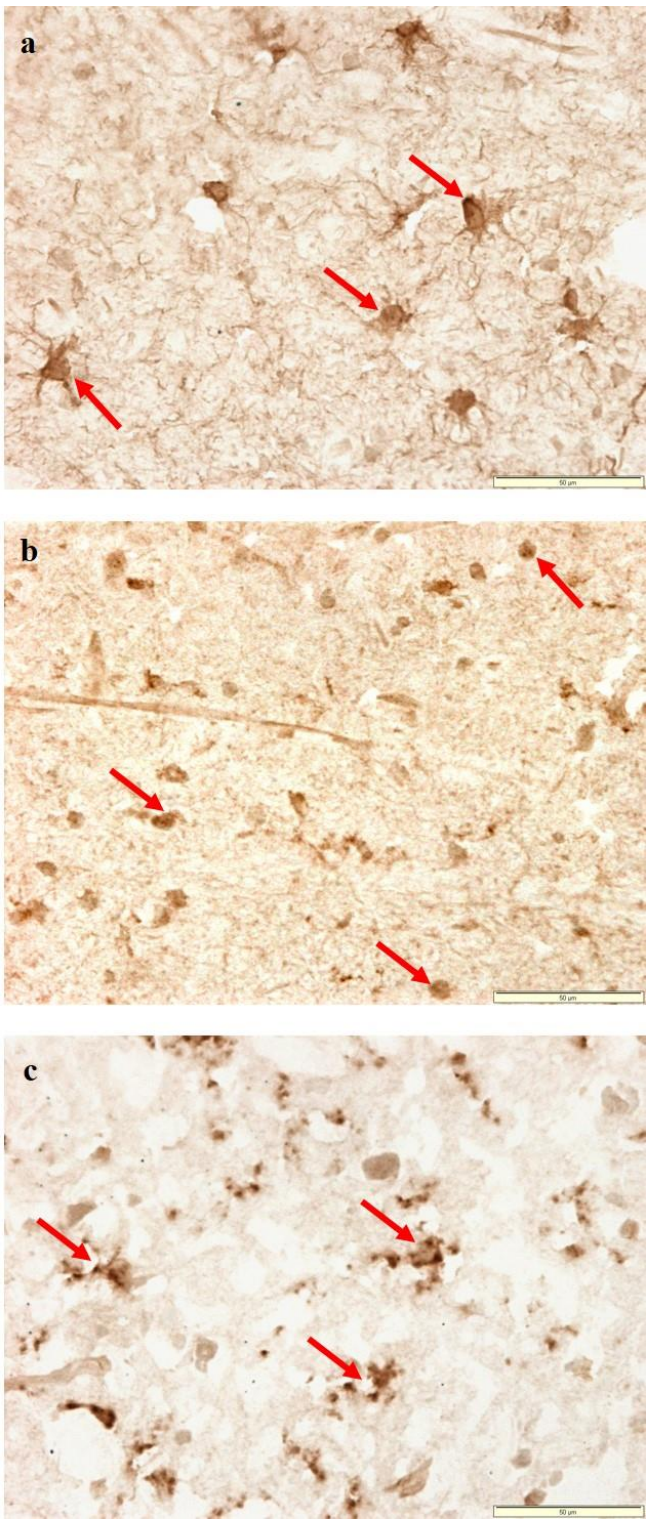

Figure 3.4 Rapid IHC detection of glial cells

GFAP (brown) labelled individual stellate astrocytes (a, red arrows). OSP (brown) labelled individual small, spherical oligodendrocytes (b, red arrows). CD68 (brown) labelled ramified branched microglia (c, red arrows). *Scale bar represents 50µm.*

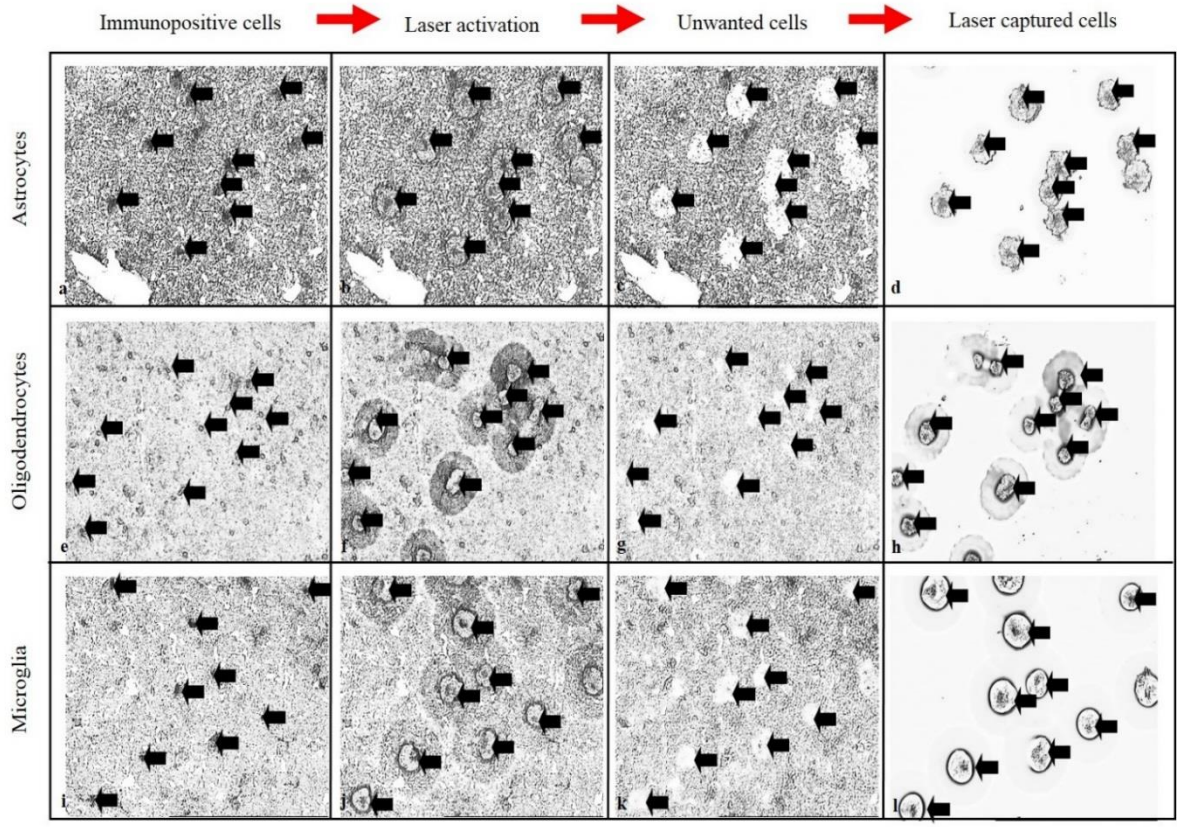

Figure 3.5 Laser capture microdissection of glial cells

$GFAP^+$ astrocytes (a), OSP^+ oligodendrocytes (e), and $CD68^+$ microglia (i) were identified by rapid immunostaining. The laser is fired causing the filmed cap to fuse with the underlying cell as indicated by the arrows in (b, f, and j). The cap is lifted off the tissue section leaving unwanted cells behind (c, g, and k), while laser captured cells adhered to the film, ready for RNA extraction (d, h, l). Figure adapted from Waller *et al* 2012.

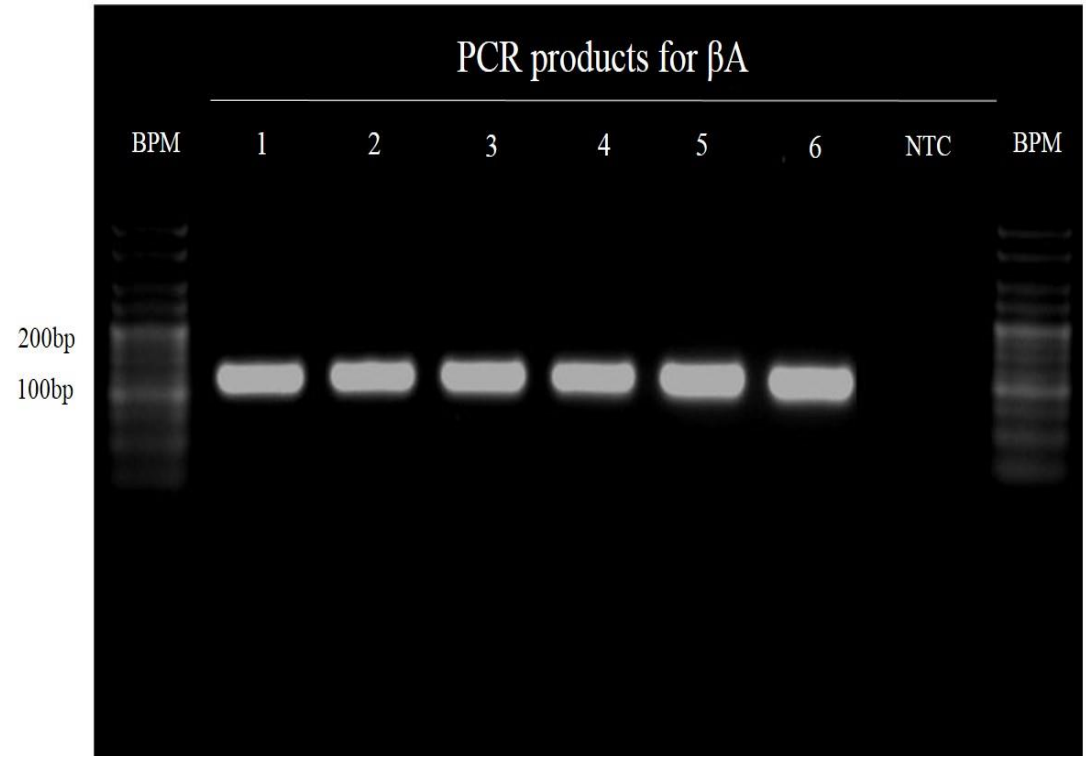

Figure 3.6 Agarose gel electrophoresis of RT-PCR cDNA products for beta-actin
The presence of βA mRNA in each of the 6 samples and absence in NTC sample confirms all extracted RNA was successfully converted to cDNA.

Key: BPM: base pair marker, NTC: no template control, βA: beta-actin, bp: base pairs.

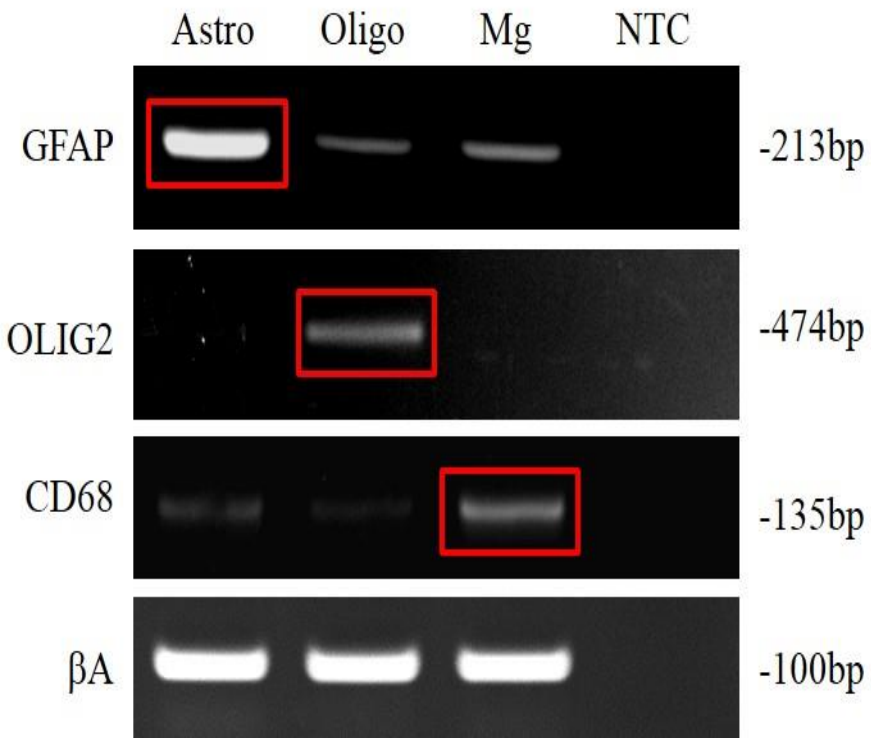

Figure 3.7 RT-PCR analysis of glial cells isolated from PM CNS tissue using immuno-LCM

Specific glial cell populations are shown to be enriched by RT-PCR. GFAP+ astrocytes are associated with higher transcript levels of GFAP and lower expression of OLIG2 and CD68 transcript (Astro column, red box). Oligodendrocyte enrichment is confirmed by higher levels of OLIG2 transcript in comparison to GFAP and CD68 transcripts (Oligo column, red box). $CD68^{+}$ microglia correlate with a higher CD68 transcript level compared to GFAP and OLIG2 transcripts (Mg column, red box). Figure adapted from Waller *et al* 2012.

Key: Astro: astrocytes, Oligo: oligodendrocytes, Mg: microglia, NTC: no template control, βA: beta-actin, GFAP: glial fibrillary acidic protein.

To further validate the presence of enriched glial cell populations, RT-PCR was carried out to show levels of NFL, an axonal marker. Very low NFL expression was identified in the oligodendrocyte and microglia samples (Figure 3.8) while the astrocyte population showed a slightly higher level of NFL transcripts, recognising the close proximity astrocytes have with axons. However RT-PCR confirms the enriched glial cell populations achieved using immuno-LCM.

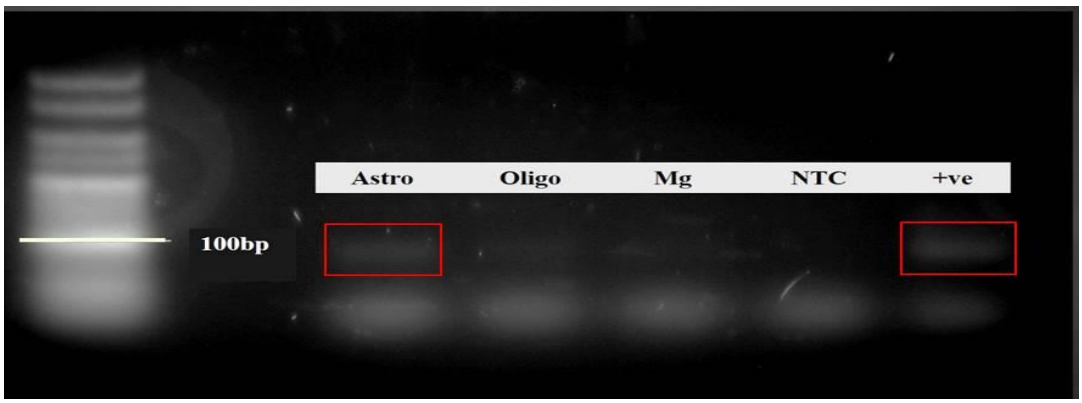

Figure 3.8 Neurofilament light RT-PCR analysis of glial cells isolated from PM CNS tissue using immuno-LCM

Low levels of neurofilament light (NFL) transcripts were detected in the astrocyte samples reflecting their close proximity to axons, no NFL transcripts can be detected in the oligodendrocyte or microglia samples.

Key: Astro: astrocytes, Oligo: oligodendrocytes, Mg: microglia, NTC: no template, +ve: positive neuronal control, bp: base pairs.

3.5 Discussion

In this study the isolation of enriched populations of glial cells from frozen human PM CNS was demonstrated using a novel rapid immuno-LCM method. Using 3 specific, recognised glial-specific antibodies: GFAP (astrocytes), OSP (oligodendrocytes) and CD68 (microglia), a rapid IHC method combined with LCM was developed, which limited RNA degradation thereby enabling downstream applications such as RT-PCR to be carried out. Confirmation of glial cell enrichment was demonstrated by RT-PCR for glial-specific transcripts. In addition, the number of cells required to gain sufficient starting material for downstream applications such as microarray analysis, was confirmed as in a previous study (Simpson *et al* 2011). Isolation of approximately 1000 astrocytes, 1500 oligodendrocytes and 1000 microglia was required to obtain 50ng of total RNA. This technique enables the isolation of specific cell types from both disease and control PM CNS samples for transcriptomic and proteomic studies, an advantage over the studies to date which have investigated heterogeneous cell populations, and it enables specific disease processes and pathological mechanisms to be linked to cell type. This approach may also identify potential biological disease biomarkers and be beneficial in identifying therapeutic targets for a range of neurological diseases, including MS.

3.5.1 LCM as a tool to investigate neurological disease

With the continuing advancements in 'omics' technology the potential to identify differentially expressed genes/proteins in single cell populations is made more achievable using LCM techniques. An increasing number of studies, both in animal models and human subjects, of a range of neurological diseases have investigated gene expression of LCM-ed material by means of RT-PCR and microarray platforms (Boone *et al* 2013, Chu *et al* 2009, Kumar *et al* 2013, Pietersen *et al* 2009, Simpson *et al* 2011, Torres-Munoz *et al* 2004). In relation to MS, the technique has only been used to isolate specific regions of interest thus far. For example, LCM was used to isolate CAL and gene expression microarray analysis identified significant transcriptional changes in heat shock proteins in areas of chronicity compared to surrounding NAWM (Mycko *et al* 2012). Similarly, carrying out RT-PCR on specific anatomical areas of the MS brain including normal appearing, perilesional and lesional identified a significant expression of endoplasmic reticulum genes in lesional tissue (Cunnea *et al* 2011). An earlier study by the same group used LCM to isolate blood vessels from MS patients, through microarray analysis the significant upregulation of a disintegrin and metalloprotease

domain (ADAM)17 and other MMPs associated with the breakdown of the BBB were identified in the MS cases compared to control cases (Cunnea *et al* 2010). Relatively few studies have investigated the use of LCM in the brain to look at protein expression in relation to specific cell populations or ROI, due to a number of issues to be discussed later in this chapter. However, proteomic analysis has been possible on LCM-ed dentate granule cells from patients with frontotemporal lobar degeneration (FTLD) (Gozal *et al* 2011) and IHC assisted LCM was used to identify Lewy bodies from patients with dementia with Lewy bodies (Leverenz *et al* 2007), with similar IHC-LCM performed to isolate neurofibriallary tangles in patients with AD (Wang *et al* 2005). The only proteomic LCM study in MS demonstrated the isolation of three separate lesion types from patients, the extracted protein resolved using sodium dodecyl sulphate polyacrylamide gel electrophersis (SDS-PAGE), and protein bands digested with trypsin and analysed on a nanoliquid chromatography tandem mass spectrometer. 158, 416 and 236 unique proteins were identified across the acute, CAL and chronic lesions, with more than half the identified proteins having unknown function, while the analysis showed CAL displayed high expression of coagulation proteins (Han *et al* 2008).

3.5.2 Limitations of LCM for genomic work

The use of LCM to isolate specific regions/cells and identify potential gene/protein changes can be used to identify changes that may contribute to disease pathogenesis. To date, however there are relatively few studies which have employed LCM on human PM CNS material, which can be explained by a number of factors, many of which need to be considered prior to commencing any work applying LCM to PM tissue (Ordway *et al* 2009).

When carrying out transcriptomic studies, using the RIN as a measure of RNA quality, enables the identification of potential suitable, usable cases for LCM. As identified in this study, not all PM CNS material appears to be suitable owing to a number of factors known to affect the RIN including the agonal state of the patient at death, as prolonged hypoxia can affect RNA and protein stability (Harrison *et al* 1991, Kingsbury *et al* 1995, Trabzuni *et al* 2011). Also, RNA quality of tissue has been shown to deteriorate with increasing numbers of antemortem events (Durrenberger *et al* 2010). Another factor to consider in determining suitable cases for LCM is the pH of the patient's CSF, shown to be a good indicator of RNA quality of tissue (Durrenberger *et al* 2010), as pH levels below 6.0 have been shown to be detrimental and affect the RNA quality of PM CNS tissue (Kingsbury *et al* 1995). Additionally, the brief freeze-thaw of the snap

frozen samples during LCM preparation can contribute to a loss in RNA quality (Mazurek *et al* 2013). In the current study, the tissue preparation time from section cutting, rapid IHC through to section dehydration in xylene was kept to a minimum (no longer than 25 minutes), despite the actual total LCM process taking around 2.5 hours. It is vital that the rapid immuno-protocol was implemented and sections were thoroughly dehydrated into xylene as quickly as possible to prevent RNA degradation, as aqueous condition have been shown to increase RNA degradation (Bernard *et al* 2011). Tissue preparation beyond this short time period can affect the RNA integrity of the sample (Burgess & McParland 2002, Fend *et al* 1999, Keays *et al* 2005, Mojsilovic-Petrovic *et al* 2004, Strand *et al* 2007). Also the LCM procedure itself can affect the RNA integrity of samples, including the duration of capture, which must be kept to a minimum (Michel *et al* 2003, Nawshad *et al* 2004). During this study each LCM sitting lasted no longer than 1 hour, accounting for around 10 minute capturing per section/slide, thereby preserving the RNA integrity of the sample from the effects of the laser power. Overall the actual processing and isolation of cells from tissue sections of different cases, using LCM, can be time consuming and, when implementing rapid IHC techniques with concentrated antibody titres, expensive experimental costs can occur (Kuhn *et al* 2012). However more automated LCM systems that incorporate an image analysis software designed to identify stained areas of tissue can improve the speed and automation of the LCM procedure (Tangrea *et al* 2011).

Another consideration is the type of laser employed to isolate the cells, which can affect the RNA quality of the isolated tissue. An LCM system can be utilised with either a UV or IR laser, the former being of higher power and hence potentially more damaging to the quality of mRNA obtained from the LCM-ed tissue (Vandewoestyne *et al* 2013). Furthermore, it should be noted that most PM cases are at end stage of disease and this additional factor must be considered when interpreting LCM derived transcriptomic data in relation to potential disease mechanisms. Interpreting ‘omics’ data from LCM samples must be viewed with caution, as the technique can only ensure an 'enriched cell' sample which may not be entirely pure, as was observed in the current study where an NFL transcript was present in the astrocyte enriched population, presumably due to the close proximity of astrocytes with axons. Therefore to confirm any data derived from LCM-ed material, validation must be carried out at both the transcriptomic and proteomic level. This type of validation may include implementing additional techniques such as qPCR to look at gene expression, and WB, IHC and mass spectrometry to assess protein expression.

3.5.3 Investigating tissue proteomics using LCM

Understanding a cell's genomic and proteomic profile in health and disease is vital in associating potential pathogenic roles to particular cell types. Investigating the transcriptome of cells isolated from tissue using LCM has been carried out in an array of settings as discussed, however the majority of a disease phenotype is the product of protein expression rather than gene expression. Therefore relating the role of a particular cell's protein expression in disease compared to health is crucial to improving disease understanding and can also assist in the development of protein biomarkers (Xu *et al* 2009).

LCM has been used to isolate regions of interest or enriched cell populations, and protein expression analysed, particularly in a number of studies in cancer (Baker *et al* 2005, Cha *et al* 2010, Liu *et al* 2012, Mu *et al* 2013, Patel *et al* 2008). However, a major limitation to using LCM as a method of generating proteomic information is the small amount of sample availability, especially from biopsy specimens in clinics and an absence of any *in vitro* amplification steps as in gene expression studies (Baker *et al* 2005). Consequently in order to overcome this there is a need for increased sensitivity in protein detection systems and improved cell isolation from tissue, while preserving tissue morphology.

There is a range of different systems currently available to study the proteome including: two-dimensional differential gel electrophoresis (2D-DIGE), liquid chromatography-tandem mass spectrometry (LC-MS/MS), MALDI-MS as well as WB. Over the years, the sensitivity of protein detection systems have developed to enable identification of protein expression in LCM material.

Conflicting findings have identified that methods of tissue processing as being a fundamental factor as to the amount of protein recovered from the LCM-ed tissue. One early study using 2D-DIGE proteomic analysis, identified that histologically staining brain tissue prior to LCM acted as a hindrance to recovering protein using gel electrophoresis (Mouledous *et al* 2002). However immunostaining of brain tissue showed improvement of protein recovery but only with the use of fluorescently labelled antibodies rather than the traditional enzymatic avidin biotin system, which gave a poorer protein recovery (Mouledous *et al* 2003b). In conclusion, using the traditional ABC IHC kits, high antibody titres and short incubation times are required when preparing tissue for LCM. This method of preparing tissue for LCM using enzymatic

detection based-IHC has been shown not to affect RNA integrity but the ability to identify low abundant antigens by 2D electrophoresis was hindered. In contrast, fluorescent detection based-IHC for LCM showed very little difference in the amount of proteins extracted and detected compared to the unstained samples. However, their appeared to be reproducibility variations as to the intensity of some protein spots, mostly affecting low molecular weight proteins (Mouledous *et al* 2003b). This group used navigated LCM as a means of avoiding problems with protein recovery of immuno-processed sections, whereby a serial section is histologically stained to help guide the LCM process of an unstained section. This technique was shown to be useful in identifying regions of interest but not absolute for the isolation of particular cells of interest (Mouledous *et al* 2003a).

More recently improved proteomic detection systems have enabled the use of histological staining or IHC of tissue sections prior to LCM and generated adequate protein for use in WB and mass spectrometry studies. For example S100B labelled astrocytes were isolated using LCM and WB used to confirm cell enrichment from human brain tissue (Koob *et al* 2012). Also haematoxylin stained germinal cells in human tonsils were analysed by WB for β-actin and procaspase-3 (Martinet *et al* 2004). To overcome the issue of limited sample availability from LCM, pooled microdissected protein extracts have been used in WB studies to identify differentially expressed proteins in LCM-ed isolated H&E stained stromal cells from colon adenocarcinoma tissue (Mu *et al* 2013).

Traditionally the use of 2D-DIGE combined with mass spectrometry techniques has enabled protein expression and comparison between diseased and control tissue to be made. The limitation with 2D-DIGE is that some proteins cannot be separated in this way due to size, hydrophobicity and specific isoelectric point (pI) as well as the laborious, non-automated method of identifying and dissecting out the many protein spots on a gel. Apart from 2D-DIGE, protein extracts from LCM-ed samples have been separated by traditional gel electrophoresis based on molecular weight. In breast cancer, around 60,000 tumour epithelial cells were isolated by LCM prior to protein extraction and gel electrophoresis to enable the identification of proteins based on their molecular weight. LC-MS/MS was used on the tryptic digested proteins to identify 298 differentially expressed proteins between malignant and control samples (Cha *et al* 2010).

Continuingly improved methods of tissue processing, LCM and protein extraction have enabled the use of mass spectrometry to identify proteins direct from LCM isolated tissue samples, with no need for prior protein separation by some kind of gel electrophoresis. Proteomic analysis of squamous cell carcinoma of the head and neck (HNSCC) used LCM to isolate 20,000 tumour epithelial cells, which were tryptically digested and peptides run on an LC-MS/MS system to determine around 700 expressed proteins (Patel *et al* 2008). Three skin regions were isolated using LCM and the proteomic components of each region determined by mass spectrometry (Mikesh *et al* 2013). Ultimately these studies avoid the limitations of gel electrophoresis including protein instability, limited fractionation ranges and protein recovery (Baker *et al* 2005).

In conclusion, the advancement of proteomic techniques and the application of LCM to isolate particular regions or enriched cell populations is opening up a library of proteomic data, some of which is currently beyond the knowledge of present understanding of expressed proteins and their relevance in the human body (Han *et al* 2008). Yet this data along with increasing data sets of future studies has the potential to support many new discoveries and help develop new therapeutic interventions and improve disease understanding.

3.5.4 Potential use of FFPE in LCM studies

To avoid the number of factors that can affect the RIN of frozen CNS sample and their unsuitability for LCM derived transcriptional studies, an alternative strategy would be to use FFPE tissue when carrying out LCM. One advantage of using FFPE tissue in molecular investigations such as in IHC, is the preserved morphology of FFPE tissue compared to snap frozen tissue (Shi *et al* 2008). Also storing such material is easier than the requirements of frozen material, with the majority of archival tissue samples stored as FFPE samples. However extracting usable mRNA from FFPE tissue is challenging and to date methods of RNA extraction from such tissue are still developing and have proven to be unreliable. Owing to its ability to intercalate into nucleic acids, formalin has a degrading effect on both RNA and DNA, however studies have carried out transcription expressions studies (qPCR) on extracted RNA from LCM-ed material from FFPE tissue (Joseph & Gnanapragasam 2011). Very few studies have used RNA extracted from LCM-ed FFPE tissue for gene expression microarray studies and snap frozen material is still the preferred choice of RNA (Coudry *et al* 2007). In the same manner the use of FFPE tissue for LCM-ed proteomic studies is hampered by the formalin fixing causing methylene bridges between proteins leading to a huge degree of

protein cross linking, therefore the amount of protein recovery from FFPE tissue sections is limited. Consequently when analysing the proteomics of LCM-ed material frozen tissue is the preferred choice while FFPE tissue is not recommended for such use (Hernandez & Lloreta 2006, Rodriguez *et al* 2008a).

3.5.5 Conclusion

In conclusion, this study has identified a robust method to isolate an enriched population of specific glial cells from human PM CNS tissue using immuno-LCM. In addition the study identifies the required number of each cell type to achieve a suitable amount of mRNA (50ng) needed for downstream investigations, such as microarray analysis. There are a number of limitations when employing LCM on human PM CNS tissue, however the potential information which may be realised using this technique and from this valuable resource in relation to disease pathogenesis is vital, and superior to cell lines and animal models that fail to fully replicate human disease (Jucker 2010). Glial cells play a key role in the pathogenesis of many neurodegenerative disorders. Gaining a greater knowledge of each specific cell type's role is vital to understanding the underlying pathology of neurological disease and this method described here has the potential to allow their use in the study of disease.

CHAPTER 4

MICROARRAY ANALYSIS OF THE ASTROCYTE TRANSCRIPTOME IN MULTIPLE SCLEROSIS NORMAL APPEARING WHITE MATTER

4.1 Introduction: Gene expression profiling in multiple sclerosis

A large amount of MS research has focussed on the pathological and immunological differences between demyelinated lesions, the pathological hallmark of the disease, compared to control WM. However, these studies do not identify the influence of early pathological events in relation to disease pathogenesis. Recent advancement in the transcriptomic field has allowed microarray technology to investigate the gene expression profile of individual samples, allowing for comparisons between differentially expressed genes in disease and control samples subjects to be achieved.

Microarrays are comprised of complementary DNAs (cDNAs), PCR product or oligonucleotides covalently bound to a solid support (Lock & Heller 2003). Depending on the species to be analysed, the array can cover the whole genome, to gain a full understanding of the major genes contributing to disease susceptibility (Kinter *et al* 2008) or can be designed specifically to investigate the expression of a selected panel of genes (Affymetrix, 2009). The method by which an array can be prepared varies from using modified ink-jet printing, photolithography or microspotting onto a glass surface or membrane (Lock & Heller 2003). Over 20,000 genes and more than 47,000 transcripts are represented on each Affymetrix human genome U133 Plus 2.0 microarray as used in the current study, with each gene being represented by a probe set consisting of 11 25-mer oligonucleotides (Affymetrix 2009). There are numerous microarray platforms available to investigate gene expression profiling, which differ by a number of factors including the number of gene sequences covered by the array and the length of probes (Comabella & Martin 2007, Kinter *et al* 2008). Also, the pre-processing of sample RNA must be considered such as the various RNA amplification protocols available, antisense RNA (aRNA) labelling and hybridisation (Comabella & Martin 2007, Kinter *et al* 2008). In general, labelled amplified aRNA samples are fragmented and hybridised to the microarray chips and scanned. The signal intensity of each spot on an array is directly proportional to the amount of the labelled aRNA bound to the chip (Figure 4.1), and can be used for statistical comparisons between samples.

The first microarray study on human MS brain tissue was published in 1999 (Whitney *et al* 1999). Since then, advancements in microarray technology, including an increased number of represented genes and reproducibility between arrays, has led to numerous gene expression studies in MS tissue using microarray technology, as summarised in Table 4.1, and recently reviewed (Dutta 2013, Dutta & Trapp 2012).

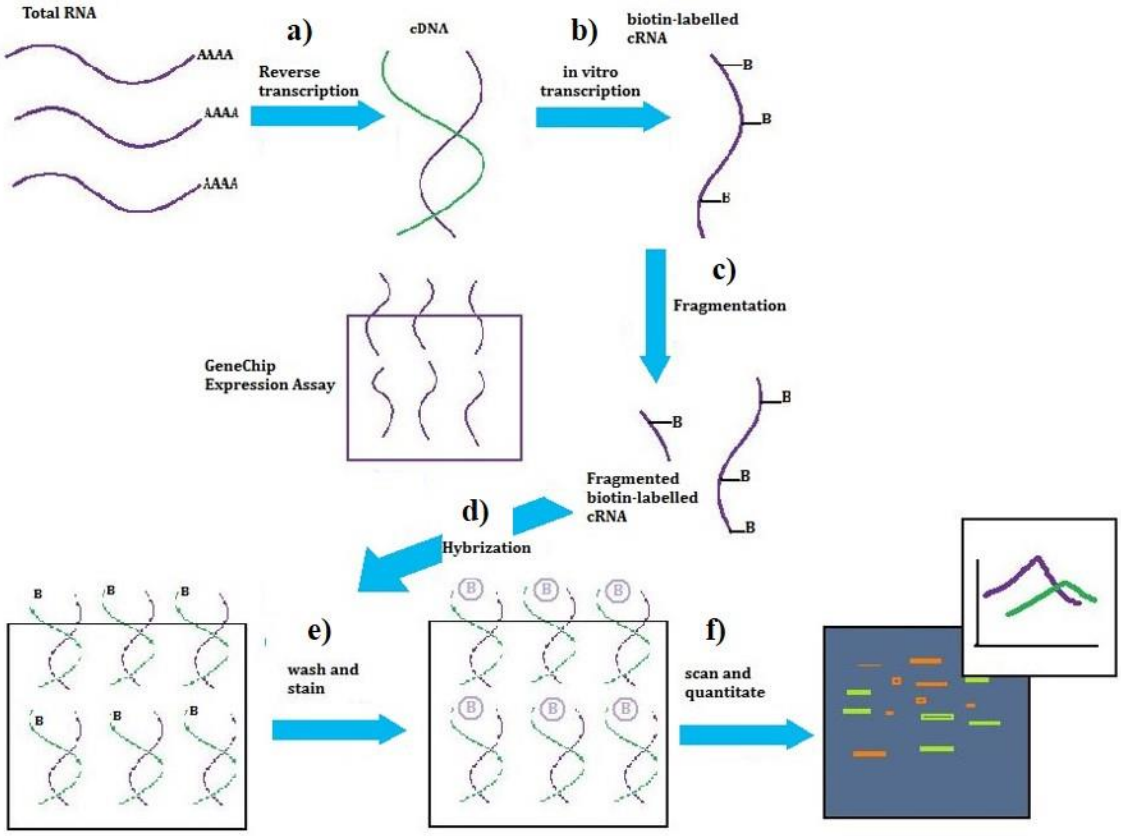

Figure 4.1 Sample preparation and microarray technique

A RNA sample (poly-A + mRNA) is reverse transcribed (a) to double stranded cDNA, *in vitro* transcription (IVT) synthesises multiple single strands of biotin labelled complementary aRNA (b) which is then fragmented (c) and hybridised to the array chip (d). After washing and staining, the array map is scanned and quantified using a scanner (e-f). The intensity of each specific array spot is directly proportional to the amount of RNA that is bound to the array and therefore quantification can be assessed for each gene product.

White matter (WM) microarray studies in MS	
Main study findings	**Reference**
1xMS (PP) (2x AL, 1x NAWM) • Differentially expressed genes in AL compared to NAWM associated with immune response, cell cycle and growth, intracellular signaling, adhesion, transport and myelin.	(Whitney *et al* 1999)
2xMS (PP: 1x EA and 1x LA lesion) (RR: 16x LA lesions) **3xCO** (pooled samples) • Proinflammatory leukotriene genes upregulated in all MS cases.	(Whitney *et al* 2001)
4xMS (SP) (1x AL, 2x CAL, 2x IA lesions) **2xCO** • An increase in inflammatory related genes and decrease in neuronal molecules and myelin associated genes.	(Lock *et al* 2002)
10xMS NAWM 7xCO • Upregulation of genes associated with signaling pathways related to oxidative stress and ischaemic preconditioning. • Upregulation of genes involved in inflammation in the NAWM.	(Graumann *et al* 2003, Zeis *et al* 2008)
5xMS (SP) (3x CAL, 2x AL) **CO** (No. unknown) • Associations with cytoskeletal reorganization, cell motility and immune response were common between the two lesion types.	(Tajouri *et al* 2003)
4xMS (SP) (2x CAL, 2x IAL) • At the CAL margins immune mediator genes were expressed. • IALs genes were associated with cell death.	(Mycko *et al* 2003, Mycko *et al* 2004)
6xMS (SP) (4x matched CAL & NAWM, 1x CAL only 1x NAWM only) **8xCO** • Differentially regulated immune response and neural homeostasis genes in lesions. • Differentially regulated immune response genes in NAWM.	(Lindberg *et al* 2004)
LCM microarray studies in MS	
Main study findings	**Reference**
12xMS (4xPP 8xSP) (4x CAL, 4x IAL, 4x NAWM) **4xCO** • Endothelial cell activation genes differentially expressed in lesions compared to control or NAWM.	(Cunnea *et al* 2010)
5xMS (SP) All CAL (5x lesion margins 3x lesion centre and 5x NAWM regions) • Heat shock protein (HSP) genes were upregulated in different areas of CALs. • Transcriptional changes were observed between demyelinated regions and NAWM.	(Mycko *et al* 2012)

Grey matter (GM) microarray studies in MS (continued)	
Main study findings	**Reference**
6xMS (1xPP, 5xSP) (non- lesional GM) **6xCO** • Differentially regulated genes in MS non lesional GM compared to control GM related to oxidative phosphorylation, synaptic transmission, cellular transport, and immune response.	(Dutta *et al* 2006, Klegeris & McGeer 2005)
6xMS (5xSP, 1x n/a) (GM Lesion and NAGM) **8xCO** • Upregulation of Ig-related genes in MS GM compared with CO GM.	(Torkildsen *et al* 2010)
8xMS (2xPP, 6x SP) (4x myelinated, 4x demyelinated hippocampal areas) **4xCO** • Between the lesional and myelinated hippocampus differentially altered genes associated with axonal transport, glutamate neurotransmission, synaptic maintenance, memory and learning.	(Dutta *et al* 2011)
FFPE tissue **3xMS** (SP, 1x AL, 2x CAL) **3xAD 3xTM 3xCO** • MS specific genes belonging to inflammation, immune cell activation/migration, oxidative injury, DNA damage/repair, cell death and tissue repair/regeneration.	(Fischer *et al* 2013)

Table 4.1 Summary of all microarray studies published on MS tissue

Key: MS: multiple sclerosis, PP: primary-progressive multiple sclerosis, SP: secondary-progressive multiple sclerosis, AD: Alzheimer's disease, TM: tuberculous meningitis, CO: control, AL: acute lesion, CAL: chronic active lesion, IAL: inactive lesion, NAWM, normal appearing white matter, NAGM: normal appearing grey matter, WM: white matter, GM: grey matter, Ig: immunoglobulin, n/a: not available.

To date, gene expression microarray studies in MS have primarily concentrated on peripheral blood mononuclear cells (PBMC) from patients. The number of studies investigating gene expression profiling in MS PBMC has risen rapidly in recent years, likely reflecting the ease of sampling and improved genomics technology, and to date almost 30 studies have been reported. These studies primarily focus on identifying potential biological markers in MS (Achiron *et al* 2010, Goertsches & Zettl 2007), tracking of disease course (Ratzer *et al* 2013) and examining patients' response to treatment (Kress-Bennett *et al* 2011, Munro & Perreau 2009). A number of PBMC studies have identified the activation of genes associated with the inflammatory response including B and T cells, when compared to the gene expression profile of control patients' PBMC (Bomprezzi *et al* 2003, Ramanathan *et al* 2001). Further experiments have monitored gene expression of PBMC throughout the disease course in relapsing patients compared to those in remission, and demonstrated an increased expression of genes related to T cells, epitope spreading and evasion of immune regulation in the former group (Mashayekhi *et al* 2010).

However, investigating PBMC in the periphery of patients may not parallel what is happening in the CNS in MS, and may reflect the systemic response to disease. Due to the huge case-to-case variability and lack of suitable, adequate human CNS tissue for microarray analysis, animal models of MS are favoured for investigating the pathophysiological changes associated with disease progression (Munro & Perreau 2009). Consequently several studies have investigated large scale gene expression changes in these MS animal models, with 20 published microarray studies in EAE to date (Table 4.2). Nonetheless investigating the transcriptome of EAE models has led to the inevitable bias towards changes in immunological gene expression. MS is widely regarded as more than an autoimmune disease, which is not reflected in microarray analysis of EAE models, that rely on forcefully inducing an autoimmune reaction by the administration of autoantigens (Comabella & Martin 2007). Consequently, the resulting gene expression data derived from EAE models is skewed towards the immune responses (Comabella & Martin 2007). Furthermore, EAE is induced in healthy animals, while MS most likely develops in an already compromised CNS which may in part account for the differences in the gene expression profiles between EAE and human MS (Comabella & Martin 2007).

Microarray studies in EAE	
Main findings	**Reference**
SJL/J mice; MBP_{87-99} and C57BL/6 mice; MOG_{35-55} induced EAE – CNS tissue • 5-lipoxygenase (5-LO) upregulation related to the biosynthesis of proinflammatory leukotrienes.	(Whitney *et al* 2001)
Lewis rats; guinea pig spinal cord homogenate induced EAE – CNS tissue • Upregulation of osteopontin in EAE rats.	(Chabas *et al* 2001)
C57BL/6 mice MOG_{35-55} induced EAE – CNS tissue • 61 genes linked to EAE susceptibility.	(Ibrahim *et al* 2001)
C57BL/6 mice MOG_{38-50} induced EAE – CNS tissue • Two groups of genes: 1. Genes encoding ion channels, neurotransmitters and growth factors. 2. Genes important for nervous system regeneration.	(Carmody *et al* 2002)
T cell receptor double transgenic B10.PL mice; MBP induced EAE - Spleen cells • Gene expression profile of isolated spleen cells identified that oestrogen treatment generated protection from EAE.	(Matejuk *et al* 2002)
MBP-Ac1-1-specific T cell receptor double transgenic mice; spontaneous EAE – CNS tissue • The gene expression profile delineates the encephalitogenic process in absence of immunisation and adjuvants as seen in spontaneous EAE.	(Matejuk *et al* 2003)
Lewis rats; guinea pig MBP induced EAE – CNS tissue • Alterations in calcium balance and neurotransmitter exocytosis may lead to EAE onset.	(Nicot *et al* 2003)
B10.PL mice; MBP induced EAE – CNS tissue • EAE symptoms reversed on treatment with vitamin D associated with increased apoptosis of inflammatory cells.	(Spach *et al* 2004)
C57B1/6 (B6) and C57B1/10.S (B10) mice; MOG_{35-55} induced EAE – lymph nodes • Gene expression profiling on lymph nodes mapped genes to known EAE-linked loci.	(Mix *et al* 2004)
Lewis rats: MBP induced EAE – CNS tissue • Treatment with Lovastatin altered 158 immune-related genes, identifying protective mechanisms provided by statins.	(Paintlia *et al* 2004)

Microarray studies in EAE (continued)	
Main findings	**Reference**
SJL/J mice; MBP induced EAE – CNS tissue • Study surrounding gene profiling in cell junction, adhesion and extracellular matrix.	(Brand-Schieber *et al* 2005)
C57/bl mice; MOG_{35-55} induced EAE – CNS tissue • EAE mice treated with an antioxidant showed gene expression profiles similar to control healthy mice.	(Gilgun-Sherki *et al* 2005)
WT C57/BL/6 and PAF receptor knock-out mice; MOG_{35-55} induced EAE – CNS tissue • In KO-mice an overall lower expression of inflammatory mediators in the CNS tissue.	(Kihara *et al* 2005)
NOD mice: MOG_{35-55} induced EAE – CNS tissue • Well defined expression pattern identified at specific stages of EAE.	(Baranzini *et al* 2005)
WT and C57BL/6 mice deficient in IFNγ and IL-12p35; MOG_{35-55} induced EAE – CNS tissue • Genes regulated across the three mouse models were likely to be regulated in MS patients.	(Jelinsky *et al* 2005)
Lewis rats; guinea pig $MBP_{68–86}$ induced EAE – Lymph nodes • Study identified 2 genes consistently regulated in the rats that developed EAE resistance.	(Liu *et al* 2006)
SJL mice; $PLP_{139-151}$ induced EAE – Lymph nodes • Genes associated with immune cell function and cell-to-cell interactions influenced by Atorvastatin treatment.	(Mix *et al* 2006)
C57BL/6J mice; MOG_{35-55} induced EAE – CNS tissue • Upregulation of angiogenic genes in acute EAE.	(Roscoe *et al* 2009)
C57BL/6 and SJL female mice $MOG_{35–55}$ induced EAE – CNS tissue • Treatment with triterpenoids suppresses proinflammatory genes and induces anti-inflammatory genes.	(Pareek *et al* 2011)
Lewis rats; MBP induced EAE – CNS tissue • Increased expression of immune related genes in the EAE models. Inflammatory response and antigen processing/presentation were the most upregulated genes.	(Inglis *et al* 2012)

Table 4.2 Summary of microarray studies published in EAE

Key: CNS: central nervous system, EAE: experimental autoimmune encephalomyelitis, KO: knock-out, MBP: myelin basic protein, MOG: myelin oligodendrocyte glycoprotein, PLP: proteolipid protein, WT: wild-type.

An alternative method of analysing the potential pathogenic mechanisms in MS is to investigate the transcriptome of cell culture models. Many studies have used microarray analysis to investigate the gene expression profile of specific cells under treatment in culture. A summary of microarray studies, with a focus on astrocytes, is shown in Table 4.3. Such investigations have included analysing the cells' response to different treatments, such as treatment with cytokines associated with MS (Argaw *et al* 2006, Zhang *et al* 2006) or the gene expression profile of different astrocyte phenotypes known to exist in MS (Daginakatte *et al* 2008, Nash *et al* 2011b). However, it should be noted that the expression profile of astrocytes in culture will be different to a physiological setting where astrocytes interact with several other cell types. Also many of these studies derive from primary astrocytes from either mouse/rat or from human foetuses, which is not a true reflection of mature astrocytes.

Ultimately, using RNA extracted directly from human CNS tissue is fundamental to identifying the transciptomic modifications in relation to human disease pathogenesis. However there are a number of confounding variables which must be considered when carrying out large-scale gene expression studies on human tissue, which have been discussed in the previous chapter and reviewed in detail in the literature (Bahn *et al* 2001, Bradl & Lassmann 2012, Kinter *et al* 2008, Stan *et al* 2006, Weis *et al* 2007). In the case of MS, understanding the gene expression profiles derived from the different microarray studies is complicated and comparability between microarray studies is challenging due to the different population of cells/tissue researched, and/or the different lesion type(s) investigated. Also, considerations must be made about the number of cases to be used in a study, as well as the staging of the disease, choice of appropriate control tissue and the different microarray platforms utilised (Bradl & Lassmann 2012, Kinter *et al* 2008).

It is well established that MS is an ongoing, hugely variable disease where the architecture of the brain is constantly changing depending on the stage of the disease and between different patients (Bradl & Lassmann 2012). To identify the initiating factors that lead to lesion formation in MS, studies into the NAWM surrounding lesions, traditionally defined as WM devoid of pathology, are required.

Microarray studies in astrocyte cell culture	
Main findings	**Reference**
Human 1321N1 astrocytoma cells • Treatment with $P2Y_2$ receptor agonist UTP, upregulated neurotrophins, neuropeptides and growth factor gene expression. **MS relevance** The upregulation of $P2Y_2$ receptors in response to stress maybe important in neuronal survival and facilitating neuroprotective mechanisms in MS.	(Chorna *et al* 2004)
Primary human fetal astrocyte • IL-1β induced the expression of genes associated with vessel plasticity, including *HIF-1α* and its target, *VEGF-A*. **MS relevance** IL-1β contributes to BBB permeability in MS by activating the HIF–VEGF pathway.	(Argaw *et al* 2006)
Human astrocytes prepared from neuronal progenitor (NP) cells (human foetus at 18.5 weeks) • Etoposide-treated astrocytes led to the upregulation of p53-responsive genes (including 14-3-3σ) and downregulation of mitotic checkpoint-regulatory genes. **MS relevance** The astrocytic expression of 14-3-3σ might serve as a marker of oxidative and DNA-damage in MS.	(Satoh *et al* 2006)
Astrocyte cultures prepared from PM human foetal CNS tissue (19–22 weeks of gestation) • IL-1β treated astrocytes – regulated expression of chemokines, cytokines, cell adhesion molecules, and vascular remodelling genes – supporting its role in CNS inflammation and BBB permeability in MS. • IFNγ treated astrocytes – similar gene expression as seen with IL-1β treatment, but milder effect. • TGF-β1 treated astrocytes – induced or controlled ECM deposition and remodelling associated genes, supporting its role in the regulation of repair in MS.	(Zhang *et al* 2006)
Astrocyte cultures prepared from newborn SJL/J and BALB/c Cum mice • TMEV treated astrocytes showed the overexpression of chemokine genes. **MS relevance** The increased expression of chemokines, including CXCL1 in TMEV treated astrocytes is chemoattractant for destructive immune cells.	(Rubio & Sanz-Rodriguez 2007)
Primary astrocyte cultures prepared from postnatal day 1−3 WT C57BL/6 mice • A number of growth control genes were regulated in two separate models of reactive astrocytosis. **MS relevance** The upregulation of particular genes in reactive astrocytes *in vitro* and *in vivo* may limit the damage produced by ischemia or inflammation.	(Daginakatte *et al* 2008)

Microarray studies in astrocyte cell culture (continued)	
Main findings	**Reference**
<u>Mixed glial</u> culture prepared from neonatal rat brain • Th1, M/M and Th2 cytokine treatment. • Differentially regulated gene expression related to metabolism and signaling, neuroprotection, axon/glial interactions and immune-system. **Relevance to MS** A balance between Th1, M/M and Th2 cytokines in the CNS may be paramount in MS lesion development.	(Lisak *et al* 2009, Lisak *et al* 2007, Lisak *et al* 2006)
Astrocyte cultures differentiated from neurospheres generated from striata of Sprague Dawley rats • A direct correlation of astrocyte phenotype with their ability to support myelination. • Comparison of quiescent and activated astrocyte resulted in the upregualtion of distinct genes including THBS4, CTGF and CXCL10, all of which have been associated with myelination. **MS relevance** Potential therapeutic intervention to promote CNS remyelination in demyelinating diseases such as MS.	(Nash *et al* 2011b)
Astrocyte cultures prepared from 1.5-day-old C57Black 6 mice • ROCK inhibitor treatment of astrocytes led to changes in biological processes regulating cellular shape and motility. **MS relevance** Pharmacological manipulation of reactive astrogliosis could ensure beneficial and pro-survival outcomes.	(Lau *et al* 2012)

Table 4.3 Summary of microarray studies published in astrocyte cultures

Key: BBB: blood brain barrier, CTGF: connective tissue growth factor, CXCL: chemokine (C-X-C motif) ligand, ECM: extracellular matrix, HIF-1α: Hypoxia-inducible factor 1-alpha, IL: interleukin, IFN: interferon, M/M: monocyte/macrophage, ROCK: Rho Kinase, σ: sigma, THBS4: Thrombospondin-4, TMEV: Theiler's murine encephalomyelitis virus, TGF-β1: Transforming growth factor-beta 1, VEGF: Vascular endothelial growth factor, WT: Wild-type.

To date, only 3 microarray studies have investigated NAWM (Graumann *et al* 2003, Lindberg *et al* 2004, Zeis *et al* 2008), all of which have identified the upregulation of genes predominantly related to the immune response. It is important to study the NAWM rather than established lesions in MS to determine either factors which may initiate and/or prevent disease progression. In order to advance the transcriptomic data obtained from these microarray studies a technique is required which limits the potential bias as a result of whole tissue sampling. LCM allows for the isolation of a particular ROI or specific cell type from tissue, and when used in conjunction with microarray analysis can identify differentially expressed genes in relation to an enriched cell population. In MS, LCM combined with microarray analysis has recently been published in two separate studies (refer to Table 4.1). The first of these studies used microarray analysis to identify differential expressed genes in LCM-ed blood vessels from different regions within MS brain (Cunnea *et al* 2010). These regions included NAWM, chronic active and IA lesions, and identified specific gene changes in endothelial cells related to alterations in BBB function. The second study performed microarray analysis on isolated WML and NAWM from well characterised MS tissue and identified the upregulation of genes associated with the heat shock protein families in relation to lesion activity (Mycko *et al* 2012).

In other neurological diseases and settings, LCM has been used to isolate specific cell types prior to microarray analysis to help provide an insight into cell activity and disease pathogenesis. Microarray analysis has been carried out on LCM-ed isolated amoeboid and ramified microglia from the corpus callosum of rat brain, identifying genes that are specific to each cell type (Parakalan *et al* 2012), motor neurons isolated from human ALS patients (Brockington *et al* 2013, Kirby *et al* 2011), astrocytes in the ageing brain (Simpson *et al* 2011) and astrocytes in the animal model of ALS (Ferraiuolo *et al* 2011). Having a more definitive transcriptomic analysis of enriched cell types in relation to disease, compared to control cases, may identify potential pathological mechanisms of disease and open up new approaches to therapy.

With this in mind, and with clear evidence of astrocyte changes in both disease models of MS (Inglis *et al* 2012, Kipp *et al* 2011) and MS tissue (Black *et al* 2010, Brosnan & Raine 2013, De Keyser *et al* 2010, Holley *et al* 2003, Nishie *et al* 2004, Rejdak *et al* 2007, Williams *et al* 2007, Zeinstra *et al* 2000), identifying changes in the astrocyte transcriptome is needed to gain a greater understanding of the astrocytes' role in MS (Goertsches & Zettl 2007). As previously mentioned, to date there are very few

microarray studies in human MS subjects and even fewer which have implemented LCM to investigate gene expression changes in an enriched ROI/cells. A detailed characterisation of the astrocyte transcriptome in human MS NAWM will identify specific changes in the astrocyte gene expression compared to normal control and may elucidate whether astrocytes are driving or preventing disease progression in MS. Furthermore, such a transcriptomic study may provide novel gene candidates that have the potential to enhance the understanding of the causes and molecular mechanisms of MS.

4.2 Aims and objectives of the study

The aims of this study were to:

- Identify disease-specific changes in the transcriptomic profile of astrocytes in MS NAWM compared to control WM, using combined immuno-LCM and gene expression microarray analysis.
- To determine if the gene expression profile of astrocytes suggests they are contributing to or preventing lesion development and disease progression.

4.3 Materials and methods

4.3.1 Suppliers

Affymetrix UK., Voyager, Mercury Park, Wycombe Lane, Wooburn Green High Wycombe HP10 0HH, United Kingdom; **Agilent Technologies Inc.**, 5301 Stevens Creek Blvd, Santa Clara CA 95051, United States; **Epicentre Biotechnologies.**, 5602 Research Park Blvd., Suite 200 Madison, WI 53719, United States; **Life Technologies Ltd.**, (Invitrogen, Arcturus) 3 Fountain Drive, Inchinnan Business Park, Paisley, PA4 9RF, UK.

4.3.2 Case selection

All frozen tissue used in this study was obtained from the UK Multiple Sclerosis Society Tissue Bank and full ethical permission was obtained (Appendix I). Full clinical information for each case/brain block investigated is described in Appendix III. Thorough neuropathological assessment of each case was carried out through H&E, LFB and CD68 IHC as described in Chapter 2. As only frozen material was used, the sections did not require dewaxing or antigen retrieval, but were fixed in ice-cold acetone for 10 minutes (95% ethanol for LFB) prior to staining. Altogether in this study 20 separate brain blocks from 13 MS cases and 16 separate brain blocks from 10 control cases were initially characterised (Appendix III). Selected MS NAWM and control cases for use in this microarray study were selected based on a number of factors including no evidence of inflammatory infiltrates, demyelination or presence of amoeboid microglia, suggestive of phagocytic activity. Also the RIN of each case was determined pre and post LCM (see section 3.3.3 for method). All chosen cases were from similar anatomical brain regions, from either P1 or P2 coronal brain slice (Table 4.4) refer to Appendix II for illustration of brain block preparation for this study. Cases were also matched based on age, MS NAWM mean 77 years old (range 46-86 years old), control mean 71 years old (range 35-91 years old) and sex (MS NAWM 4F:1M, control WM 3F:2M) and had an overall mean PMI time of 16 hours (range 5-33 hours). Based on the above criteria, in total 5 MS NAWM and 5 control cases were used in the study (Table 4.4) which is considered an adequate number of cases to identify differentially expressed genes (Pavlidis *et al* 2003).

Case	Region	Age	Gender	PMI (hours)	CSF pH	RIN (Pre-LCM)	RIN (post-LCM)	MS classification
MS50	P1E4	72	F	8	n/a	4.0	2.2	SPMS
MS57	P1A6	77	F	9	6.62	5.2	3.5	SPMS
MS67	P2C7	86	F	11	6.57	4.0	2.2	SPMS
MS71	P2C3	78	F	5	7.15	5.1	3.5	SPMS
MS100	P2B3	46	M	7	n/a	4.4	3.0	SPMS
CO22	P1C2	69	F	33	7.80	3.3	n/a	N/A
CO25	P2A3	35	M	22	n/a	3.5	n/a	N/A
CO30	P2A2	75	M	17	6.60	7.1	2.4	N/A
PDCO16	P1B1	91	F	22	n/a	4.3	2.3	N/A
PDCO23	P2B4	78	F	23	n/a	6.6	2.3	N/A

Table 4.4 The microarray case cohort

5 MS and 5 control cases were identified as suitable for this transcriptomic microarray study based on their disease type, age, sex, post mortem interval (PMI) anatomical location, neuropathological assessment and RIN pre and post LCM.

Key: N/A: Not applicable, n/a: not available.

4.3.3 Laser capture microdissection and RNA extraction

In brief, for each MS NAWM and control case, 7 µm sections were cut on a cryostat (Leica, UK) and rapidly immunostained for GFAP (refer to section 3.3.5). Under microscopy $GFAP^+$ astrocytes were identified and LCM was employed on each case to isolate these cells from the tissue sections. The captured cells were used for RNA extraction (refer to sections 3.3.6 and 3.3.7). Following RNA extraction, the quantity and quality of extracted RNA was checked prior to amplification using the NanoDrop and Bioanalyser, respectively (section 3.3.4).

4.3.4 Background to RNA amplification

In order to carry out successful gene expression microarray studies, up to 15 µg of labelled RNA is needed (Affymetrix 2009). However, owing to the low concentration, on average 50ng, of RNA extracted from isolated astrocytes using LCM, RNA amplification is required to produce amplified and biotin labelled RNA. There are a number of commercially available amplification kits that claim to successfully amplify RNA from small quantities. However, to achieve optimal amplification from these kits samples must be pure and of good RNA integrity, which are both limiting factors in RNA extracted from LCM-ed PM material.

Consequently during this study a number of different amplification protocols were assessed to achieve the optimum protocol that provided 6.5 µg aRNA for use in downstream microarray analysis. In general, all amplification protocols were derived from a method using T7 RNA polymerase (Frisen *et al* 1993). In this current study approximately 50ng total RNA was achieved from each LCM-ed sample, therefore amplification involving cycles of cDNA synthesis and *in vitro* transcription (IVT) were required to gain 6.5 µg of labelled aRNA for microarray analysis.

In this study three separate amplification kits were assessed, each protocol was optimised and tested with use of alternative clean-up and purification kits. A final optimum protocol was determined and used on all samples in this study. Outlined below are the details of the three main amplification kits used to enhance aRNA recovery from LCM-ed PM material.

4.3.4.1 Two round linear amplification

Initially two separate RNA amplification kits were employed, the Two-cycle Target labelling protocol (Affymetrix, UK) and TargetAmp 2-Round biotin-aRNA amplification (Epicentre, USA), each protocol followed a similar two-round

amplification procedure but varied in the amount of starting material required. For the first round of amplification using the Affymetrix kit, 50ng total RNA or with the Epicentre kit 500pg total RNA from each sample was reverse transcribed along with Poly-A control RNA using a T7-oligo(dT) promoter primer which anneals to the poly-A tail of mRNA. Poly-A controls are *in vitro* synthesised polyadenylated transcripts corresponding to the *B.subtilis* genes, *lys, phe, thr* and *dap*. The expression levels of the Poly-A control probe sets on the microarray are used to check the RNA amplification efficiency independent of sample quality or quantity. Second strand complementary cDNA synthesis was achieved using a MM containing DNA polymerase I following an RNase H action, which incorporates the T7 polymerase promoter into the double stranded cDNA (dsDNA), while RNaseH breaks down the RNA template strand. This dsDNA product was purified and served as a template for the first round IVT reaction. The IVT reaction used a T7 RNA polymerase and unlabelled ribonucleotide mix to generate multiple copies of aRNA. In the second round of amplification numerous copies of aRNA were reverse transcribed with random primers and second strand cDNA synthesis generated using T7-oligo(dT) promoter primers and a MM containing DNA polymerase I and dNTP to create a cDNA template for the second IVT reaction. dsDNA was transcribed into aRNA using biotinylated conjugated nucleotides in the second round IVT reaction. At this stage the biotin labelled aRNA was purified using a column based clean-up kit to remove enzymes, salts and any unincorporated nucleotides (Figure 4.2).

4.3.4.2 One round linear amplification

The optimum RNA amplification kit used in this study was the GeneChip 3' IVT Express Kit (Affymetrix, UK) which involved one round of amplification employing the T7 IVT step a well-established method for preparing samples for gene expression analysis. Initially total RNA (50ng) and poly-A control RNA was reverse transcribed with an enzyme and buffer MM containing T7 oligo(dT) primers to synthesise first strand cDNA containing a T7 promoter sequence. cDNA was converted to dsDNA by the use of an enzyme and buffer MM containing DNA polymerase I and RNase H to act as a template for the IVT reaction. IVT synthesised multiple copies of amplified aRNA incorporating biotin conjugated nucleotides. The biotin labelled aRNA was purified using RNA binding magnetic beads to remove enzymes, salts, and any unincorporated nucleotides to aid in a high recovery of aRNA (Figure 4.3).

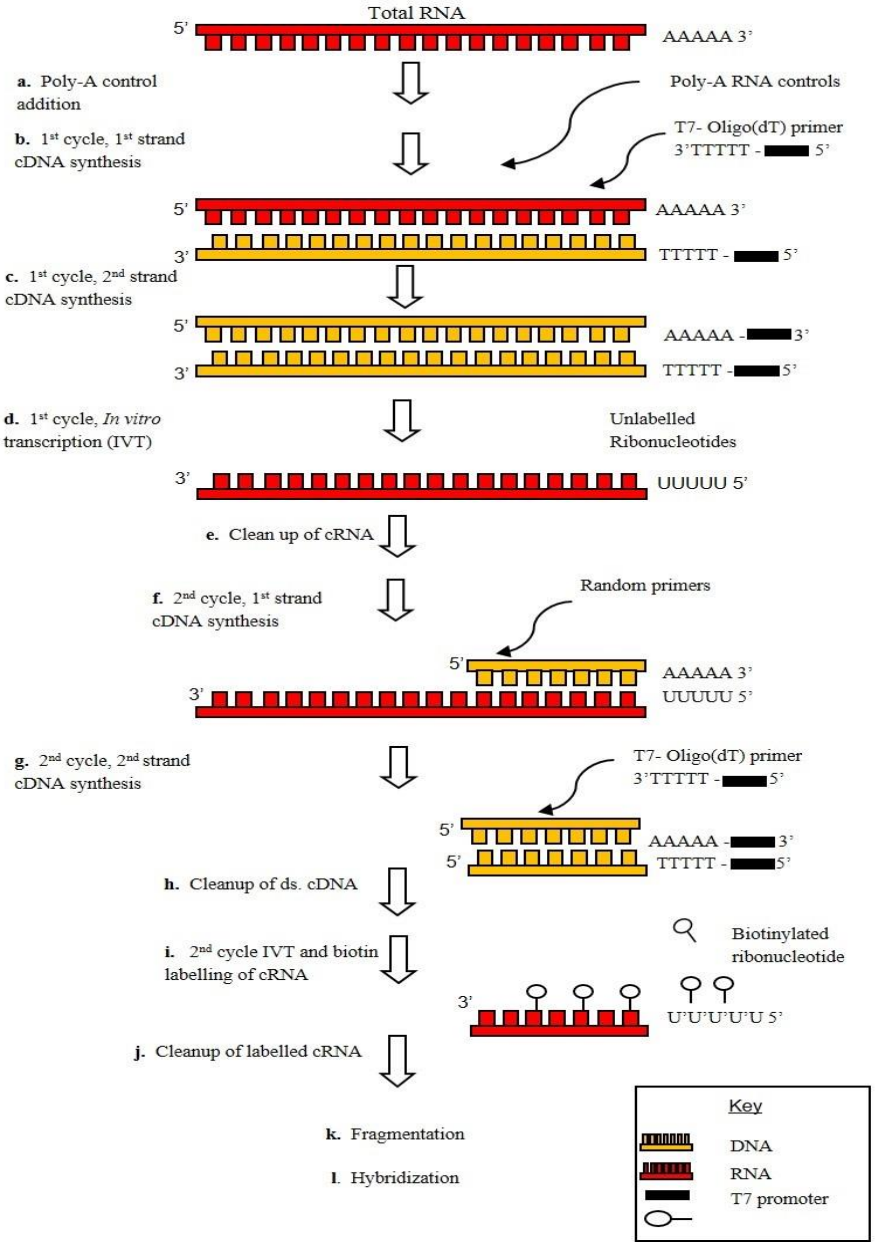

Figure 4.2 Two round amplification method of extracted RNA from isolated astrocytes

RNA and poly-A controls primed with T7 oligo (dT) primers were reverse transcribed into cDNA (a, b). Single stranded cDNA was converted to dsDNA (c) using DNA polymerase and RNase H action. This dsDNA acts as a template in the first round IVT reaction where multiple copies of aRNA were generated (d). A second round of amplification followed an aRNA clean-up (e) where aRNA product from the first round of amplification was reverse transcribed into cDNA (f). dsDNA was generated (g) and a second round IVT reaction produced multiple copies of biotin labelled aRNA from the dsDNA template (h, i). aRNA was purified to remove any unincorporated NTPs, salts, enzymes (j) aRNA ready for fragmentation and hybridisation to the GeneChip (k, l). Figure adapted from Affymetrix, 2009.

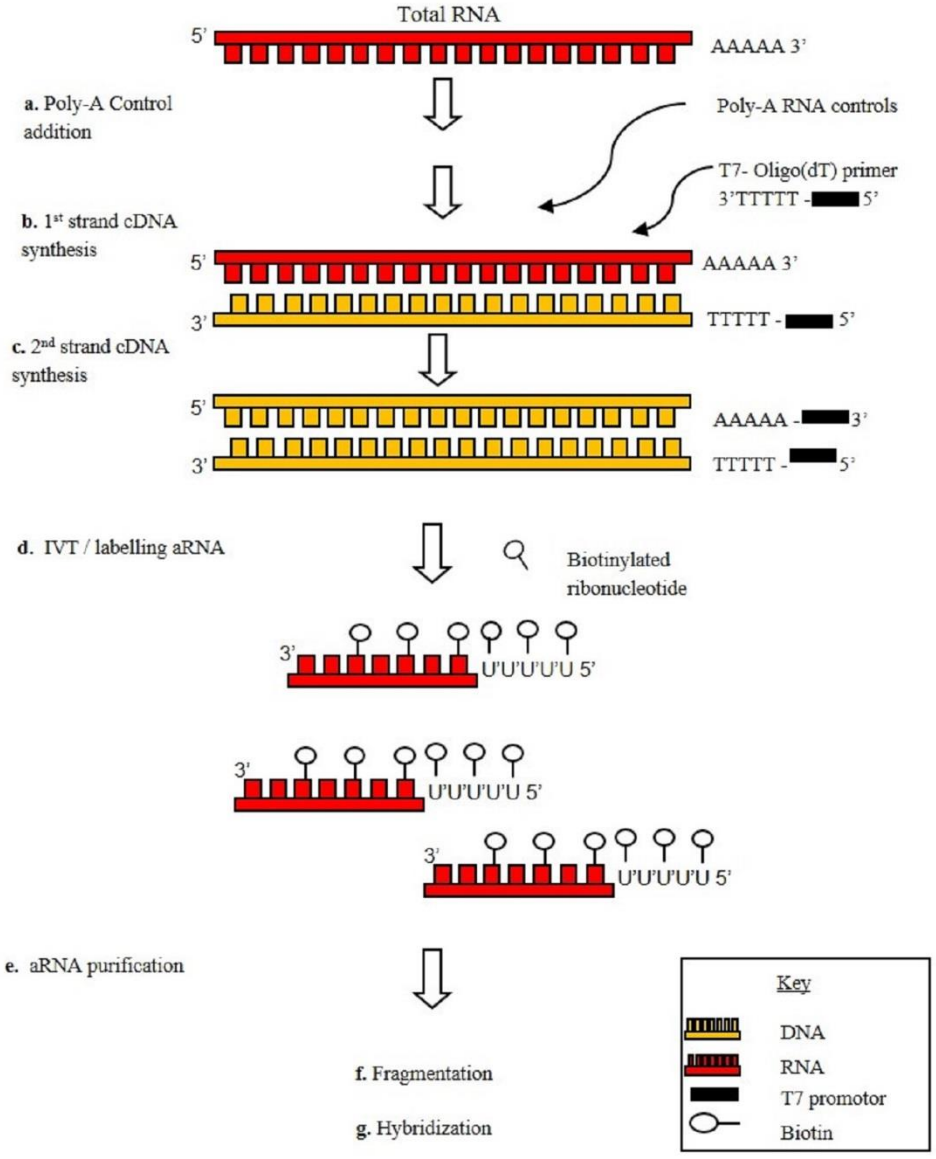

Figure 4.3 One round amplification method of extracted RNA from isolated astrocytes

RNA and poly-A controls primed with T7 oligo(dT) primers were reverse transcribed into cDNA (a, b). Single stranded cDNA was converted to ds(DNA) (c) using DNA polymerase and RNase H action. This dsDNA acts as a template in the IVT reaction where multiple copies of biotin labelled aRNA were generated (d). aRNA was purified in RNA binding magnetic beads to remove any unincorporated NTPs, salts, or enzymes (e) aRNA ready for fragmentation and hybridisation to the GeneChip (f, g). Figure adapted from Affymetrix, 2009.

4.3.4.3 Assessment of amplified RNA quantity and quality

Following elution from the RNA magnetic beads, the quantity of amplified aRNA was analysed on the NanoDrop spectrophotometer (as described in section 3.3.4). And quality of aRNA checked by loading 1µl aRNA onto a Nano LabChip 6000 (capable of measuring 25–500 ng/µl total RNA) using the Agilent 2100 Bioanalyser.

4.3.5 Microarray procedure

4.3.5.1 Affymetrix Human Genome U133 Plus 2.0 microarrays – the structure

The use of Affymetrix Human Genome U133 Plus 2.0 arrays enables measurement of gene expression over the entire human genome in a single hybridisation. More than 54,000 probe sets are used to analyse the expression level of more than 47,000 transcripts and variants, including approximately 38,500 characterised human genes. Known gene/transcripts are represented on the microarrays by a probe set which consists of 11 25-mer oligonucleotides that are designed to be a perfect match to a region on the expressed transcript, these probes are synthesised in discrete areas (features) on the microarray. To control for non-specific hybridisation during analysis and interfering background noise, each perfect match probe sequence is paired to a mismatch probe sequence containing a single base substitution at the 13th nucleotide of the probe. Any difference in signals between the perfect match and mismatch paired probes is a measure of probe set specificity and can be used to determine the overall signal by a specific probe set.

4.3.5.2 RNA fragmentation, hybridisation and microarray scanning

In order to increase the specificity and intensity of each array, aRNA fragmentation is required to limit the RNA molecule size to eliminate steric hindrance and non-specific cross-hybridisation on the microarray. Hence 6.5µg of biotin labelled aRNA from each sample was fragmented using an array fragmentation buffer which contains Mg^{2+} ions and is part of the 3' IVT express kit. To aid the reaction, samples were heated to 94°C for 25 minutes. Following fragmentation, 1µl of aRNA was loaded on to a Nano LabChip 6000 and run on the 2100 Bioanalyser (Agilent, USA) to analyse the size of fragmentation reaction products (Figure 4.4). Meanwhile the microarray chips were preconditioned with 200µl prehybridisation mix for at least ten minutes at 45°C, rotating at 60 rpm in a hybridisation oven (Affymetrix, UK). 6.5µg fragmented and labelled aRNA was mixed in a hybridisation cocktail containing serial concentrations of hybridisation controls (bioB, bioC, bioD, and cre genes) and positive oligonucleotide B2 control (B2 oligo). By using hybridisation controls the overall RNA hybridisation

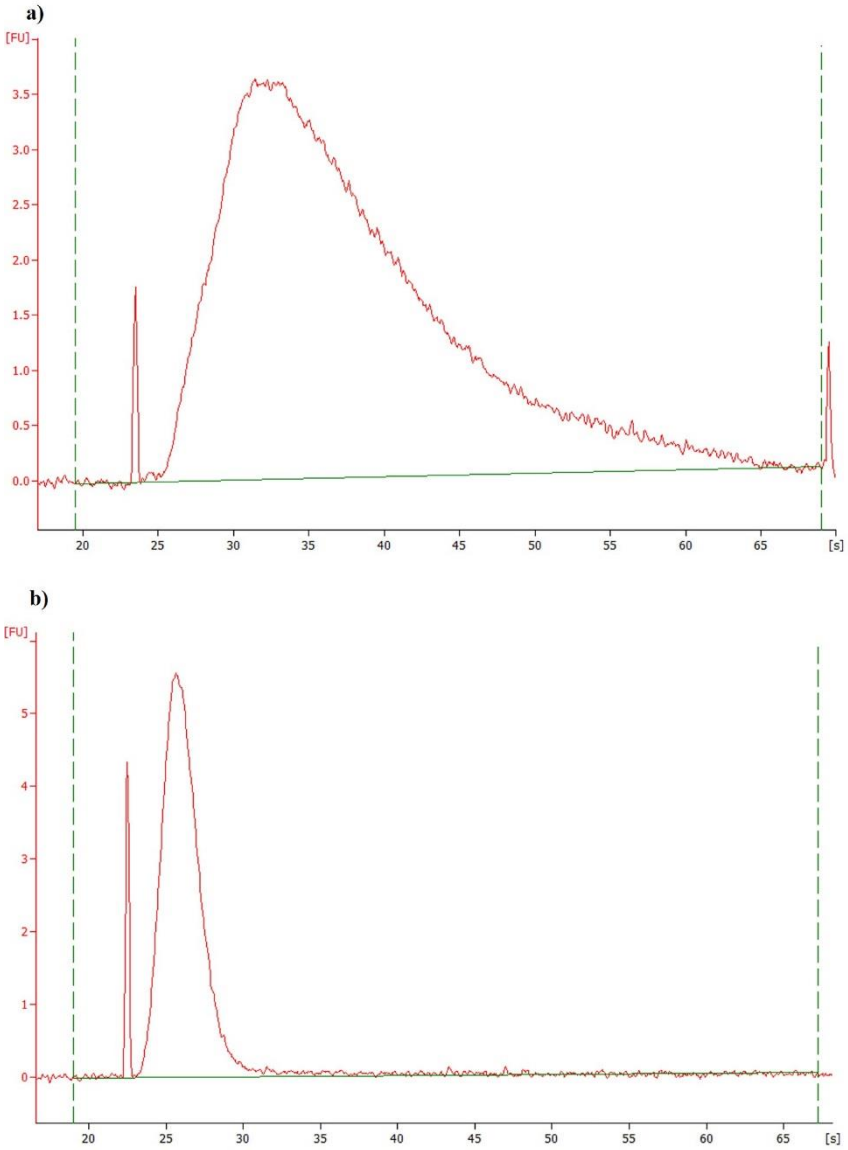

Figure 4.4 Pre and post fragmented aRNA analysis using the Agilent 2100 Bioanalyser

An example electropherogram of amplified aRNA (a) and fragmented amplified aRNA (b).

y-axis represents fluorescence units, (FU) and *x-axis* represents runtime in seconds, (s).

efficiency of the array can be assessed, with the signal intensity of each control reflecting their applied concentration. Whilst the B2 oligo was used to align the processing data at the corners and border of each array. After conditioning the microarray chips, the aRNA hybridisation cocktail replaced the preconditioning hybridisation solution and hybridisation took place overnight (o/n) for 16 hours at 45°C, rotating at 60 rpm. After 16 hours the hybridisation cocktail was removed from each microarray chip and the washing and staining of each microarray was carried out in the GeneChip Fluidics Station 400 (Affymetrix, UK). Firstly a low stringency wash solution was applied to the microarrays, followed by a high stringent wash to remove any unbound RNA, before staining with the light sensitive streptavidin phycoerythrin (SAPE). Another low stringent wash step followed prior to the application of a biotinylated anti-streptavidin antibody and an additional stain in SAPE followed by final wash steps. Each microarray chip was scanned in the GeneChip 3000 scanner with the use of a high-resolution laser to determine the fluorescent intensity of hybridised transcripts.

4.3.6 Microarray data analysis

The transcriptional profile of astrocytes isolated from MS NAWM and Control WM was compared on Affymetrix U133 Plus 2.0 microarrays. Affymetrix Gene Expression Console was used for quality and control analysis of the data and the image or CEL files were imported to GeneSpring version 7.0 (Agilent, USA) and normalised to the median of all genes prior to statistical analysis to identify differentially expressed genes. As a restrictive cut-off point, differentially expressed genes were genes from MS NAWM cases that were upregulated (≥ 1.5 fold change and ≤ 0.05 p-value) or downregulated (≥ -1.5 fold change and ≤ 0.05 p-value) compared to control cases. Significantly altered genes were identified through the Database for Annotation Visualisation and Integrated Discovery (DAVID) allowing genes to be grouped based on their biological function and the use of Kyoto Encyclopedia of Genes and Genomes (KEGG) pathway analysis, to identify any specific biological pathways of related genes.

4.4 Results

4.4.1 Classification of suitable cases for LCM

In total, 8 MS cases (14 blocks) and 11 control cases (16 blocks) were histologically characterised and subjected to pre LCM RNA analysis. One MS case investigated had evidence of inflammation as indicated by the presence of perivascular inflammatory cell infiltrates and the presence of $CD68^+$ amoeboid microglia (Figure 4.5) therefore case MS93 was eliminated from further investigation. In addition, MS103 failed to provide a pre-LCM RIN and appeared histologically abnormal with $CD68^+$ amoeboid microglia and slight perivascular cuffing, and was therefore also eliminated from the study. Case MS159 gave a low pre-LCM RIN of 2.5 and histologically the case appeared abnormal with perivascular cuffing and the presence of $CD68^+$ amoeboid microglia, therefore this case was also eliminated from the study. The majority of control cases showed no evidence of pathology, however one case from the SBTB showed evidence of inflammation and therefore was eliminated from further investigation. Of the remaining control cases, selection was based on anatomical location, PMI, RIN, sex and age matching with the selected MS cases. After exhausting samples from both the UK MS Society Tissue Bank and the SBTB for snap frozen material, 5 suitable MS NAWM and 5 controls were selected to be used in the study (refer to Table 4.4).

4.4.2 RNA amplification from LCM-ed material

On average approximately 1500 astrocytes were isolated per case using LCM, from 6-8 GFAP rapid-immunostained sections, (5 hours maximum of LCM per case) and provided approximately 50ng of starting total RNA. Each amplification kit used in this study to amplify extracted RNA from isolated astrocytes gave varied results, examples of which are presented here. Initial experiments using the two round amplification method (Affymetrix kit) employed 50ng starting RNA from each sample, only one sample (MS71 P2C3) amplified to the required amount of biotin labelled aRNA needed for microarray analysis (7.26 µg). LCM was therefore repeated on all samples and the amplification protocol was repeated using a higher amount of starting RNA (70ng), which gave varying results ranging from 0.52-1.81µg biotin labelled aRNA (Table 4.5).

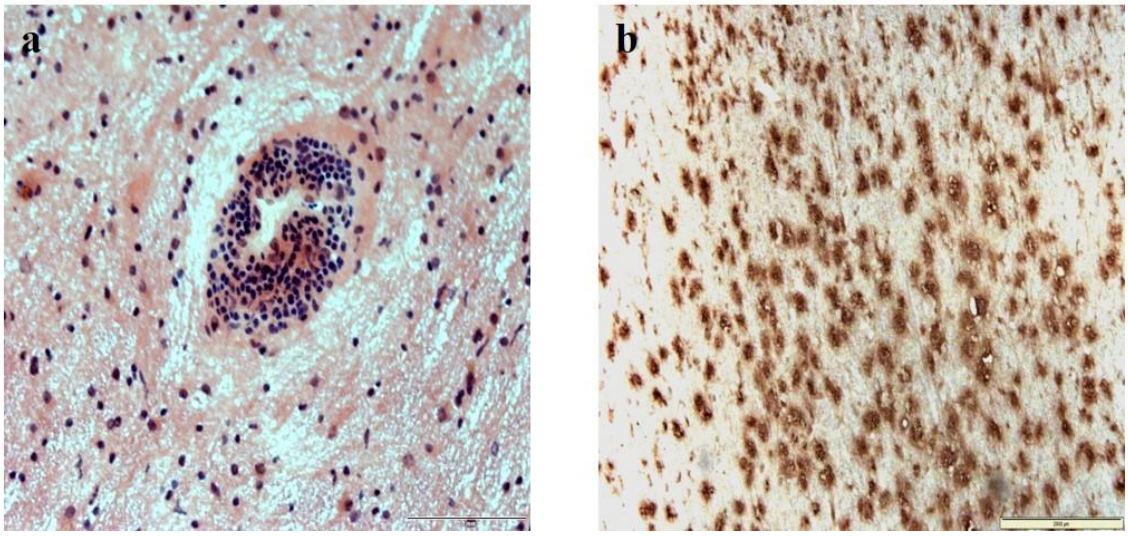

Figure 4.5 Perivascular cuffs and CD68^{+} amoeboid microglia

An example of a MS NAWM cases which was eliminated from the study due to evidence of perivascular infiltration (a), and positive CD68 amoeboid microglia which suggests a phagocytic phenotype (b). *Scale bar represents 200 µm.*

	Starting RNA [50ng]	Starting RNA [70ng]
Case	Amplified RNA [µg]	Amplified RNA [µg]
MS50 P1E4	1.63	1.00
MS57 P1A6	2.00	1.81
MS67 P2C7	1.19	1.57
MS71 P2C3	7.27	1.32
MS100 P1B3	1.23	0.90
PDC016 P1B1	0.70	1.05
PDC023 P2B4	1.01	1.32
CO22 P1C2	0.97	1.08
CO25 P2A3	0.99	1.17
CO30 P2A2	1.73	0.52

Table 4.5 Two-round amplification optimisation (Affymetrix)

Amplification was carried out on all samples with different starting amounts of RNA ranging from 50ng and 70ng. Only RNA from case MS71 P2C3 with 50ng starting RNA amplified to the sufficient amount required for microarray analysis.

Due to the limitations of the Affymetrix amplification kit and its removal from sale by the manufacturer the use of an alternative amplification kit, the TargetAmp 2-Round biotin-aRNA amplification (Epicentre, USA) was evaluated. This kit claimed to amplify very small amounts of RNA (a minimum of 500pg) and therefore appeared more suited for the limited amount of extracted RNA from samples used in this study. Initial studies with this kit yielded 1.9-2.5 µg aRNA, very little advancement in this value was attained by implementing 1000pg starting RNA (Table 4.6). However with continued use on repeated samples the kit proved unreliable and insufficient amounts of aRNA were obtained. Samples from each round of amplification (on average approximately 4 rounds of amplification were needed per case) were pooled together to provide approximately 6.5µg aRNA. Sample fragmentation was carried out and two samples hybridised onto microarray chips but only 11.3% probe set coverage for the MS sample and 1.4% coverage for the control sample was obtained. As both the NanoDrop and Bioanalyser gave ambiguous findings related to the small amounts of RNA being amplified in the Epicentre kit, a final separate amplification kit was employed, the GeneChip 3' IVT Express Kit (Affymetrix, UK). This method employed a single round of RNA amplification and alternative RNA magnetic bead purification step to which a higher yield of aRNA was attained per sample (Table 4.7) a minimum of 6.5 µg biotin labelled aRNA was obtained from 50ng starting RNA from one round of amplification, except for one case (CO25 P2A3) where two independent single rounds of amplification were needed and the two samples pooled to obtain 6.5 µg aRNA.

4.4.3 Gene expression profiling and quality control

The GeneChip Operating Software (GCOS) generated data files containing information from each of the ten microarray chips analysed. Through Expression Console (Mas5.0 analysis) quality reports of the transcriptional profile of each sample were produced including a number of quality control and normalisation factors to consider. The number of probe sets present for each array is calculated as a percentage (%) relative to the number of total probe sets on the array, comparative arrays should therefore share similar % probe sets. Hybridisation controls are also used to assess the quality of replicated RNA samples, the overall intensity of the controls of each gene array is compared to an expected target intensity value to calculate the appropriate scaling factor. Using the scaling factor normalises the data to a set value, so that the 10 arrays can be compared. Consequently a sample that is degraded or poorly amplified and labelled in the microarray procedure will yield a lower intensity, so when samples are

	Starting RNA [500pg]	Starting RNA [1000pg]
Case	Amplified RNA [µg]	Amplified RNA [µg]
MS50 P1E4	1.93	2.34
CO30 P2A2	2.57	2.43

Table 4.6 Two-round amplification optimisation (Epicentre)

Amplification was carried out initially on two samples with different starting amounts of RNA ranging from 500pg and 1000pg. A significant amount of RNA was amplified but not enough for microarray analysis.

Case	aRNA [µg]
MS050 P1E4	6.65
MS057 P1A6	8.37
MS067 P2C7	8.62
MS071 P2C3	7. 27
MS100 P2B3	7.25
PDC016 P1B1	8.10
PDC023 P2B4	7.14
CO22 P1C2	6.70
CO25 P2A3*	5.20 4.60
CO30 P2A2	6.90

Table 4.7 One-round GeneChip 3' IVT Express amplification

A minimum of 6.5 µg biotin labelled aRNA was achieved in one round of amplification, suitable for microarray analysis. (Two independent single round amplification of sample CO25 P2A3 was completed and the two samples pooled together).

compared and normalised to the same target intensity the scaling factor for that poor, degraded sample will be higher than for more intact samples. Considering these two independent factors, 3/10 array samples (two control and one MS NAWM) were eliminated from further analysis. CO22 P1C2, CO25 P2A3, and MS100 P2B3 had lower % probe sets present (20.01%, 7.47%, and 22.54%) in comparison to the remaining seven samples which gave a mean % probe set present of 34.82% (32.06%-38.15%). As well the scale factors were considerably higher in these three samples (CO22 P1C2: 23.17, CO25 P2A3: 58.35, and MS100: P2B3 19.26) in comparison to the remaining seven samples with a mean scale factor: 8.22 (5.16-11.00). Other factors measured included: the average background and RAW noise (RawQ). There is no official limit for background values but Affymetrix recommends values, ranging between 20-100 are adequate and replicate arrays should have comparable background values. In this study, the mean background signal for the seven samples was 26.18 (26.08-27.18). RawQ measures the pixel-pixel variation of probe cells on the array, the noise comes from two factors: electrical noise from the scanner and the sample quality, comparable RawQ values between replicate arrays should exist, from the seven samples analysed, the mean RawQ value was 0.67 (0.66-0.71). Specifically the internal control gene, glyceraldehyde 3-phosphate dehyrogenase (GAPDH), is used to provide information on the sample quality and efficiency of amplification and is calculated based on the 3' probe sets for GAPDH compared to the signal values of the corresponding 5' probe sets. These results are summarised in (Table 4.8).

Quantification of transcript abundance for each probe set was generated based on the MAS5.0 algorithm (Affymetrix 2002); the logged average ratio of fluorescence between the perfect match and mismatch probe sets. In order to visualise the variation of transcript abundance between microarrays, a logarithmic scaled boxplot of each array's distribution of probe set intensities is calculated from the median signal intensity across all the arrays (Figure 4.6). This visual representation of microarray findings supports the results from the initial quality control analysis (refer to Table 4.8) indicating three outlier samples (CO22 P1C2, CO25 P2A3 and MS100), which were eliminated from further analysis.

4.4.4 Confirmation of astrocyte enrichment

In order to confirm that the extracted RNA from each sample represented a significantly enriched astrocyte population, specific transcript expressions were investigated. High levels of GFAP transcripts (astrocyte: probe set id 203540_at, mean signal intensity

Sample	Probe sets % present	Background signal	RawQ	Scale-factor	GAPDH 3'-5' ratio
MS100 P2B3	22.54	26.88	0.65	19.62	46.33
MS67 P2C7	34.04	26.57	0.65	8.35	123.25
MS57 P1A6	36.35	27.18	0.67	7.24	212.30
MS50 P1E4	32.06	26.38	0.68	10.58	95.08
MS71 P2C3	35.59	26.27	0.68	7.04	109.64
PDCO16 P1B1	35.02	26.46	0.67	8.15	300.30
CO22 P1C2	20.01	25.82	0.68	23.17	14.89
CO25 P2A3	7.47	27.93	0.70	58.35	53.77
CO30 P2A2	32.56	26.08	0.66	11.00	58.39
PDCO23 P2B4	38.15	27.13	0.71	5.16	129.19

Table 4.8 Sample quality control analysis post microarray

Considering the different variables, samples MS100 P2B3, CO22 P1C2 and CO25 P2A3 (orange) were eliminated from the cohort based on their lower % probe sets present and high scale-factor scores.

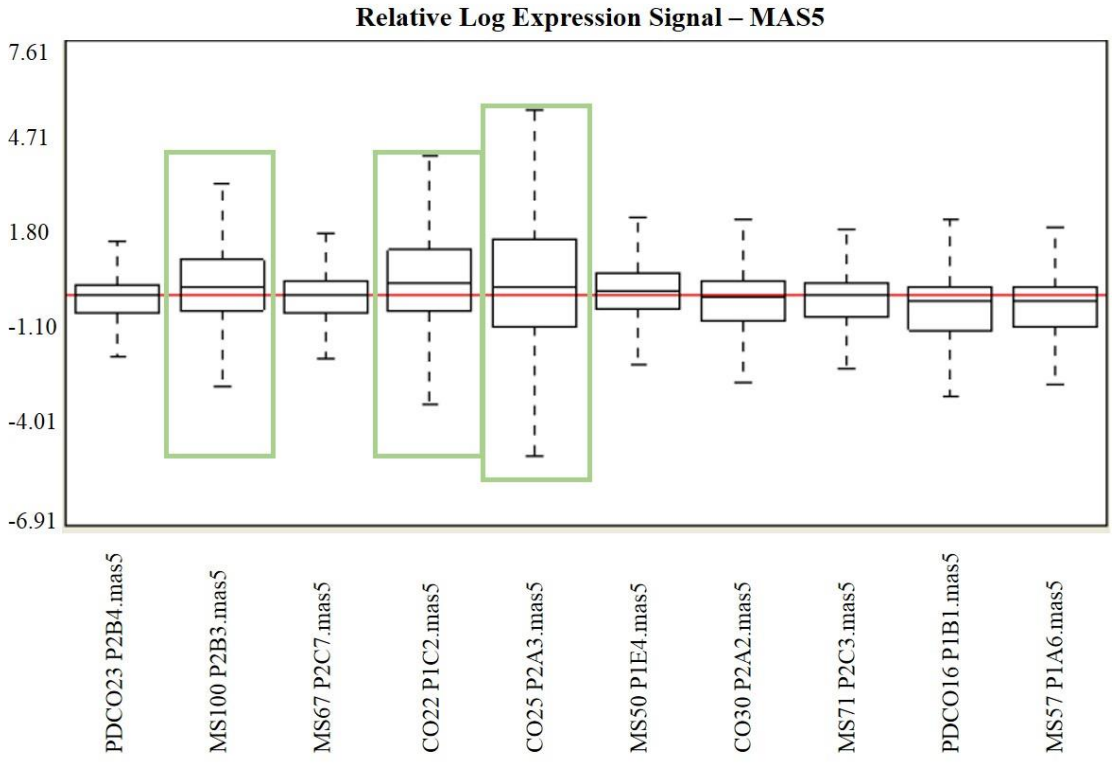

Figure 4.6 The relative expression signal for each array generated in Expression Console (MAS5.0 algorithm)

The median gene expression across all 10 arrays is identified (red line) and the overall deviation from the corresponding median is identified for each microarray chip. The Y-axis is the relative log expression signal for all 10 samples (X-axis).

5995.0; range, 1263.7-20549.3) but low levels of CD34 (endothelial cell: probe set id 209543_s_at, mean signal intensity 50.6; range, 14.7-98.4), CD68 (microglia: probe set id 203507_at, mean signal intensity 23.7; range, 4.1-64.1), and OLIG-2 oligodendrocyte: probe set id 213825_at, mean signal intensity 290.3; range, 133.5-520.7) confirming the extracted RNA from LCM-ed cells was an enriched astrocyte population. Moderately high levels of a neuronal transcripts were detected (NFL: probe set id 221805_at, mean signal intensity 3328.6; range, 368.9-5264.2), which may reflect the close proximity of astrocytes to axons which will be isolated along with the immunopositive astrocytes as a result of the LCM process.

4.4.5 Identifying differentially expressed genes associated with astrocytes isolated from MS NAWM in comparison to astrocytes from control WM

GeneSpring analysis was used to identify the differentially significant transcriptional changes in astrocytes isolated from MS NAWM compared to control WM. In total across the seven samples (four MS and three control) 3375 genes were differentially expressed (1778 upregulated and 1596 genes downregulated). Following GeneSpring analysis, transcripts were identified as significantly differentially expressed (up or down-regulated) if the expression level in the NAWM samples was altered with a fold change of ≥ 1.5, and a p-value ≤ 0.05 when compared to the control samples (Table 4.9).

4.4.6 Investigating differentially expressed genes in MS NAWM astrocytes compared to control WM astrocytes using DAVID

Significant differentially expressed gene lists (up and downregulated) were imported into DAVID, a tool used to group genes into pathways based on their biological function (Huang da *et al* 2009a, Huang da *et al* 2009b). Genes associated with immune response (Table 4.10), homeostasis (Table 4.11), cell signaling (Table 4.12), cytoskeleton (Table 4.13) and RNA processing/protein metabolism (Table 4.14) were grouped (Table 4.15) full tables of genes are listed in Appendix V. However when manually assessing gene expression from the top 20 differentially upregulated genes (Table 4.16), 6 genes (metallothionein 1X [MT1X], metallothioenin 1G [MT1G], metallothionein 2A [MT2A], metallothionein 1 pseudogene 2 [MT1p2], ferritin light chain [FTL], and transferrin [TF]) related to the homeostasis of metal iron, were confirmed through literature searching to be associated with oxidative stress and MS (Hametner *et al* 2013, Williams *et al* 2012).

	Total number of genes	Total number of up-regulated genes	Total number of down-regulated genes
GeneSpring analysis (total gene count) (4 MS vs. 3 CO)	3375	1778	1596
GeneSpring analysis FC ≥1.5 and P-value ≤0.05	452	208	244

Table 4.9 Total number of genes identified from the microarray study using GeneSpring software (MS NAWM vs control)

Probe Set ID	p-value	Fold change	Gene Symbol	Gene Title
209619_at	0.0075	2.73	CD74	CD74 molecule, major histocompatibility complex, class II invariant chain
225353_s_at	0.0164	1.77	C1QC	complement component 1, q subcomponent, C chain
217767_at	0.0352	1.94	C3	complement component 3
224079_at	0.0393	1.54	IL17C	interleukin 17C
203233_at	0.0130	1.54	IL4R	interleukin 4 receptor
211990_at	0.0026	2.01	HLA-DPA1	major histocompatibility complex, class II, DP alpha 1
201137_s_at	0.0056	1.85	HLA-DPB1	major histocompatibility complex, class II, DP beta 1
204748_at	0.0205	-1.56	PTGS2	prostaglandin-endoperoxide synthase 2 (prostaglandin G/H synthase and cyclooxygenase)
201331_s_at	0.0360	-1.73	STAT6	signal transducer and activator of transcription 6, interleukin-4 induced

Table 4.10 Differentially expressed immune response genes identified in astrocytes isolated from NAWM compared to control WM

Upregulated genes (black), downregulated genes (red).

Probe Set ID	p-value	Fold change	Gene Symbol	Gene Title
212788_x_at	0.0304	2.24	FTL	ferritin, light polypeptide
211456_x_at	0.0435	2.22	MT1P2	metallothionein 1 pseudogene 2
204745_x_at	0.0313	2.26	MT1G	metallothionein 1G
208581_x_at	0.0416	2.23	MT1X	metallothionein 1X
212185_x_at	0.0318	2.52	MT2A	metallothionein 2A
205970_at	0.0157	2.02	MT3	metallothionein 3
214064_at	0.0478	2.21	TF	transferrin
229463_at	0.0101	-3.11	NTRK2	neurotrophic tyrosine kinase, receptor, type 2
209747_at	0.0235	1.55	TGFB3	transforming growth factor, beta 3

Table 4.11 Functional grouping of the differentially expressed genes identified relating to dysregulation of homeostasis in astrocytes isolated from NAWM compared to control WM

Upregulated genes (black), downregulated genes (red).

Probe Set ID	p-value	Fold change	Gene Symbol	Gene Title
201460_at	0.0387	1.70	MAPKAPK2	mitogen-activated protein kinase-activated protein kinase 2
218181_s_at	0.0160	1.54	MAP4K4	mitogen-activated protein kinase kinase kinase kinase 4
209281_s_at	0.0488	-1.58	ATP2B1	ATPase, Ca^{2+} transporting, plasma membrane 1
203685_at	0.0468	1.76	BCL2	B-cell CLL/lymphoma 2
227751_at	0.0377	-1.75	PDCD5	programmed cell death 5
200788_s_at	0.0221	1.53	PEA15	phosphoprotein enriched in astrocytes 15
205117_at	0.0101	2.25	FGF1	fibroblast growth factor 1 (acidic)
211535_s_at	0.0039	1.63	FGFR1	fibroblast growth factor receptor 1

Table 4.12 Functional grouping of the differentially expressed genes associated with cell signaling and communication

Upregulated genes (black), downregulated genes (red).

Probe Set ID	p-value	Fold change	Gene Symbol	Gene Title
203590_at	0.0159	1.50	DYNC1LI2	dynein, cytoplasmic 1, light intermediate chain 2
203762_s_at	0.0349	-1.83	DYNC2LI1	dynein, cytoplasmic 2, light intermediate chain 1
203763_at	0.0344	-1.99	DYNC2LI1	dynein, cytoplasmic 2, light intermediate chain 1
209244_s_at	0.0053	1.80	KIF1C	kinesin family member 1C
212567_s_at	0.0191	2.05	MAP4	microtubule-associated protein 4
212566_at	0.0087	2.14	MAP4	microtubule-associated protein 4
200835_s_at	0.0198	1.62	MAP4	microtubule-associated protein 4
33850_at	0.0409	1.83	MAP4	microtubule-associated protein 4
243_g_at	0.0294	1.73	MAP4	microtubule-associated protein 4
235127_at	0.0128	1.89	PMP2	peripheral myelin protein 2
206826_at	0.0179	2.04	PMP2	peripheral myelin protein 2

Table 4.13 Differentially expressed cytoskeleton genes identified in astrocytes isolated from NAWM compared to control WM

Upregulated genes (black), downregulated genes (red).

Probe Set ID	p-value	Fold change	Gene Symbol	Gene Title
200810_s_at	0.0483	-1.97	CIRBP	cold inducible RNA binding protein
217863_at	0.0068	-1.54	PIAS1	protein inhibitor of activated STAT, 1
208616_s_at	0.0325	1.59	PTP4A2	protein tyrosine phosphatase type IVA, member 2
208732_at	0.0326	-1.99	RAB2A	RAB2A, member RAS oncogene family
208733_at	0.0032	-1.92	RAB2A	RAB2A, member RAS oncogene family
208929_x_at	0.0026	1.82	RPL13	ribosomal protein L13
212191_x_at	0.0103	1.91	RPL13	ribosomal protein L13
212933_x_at	0.0054	1.60	RPL13	ribosomal protein L13
212734_x_at	0.0023	1.95	RPL13	ribosomal protein L13
214351_x_at	0.0011	1.89	RPL13	ribosomal protein L13
200716_x_at	0.0024	1.53	RPL13A	ribosomal protein L13a
212790_x_at	0.0008	1.61	RPL13A	ribosomal protein L13a
210646_x_at	0.0007	1.59	RPL13A	ribosomal protein L13a
211942_x_at	0.0026	1.73	RPL13A /// RPL13AP25 /// RPL13AP5 /// RPL13AP6	ribosomal protein L13a /// ribosomal protein L13a pseudogene 25 /// ribosomal protein L13a pseudogene 5 /// ribosomal protein L13a pseudogene 6
200869_at	0.0141	1.68	RPL18A /// RPL18AP3	ribosomal protein L18a /// ribosomal protein L18a pseudogene 3
200003_s_at	0.0158	1.56	RPL28	ribosomal protein L28
200062_s_at	0.0014	1.71	RPL30	ribosomal protein L30
200092_s_at	0.0029	1.63	RPL37	ribosomal protein L37
201429_s_at	0.0011	1.67	RPL37A	ribosomal protein L37a
200936_at	0.0102	1.54	RPL8	ribosomal protein L8
200095_x_at	0.0056	1.55	RPS10	ribosomal protein S10
211542_x_at	0.0096	1.52	RPS10	ribosomal protein S10
200031_s_at	0.0008	1.55	RPS11	ribosomal protein S11
200819_s_at	0.0018	1.51	RPS15	ribosomal protein S15
226131_s_at	0.0029	1.52	RPS16	ribosomal protein S16
201049_s_at	0.0215	1.52	RPS18	ribosomal protein S18
202649_x_at	0.0032	1.75	RPS19	ribosomal protein S19
213414_s_at	0.0046	1.97	RPS19	ribosomal protein S19
212433_x_at	0.0018	1.55	RPS2	ribosomal protein S2
203107_x_at	0.0039	1.50	RPS2	ribosomal protein S2
200949_x_at	0.0024	1.58	RPS20	ribosomal protein S20
200834_s_at	0.0307	1.57	RPS21	ribosomal protein S21
208904_s_at	0.0013	1.53	RPS28	ribosomal protein S28
200024_at	0.0225	1.53	RPS5	ribosomal protein S5
214317_x_at	0.0140	1.59	RPS9	ribosomal protein S9
200763_s_at	0.0145	1.80	RPLP1	ribosomal protein, large, P1
202172_at	0.0208	1.54	VEZF1	vascular endothelial zinc finger 1
202173_s_at	0.0338	1.52	VEZF1	vascular endothelial zinc finger 1

Table 4.14 Differentially expressed RNA processing and protein metabolism genes identified in astrocytes isolated from NAWM compared to control WM

Upregulated genes (black), downregulated genes (red).

Functional groups	Number of genes	p-value
RNA Processing	19	0.013
Immunity and defence	34	0.021
Intracellular signalling cascade	28	0.0035
Protein metabolism and modification	70	0.0015
Cytoskeleton	35	0.026
Homeostasis		
Neuron development	12	0.046
Response to metal ion	7	0.031
Cellular cation homeostasis	10	0.046
Response to hypoxia	8	0.012

Table 4.15 DAVID analysis of significant, differentially expressed genes in astrocytes in MS NAWM versus control WM

Probe Set ID	p-value	Fold change	Gene Symbol	Gene Title
209619_at	0.008	2.73	CD74	CD74 molecule, major histocompatibility complex, class II invariant chain
225368_at	0.034	2.63	HIPK2	homeodomain interacting protein kinase 2
209343_at	0.029	2.57	EFHD1	EF-hand domain family, member D1
212185_x_at	0.032	2.52	MT2A	metallothionein 2A
225097_at	0.028	2.43	HIPK2	homeodomain interacting protein kinase 2
204037_at	0.018	2.39	LPAR1	lysophosphatidic acid receptor 1
225207_at	0.039	2.35	PDK4	pyruvate dehydrogenase kinase, isozyme 4
235617_x_at	0.044	2.29		
219236_at	0.027	2.28	PAQR6	progestin and adipoQ receptor family member VI
204745_x_at	0.031	2.26	MT1G	metallothionein 1G
205117_at	0.010	2.25	FGF1	fibroblast growth factor 1 (acidic)
211959_at	0.024	2.24	IGFBP5	insulin-like growth factor binding protein 5
212788_x_at	0.030	2.24	FTL	ferritin, light polypeptide
208581_x_at	0.042	2.23	MT1X	metallothionein 1X
229048_at	0.028	2.22		
211456_x_at	0.044	2.22	MT1P2	metallothionein 1 pseudogene 2
214064_at	0.048	2.21	TF	transferrin
201721_s_at	0.017	2.18	LAPTM5	lysosomal multispanning membrane protein 5
209000_s_at	0.037	2.18	SEPT8	septin 8
218251_at	0.011	2.16	MID1IP1	MID1 interacting protein 1 [gastrulation specific G12 homolog (zebrafish)]

Table 4.16 Top 20 differentially upregulated genes

From the top 20 differentially upregulated genes in astrocytes isolated from MS NAWM compared to control WM six genes (orange) were related to the homeostasis of iron and oxidative stress.

4.5 Discussion

In MS, it has been suggested that identifying the changes in pathology within the NAWM may elucidate the mechanisms of disease initiation and ultimate progression (Liang *et al* 2012, Melief *et al* 2013, Miller *et al* 2003, Traboulsee *et al* 2003, Zeis *et al* 2008). In this study LCM-ed isolated astrocytes from PM MS NAWM cases and control WM were subjected to gene expression microarray analysis to identify differentially expressed genes. Astrocytes perform a variety of key roles in the CNS: they maintain homeostasis by controlling ion concentrations including potassium and calcium (Sofroniew & Vinters 2010), provide nutritional metabolites to neurons and control the osmotic balance within the CNS (Sofroniew & Vinters 2010), release an array of pro- and anti-inflammatory cytokines and chemokines partaking in immune responses (Jensen *et al* 2013), and maintain the BBB (Abbott *et al* 2006). Furthermore, astrocytes respond to stimuli through a process known as astrogliosis (Zamanian *et al* 2012). The significant differentially expressed genes identified in this microarray study identified changes in functional gene groups associated with the immune response, homeostasis, cellular signaling and communication, cytoskeleton and protein metabolism. Most interestingly, from the top 20 differentially upregulated genes, six genes were related to the homeostasis of iron and the response to oxidative stress, which is an increasingly recognised factor in many neurodegenerative diseases (Al-Radaideh *et al* 2013, Bishop *et al* 2002, Carbonell & Rama 2007, Hametner *et al* 2013, Williams *et al* 2012).

4.5.1 Significant, differentially expressed genes associated with the immune response

Functional grouping of the significant differentially expressed genes identified enrichment of genes associated with the immune response (refer to Table 4.10), with the majority (16/19) of genes upregulated in MS NAWM compared to control WM. This finding supports previous gene expression studies performed on MS NAWM (Lindberg *et al* 2004, Lock *et al* 2002). However, also highlighted here and in agreement with published studies, was no significant differential expression of the commonly related inflammatory genes associated with MS such as TNFα, or IFNγ (Lindberg *et al* 2004, Lock *et al* 2002).

The upregulation of *IL-17C*, a proinflammatory cytokine previously linked to MS pathogenesis (Stromnes *et al* 2008), and increased expression of complement components (*C1QC and C3*) associated with complement mediated inflammation in MS

were identified (Brink *et al* 2005, Koning *et al* 2007, Rus *et al* 2006). Upregulation of immune response genes including *C1* and *C3* complement components have been identified in a microarray study of the MS model, Theiler's murine encephalomyelitis (Ulrich *et al* 2010) and in EAE mouse models (Matejuk *et al* 2003, Spach *et al* 2004). Corroborative studies in MS patients consistently identify an increased level of plasma C3 along with other complement factors (Ingram *et al* 2012). Through IHC the deposition of C3 expression by enlarged microglia in MS NAWM has been reported however this study failed to describe any astrocytic expression (Ramaglia *et al* 2012). Studies in EAE have shown mice deficient in C3 have reduced cellular infiltration and demyelination (Barnum 2002) with the expression of C3 required for full development of the disease (Szalai *et al* 2007), suggesting the increased expression of components of the complement cascade by astrocytes contributes to lesion pathogenesis.

A significant reduction in signal transducer and activator of transcription 6 *(STAT6)* in MS NAWM astrocytes compared to control WM was found in the current study. This finding is in contrast to previous reports of an increased *STAT6* expression associated with the presence of activated macrophage/microglia which were documented to be present throughout the NAWM cases used in that study, concluding an increased expression of *STAT6* was related to a persistent activation of macrophages/microglia in MS (Graumann *et al* 2003). These differences may reflect the stringent case selection parameters used in the current study which included the elimination of any NAWM cases which contained amoeboid $CD68^+$ microglia. Furthermore, the current study was performed on an enriched astrocyte cell population, which likely express a different transcriptomic profile to the heterogeneous cell population present in whole tissue studies. Immunohistochemical investigation of STAT6 expression in NAWM has demonstrated the colocalisation of STAT6 with myelinating oligodendrocytes and occasional $GFAP^+$ astrocytes, with no colocalisation of STAT6 expression and $CD68^+$ microglia (Zeis *et al* 2008). The downregulation of *STAT6*, which forms part of the anti-inflammatory Janus kinase/STAT (*JAK/STAT)*-signaling pathway, opposes the upregulation of its main receptor *IL-4R,* which was upregulated in the present microarray study and supports published qPCR findings (Zeis *et al* 2008). IL-4R expression may activate other unknown pathways in astrocytes as opposed to the *STAT/JAK* signaling pathway as no other *STAT* or *JAK* genes were identified in the current study, in contrast to whole tissue studies (Graumann *et al* 2003, Lindberg *et al* 2004, Zeis *et al* 2008).

The current study also identified significant downregulation of prostaglandin-endoperoxide synthase 2 *(PTGS2)* also known as cyclooxygenase-2 *(COX-2)* which is known to be expressed by inflammatory cells, infiltrating macrophages and ramified microglia close to the inflammatory infiltrates in MS (Minghetti 2004). COX-2 synthesises the production of prostanoids that contribute to chronic inflammation (Hinz & Brune 2002) and production of free radicals (Minghetti 2004). Non-steroidal anti-inflammatory drugs (NSAIDs) are a recognised treatment in MS (Klegeris & McGeer 2005, Lleo *et al* 2007) and may downregulate *COX-2* gene expression and ultimately the functioning protein, thereby having a beneficial anti-inflammatory effect. The decreased *COX-2* expression identified in this study may reflect patients' unspecified therapeutic treatment in life. Furthermore the reduction in *COX-2* expression may reflect neuroprotective action by astrocytes, limiting their production of free radicals, decreasing oxidative stress and preventing disease progression (Minghetti 2004).

4.5.2 Significant, differentially expressed genes associated with homeostasis

The current microarray study identified significant, differentially expressed genes associated with homeostasis (refer to Table 4.11), which can be subdivided into 3 groups related to neurotrophic support, metal ion binding and transcription, as shown in Table 4.15 (full gene list, Appendix V). These findings support published microarray studies in MS NAWM, which also identified significant differential expression of genes associated with cellular homeostasis and neuroprotection (Graumann *et al* 2003, Lindberg *et al* 2004, Zeis *et al* 2008). Similar to these reports, major downregulation of neurotrophic-related genes (15/21) was detected in the NAWM. However, in contrast to Lindberg's study, increased expression of transforming growth factor, beta 3 (*TGF-B3)* was detected in NAWM. TGF-B3 is an astrocyte derived regulator of neuronal survival known to enhance the action of neurotrophic factors (Krieglstein *et al* 2002), therefore the increased astrocytic expression of *TGF-B3* may potentially be neuroprotective in NAWM. Furthermore, *TGF-B3* gene expression is increased in EAE mice treated with anti-inflammatory oestrogen molecule, which also resulted in the decreased mRNA expression of the proinflammatory cytokine *TNFα* compared to untreated EAE mice (Matejuk *et al* 2002).

Neurotrophic tyrosine kinase receptor, type 2 *(NTKR2),* also known as tropomyosin receptor kinase B *(TrkB),* is activated by ligands, including brain-derived neurotrophic factor (BDNF), and contributes to neuroprotection (Colombo *et al* 2012). In the current

study, a marked reduction of *NTKR2* was identified in astrocytes isolated from MS NAWM, which is in direct contrast to other microarray studies where an upregulation of *TrkB* transcripts in MS NAWM and WML was reported (Graumann *et al* 2003, Mycko *et al* 2004). Also, TrkB protein expression was identified in active and IA lesions of MS patients (Stadelmann *et al* 2002) and in an EAE study (De Santi *et al* 2009). Conflicting accounts as to the expression of *TrkB* by astrocytes has been discussed (Colombo *et al* 2012, Song *et al* 2013). Mice that lack astrocytic TrkB are protected from EAE-induced neurodegeneration and compared to normal EAE-induced mice show a reduced cellular infiltration resulting in reduced neuroinflammation (Colombo *et al* 2012). Astrocytes in culture when stimulated with BDNF, increase their release of NO and astrocyte conditioned media was detrimental to neurons. Ultimately this suggests that NO synthesis in the CNS contributes to the development of EAE and is dependent on astrocyte expressed TrkB, with increased astrocyte expression of TrkB being detrimental due to the increased NO production (Colombo *et al* 2012).

The reduction in NTKR2 expression in isolated astrocytes from NAWM may suggest a response to the increase in NO within lesion centres, and an attempt to maintain homeostasis within the tissue. NAWM astrocytes may reduce expression of growth factor receptors to limit the potential neurodegenerative effects from interactions with neurotrophic factors such as BDNF. Increased disease incidence and severity of EAE has been reported in TrkB (+/-) heterozygous mice compared to wild type TrkB (+/+) mice (Song *et al* 2013). This contradicts previous findings that showed the upregulation of TrkB receptor expression in astrocytes in MS lesions and that the astrocyte TrkB knock-out (KO) model protected against EAE induced demyelination (Colombo *et al* 2012). The increased disease severity in the TrkB heterozygous mouse was presumed to be as a result of an increased BDNF interaction with its alternative p75 receptor because of reduced levels of TrkB. Evidently a better understanding of TrkB and its interactions in MS is needed. The discrepancies between these studies could reflect different downstream effects of TrkB signaling at different time points, or in different cell types during the disease course (Song *et al* 2013). Previous microarray studies indicating an increase in *TrkB* in MS lesions and NAWM were derived from whole tissue (Graumann *et al* 2003, Mycko *et al* 2004), however the transcriptomic data in the current microarray study originates from an enriched astrocyte population from MS NAWM, highlighting one of the advantages of using LCM based methodology in transcriptomic studies in assessing gene expression to a specific cell population.

The expression of proinflammatory molecules by activated glia plays an important role in the pathogenesis of MS and is also critical to the regulation of genes associated with oxidative stress and tissue damage (Miller *et al* 2013). Despite lack of specific expression of *IFN* genes in this study, apart from the interferon induced transmembrane protein *(IFITM)1* and *IFITM2,* which have not been reported previously in MS pathology, a number of genes were differentially expressed which play a role in limiting oxidative stress and maintaining homeostasis (Haider *et al* 2011).

The current study identified significant upregulation of various metal ion binding genes including five metallothionein *(MT)* isotypes, *TF* and *FTL*. These genes regulate levels of metal ions, in particular iron, which have been shown to accumulate in MS lesions and exacerbate oxidative damage through the conversion of hydrogen peroxide to free-radical ions (Hametner *et al* 2013). An increase in *TF* and *MT1L* expression has also been identified by microarray analysis in both acute and CAL when compared to control tissue (Tajouri *et al* 2003). Similarly microarray analysis identified the increased expression of *MT* genes, representing a stress response in MS lesions compared to control tissue was detected (Lock *et al* 2002) and *MT1* has been demonstrated in MS chronic and active lesions (Jelinsky *et al* 2005). *MT's* have been indicated in the development of lesions in both MS and EAE studies (Jelinsky *et al* 2005, Penkowa *et al* 2003b, Penkowa *et al* 2003c). These findings are in contrast to one study which did not report any significant alteration in *MT1* or *MT3* expression in the spinal cord of EAE mice (Carmody *et al* 2002). However, the expression of these two genes in the spinal cord of control C57BL/6 mice formed part of the top 20 most abundant genes in the normal CNS (Carmody *et al* 2002). Discrepancies between studies maybe due to the anatomical area investigated, as the spinal cord is not a true reflection of the whole CNS and may reflect regional variations in gene expression (Carmody *et al* 2002). Reports indicate that lactotransferrin *(Ltf),* a member of the TF family, is highly expressed at all stages of EAE in comparison to control mice (Baranzini *et al* 2005). The current study suggest that astrocytes play a key role in reducing the amount of iron within the NAWM in MS, thereby preventing the accumulation of oxidative damage and the spread of lesion formation.

4.5.3 Significant, differentially expressed genes associated with cell signaling and communication

Although KEGG pathway analysis of the microarray data did not identify alterations in specific signaling pathways, functional grouping analysis identified the differential

expression of genes related to mitogen-activated protein kinase (MAPK), insulin, calcium and ubiquitin signaling pathways, in addition to genes involved in apoptosis and cell junction/synapses. These findings support previous studies which have shown differential expression of genes associated with receptor mediated signaling pathways in NAWM compared to control WM (Graumann *et al* 2003, Zeis *et al* 2008). Dysregulation of intracellular signaling pathways is also a feature of acute MS lesions (Whitney *et al* 1999), active MS lesion margins (Mycko *et al* 2003), and cortical pathology in MS (Dutta *et al* 2007). In a recent LCM study genes associated with a cellular response to stress and/or hypoxia were identified through qPCR on LCM isolated MS NAWM in comparison to control cases (Cunnea *et al* 2011). Clearly dysregulation of signaling pathways play a key role in the pathogenesis of MS, but understanding the origins and consequences of these signals is difficult to comprehend in the heterogeneous cell population present in the CNS, yet has the potential to identify specific therapeutic targets.

The emerging role of MAPK in MS has recently been reviewed (Krementsov *et al* 2013). MAPK signaling is associated with directing cellular responses to stimuli such as heat, hypoxia, and cytokines and is involved in the control of many cellular processes, particularly those related to cell proliferation, cell stress and apoptosis (Berridge 2012). In support of the literature, the current study identified significant upregulation *of mitogen-activated protein kinase-activated protein kinase 2 (MAPKAPK2)* (Graumann *et al* 2003) and mitogen-activated protein kinase kinase kinase kinase 4 *(MAPK4)* in the NAWM (refer to Table 4.12), both of which have been linked to ischaemic preconditioning and oxidative stress associated with MS (Graumann *et al* 2003).

Calcium signaling is associated with the regulation of many cellular processes including cellular excitability, exocytosis, motility, apoptosis, and transcription (Clapham 2007). Ca^{2+} binds to and affects the localisation, association and function of proteins (Clapham 2007). Dysfunction of calcium pumps and exchangers are linked to axonal injury and neuronal dysfunction in both MS and EAE (Kurnellas *et al* 2007). Abnormal influx, extrusion, buffering and sequestration of calcium results in calcium imbalance, which may initiate detrimental mechanism(s) that ultimately result in neuronal degeneration and cell death (Kurnellas *et al* 2007).

Recent comparisons of other microarray datasets identified dysregulation of calcium/calmodulin-dependent protein kinase activity in MS (Borjabad & Volsky

2012). In the current study, a downregulation of genes associated with intracellular calcium signaling have been demonstrated, including a gene involved in the extrusion of calcium from cells, the ATPase, $Ca2^{+}$ transporting, plasma membrane 1 *(ATP2B1)* also known as plasma-membrane $Ca2^{+}$-ATPase 1 *(PMCA1)*. Although changes in the expression of this gene have not previously been linked to MS (Nicot *et al* 2005, Nicot *et al* 2003), a decreased expression of its alterative isotype *PMCA2* has been reported in both MS and EAE (Kurnellas *et al* 2007, Nicot *et al* 2005).

Apoptosis plays a key role in the removal of autoreactive T cells in EAE (Okuda *et al* 2002). However, apoptosis of immune cells can also lead to the damage and destruction of oligodendrocytes and neurons in MS (Banisor & Kalman 2004). In the current study, an upregulation of the anti-apoptotic gene *BCL2* was identified in astrocytes isolated from MS NAWM compared to control WM, supporting previous work that showed increased expression of anti-apoptotic *BCL2* and pro-apoptotic BCL2 antagonist killer *(BAK)* in MS NAWM and CAL (Banisor & Kalman 2004). It has been suggested that efficient control of inflammation in MS is due to activation of the Fas/FasL pathway resulting in cell death (Banisor & Kalman 2004). Increased expression of *BCL2* has also been reported in microarray studies investigating cortical involvement in MS (Dutta *et al* 2007). The current study identified downregulation in expression of programmed cell death 5 *(PDCD5)* gene which has not been previously been discussed in relation to MS, however PDCD5 protein is known to accelerate apoptosis and has been shown to be downregulated in many cancer studies (Du *et al* 2009, Li *et al* 2008a, Spinola *et al* 2006, Xu *et al* 2012, Yang *et al* 2006). One study investigating ischaemic damage in the brain hypothesised that the inhibition of *PDCD5*-induced apoptotic pathways is protective to neurons in ischemia by reducing apoptotic-related protein such as p53, Bax and caspase-3 (Chen *et al* 2013a). The downregulation of pro-apoptotic and upregulation of anti-apoptotic genes in isolated astrocytes from MS NAWM may reflect functional changes in the cells to limit their own death as a result of glutamate excitoxicity and oxidative stress seen in MS, therefore indirectly protecting surrounding neuronal axons. However, the particular role of these anti-apoptotic genes by astrocytes in MS NAWM is yet to be fully elucidated and further work is required.

In the CNS FGFs induce axonal growth, neurogenesis, neuroprotection and lesion repair through activation of receptors on target cells (Reuss & von Bohlen und Halbach 2003). In astrocyte culture systems, FGF-1 is released in response to cell injury such as

oxidative stress, heat shock, hypoxia, and serum starvation (Reuss & von Bohlen und Halbach 2003). Increased expression of FGF-1 by activated astrocytes has been demonstrated in MS (Kimura *et al* 1994) and in AD (Mashayekhi *et al* 2010). The current study demonstrates increased expression of *FGF-1* by astrocytes in the NAWM, which may reflect a response to insult, such as oxidative stress (Ludwin 2006, Zeis *et al* 2008) and the astrocytic attempt to prevent lesion spread.

4.5.4 Significant, differentially expressed genes associated with the cytoskeleton

The cytoskeleton is a complex network of actin filaments, microtubules and intermediate filaments, which support cell structure and function in an array of processes such as apoptosis, migration and invasion (Vergara *et al* 2009). Many neurodegenerative diseases such as ALS, PD and AD are hallmarked by changes in cytoskeletal proteins, which are categorised into either filamentous aggregates of neuronal filament proteins, or inclusions containing microtubule-associated proteins (MAP) tau (Cairns *et al* 2004). In MS, the main axon cytoskeleton proteins including the light, medium and heavy neurofilaments (NF), beta tubulin (TUB) and GAP-43 are decreased in lesions (Fressinaud *et al* 2012). However, the involvement of specific cellular cytoskeleton proteins in MS has been overlooked with the disease being branded as chronic neuroinflammatory. Consequently, the majority of research has revolved around the autoimmune and immunological responses associated with the disease, especially apparent from the work conducted on the traditional MS animal model EAE (Comabella & Martin 2007).

Astrocytes rapidly adapt to insult in the CNS, this is associated with the differential expression of genes associated with the cytoskeleton network, including GFAP. In this study the isolation of astrocytes was based on GFAP expression, therefore it is not surprising that GFAP was not significantly differentially expressed. However, GFAP signal intensities from the study were higher in MS NAWM cases compared to control cases with GFAP mean signal intensity in MS NAWM cases being 9066.4 (range; 2278.3-20549.3), compared to control cases GFAP mean signal intensity of 1899.3 (range; 1263.7-3046.4), suggesting astrocytes respond to some form of insult in MS NAWM by the increased expression of GFAP. Many of the published microarray studies in human MS tissue have failed to identify significant differential expression of genes associated with changes in cellular cytoskeleton, which may reflect analysis of whole tissue, rather than isolated enriched individual cell populations, where specific cytoskeletal changes in cells is masked or assigned to other generic functions such as

cell signaling or immune response. However, differentially expressed genes associated with the cytoskeleton were identified in MS acute and chronic lesions in comparison to control WM, in particularly the expression of *MAP4* and dynein, cytoplasmic 1, light intermediate chain 2 *(DYNC1LI2)* which were upregulated in the findings of (Tajouri *et al* 2003).

In contrast other components of the cytoskeleton signaling pathway, including dynein, cytoplasmic 2, light intermediate chain 1 *(DYNC2LI1)*, were downregulated in the current study (refer to Table 4.13). An imbalance in dynein expression in astrocytes in MS NAWM may lead to a disruption in function and altered transport of neurotrophic factors in MS, as has been seen in ALS (Chevalier-Larsen & Holzbaur 2006). A recent study modelling gene-gene interactions in a number of MS GWAS classified calcium-signaled cytoskeleton regulation as a potential neurodegenerative mechanism in MS (Bush *et al* 2011). However, none of the genes identified in that study were differentially expressed in this current one.

As in human microarray studies, the majority of EAE microarray studies identified the regulation of immune response-associated genes, with little reference to changes in genes related to the cytoskeleton. Although one study categorised a set of cytoskeleton associated genes as being differentially expressed in AT-EAE mice, with a general equal quantity of up and down-regulated genes, but no reference to specific genes was made (Brand-Schieber *et al* 2005). A similar divide of up- and downregulated genes associated with the cytoskeleton was also identified in the current study (Full gene list, Appendix V). Specifically an increased expression of kinesin family member 1C *(KIF1C)* was identified, this specific kinesin family member has not been implicated in MS before, however the expression of kinesin genetic variants has been linked to the disease (Alcina *et al* 2013, Goris *et al* 2010). Kinesin is known to play a role in supplying energy for glial cells by trafficking mitochondria along the cytoskeleton protein, tubulin, in response to the surrounding energy demands (Szolnoki *et al* 2007). Altering expression of kinesin molecules may alter the energy production by glial cells. An increased expression of KIF1C by astrocytes may lead to increased energy production, an attempt by astrocytes to help maintain myelin integrity within the NAWM (Szolnoki *et al* 2007). Kinesins traffic the myelin synthesis apparatus, therefore increased KIF1C may increase myelin synthesis, due to an increased synthesis capacity. The current study also reports the increased expression of peripheral myelin protein 2

(PIMP2), a protein component of the myelin sheath present in small amounts in CNS myelin (Majava *et al* 2010). Further investigations into the significance of these differentially expressed cytoskeletal genes by astrocytes in MS NAWM is required to gain a better understanding of their importance in respect to disease pathogenesis.

In astrocyte cell culture systems, artificial activation of the cells by H_2O_2 mediates a change in the cytoskeletal network associated with changes in actin and myosin (Zhu *et al* 2005). The cytoskeletal network has previously been reported as one of the earliest targets in oxidative stress (Dalle-Donne *et al* 2001, Zhao & Davis 1998), suggesting that alterations in cytoskeletal gene expression in astrocytes isolated from MS NAWM may reflect an early response to increased oxidative stress in the surrounding demyelinated lesions. In culture, rat astrocytes show an altered cytoskeletal organisation when treated with IFNβ, a commonly used drug in MS (Vergara *et al* 2009), suggesting changes in the cytoskeleton organisation alter the cells' morphology and possible function. Therefore, astrocytes may alter their cytoskeletal gene expression in NAWM to provide protection from disease initiating insults, including oxidative stress.

4.5.5 Significant, differentially expressed genes associated with RNA processing and protein metabolism.

From the published microarray studies on MS/EAE only one study identified a group of differentially expressed genes associated with an RNA processing function in spinal cord of EAE mice, but failed to report specific genes (Brand-Schieber *et al* 2005). However, a recent study identified the influence of cold inducible RNA binding protein (CIRBP) on inflammation, making specific reference to its possible involvement in autoimmune disorders (Brochu *et al* 2013). CIRBP responds to an array of stresses including hypoxia and UV irradiation, and plays a role in RNA processing by binding to the 3'untranslated region (UTR) of specific transcripts to stabilise them and support their transport to ribosomes for translation (Brochu *et al* 2013). This study identified the association of CIRBP with the expression of an array of transcripts related to inflammation including *IL-1β*, a cytokine also regulated by NFkB (Brochu *et al* 2013). By using small interfering RNA (siRNA) to silence *CIRBP* expression in fibroblasts, the binding capacity of NFkB is disrupted, reducing the expression of *IL-1β*. Ultimately CIRBP affects the sensitivity of cells to a variety of stresses by regulating NFkB activity, with CIRBP disruption leading to a reduced IL-1β expression, highlighting CIRBP's role in regulating inflammation. Conversely a forced increased fibroblast

expression of CIRBP led to an increased expression of IL-1β (Brochu *et al* 2013). In contrast to the study whereby (Brochu *et al* 2013) reported in response to UV stress an increased expression of CIRBP, in the current study, *CIRBP* is downregulated suggesting that in MS NAWM, astrocytes are decreasing their *CIRBP* expression to prevent an inflammatory response in the NAWM. However more work on astrocyte expression of *CIRBP* and its function related to MS is needed as it is known that CIRBP responds to a variety of stresses in different ways (Brochu *et al* 2013). Astrocytes are responsible for maintaining homeostasis within the CNS and are adaptable cells, therefore astrocytes in the NAWM may respond by initially decreasing their expression of *CIRBP* in an attempt to halt the spread of inflammation and disease progression.

Differentially expressed genes associated with the regulation of protein activity and metabolism are associated with both acute and chronic MS lesions (Tajouri *et al* 2003). Specifically, the upregulation of *RAB2* was seen in a microarray study by (Tajouri *et al* 2003) which is in contrast to the finding of a decreased expression of this transcript in the current study, while the protein inhibitor of the activated signal transducer and activator of transcription (STAT) 1 *(PIAS1)* was decreased in both studies. Differences seen in the expression of specific protein metabolism genes may in part be down to the samples used. (Tajouri *et al* 2003) investigated both chronic and acute MS tissue while the current study identified differentially expressed genes in astrocytes isolated from MS NAWM, clearly varying transcriptomes are apparent across the tissues. Protein synthesis and metabolism associated genes have also been identified in EAE mice with the decreased expression of ribosomal protein S26 *(RPS26)* (Ibrahim *et al* 2001). However, the current study identified the upregulation of a number of different ribosomal proteins in MS NAWM astrocytes (refer to Table 4.14). Again, these differences may be due to gene expression profiles being compared between EAE animals and human subjects, the tissue type and disease stage may act as confounders to these differences.

Inflammation results in increased expression of genes associated with protein synthesis and metabolism in EAE (Mix *et al* 2004), with many of the genes being linked to an increased disease susceptibility. Also, in the TME viral model of MS, genes associated with protein metabolic processes including protein tyrosine phosphatase 4A2 *(PTP4A2)* and vascular endothelial zinc finger *(VEZF1)* are differentially regulated (Navarrete-Talloni *et al* 2010), supporting the current study's findings. Again, direct comparisons

between gene expression profiles of a viral animal model of MS and human MS subjects, along with differences in cell types investigated will account for many of the conflicting results of these microarray studies.

4.5.6 The 'pros' and 'cons' of gene expression microarray analysis

Current MS microarray studies have investigated the gene expression profile of human brain tissue, circulating PBMC, and tissue/cells obtained from MS animal models. Comparison between studies is hindered by differences in patient groups, the heterogeneity of the regions investigated and the experimental design, including the use of differing microarray platforms. These differences make the comparison of data sets and the associated gene expression between studies highly problematic.

There are a number of issues to consider when performing RNA profiling of samples using microarray analysis. To date, MS microarray studies have primarily aimed to identify; 1) biomarkers of disease, 2) molecular mechanisms of disease, and 3) potential drug targets (Kinter *et al* 2008). The primary aim of the study determines which sample(s) to use, the number of samples required for statistical significance, the appropriate microarray platform and the statistical analysis to perform. This current study was a non-hypothesis driven project to investigate the role of astrocytes in MS NAWM, thereby enabling the identification of altered expression of novel genes for which further hypothesis driven research could be carried out.

The use of microarray analysis of gene expression clearly has many advantages, however there are many limitations to the technique, which should be acknowledged and which may explain the lack of consistent findings between studies (Comabella & Martin 2007). The variability in MS microarray studies may reflect the genetic variation between cases, the patient cohort size employed and the difference in disease type investigated, whether PPMS or SPMS for example. Also, the PMI of human samples is known to affect the RNA integrity and ultimately gene expression profile, and human PM tissue is only a snapshot of disease activity. In order to avoid these issues, the current study investigated NAWM obtained from similar neuroanatomical locations. However, it should be noted that the data may also be influenced by the disease course of the patient, whether in relapse or remission at time of death, which was unknown in the current study, and/or the distance of the NAWM block from a WML. Additionally the cellular makeup of tissue investigated in preceding studies and the use of different microarray platforms containing different genes and probe sets could add to the different findings between studies (Munro & Perreau 2009). Multiple RNA processing

steps could, in part, also contribute to the different gene expression profiles between studies. For instance RNA extracted from cell culture models is more intact than RNA isolated in the current study. Immuno-guided LCM was used to isolate astrocytes from PM human tissue prior to RNA extraction and amplification. Therefore, RNA integrity of samples may have been affected due to the rapid-IHC protocol used and the laser fired from the LCM. RNA extraction and multiple rounds of RNA amplification could further modify the RNA integrity of samples and ultimately the hybridisation to microarray chips. Also the various methods used for statistically analysing gene expression data may account for the diverse findings in studies, with (Lindberg *et al* 2004) defining significantly expressed genes as having a 2-fold change compared to the current study, which implemented a cut off of 1.5 fold change and 0.5 p-value as being significant. Ultimately, this may not be suitable for some genes, where only a slight change in expression (below the cut off) could account for a profound effect related to disease pathogenesis. However, from previous studies in our research group and the large quantity of data generated a balance had to be determined.

In order to improve the reliability of microarray data, additional validation studies must be carried out as discussed in detail in chapter 5. Validation of microarray data should be obtained using alternative methods such as analysing the gene expression using qPCR, but also by the use of other techniques to assess protein expression such as IHC, WB and MALDI-MS to investigate the functional proteomic profiles of these regulated genes (Comabella & Martin 2007). Validation should be completed on an additional cohort of patients where results from the validation patient cohort should support the findings from the original microarray patient cohort (Comabella & Martin 2007).

Disease heterogeneity in human subjects will always be a limiting factor in any investigative study into understanding disease, including microarray studies (Munro & Perreau 2009). However, the future direction of microarray research applied to study disease needs to consider other supplementary work to gain a fuller, broader yet specific understanding of disease pathogenesis. Consideration of the genetic background of individuals, environmental triggers, individual differences in immune reactivity towards pathological insults, and treatment responses need to be addressed (Comabella & Martin 2007). Integration studies combining transcriptomic microarray research with potential proteomic work such as MALDI-MS could ultimately help to identify potential biological biomarkers of disease (Hori *et al* 2012). However the need for a better understanding of analysis software that enables researchers to compare both

transcriptomic microarray data and proteomic mass spectrometry derived data to decipher possible links and connections is required. In order to limit the inevitable variation in human subjects, integrating microarray data with a thorough neuropathological assessment pre and post mortem, along with MRI data, could add to the knowledge of that individual's disease activity, which as has already discussed, could ultimately add to the variability.

The emerging next generation sequencing technology, the transcriptome sequencing instrumentation, also known as RNA-Seq is poised to replace microarray based technologies for transcriptome analysis (Hitzemann *et al* 2013). Compared with microarray analysis, RNA-Seq has a greater dynamic range and no issues with probe saturation (Pozhitkov *et al* 2010). The technique also detects both coding and non-coding RNAs, and is capable of identifying the expression of regulatory micro RNA (miRNA) (Ziats & Rennert 2013), and can also detect alternative spliced transcripts and allele specific expression and nucleotide polymorphisms (Hitzemann *et al* 2013). The subsequent transcriptomic data derived from this technology is not biased to the 3' UTR as observed with many microarray derived datasets. However, RNA-Seq technology has its own limitations and disadvantages, including the interpretation and analysis of the huge data sets, and the cost of running samples using this technology. However, with increasing acknowledgment of the diversity and complexity of disease transcriptomics, RNA-Seq is a sophisticated technology that will undoubtedly aid in future transcriptomic studies of many diseases.

4.5.7 Conclusion

The current microarray study demonstrated that astrocytes isolated from MS NAWM are involved in a number of different functions within the NAWM associated with the immune response, cell signaling, cytoskeletal changes and the regulation of homeostasis. The most significant, differentially upregulated genes were related to the regulation of iron and oxidative stress. Therefore, astrocytes in MS NAWM may be playing a neuroprotective role by attempting to maintain homeostasis within the brain by regulating iron concentration and subsequent oxidative stress established in MS lesions in order to prevent lesion spread and ultimately disease progression.

CHAPTER 5

THE NEUROPROTECTIVE ROLE OF ASTROCYTES IN REGULATING IRON HOMEOSTASIS AND OXIDATIVE STRESS IN MULTIPLE SCLEROSIS NORMAL APPEARING WHITE MATTER

5.1 Introduction

Iron is vital in many biochemical and enzymatic reactions within the human body and is critical in the synthesis of ATP, DNA, myelin and neurotransmitters, within the CNS (Crichton *et al* 2011, Todorich *et al* 2009). Iron is capable of being oxidised and reduced between its ferric (Fe^{3+}) and ferrous (Fe^{2+}) state (Papanikolaou & Pantopoulos 2005). This ability to accept and donate electrons is pivotal in both its physiological role and its proposed pathological role in neurodegeneration. The regulation of iron is strictly regulated, since insufficient or excess impacts cell viability. The current study identified dysregulation of genes responsible for the regulation of iron homeostasis and oxidative stress in isolated astrocytes from MS NAWM.

To date, the mechanism(s) of iron transport and metabolism within the brain are not fully understood due to a number of factors (Ke & Qian 2007). Firstly, the lack of serum and blood in the abluminal surface of the BBB, which is shown to be involved in the well-established mechanism of iron transport and metabolism in other organs (Johnstone & Milward 2010). Additionally, research regarding the expression of iron exporter proteins throughout the BBB and CNS is contradictory, for example reports on the expression of divalent metal transporter 1 (DMT1) by blood vessel endothelial cells (BVEC) is inconsistent (Moos *et al* 2006, Siddappa *et al* 2002). Furthermore, as yet uncharacterised novel mechanisms/proteins involved in iron regulation in the brain may account for the lack of understanding of iron transport and metabolism in the brain (Johnstone & Milward 2010). However, it is established that the brain is unique in its method of regulating the transportation and release of iron. An increased understanding of how iron is transported, metabolised and regulated within the brain could help in understanding the relationship between iron and neurodegenerative diseases.

Within the human body there is around 4-5g of iron (Zheng & Monnot 2012), the majority of which is within haemoglobin, within erythrocytes and is termed 'heme-iron', accounting for at least 75% of the total body's iron (Gaasch *et al* 2007). The remaining iron within the body is bound to plasma proteins, such as the iron transporter protein TF, or the storage molecule ferritin (FT) (Gaasch *et al* 2007). Iron is believed to enter the CNS from the circulation via BVEC, primarily as TF-bound iron (Moos *et al* 2007). Within the brain, iron is widely distributed with varying concentrations in different regions, associated with different cell types, accumulating progressively with age and neurodegenerative disease (Khalil *et al* 2011b, Moos *et al* 2007, Ramos *et al* 2013). Levels of iron are higher in motor-related areas of the brain compared to non-

motor regions (Chen *et al* 2013b, Koeppen 1995, Zhang *et al* 2010), suggesting an imbalance of iron regulation in these regions may contribute to movement disorders.

In order to understand the relationship between iron and neurological diseases, an understanding of the mechanisms of iron transport into the brain, the cellular distribution/regulation of iron in the brain parenchyma and the process by which iron is removed from the CNS is needed. The brain cannot take up iron directly from the circulatory system, instead iron crosses the BBB via endocytosis into BVEC (Figure 5.1) or transcytosis across BVEC (Figure 5.2). The proposed main route of iron entry into the brain involves TF/Transferrin receptor-1 (TFR1) interaction, whereby BVEC acquire iron from circulatory TF via TFR1 expression on the cells' membrane. Iron passes into and across the BBB via vesicles and is exported as ferrous iron into the brain parenchyma. There is huge debate and less understanding as to the processes behind free iron exportation into the brain parenchyma (Deane *et al* 2004, Moos & Morgan 1998, Takeda *et al* 2002). As previously mentioned there is conflicting evidence of DMT1 expression by BVEC (Moos *et al* 2006, Siddappa *et al* 2002). Likewise discrepancies in ferroportin (FPT) expression by BVEC have been reported (Moos *et al* 2007, Wu *et al* 2004). It has been suggested that in the absence of DMT1 expression by BVEC, astrocytes that form up to 95% of the lining of the abluminal surface of the BBB (Cecchelli *et al* 2007) express DMT1 *in vivo* at their perivascular endfeet (Burdo & Connor 2003). Yet again, the expression of DMT1 by astrocytes is debatable (Moos & Morgan 2004). However, astrocytes release citrate and ATP forming complexes with iron in the extracellular space and are responsible for an alternative method of iron exportation into the brain (Leitner & Connor 2012, Ma *et al* 2009, Moos *et al* 2007, Qian & Shen 2001). Astrocytes are also capable of delivering transported iron to neurons via the action of FPT and ceruloplasmin (Cp) that results in exported ferric iron binding to locally circulating TF in the brain (Moos *et al* 2007). Brain TF can deliver iron to TFR1-expressing cells in the CNS including neurons, and OPC where iron is released via endocytosis to carry out its functional role.

Alternatively, iron can cross the BBB bound to TF via transcytosis (Fishman *et al* 1987, Moos 2002), where iron bound TF directly interacts with TFR1 expressed on neurons. Iron can cross the BBB bound to FT via T cell mucin domain containing receptor 2 (Tim2) by receptor mediated transport (Todorich *et al* 2008).

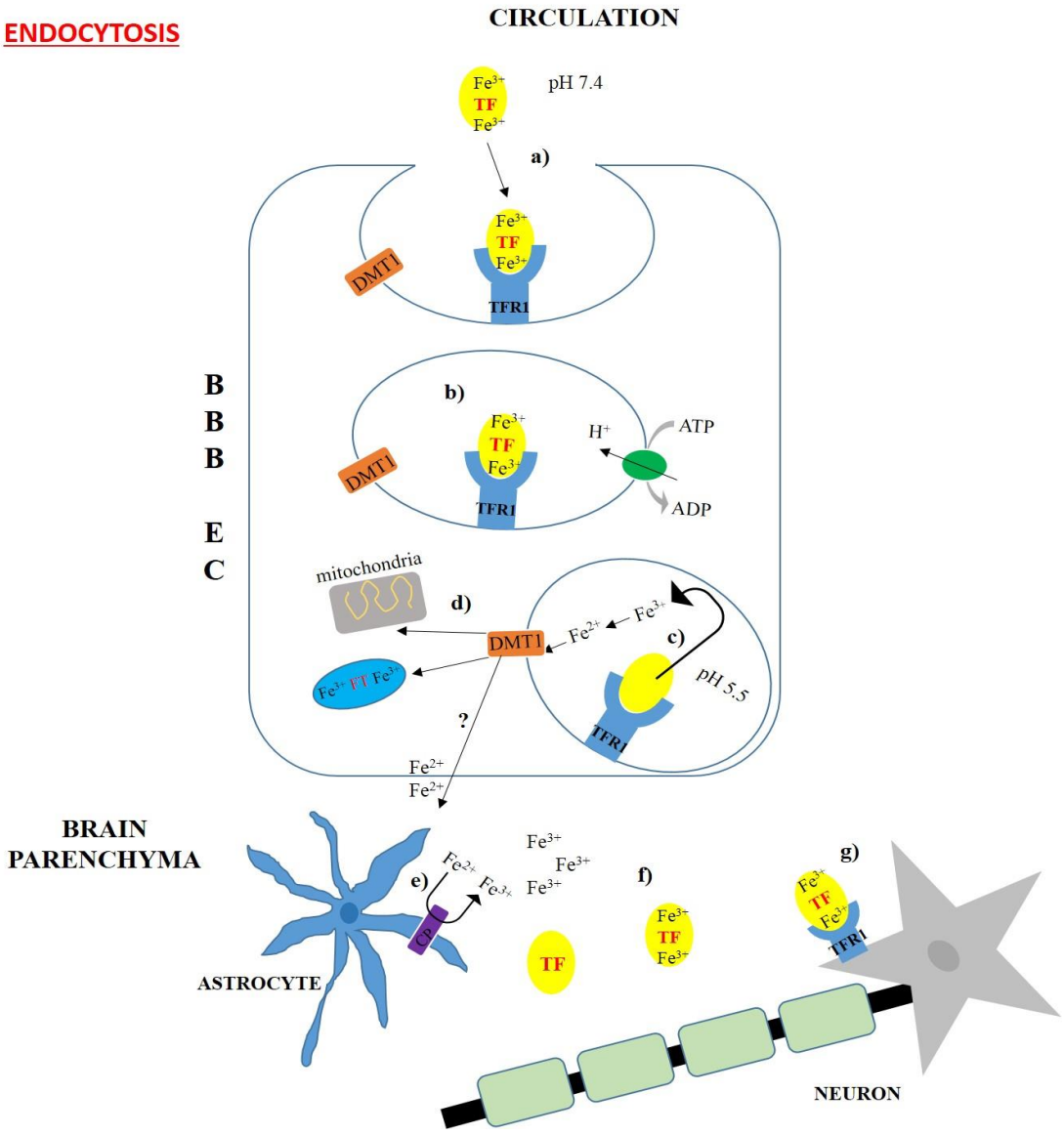

Figure 5.1 The regulation of iron transport into the brain via endocytosis

TF- bound iron in the circulatory system binds TFR1 expressed on endothelial cells of the BBB (a). This complex is endocytosed into the cells. Endocytic vesicles possess ATPases that pump protons into vesicles resulting in increased acidity (b), the reduction in pH causes iron to dissociate from TF (c). Reduced iron is transported into the cytosol by the DMT1 (d). Iron can be stored in FT or used in metabolic cellular processes, such as in the electron transport chain of mitochondria. Also, free iron inside the cell can cross into the brain through an unknown exportation mechanism. Iron can be reoxidised by the action of Cp expressed by astrocytes (e) and bind to circulating TF in the brain (f). TF-bound iron binds to TFR1 expressed on neurons and is endocytosed into the endolysosome where iron is dissociated from TF to carry out its neuronal functions.

Key: BBB: blood brain barrier, Cp: ceruloplasmin, DMT1: divalent metal transporter 1, EC: endothelial cell, FT: ferritin, TF: Transferrin, TFR1: transferrin receptor-1.

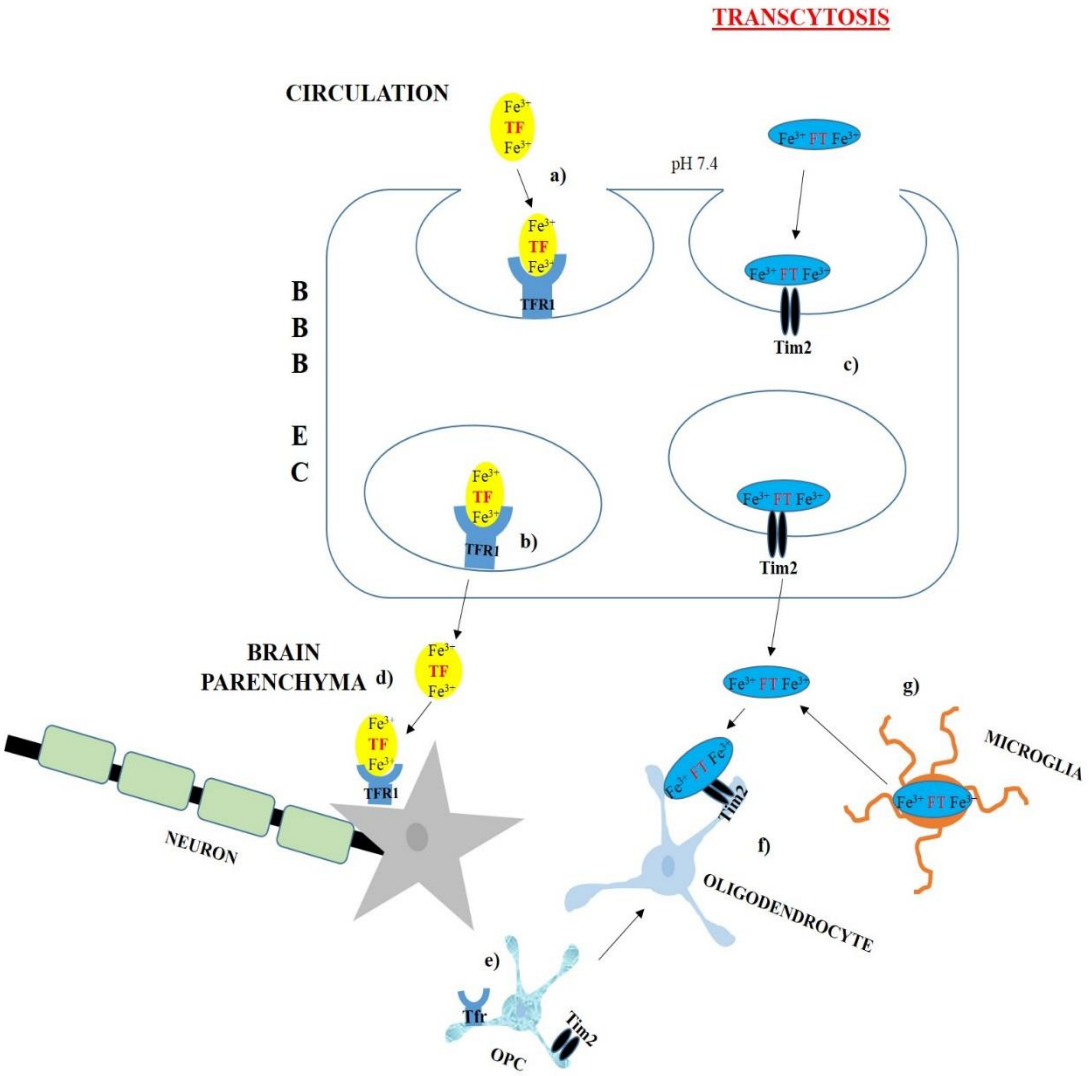

Figure 5.2 The regulation of iron transport into the brain via transcytosis

TF-bound iron in the circulatory system binds TFR1 expressed on the endothelial cells of the BBB (a). This TF-bound iron complex can be transcytosed across the endothelial cells mediated by TFR1 (b) or FT bound iron is transcytosed through receptor mediated transport via Tim2 (c). Once TF-bound iron crosses the BBB, it binds to TFR1 on neurons and is endocytosed into the endolysosome where iron is dissociated from TF to carry out its neuronal functions (d). OPCs express TFR1 and may take up TF-bound iron (e) however, mature oligodendrocytes cells no longer express TFR1 but acquire iron from FT through their expression of Tim2 (f). Microglia do not express TFR1 and obtain iron via phagocytosis of FT, which can also be secreted by microglia to support supply of iron to oligodendrocytes (g).

Key: BBB: blood brain barrier, DMT1: divalent metal transporter 1, EC: endothelial cell, FT: ferritin, OPC: oligodendrocyte precursor cell, Tim2: T cell mucin domain containing receptor 2, TF: Transferrin, TFR1: transferrin receptor-1.

Mature oligodendrocytes lose their expression of TFR1 and acquire iron from FT via their expression of Tim2 (Todorich *et al* 2008). Microglia do not express TFR1 and acquire iron via phagocytosis of FT. Microglia can also release FT, further supplementing the iron source for oligodendrocytes. Excess iron in neurons and glial cells diffuses into the interstitial fluid in the brain, where free or TF-bound iron is released into the CSF. Choroidal epithelia interact with free iron via DMT1 or TF-bound iron via TFR1 and transport the excess iron into the blood (Zheng & Monnot 2012).

Levels of iron in the CNS are regulated in part by the binding of TF with TFR1. The expression of TFR1 can be altered by the overall iron concentration present in the CNS through iron-regulatory proteins (IRP). When iron levels are low, a conformational change in IRP1 increases its binding with the iron-responsive element (IRE) sequence at the 3' UTR of TFR1 mRNA. This binding stabilises TFR1 mRNA and increases its protein translation, therefore binding with TF increasing the amount of iron delivered into the cells (Leitner & Connor 2012). When iron levels are increased in the CNS, IRP1 binding to the IRE sequence on TFR1, and DMT1 is reduced, destabilising TFR1, and DMT1 mRNA and reducing their translation, preventing the toxic increase in iron that can cause oxidative stress (Leitner & Connor 2012, Zheng & Monnot 2012). CNS iron levels are tightly regulated, but when iron homeostasis is compromised, the resulting increased iron levels contribute to neurodegenerative pathologies (Gaasch *et al* 2007).

In MS, iron accumulation has been proposed to contribute to several pathological and physiological processes (Bagnato *et al* 2011). Excess iron can amplify the activation state of microglia causing an increase in proinflammatory cytokine expression (Williams *et al* 2012) that can drive oxidative stress. Increased intracellular iron can damage mitochondria directly, while inadequate control of iron can produce damaging ROS resulting in oxidative stress (Morelli *et al* 2012, Williams *et al* 2012). In the brain, oxidative stress is associated with detrimental effects including lipid peroxidation, impairment of glutamate and glucose transport, exacerbation of mitochondrial dysfunction, increased intracellular calcium concentration and resulting cell dysfunction and death (Halliwell 2006, Salvador 2010).

Within the CNS in MS an increase in iron has been identified in areas adjacent to veins (Williams *et al* 2011), and at perilesional margins (Bagnato *et al* 2011, Hametner *et al* 2013). Increased iron deposition in MS is associated with increased oligodendrocyte and myelin loss (Bagnato *et al* 2011). Similarly, the release of iron from proteins whose degradation is induced by respiratory burst molecules, produced by microglia and macrophages during inflammation, have been linked with increased iron deposition in MS (Bagnato *et al* 2011, Lassmann *et al* 2012). Cellular toxicity in MS as a result of iron accumulation is mainly due to the Fenton reaction and the effects of respiratory burst, as demonstrated in (Figure 5.3). Free iron reacts with cellular metabolites including H_2O_2 and superoxide anion (O_2^-) to produce highly reactive and damaging free radicals, such as the $OH^\bullet$ (Khalil *et al* 2011b). O_2^- can also react with ferric iron in the Haber-Weiss reaction to produce ferrous iron in a process known as redox cycling, which further exacerbate free radical production (Khalil *et al* 2011b).

In the CNS, the prominent damaging effects of oxidative stress are associated with mitochondrial inner membrane respiratory complexes (Shamoto-Nagai *et al* 2006). Iron-induced cell death occurs as a result of the saturation of iron binding, transport and storage proteins in cells (Gaasch *et al* 2007). Consequently, the amount of free circulating iron increases, which enters already iron-saturated cells, such as neurons and oligodendrocytes, leading to an increased intracellular level of free iron. Oxidative damage of DNA can lead to the increased expression of p53 and caspase 3, while mitochondrial dysfunction caused by iron results in the release of cytochrome c (Gaasch *et al* 2007).

Astrocytes are resilient to the neurotoxic effects of excess iron (Gaasch *et al* 2007), which may reflect the high antioxidant and metal binding capabilities of molecules such as metallothionein (Pedersen *et al* 2009, Penkowa *et al* 2006, Sawada *et al* 1994). Although astrocytes can accumulate iron and have the capacity to store iron as FT, they rarely contain large amounts of either, suggesting astrocytes transport iron to other cells (Dringen *et al* 2007). As with much of the published work on iron metabolism in the brain, conflicting literature on the expression of TF and TFR by astrocytes is apparent. To date, astrocytes have been shown to express TFR1 *in vitro*, (Hoepken *et al* 2004), but not *in vivo*. In order to gain a better understanding of the role of astrocytes in regulating CNS levels of iron and their role in neurological disease, more research is required.

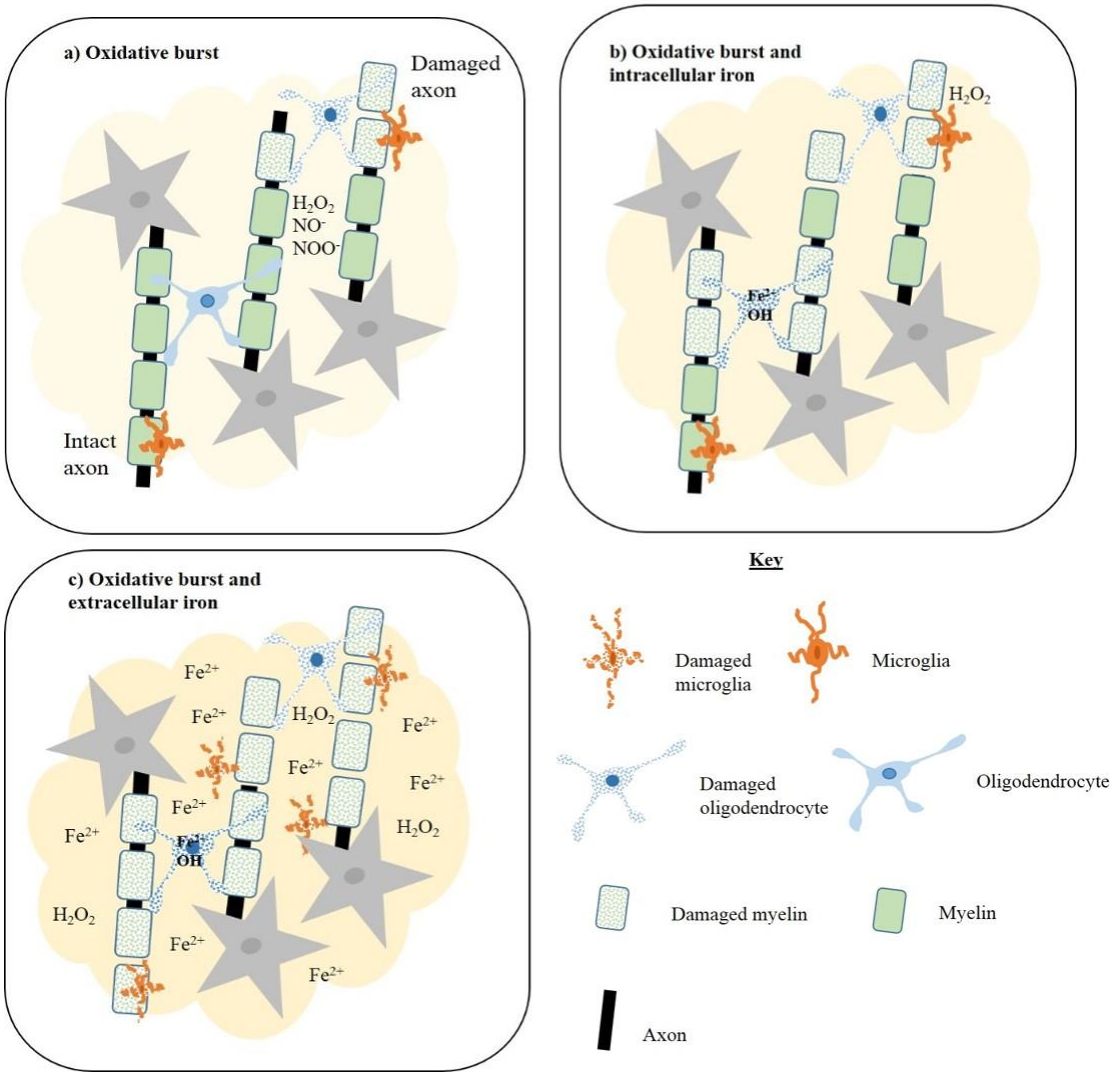

Figure 5.3 Respiratory burst and associated tissue damage in MS

During inflammation in MS, activated microglial undergo a respiratory burst with increased glucose and oxygen consumption resulting in the release of H_2O_2 (a, yellow shaded area). In combination with NO and $ONOO^-$ radicals, these factors lead to destruction of axons, myelin and oligodendrocytes. Tissue damage in the absence of Fe^{2+} occurs in local tissue surrounding activated microglia where H_2O_2 is at its highest (a). With Fe^{2+} accumulation in oligodendrocytes, H_2O_2 diffuses into these cells, where ROS are formed leading to cell death (b). Astrocytes do not contain the same level of stored iron as oligodendrocytes and are not as affected by ROS. Free Fe^{2+} released from damaged oligodendrocytes is taken up by microglia which causes these cells to become damaged and degenerate resulting in a second surge of Fe^{2+} release triggering further oxidative damage and lesion spread and development (c). Figure adapted from Lassmann *et al* 2012.

This chapter describes the detailed investigation of the astrocytic expression of a panel of iron regulatory molecules identified as being the most significantly upregulated genes in astrocytes isolated from PM MS NAWM, in comparison to controls in the preceding microarray study. A dysregulation of iron and oxidative stress have been suggested to be involved in a number of neurological diseases and also in MS. Therefore, we hypothesise that astrocytes are neuroprotective in MS NAWM involved in regulating iron homeostasis and reducing oxidative damage and consequently lesion development and disease progression. qPCR, WB, IHC and MALDI-MS were employed to attempt to verify the microarray candidates and confirm the potential neuroprotective role of astrocytes in MS NAWM.

5.2 Aims and objectives of the study

The aims of this study were to:

Investigate the potential neuroprotective role of astrocytes in MS NAWM.

- Verify the increased expression of *MT, TF* and *FTL* in astrocytes isolated from MS NAWM compared to control cases using qPCR.
- Confirm the increased astrocytic expression of MT, TF and FTL in MS NAWM compared to control WM by IHC.
- Quantify the expression of FTL and MT in MS NAWM compared to control WM using SDS-PAGE and WB.
- Evaluate the presence and distribution of MT, FTL and TF in MS NAWM and control WM using MALDI-MS and MALDI-MS imaging.

5.3 Materials and methods

5.3.1 Suppliers

Abcam, 330 Cambridge Science Park, Cambridge, CB4 0FL, UK; **AB Sciex UK**, Limited Phoenix House, Lakeside Drive, Centre Park Warrington, Cheshire WA1 1RX, UK; **Agilent Technologies Inc.**, (Stratagene), 5301 Stevens Creek Blvd, Santa Clara CA 95051, USA; **Applied Biosystems Inc.**, 850 Lincoln Centre Drive, Foster City, CA 94404, USA; **BIOplastics**, Rötscherg 61, 6374 XW Landgraaf, The Netherlands; **Bio-Rad Laboratories Ltd.**, Bio-Rad House, Maxted Road, Hemel Hempstead, Hertfordshire, HP2 7DX, UK; **Bruker UK Ltd.**, Banner Lane, Coventry, CV4 9GH, UK; **DAKO UK Ltd.**, Cambridge House, St Thomas Place, Ely, Cambridgeshire, CB7 4EX, UK; **Eurofins MWG Operon**, Anzinger Str. 7a 85560 Ebersberg, Germany; **Fisher Scientific Inc.**, Bishop Meadow Road, Loughborough, Leicestershire, LE11 5RG, UK; **GE Healthcare Life Sciences**, Pollards Wood, Nightingales Lane, Chalfont St Giles, Buckinghamshire, HP8 4SP, UK; **HTX Technologies**, LLC PO Box 1036 Carrboro, North Carolina (NC), 27510, USA; **Labcyte Europe**, Unit 12 Enterprise Centre Pearse Street Dublin 2, Ireland; **Leica Microsystems Ltd.**, Davy Avenue, Knowhill, Milton Keynes, MK5 8LB Buckinghamshire, UK; **LI-COR Biosciences UK Ltd.**, St. John's Innovation Centre, Cowley Road, Cambridge, CB4 0WS, UK; **Life Technologies Ltd.** (Invitrogen, Arcturus, Novex®), 3 Fountain Drive, Inchinnan Business Park, Paisley, PA4 9RF, UK; **MathWorks**, 3 Apple Hill Drive Natick, MA 01760-2098, USA; **Olympus**, KeyMed House, Stock Road, Southend-on-Sea, SS2 5QH, UK; **Sigma-Aldrich**, The Old Brickyard, New Road, Gillingham, Dorset, SP8 4XT, UK; **SunChrom**, Wissenschaftliche Geräte GmbH, Industriestr. 27, 61381, Friedrichsdorf, Germany; **Vector laboratories Ltd.**, 3 Accent Park, Bakewell Road, Orton Southgate, Peterborough, PE2 6XS, UK; **VWR International Ltd.**, (Quanta Biosciences), Hunter Boulevard, Magna Park, Lutterworth, Leicestershire, LE17 4XN, UK.

5.3.2 Case selection

All frozen tissue used in this study was obtained from the UK Multiple Sclerosis Society Tissue Bank (Appendix I). Clinical information for each case is described in Appendix III. Due to the limited availability of NAWM snap frozen tissue, the stringent criteria set out in the original microarray for case selection was reduced in this selection of the validation cohort. The criteria for inclusion into the study was based solely on the neuropathological assessment of each case (Table 5.1) and not the RIN. Selected cases

Case	Region	Age	Gender	PMI (hours)	CSF pH	H&E	CD68	LFB	RIN (Post-LCM)	MS classification
MS103	A3B4	77	F	7	n/a	Normal	Normal - ramified microglia, no amoeboid microglia present	Positive	n/a	SPMS
MS105	A4B2	73	M	8	6.47	Normal	Normal - ramified microglia, no amoeboid microglia present	Positive	2.0	SPMS
MS106	P5B1	39	F	18	6.48	Normal	Normal - ramified microglia, no amoeboid microglia present	Positive	n/a	n/a
MS107	P4C3	38	M	19	6.90	Normal	Normal - ramified microglia, no amoeboid microglia present	Positive	2.0	RPMS
MS200	P1D2	44	F	20	6.90	Normal	Normal - ramified microglia, no amoeboid microglia present	Positive	1.9	SPMS
MS235	P3D2	53	M	14	6.90	Normal	Normal - ramified microglia, no amoeboid microglia present	Positive	n/a	SPMS
CO14	P2C2	64	M	18	n/a	Normal	Normal - ramified microglia, no amoeboid microglia present	Positive	n/a	N/A
CO22	P1C2	69	F	33	7.8	Normal	Normal - ramified microglia, no amoeboid microglia present	Positive	n/a	N/A
CO25	P1B1	35	M	22	n/a	Normal	Normal - ramified microglia, no amoeboid microglia present	Positive	2.2	N/A
CO26	P1B1	78	F	33	6.7	Normal	Normal - ramified microglia, no amoeboid microglia present	Positive	2.5	N/A
PDCO01	P2E4	76	M	24	n/a	Normal	Normal - ramified microglia, no amoeboid microglia present	Positive	2.3	N/A
PDCO22	P2B1	65	M	12	7.7	Normal	Normal - ramified microglia, no amoeboid microglia present	Positive	2.6	N/A

Table 5.1 The validation patient cohort

Due to the limited availability of snap frozen material, the selection of 6 MS NAWM and 6 control cases for this validation study was based on neuropathology and not stringent RNA integrity.

Key: N/A: not applicable, n/a not available.

were chosen based on no evidence of inflammatory infiltrates, demyelination or presence of amoeboid microglia, suggestive of phagocytic activity confirmed by carrying out a thorough neuropathological assessment of each case as described in detail in Chapter 2.

5.3.3 The principles of quantitative PCR

qPCR is a tool that allows the detection and quantification of particular genes of interest and is commonly used to compare gene expression levels of mRNA targets between diseased and control samples. The technique uses a series of heat dependant amplification steps employing the typical three stage PCR workflow; dsDNA is firstly *denatured* followed by primer *annealing* and *extension* of cDNA through a series of 30-40 cycles. The dsDNA product is measured after each amplification cycle and can be detected via two common methods; firstly through the use of fluorescent tags which only omit fluorescence when incorporated into dsDNA, or secondly the use of sequence specific DNA probes containing fluorescently labelled oligonucleotides which are only detected upon hybridisation of the probe with its complementary sequence.

Prior to PCR, mRNA is reverse transcribed using reverse transcriptase enzymes to cDNA. In this study, qPCR products were quantified in the exponential phase of the reaction, through each PCR cycle the product doubles and is measured by SYBR green fluorescent dye that bind to dsDNA. qPCR provides more accurate data than traditional PCR where only semi-quantitative analysis can be completed at the end of the PCR reaction, relying on good band separation and resolution by agarose gel electrophoresis. In qPCR two values are measured, the threshold line and the cycle threshold (Ct) value. The threshold line is the point in the reaction when the fluorescence from the reaction is significantly higher than the background fluorescence, generally 10 standard deviations above the mean baseline fluorescence (Agilent Technologies, 2012). The Ct value is the point in the reaction when the sample reaches this threshold. Consequently, samples with higher expression of the transcript of interest will have lower Ct values compared to those samples with less transcript which will have a higher Ct value.

Natalie Rounding, a University of Sheffield undergraduate student supervised by Rachel Waller assisted in the primer optimisation and IHC work completed in this chapter.

5.3.3.1 cDNA synthesis

Using an identical method to the microarray experiments, RNA was extracted from $GFAP^+$ astrocytes by LCM in 12 additional cases (6 MS NAWM and 6 control WM

cases refer to Table 5.1) which had not been used for the microarray study. Total RNA was converted to cDNA using qScript cDNA mix/supermix (Quanta, UK) as described in section 3.3.8.

5.3.3.2 Primer design

qPCR primers were designed using Primer-BLAST (basic local alignment search tool) software (NCBI, http://blast.ncbi.nlm.nih.gov/Blast.cgi) or for the different metallothionein isotypes and FTL, sequences were taken from published studies (Gebril *et al* 2011, Sequeira *et al* 2012). When designing qPCR primers a number of considerations were made, the primers, where possible, were designed to span an exon-exon boundary to avoid possible genomic DNA influence. Primers were designed with an amplicon length of 70-150 bp, a melting temperature (Tm) between 57-63°C, and 20-80% GC content. Similar to the IVT microarray probes, primers were designed against the 3' end of the gene to compensate for the poorer RNA integrity of PM, LCM-ed RNA samples. Probeset IDs of genes to be validated were searched for using NetAffx (http://www.affymetrix.com/), providing details of the sequence used to build the probe on the 3' IVT microarrays. All primers for qPCR (Table 5.2) were purchased from Eurofins MWG Operon, Germany.

5.3.3.3 Primer optimisation and efficiencies

In order to compare gene expression using qPCR it is vitally important that the primer efficiencies of the target genes and housekeeping (HK) genes are approximately equal. The efficiency of primers represents the amount of PCR product increase after each cycle, ideally a PCR reaction will contain primers with near to 100% efficiency. Dissimilar primer efficiencies between the HK and target gene can falsely calculate differences in the expression ratio (Pfaffl *et al* 2002).

Therefore establishing the primer efficiency along with the optimum combination of primer concentrations was required. qPCR was initially carried out using different concentration combinations of forward and reverse primers. For primer optimisation, 1µg of total RNA extracted from the astrocytes of a control case was reversed transcribed to cDNA as outlined in section 3.3.8. qPCR was performed with [25ng] astrocyte cDNA, 1X Brilliant II SYBR Green PCR MM (Agilent, UK), along with appropriate volumes of forward and reverse primers (Table 5.3), adjusted with d.H_2O to

Gene name	Gene	Primer sequence	Length (bp)	Concentration (Nm)
Metallothionein 1G	MT1G	F: 5'GGAACTCTAGTCTCGCCTCGG3' R: 5'AGGAGACACCAGCGGCAC3'	64	300 300
		F: 5'GCCCTGCTCCCAAGTACAAATA3' R: 5'GAATGTAGCAAAGGGGGTCAAGAT3'	**87**	**300 300**
Metallothionein 1X	MT1X	**F: 5'GTGGGCTGTGCCAAGTGTG3' R: 5'TGCACTTGTCTGACGTCCCTT3'**	**58**	**300 300**
Metallothionein 2A	MT2A	F: 5'ACAGCCCCGCTCCCAGATGT3' R: 5'GCAAACGGTCACGGTCAGGGT3'	81	600 600
		F: 5'CTGATGCTGGGACAGCCC3' R: 5'TTGTGGAAGTCGCGTTCTTTAC3'	**52**	**300 600**
Transferrin	TF	**F: 5'ACCTGGCCAGAGCCCCGAAT3' R: 5'TGCCCGAGCAGTCAGTTACGTT3'**	**119**	**300 300**
Ferritin Light Chain	FTL	**F: 5'TTCGACCGCGATGATGTG3' R: 5'TTCTCCTCGGCCAATTCG3'**	**64**	**300 300**
β-Actin	βA	**F: 5'GTGGCTTTTAGGATGGCAAG3' R: 5'ATCCCCCAAAGTTCACAATG3'**	**100**	**300 300**

Table 5.2 qPCR primers used for microarray validation

qPCR primer sequences and optimised concentrations for microarray validation (optimised primer sequence and concentration in bold).

Forward Primer [nM]	Reverse primer [nM]	SYBR green MM (2X)	cDNA [25ng]	Water
150 (0.6µl)	150 (0.6µl)	10.0µl	1.0µl	7.8µl
150 (0.6µl)	300 (1.2µl)	10.0µl	1.0µl	7.2µl
300 (1.2µl)	150 (0.6µl)	10.0µl	1.0µl	7.2µl
300 (1.2µl)	300 (1.2µl)	10.0µl	1.0µl	6.6µl
300 (1.2µl)	600 (2.4µl)	10.0µl	1.0µl	5.4µl
600 (2.4µl)	300 (1.2µl)	10.0µl	1.0µl	5.4µl
600 (2.4µl)	600 (2.4µl)	10.0µl	1.0µl	4.2µl
300 (1.2µl)	300 (1.2µl)	10.0µl	(NTC)	7.6µl

Table 5.3 Primer optimisation

For each of the five primer pairs (MT1G, MT2A, MT1X, TF and FTL), appropriate volumes of forward and reverse primers were added to the PCR mix to test a range of primer concentrations. (Primer stock concentration 5pmol/µl).

a final volume of 20µl. Each sample was assessed in triplicate and analysed in a PCR plate sealed with PCR caps (BIOplastics, The Netherlands) on an MX3000P Real-Time PCR system (Stratagene, USA). The PCR programme consisted of denaturation at 95ºC for 10 minutes, products were amplified (40 cycles of 95ºC for 30 seconds, and 60ºC for 1 minute) followed by a final cycle at 95ºC for 1 minutes, 55ºC for 30 seconds, and 95ºC for 30 seconds. To ensure the primers were efficient over a range of cDNA template concentrations, qPCR was also carried out with serial dilutions of cDNA (12.5ng/µl - 0.15 ng/µl) using the determined optimal primer concentrations for each gene of interest (Table 5.2) and a standard curve prepared and primer efficiencies compared.

5.3.3.4 Selection of a housekeeping gene

A housekeeping gene is required as a reference gene and is used for normalisation of target gene expression in all qPCR experiments. Analysis of the signal intensities of corresponding β-actin and GAPDH probe sets from the original microarray data helped to define the most suitable HK gene for qPCR.

5.3.3.5 qPCR validation attempt of candidate iron related genes

Iron-homoeostasis candidate genes, which showed significant altered expression in the original microarray study, were validated by qPCR. For each gene of interest, qPCR was performed using the optimised primer concentrations determined in the primer optimisation investigations (refer to Table 5.2). Each of the validation samples (6 MS NAWM and 6 control WM) was run in triplicate, alongside HK controls (β-actin) for each sample. The PCR programme followed is outlined in 5.3.3.3.

The fluorescent signal generated by each sample at the end of each cycle of the PCR was analysed using MxPro software (Stratagene, USA) and the gene expression normalised to the HK gene β-actin using the comparative Ct, (delta-delta ΔΔCt) method of quantification (ABI PRISM 7700 Sequence Detection System protocol, Applied Biosystems, USA). Initially all triplicate Ct values were averaged for each sample's target gene and HK gene. The difference between both the samples target gene Ct value and HK gene Ct value (ΔCt) was taken as an indication of the expression level of the studied gene. An average Ct value from all control cases was taken as a reference for relative gene expression. ΔΔCt is the difference between the ΔCt for individual samples and the average Ct from all control samples. In order to account for the exponential nature of PCR the ΔΔCt values were converted into linear form by raising the ΔΔCt to $2^{-\Delta\Delta Ct}$, which generates the relative gene expression in MS NAWM compared to control

cases. qPCR data was analysed using a non-parametric Mann-Whitney U test performed in GraphPad and the relative gene expression differences were assessed between MS NAWM and control WM for each of the candidate genes. Significance was set at p=<0.05.

5.3.4 Immunohistochemistry

5.3.4.1 Single labelling IHC for iron related proteins in MS NAWM and control cases

IHC was carried out on the validation cohort, to identify the expression and localisation of MT, FTL and TF and determine the colocalisation of these proteins with astrocytes. Primary antibody optimisation was carried out using a range of dilutions (Table 5.4), based on the manufacturer's recommendation, in order to find the concentration that provided specific IHC staining with minimal non-specific background stain. 10 µm sections were cut on the cryostat and mounted onto poly-lysine coated microscope slides (Leica, UK). These sections were fixed in ice-cold acetone for 10 minutes prior to IHC using the using the ABC-HRP technique and Vectastain Elite kit (Vector Laboratories, UK) with DAB (Vector Laboratories, UK) as substrate (refer to section 2.3.7 for full details).

5.3.4.2 Dual labelling IHC for colocalisation of iron related proteins with astrocytes

Single IHC was carried out with the optimum primary antibody concentration, determined from the single labelling optimisation studies using the ABC-HRP technique and Vectastain Elite kit (Vector Laboratories, UK) with DAB (Vector Laboratories, UK) as substrate. Following the DAB incubation, the sections were re-blocked in 1.5% normal goat serum (150 µl in 10 ml TBS) for 30 minutes at RT. Excess block was removed and avidin applied for 15 minutes at RT (a component of the Avidin/Biotin blocking kit, Vector Laboratories, UK). Sections were quickly rinsed with TBS, and the second component of the blocking kit, biotin, was added to the sections and left to incubate for 15 minutes at RT. Sections were tapped to remove excess biotin and a more concentrated GFAP antibody than used in the previous single-labelled astrocyte phenotype study (1:500) was applied to the sections and left to incubate o/n at 4ºC. Following the o/n incubation sections were thoroughly washed in TBS for 10 minutes. Biotinylated species-specific secondary antibody was prepared, by adding 150 µl goat/horse serum in 10 ml TBS and then adding 50 µl of biotinylated secondary antibody. Secondary antibody was left to incubate for 1 hour at RT prior to

Primary antibody	Species	Clonality	Isotype	Supplier	Dilution
Anti-Metallothionein Clone E9 **(MT)**	Mouse	Monoclonal	IgG	Dako, UK	1:50 1:100 **1:200** 1:400
Anti-Ferritin Light Chain antibody **(FTL)**	Rabbit	Polyclonal	IgG	Abcam, UK	1:50 1:100 1:200 **1:400**
Anti-Human Transferrin **(TF)**	Mouse	Monoclonal	IgG1	AbD Serotec, UK	1:50 **1:100** 1:250
Glial fibriallary acidic protein **(GFAP)**	Rabbit	Polyclonal	IgG	Dako, UK	**1:500**

Table 5.4 Details of the primary antibodies used in the iron IHC study

All dilutions were made in the appropriate blocking serum, the optimum concentration used in the study are shown in bold.

being washed with TBS for 10 minutes. The alkaline phosphatase ABC reagent was prepared (Vectastain ABC-AP kit, Vector Laboratories, UK) by adding 100 µl reagent A and 100 µl reagent B to 5 ml TBS, this was prepared at least 30 minutes prior to use. ABC-AP reagent was added to the sections and left to incubate at RT for 1 hour, prior to washing with TBS for 10 minutes, ensuring all excess TBS was removed prior to the addition of the alkaline phosphatase substrate. The alkaline phosphatase substrate (VECTOR Red Alkaline Phosphatase Substrate Kit, Vector Laboratories, UK) was prepared by adding 100 µl reagent 1, 2, and 3 to 5 ml Tris-HCl, 100mM. The substrate was added to the sections and left for 10-20 minutes for the reaction to develop, which was stopped by washing the sections in d.H_2O. Sections were counterstained in haematoxylin for 30 seconds, rinsed in tap water until the water ran clear, dehydrated in graded alcohols and mounted using DPX and glass coverslips. For internal controls, the primary antibody was omitted to ensure the absence of non-specific binding from the secondary antibody.

5.3.4.3 Image analysis

All IHC and histology was examined using the BX61 Olympus microscope and CellR image software system (Olympus, UK). A qualitative description of the staining pattern of each antibody and it's colocalisation with astrocytes was noted across the MS NAWM and control samples.

5.3.5 Western blotting technique

WB, also known as immunoblotting, is often used to separate and identify proteins (Figure 5.4). Ruth Thomas, a Welcome Trust funded undergraduate student supervised by Rachel Waller assisted in the WB work completed in this chapter. In this technique a mixture of proteins is separated based on molecular weight, through gel electrophoresis (Mahmood & Yang 2012). Separated proteins are identified as distinct bands on the gel. The separated protein bands are then transferred from the gel onto a membrane and the membrane probed with antibodies specific to the protein of interest. As specific antibodies are used, only the protein of interest should be visible after probing, the density of the band corresponds to the amount of protein present in the sample (Mahmood & Yang 2012).

5.3.5.1 Tissue protein extraction

Protein lysates from each validation case (5MS NAWM and 5 control WM) were prepared by the addition of 300 µl of CelLytic™ Mammalian Tissue lysis buffer (Sigma-Aldrich, UK) supplemented with 30 µl of protease inhibitor cocktail

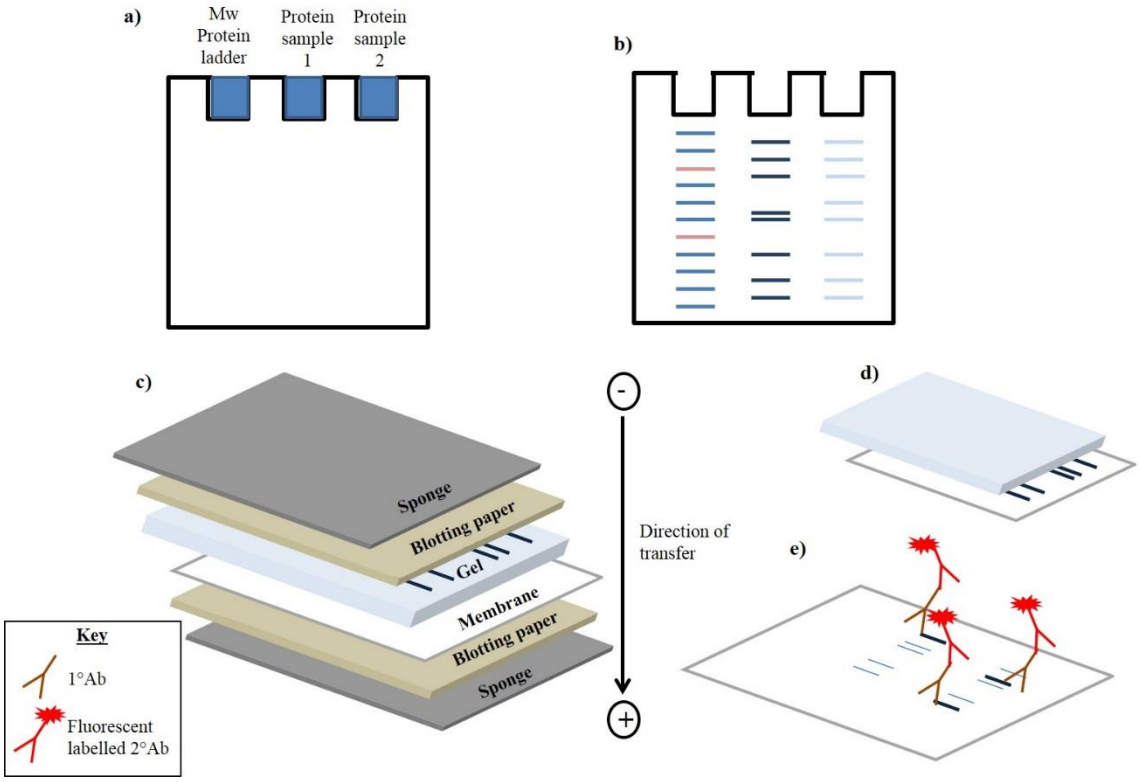

Figure 5.4 Western blot technique

Denatured protein samples are loaded onto an SDS-PAGE gel alongside a molecular weight protein ladder standard (a) and separated via gel electrophoresis based on their molecular weight (b). The separated proteins are transferred onto a nitrocellulose membrane (c&d). The transferred membrane is immunoprobed with an antibody specific to the protein of interest, followed by the incubation of a fluorescently labelled secondary antibody, the protein is then visualised using the Li-Cor Odyssey® imaging system.

(Sigma-Aldrich, UK) to 10x30 µm WM sections (the cortex from each section was removed using a sterile disposable scalpel). The samples were homogenised using a hand held homogenizer to break down the tissue, and sonicated on ice for 15-20 seconds. The lysed samples were centrifuged at 4°C for 30 minutes at 14,000 rpm to pellet the tissue debris. The protein containing supernatant was transferred to a chilled sterile Eppendorf and stored until uses at -80˚C.

5.3.5.2 Determination of protein concentration – Bradford protein assay

Prior to WB, protein concentration of each sample was determined using the Bradford protein assay and to allow equal protein loading on to the gel. The Bradford assay relies on the binding of a Coomassie Brilliant Blue G-250 dye to proteins (Bradford 1976). Prior to binding with the protein samples the cationic Commassie Blue exists in an acidic doubly protonated red form. Once protein is added the Commassie Blue is changed into to an unprotonated anionic blue form which is detectable at A_{max} 595nm using a spectrophotometer. Therefore the increasing absorbance is proportional to the amount of protein bound to the dye and therefore the higher the protein concentration of that particular sample. A standard curve can be created using known concentrations of bovine serum albumin (BSA) (Sigma-Aldrich, UK) to which the unknown sample concentration can be determined using linear regression analysis;

y=mx+c **(y=**absorbance, **m=**gradient, **x=**protein concentration, **c=**y intercept.)

5.3.5.3 Western blotting for ferritin light chain and metallothionein

Protein samples were separated on a pre-cast 18% Novex Tris-glycine gel using the traditional SDS-PAGE technique, a range of protein concentrations were used in the WB optimisation experiments [5-40 µg]. All buffers and reagents for WB were purchased from Life Technologies unless otherwise stated, and recipes found in Appendix IV. Samples were prepared by adding 30 µg sample to 6x sample buffer (prepared in house, Appendix IV) and adjusting the volume to 20 µl with d.H_2O. Samples were denatured on a heat block at 70°C for 10 minutes and immediately placed on ice until use. Pre cast gels were placed in a Novex® electrophoresis gel tank containing Novex® Tris-Glycine SDS Running Buffer. Each 30 µg sample was loaded into each well along with 2 µl Precision Plus protein dual extra standard ladder (Bio-Rad, UK). Electrophoresis was carried out at 125V for 90 minutes, until the dye front reached the bottom of the gel. Separated proteins were transferred via WB onto a nitrocellulose membrane (NCM) (Hybond-C extra, GE Healthcare Life Sciences, UK). Before the transfer, all materials required for the western blot including the NCM,

blotting paper, and sponges were pre-soaked in cold Novex® Tris-glycine transfer buffer. The transfer sandwich was assembled (refer to Figure 5.4) submerged in cold transfer buffer, to ensure no bubbles were formed between the sandwich layers. The assembled sandwich was placed in a transfer tank containing surplus cold transfer buffer and protein transfer from the gel to the membrane was carried out for 1 hour at 100V on ice. For confirmation of successful protein transfer, the transferred membrane was stained with Ponceau S red (Sigma-Aldrich, UK), which is a highly sensitive red stain for proteins, such that all transferred protein can be visualised, this stain was removed with water prior to immunoprobing (Harper & Speicher 2001).

5.3.5.4 Immunoprobing

All transferred membranes were blocked for 1 hour at RT in 5% blocking buffer in TBS-Tween20 (TBS-T). All antibody solutions were made up in 5% blocking solution to an appropriate concentration, (refer to Table 5.5 for all antibody titrations used throughout the WB experiments). The primary antibodies were applied to the membrane and incubated o/n at 4°C on a flatbed shaker. An anti-β-actin was ran alongside the primary antibody of choice, as a house-keeping and loading control. To confirm specificity of antibody binding, negative controls were also used for each WB by omitting the primary antibody and incubating in blocking solution alone. Membranes were washed thoroughly in TBS-T) (3 x 10 minutes) on a flatbed shaker to remove any unbound primary antibody. Appropriate labelled secondary antibodies were diluted in blocking solution (refer to Table 5.5 for antibody concentrations) and applied onto the membranes and left to incubate for 1 hour at RT on a flatbed shaker (in the dark). Membranes were finally washed with TBS-T (3 x 10 minutes) and visualised using the LICOR Odyssey® imaging system.

5.3.5.5 Statistical analysis of western blots

Data was normalised with respect to the loading control used, β-actin. Densitometric data was analysed using a non-parametric Mann-Whitney U test and comparisons between NAWM and control tissues made. Significance was set at $p < 0.05$.

Specificity of primary antibody	Species	Clonality	Source	Dilution
Anti-Ferritin Light Chain antibody **(FTL)**	Rabbit	Polyclonal	Abcam, UK	1:500 **1:1000**
Anti-Metallothionein Clone E9 **(MT)**	Mouse	Monoclonal	Dako, UK	1:100 1:500 1:1000
β-actin (for MT)	Rabbit	Polyclonal	Sigma, UK	1:500 **1:1000**
β-actin (for FTL)	Mouse	Monoclonal	Abcam, UK	1:500 **1:1000**

Target of secondary antibody	Clonality	Conjugate	Source	Dilution
Goat anti-Mouse IgG	Polyclonal	IR800 CW	Licor, UK	1:500 (MT) 1:1000 (MT)
Goat anti-Mouse IgG	Polyclonal	IR 680 CW	Licor, UK	1:1000 (MT) 1:5000 (MT) **1:15,000 (β-actin for FTL)**
Goat anti-Rabbit IgG	Polyclonal	IR800 CW	Licor, UK	1:1000 (β-actin for MT) **1:15,000 (β-actin for MT)** 1:10,000 (FTL) **1:15,000 (FTL)**

Table 5.5 Details of the primary and secondary antibodies used in western blotting for the analysis of protein expression in MS NAWM and control WM tissue

The optimal antibody concentration was determined through optimisation experiments, with the optimum concentration in bold.

Key: FTL: Ferritin light chain, MT: Metallothionein.

5.3.6 An introduction to mass spectrometry

Mass spectrometry is an analytical technique allowing the molecular weight of a wide range of molecules and biomolecules to be determined. It is a highly sensitive technique, capable of generating data within seconds to measure analytes in the femtomole range (So *et al* 2013). Mass spectrometry works on the principle of generating ions from molecules that are measured on the basis of their mass-to-charge (*m/z*) and can also be used to determine the chemical structure of molecules such as peptides by fragmenting larger proteins and determining their amino acidic sequence through the *m/z* of the fragments (Domon & Aebersold 2006).

There are three main components to a mass spectrometer namely: (i) the ionisation source in which molecules are ionised, (ii) a mass analyser in which ions are separated based on their *m/z*, (iii) the detector by which ions are revealed (Figure 5.5). Each part of a mass spectrometer can be altered depending on the species/molecules being investigated, whether these be lipids, peptide, drugs, metabolites, or proteins.

Ionisation techniques such as electron ionisation (EI) and chemical ionisation (CI) allow for the ionisation of small molecules, (mass range up to 1000 Da) that are volatile and thermally stable (Glish & Vachet 2003). However, with larger biomolecules, such as proteins and peptides, these two methods of ionisation are not suitable, due to the use of harsh conditions causing analyte fragmentation (Domon & Aebersold 2006). Electrospray ionisation (ESI), exploitable mass range less than 200 kDa (Fenn *et al* 1989) and MALDI, exploitable mass range less than 500 kDa (Hillenkamp *et al* 1991), are considered 'soft' ionisation techniques. Both ionisation methods allow the transfer of the analyte into the gas phase, with little or no sample fragmentation, and are typically the ionisation methods of choice when investigating protein/peptides via mass spectrometry, though the research reported throughout this chapter has been undertaken exclusively via MALDI-MS.

5.3.7 Matrix Assisted Laser Desorption Ionisation (MALDI)

MALDI is a versatile soft ionisation technique that has been employed to investigate a wide range of molecules including, besides proteins and peptides, other involatile and thermally labile compounds such as organic drugs (Dong *et al* 2010, Galano *et al* 2012), metabolites, (Galano *et al* 2012, Yukihira *et al* 2010), polysaccharides,

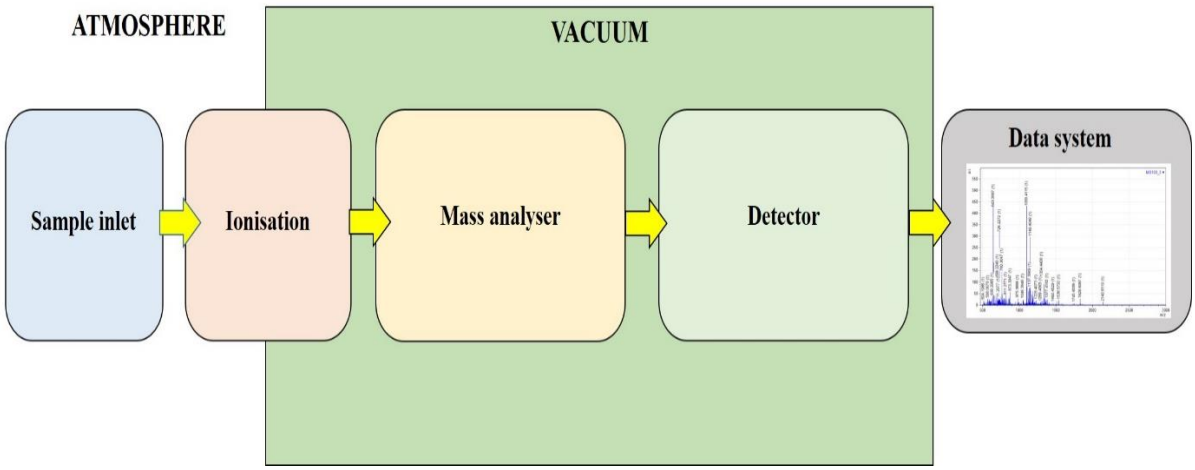

Figure 5.5 Block scheme diagram of a mass spectrometer

(Halinski & Stepnowski 2013) polymers (Barrere *et al* 2012) and nucleic acids (Joyner *et al* 2013). In MALDI, the ionisation of the analyte is supported by a compound known as the matrix. This is in general a small organic acid with an extended conjugation of double bonds capable of absorbing UV light. The matrix absorbs the energy from a laser firing in the UV region and transfers it to the analyte (Kafka *et al* 2011). The matrix composition is vital for the optimal ionisation of the analyte and its optimisation is required for the specific compound being investigated.

After mixing the matrix with the sample and depositing onto a MALDI plate, co-crystallisation occurs upon evaporation of the solvent component of the matrix. Under vacuum, a laser is pulsed over the sample, and the heat generated causes desorption of the matrix and analyte ion clusters into the gas phase (Yates *et al* 2009). A number of different lasers have been used in MALDI, which operate at different wavelengths and emit different levels of energy (Hoffmann 2007). Commonly used lasers in MALDI operate in the UV region such as a nitrogen (N_2) laser at wavelength of 337 nm, or neodymium-doped:yttrium aluminum garnet (Nd:YAG) lasers at wavelength of 335 nm. Due to the longer lifespan of Nd:YAG lasers these tend to be used more so than N_2 lasers (Trim *et al* 2012).

The ionisation mechanism in MALDI is not fully understood, however it is generally accepted that as the laser is fired onto the co-crystallised matrix/analyte complex, a desorption process occurs by which clusters of matrix and analyte are transferred into the gas phase. At the same time, the matrix absorbs the laser energy thus reaching an excited state. The matrix is stabilised by transferring a proton to the analyte. This generates mostly monoprotonated ions, thus minimising spectral complexity and enabling easier interpretation of *m/z* values. The matrix is used in great excess thus protecting the analyte from the direct impact of the laser and minimising analyte fragmentation (Figure 5.6).

5.3.7.1 MALDI coupled mass analysers

There are a number of mass analysers available that separate ions based on their *m/z* ratio, which differ based on their accuracy and mass resolving power. Suitable mass analysers coupled to a MALDI source include the time-of-flight (TOF) analyser that separates ions based on the time it takes for ions to reach the detector traveling along the analyser (the drift tube). An alternative mass analyser is the quadrupole (Q), separating ions based on their stability in an oscillating electrical field. Q analysers are

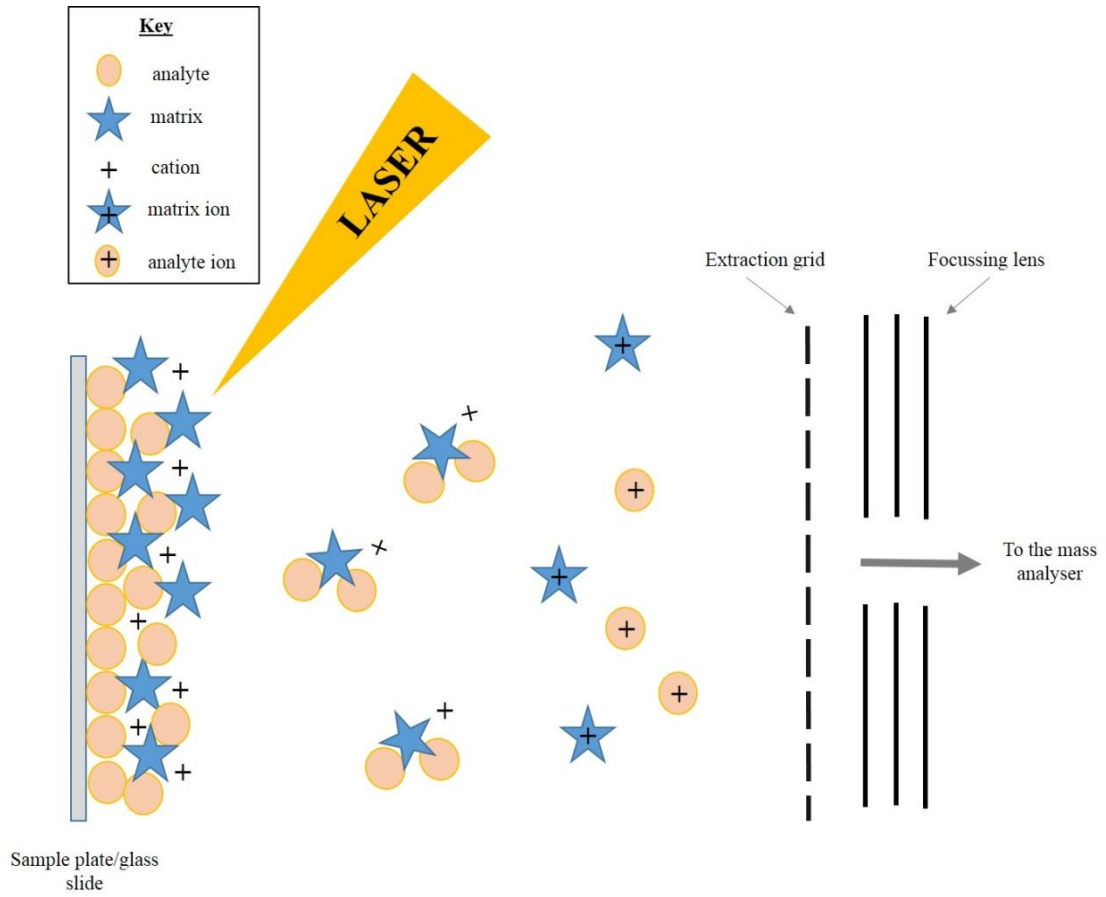

Figure 5.6 The mechanism of matrix assisted laser desorption ionisation (MALDI)
In MALDI analysis a matrix solution is deposited onto the sample and left to co-crystallise. The laser firing heats and excites the matrix and analyte crystallised species, causing both molecules to expand and enter into a gas phase. Excited matrix ions are stabilised by the transfer of protons to analyte molecules in the process known as ionisation, the analyte ions are then accelerated under vacuum into the mass analyser.

not generally coupled to a MALDI source unless they are followed by a second mass analyser; hybrid mass analysers can be employed, which offer the advantages of both TOF and Q with higher sensitivity and mass accuracy allowing for mass spectrometry and tandem mass spectrometry (MS/MS) acquisition on the same samples.

In the TOF analysers formed ions are accelerated through the drift tube at a suitable potential (20-25 kV) (Andersson *et al* 2010). The TOF depends on the *m/z* of the ions, with lower *m/z* ions having a higher kinetic energy and reaching the detector more quickly than higher *m/z* ions with lower kinetic energy (Hoffmann 2007). Mass resolution can be improved by using a reflectron, which helps the focussing of high energy ions thus improving mass accuracy. A reflectron consists of a decelerating and reflecting field, which work by altering the flight direction of the ions. Ions with the same *m/z* but differing velocities will enter the reflectron and those with higher kinetic energy and velocity will penetrate the decelerating component of the reflectron further than ions with lower kinetic energy and velocity. Consequently, the faster ions will spend more time in the reflecting field and catch up with the slower ions on release from the reflectron (Hoffmann 2007). Changing the direction of the ions to the detector compensates for small differences in velocities of ions with the same *m/z* values (Glish & Vachet 2003). Molecules up to 3000 Da including peptides benefit from the use of the analysis in reflectron mode.

Q analysers are generally popular due to their low cost, small size and lower voltage used to accelerate ions from the source to the analyser (V compared to kV) (Glish & Vachet 2003). Q are an arrangement of four metal rods in a cylindrical shape with applied potentials. Separation of ions in a Q is due to the ions motion and stability in an electric field dependant on their *m/z*, not on their velocity, as in the TOF analysers (Glish & Vachet 2003, Yates *et al* 2009). The ratio between the radio frequency (rf) voltage and direct current voltage over the Q determines the analysers function. The size of the Q and rf are kept constant so that the analyte ions are separated based on their *m/z*, with each ion reaching the detector by alterations of the rf and DC voltages (Glish & Vachet 2003). For example, only ions with a particular *m/z* will reach the detector for a given voltage, while the other ions will be unstable, colliding with the rods.

Hybrid mass analysers include the Q-TOF, in normal mass spectrometry acquisition the Q guides the ions to the TOF analyser (Domon & Aebersold 2006) where the whole mass spectrum is measured.

For MS/MS acquisition a known precursor ion can be selected in the Q and fragmented in the collision cell, and the resulting ion products analysed in the TOF section (Loboda *et al* 2000, Shevchenko *et al* 2000). Q-TOF allows for both peptide fingerprinting (MS acquisition) and MS/MS of precursor ions to be acquired from the same sample preparation. These devices are highly sensitive, have high resolving power and mass accuracy (Loboda *et al* 2000).

5.3.7.2 MALDI-mass spectrometry profiling (MALDI-MSP)

MALDI-mass spectrometry profiling (MALDI-MSP) is the method of choice when one is interested in the molecular pattern within specific areas or anatomical regions of a tissue section. By depositing matrix in defined spots across the ROI on the tissue MSP can be completed in minutes with acquired ion profiles of species confined to that specified matrix spot. Within MALDI-MSP the spectra are usually generated from a small number of spots at random or from specific areas on the tissue section. For example, concerning the work presented in this thesis, MALDI-MSP was employed to generate specific regional mass spectral profiles targeting the WM of the brain yet, due to the nature of the matrix, spraying was used instead of the conventional spotting of matrix for MSP, as discussed later in the chapter (Figure 5.7).

5.3.7.3 MALDI-mass spectrometry imaging (MALDI-MSI)

MALDI-mass spectrometry imaging (MALDI-MSI) is advantageous over other proteomic methods which require the use of specific antibodies like in IHC and WB. Carrying out WB requires sample homogenisation and time consuming protein extraction, purification and separation steps which are avoided when using MALDI-MSI. Furthermore, MALDI-MSI maintains cellular and molecular integrity within a tissue section which is lost when investigating protein expression by WB (Wisztorski *et al* 2008). Firstly introduced in 1997 by Caprioli and colleagues, continuing developments in MSI have made the technique more sensitive, robust and useful in applications such as cancer research, neuroscience and pharmaceutical development (Goodwin *et al* 2008, Reyzer & Caprioli 2007). MALDI-MSI allows the distribution of hundreds of species in intact biological tissue sections to be visualised in a single measurement (Caprioli *et al* 1997). The technique has been used to image lipids, peptides, proteins or drugs in a range of different biological settings (Carter *et al* 2011, Chaurand *et al* 2006, Eberlin *et al* 2011, Hanrieder *et al* 2013a, Rohner *et al* 2005, Trim *et al* 2008). When carrying out MALDI-MSI on tissue sections, the matrix is applied to the section as a homogeneous layer by a number of matrix deposition devices as

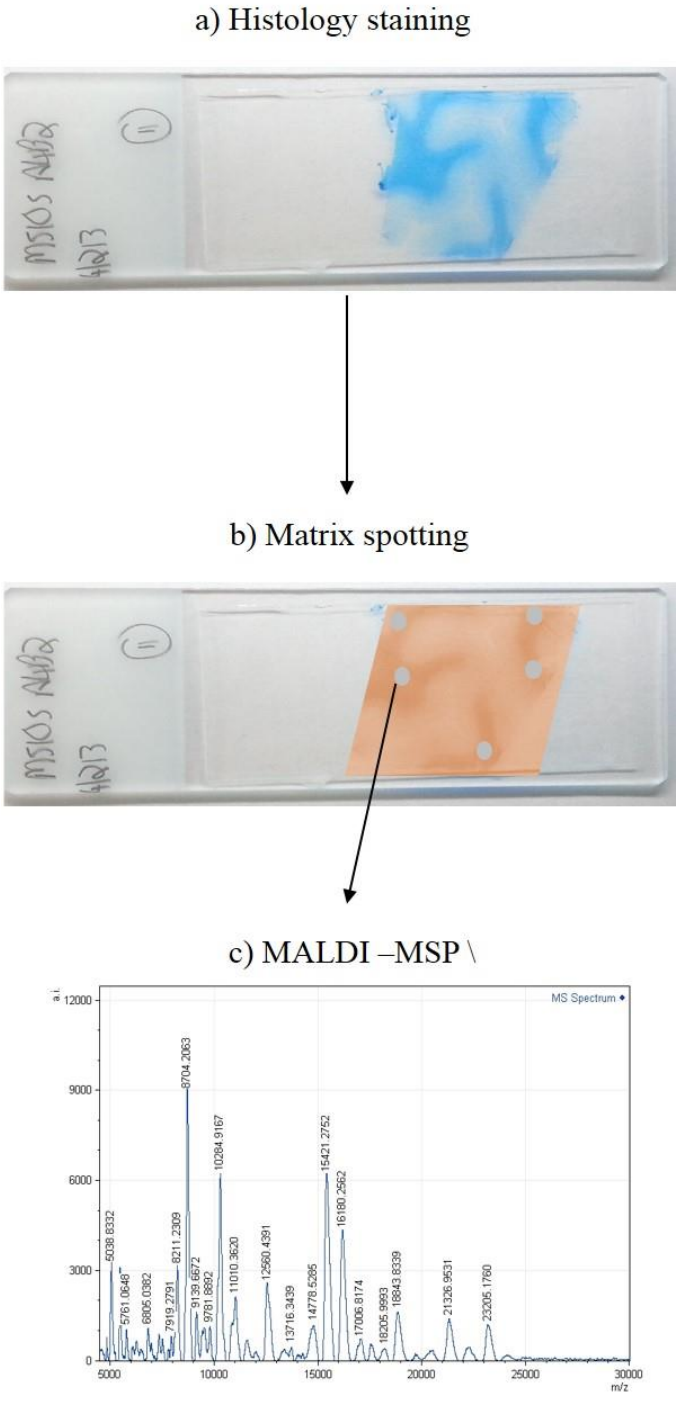

Figure 5.7 Matrix assisted laser desorption ionisation-mass spectrometry profiling (MALDI-MSP)

Tissue sections can be histologically stained to define specific areas of interest. For example in brain tissue, WM and cortex are identified by LFB (a). On a consecutive tissue section matrix can be deposited on to the area of interest (WM) (b) and MALDI-MSP can be carried out for each specified spot (c). Comparisons of mass spectrum can be made between disease tissue and control tissue.

explained in section 5.3.7.4. Matrix coated tissue sections are introduced into the mass spectrometer and a laser is delivered onto the section on each point of known x,y coordinates in a pre-defined raster. The spatial resolution achievable by MALDI-MSI can range between 10-150 µm dependent on the instrument used. From a single analysis on one tissue section, a single mass spectrum is generated from each raster point. From these mass spectra it is possible to plot the relative intensity of each *m/z* peak and visualise the ion distribution across the tissue section as an image (Goodwin *et al* 2008). A representative example of the MALDI-MSI process is shown in Figure 5.8.

5.3.7.4 Matrix composition and application

The success of a MALDI-MS study is associated with: sample preparation, the type of matrix used and method of matrix deposition. The choice of the matrix depends on the type of compound being investigated by MALDI-MS (Table 5.6). There are a number of different methods of matrix delivery to biological tissue sections, according to whether MSP or MSI is employed, with the ultimate aim of maximising analyte extraction, while minimising analyte delocalisation. MALDI matrix can be delivered as individual droplets (spotted) or as a homogenous layer (coated) onto biological tissue sections. Spotting matrix can be completed manually using a pipette or using specific automated matrix spotter instruments such as the Potrait® 630 Spotter (LABCYTE™, Ireland). This instrument automatically spots matrix across a tissue section using acoustic droplet ejection (ADE) (Aerni *et al* 2006). Advantages of matrix spotting over spray coating is that the reproducibility between samples is higher because the analyte extraction is more efficient. The instrument is able to alter spot size deposited, with smaller closer packed matrix spots preferred for higher resolution MSI, while larger matrix spots spread and have the possibility to delocalise the samples and tend to be better for MSP (Aerni *et al* 2006). Coating sections can be undertaken manually or using automatic matrix depositors; such automated instrumentation include the ImagePrep (Bruker Daltonics, UK) a robotic matrix deposition system.

Alternatively the SunCollect™ automater sprayer (SunChrom, Friedrichdorf, Germany) and the automated TM Sprayer (HTX Technologies, USA) can be used, as in the current research. Both these systems use pneumatic atomisation to spray matrix uniformly onto MALDI sample plates or glass slides, the pressurised air ensures the constant spray conditions, regardless of surrounding environmental factors, such as temperature and humidity. The advantage of automated sprayers is that under pressure the spray is very directional, ensuring a precise location of matrix deposition onto small surfaces.

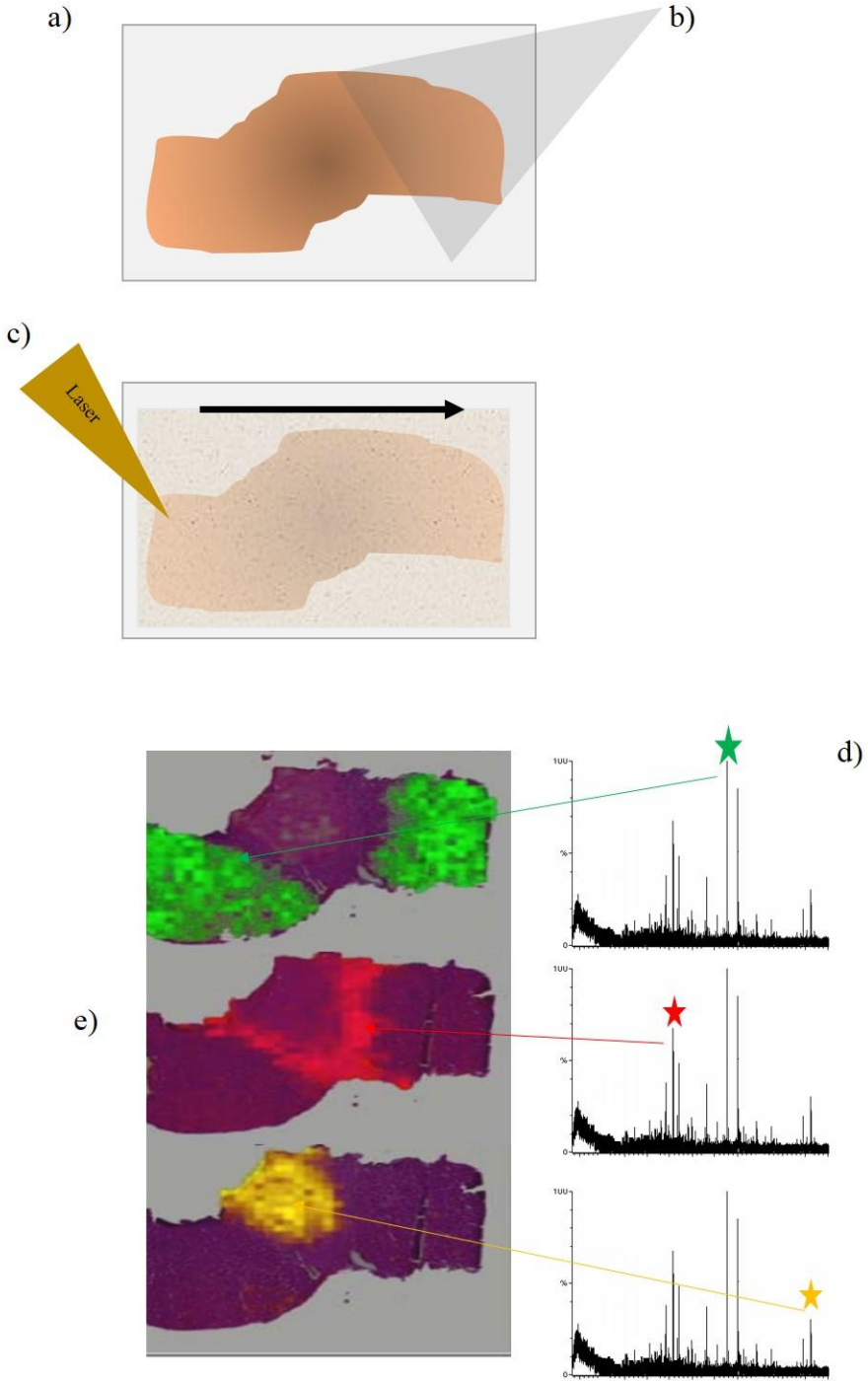

Figure 5.8 Matrix assisted laser desorption ionisation-mass spectrometry imaging (MALDI-MSI) work flow

Tissue sections are cut and mounted on to a glass slide or MALDI plate (a), and matrix deposited onto the section (b). A laser is fired at set raster points across the tissue section (the black arrow showing direction of laser movement across the tissue section) (c), at each raster point, a mass spectra is generated (d). Specific *m/z* ions can be identified from the mass spectra and their distribution identified in the tissue section (e). Figure adapted from Walch *et al* 2008.

Matrix	Matrix abbreviation	Analyte
α-cyano-4-hydroxycinnamic acid	CHCA	Proteins/peptides, small molecules, lipids, drugs and carbohydrates
1,7-bis-(4-hydroxy-3-methoxy-phenyl)-hepta-1,6-diene-3,5-dione (Curcumin)	Curcumin	Drugs and lipids
Trans-2-(3-(4-tert-Butylphenyl)-2methyl-2-propenylidene)malononitrile	DCTB	Inorganic molecules
2,5-dihydroxybenzoic acid	DHB	Proteins/ peptides, small organic molecules, synthetic polymers, glycoproteins and carbohydrates.
Dithranol	DIT	Lipids, synthetic polymers
(E)-3-(4-hydroxy-3-methoxy-phenyl)prop-2-enoic acid (Ferulic acid)	FA	Proteins
Hydroxypicolinic acid	HPA	Oligonucleotides
Trans-3-indoleacrylic acid	IAA	Synthetic polymers
Hydroxycinnamic (sinapinic) acid	SA	Proteins/peptides
Trihydroxyacetophenone	THAP	Carbohydrates, oligonucleotides

Table 5.6 Common matrices used in MALDI-MS

Table adapted from Hoffmann 2007.

As well the ability to optimise parameters that control the level of protein extraction and matrix crystallisation, automated spraying systems prevent sample delocalisation. For example, the distance between the spraying nozzle and the tissue section can be controlled (SunCollect), while nozzle velocity and gas flow can control the matrix drying time (TM Sprayer/SunCollect), while a faster rate of solvent evaporation through the use of heat prevent the formation of large matrix crystals, known to create heat spots (TM Sprayer). Throughout this study, application of matrices was completed using the TM Sprayer, while trypsin was delivered using the SunCollect.

5.3.7.5 MALDI-MS – tissue preparation

From the validation patient cohort (5 MS NAWM and 5 control cases – refer to Appendix III) 10 µm tissue serial sections were cut on the cryostat (Leica, UK) and mounted on to poly-lysine glass slides (Leica, UK). All prepared tissue sections were used immediately or stored in an airtight slide box at -80°C until use. One section from each case was stained with LFB (refer to section 2.3.5 for method) to differentiate between the WM and cortex within each case. Whether profiling for proteins or imaging for peptides, sections were removed from -80°C and placed in a vacuum dessicator for 15 minutes to allow the tissue to come to RT and remove any excess moisture. Tissue sections were washed sequentially with 80% ethanol, 90% ethanol and chloroform for 30 seconds in each and left to dry in a vacuum dessicator for 10 minutes prior to matrix/trypsin deposition.

5.3.8 Intact protein profiling (MALDI-MSP)

For each of the cases investigated (5 MS NAWM and 5 controls), protein profiling was completed on six biological repeats with six mass spectra (technical repeats) generated from six random ROIs on each biological repeat.

5.3.8.1 MALDI matrix preparation and deposition

In this study a range of different matrices were trialled at various concentrations and solvent compositions (Table 5.7). For final MALDI-MSP of intact proteins, the optimum matrix composition was 5mg/ml ferulic acid (FA) in 50/33/17 (%v/v) d.H_20/acetone/formic acid. FA matrix was sprayed onto the tissue sections using the automated TM Sprayer (HTX Technologies, USA), block temperature: 80ºC, velocity: 1300 mm/minute, matrix flow rate: 100 µl/minute, line spacing: 1.5 mm, matrix layers (passes): 22, air pressure: 10 psi.

Matrix	Concentration (mg/ml)	Solvent composition
α-cyano-4-hydroxycinnamic acid (CHCA)	5 / 10	ACN:H_2O:TFA (70%:30%:0.5%)
Sinapinic acid (SA)	5	ethanol:H_2O:TFA (50%:50%:0.5%)
	5	ethanol:H_2O:TFA (80%:20%:0.3%)
	5	ACN:H_2O:TFA (70%:30%:0.5%)
	5	ACN:H_2O:TFA (70%:30%:0.5%) + 2.4µl aniline*
	5	ACN:H_2O:TFA (50%:50%:0.3%)
	25	ACN:H_2O:TFA (50%:50%:0.2%)
	25	ACN:H_2O:TFA (50%:50%:0.2%) + 2.4µl aniline*
Curcumin	2	Acetone:H_2O (70%:30%)
	2	ACN:H_2O (70%:30%)
	2	Acetone:H_2O:TFA (70%:30%:0.2%)
	2	ACN:H_2O:TFA (70%:30%:0.2%)
Ferulic acid	10	ACN:H_2OTFA (70%:30%:0.1%)
	12 / 20	ACN:H_2O:TFA (50%:50%:0.1%)
	10	ACN:H_2O:TFA (70%:30%:0.5%)
	5 / 10 / 20	**Acetone:formic acid:water (33%:17%:50%)**

Table 5.7 Details of the different matrices and solvent compositions trialled for intact protein profiling

Final optimised conditions in red.

Key: ACN: acetonitrile, TFA: trifluoroacetic acid.

*****Equimolar amounts of aniline were added to the SA solution, therefore 1 ml 5mg/ml SA solution contained 2.4 ml of aniline.

5.3.8.2 MALDI-MSP Instrumentation

The mass spectrometer used in the intact protein profiling work was a Voyager De Pro MALDI-TOF (Applied Biosystems/MDS Sciex, USA) with a Nd:YAG laser. The instrument was operated in linear mode, using a delay time of 750 nsec, 150 laser shots were fired per spectrum, at an intensity of 2900 (arbitrary units). For each case, six biological repeats were analysed, generating six random technical repeats in the defined WM in both the MS cases and control cases (as determined from the LFB stained section of each case). The mass spectrometer was calibrated before each sample was analysed using a mixed protein calibration standard of insulin (5734 *m/z*) apomyoglobin (MH^{2+} 8476 *m/z*, MH^{+} 16952 *m/z*), cytochrome C 12361 *m/z*, using the same parameters as stated above.

5.3.9 Peptide digest imaging (MALDI-MSI)

For each case investigated (5 MS NAWM and 5 controls), MALDI-MSI was completed on five biological repeats.

5.3.9.1 In situ tissue digestion

In situ tryptic digests were performed on the tissue sections prior to matrix deposition. Trypsin solution was prepared at 20 µg/ml by the addition of 50 mM ammonium bicarbonate (NH_4HCO_3) containing (0.5%) Octyl-α/β-glucoside (OcGlc), all reagents supplied by Sigma-Aldrich, UK. The automated pneumatic SunCollect (SunChrom, Friedrichdorf, Germany) was used to spray the trypsin solution onto the sections in a series of five layers, at a flow rate of 2 µl/min. Trypsin coated sections were incubated in a humidity chamber containing d.H_2O for 3 hours at 37°C and 5% CO_2/95% air.

5.3.9.2 Matrix preparation and deposition

For peptide imaging, the matrix α-cyano-4-hydroxycinnamic acid (CHCA) prepared in 50/0.5 (%v/v) d.H_2O/trifluoroacetic acid (TFA) (Fisher, UK) and 25/25 (%v/v) ethanol/acetonitrile (ACN) was sprayed using the TM Sprayer (HTX Technologies, USA), block temperature: 80ºC, velocity: 1300 mm/minute, matrix flow rate: 100 µl/minute, line spacing: 1.5 mm, matrix layers (passes): 10, air pressure: 10 psi.

5.3.9.3 MALDI-MSI instrumentation

Peptide images were acquired using a Q-Star Pulsar/Q-TOF mass spectrometer (Applied Biosystems/MDS Sciex, USA) fitted with a variable rate ND: Yttrium vanadate (Nd:YVO_4) laser using a continuous raster, imaging at a laser repetition rate of 5 KHz. Image acquisition was performed at 150 µm spatial resolution.

5.3.10 Mass spectrometry data processing

MSI data was imported into BioMap 3.7.5.5 software (http://www.maldi-msi.org/) for image processing. Within BioMap, the WM ROI was manually outlined in each biological repeat using the LFB stained section as a guide. The data was normalised against the total ion count (TIC) and the same contrast/brightness applied to the images. The data list generated from the ROI of each biological repeat was exported from BioMap and converted to a text file.

Prior to statistical analysis, the accumulated text files from each case, representing data lists exported from either BioMap 3.7.5.5 (peptide imaging) or from Voyager data explorer (intact protein profiling) were imported into SpecAlign (Oxford, UK) to undergo data alignment processing. This software generated an average spectrum for each case from which all peaks in all spectra being analysed were aligned to, and all spectra were normalised against the TIC. Both peptide and protein spectra were then processed using mMass (Strohalm *et al* 2010), an open source mass spectrometry tool, to allow for peak selection.

5.3.11 Statistical analysis

Post SpecAlign, and peak selection in mMass, a collective group of protein text files representing each of the 6 technical repeats of the 6 biological repeats of each of the 10 cases (5 MS NAWM and 5 controls), or a collective group of peptide text files representing each of the 5 biological repeats of the 10 cases (5 MS NAWM and 5 controls) were imported into Marker View software 1.2 (Applied Biosystems, USA) and data were rearranged into a table format. For protein analysis a minimum intensity of 0.1 was selected, with a maximum number of peaks of 5,000. For peptide analysis a minimum intensity of 0.1 was selected, with a maximum number of peaks of 10,000; only monoisotopic peaks selected in Marker View were used in the statistical analysis. Principal components analysis (PCA) and partial least squares regression discriminant analysis (PLSDA) was performed using MATLAB® (R2012a) (MathWorks, Inc., USA).

5.4 Results

5.4.1 Optimised primer concentration and efficiencies

Initial qPCR optimisation studies determined the optimum concentration of primers. The optimum forward and reverse primer concentration for each gene of interest was selected based on the lowest Ct value, and the amplification of a single product indicating the absence of primer dimers. Initially all 5 primers were optimised by Natalie Rounding. MT1X, TF and FTL primers were optimised at 300nM/300nM, and gave a single amplified product with no evidence of primer dimer formation (Figure 5.9). The primers were efficient over a range of cDNA template concentrations, as shown by the standard curves for each of the primers and their corresponding efficiency scores; MT1X: 105.9%, TF: 99.5%, FTL: 99.8% (Figure 5.9). In comparison, MT1G and MT2A primers produced multiple peaks at varying combinations of primer concentrations and their efficiency over a range of cDNA concentrations was poor; MT1G: 91.4%, MT2A: 106.7%, (Figure 5.10). Consequently these two primers were redesigned and after repeated optimisation studies, the optimum concentration of MT1G primer pair was 300nM/300nM and MT2A primer pair was 300nM/600nM. Both primers gave single products, with good efficiencies over a range of template concentrations: MT1G: 106.9%, MT2A: 112.2% (Figure 5.11).

5.4.2 Housekeeping gene selection

Based on analysis of the original microarray data, three probe sets for β-actin and three probe sets for GAPDH were represented in all seven of the original cases used in the microarray study. The signal intensity across these probe sets was relatively high for the β-actin probes compared to the GAPDH probes (Table 5.8), therefore β-actin was used as the HK control in all subsequent qPCR experiments.

5.4.3 Opposing gene expression changes in MS NAWM compared to control WM

From the five candidate genes identified as significantly upregulated in MS NAWM astrocytes compared to control WM astrocytes in chapter 4, qPCR validation failed to replicate these microarray findings in the validation patient cohort (Figure 5.12). However, an additional qPCR carried out on remaining cDNA from a selection of cases used in the original microarray study (2 MS cases and 2 control patients) showed upregulation in expression of MT1X, TF and FTL in the MS NAWM (Figure 5.13). However, due to the study size this expression failed to reach statistical significance, yet helps to support the findings of the original microarray data.

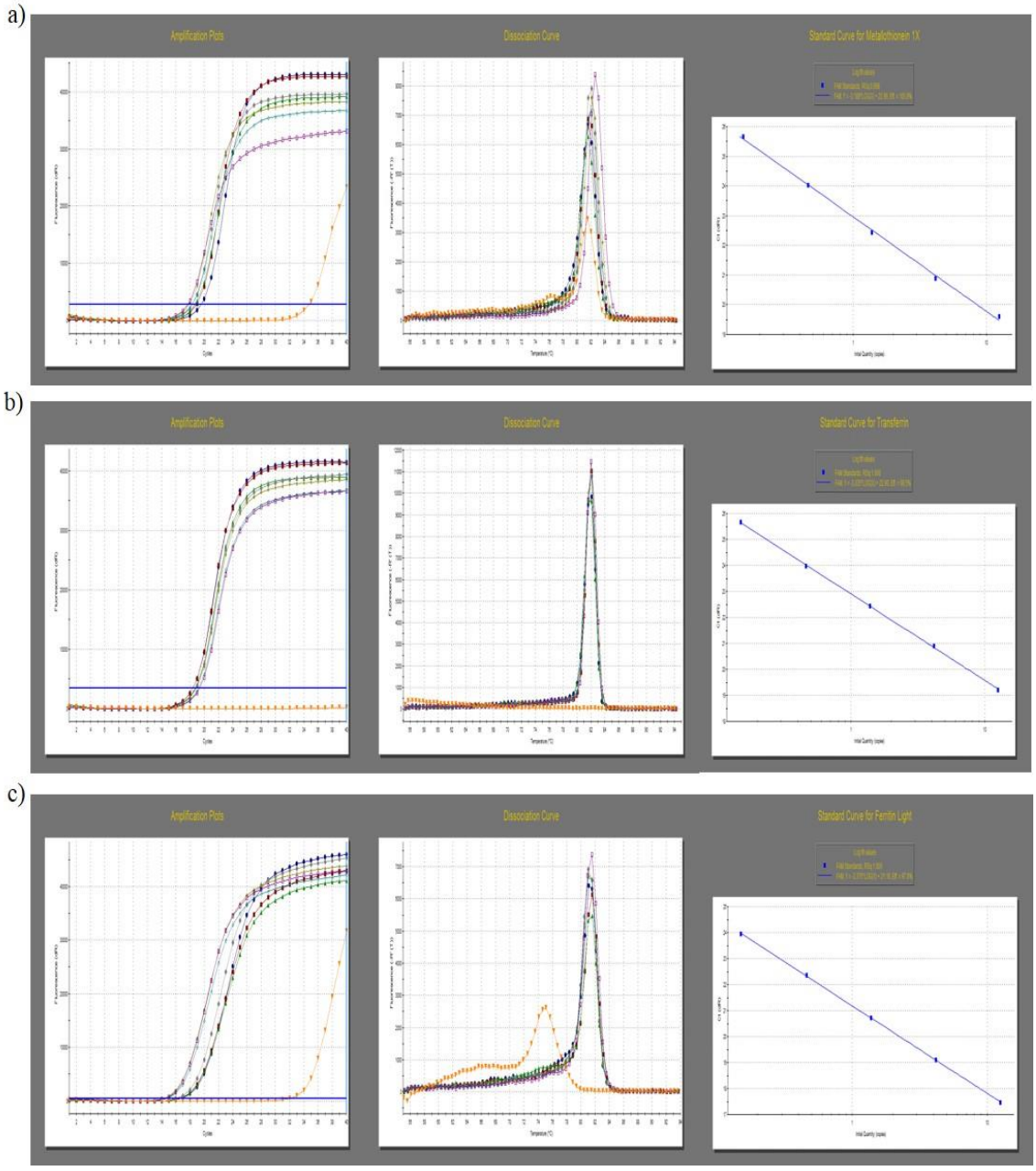

Figure 5.9 Successful primer pair optimisation for qPCR

Optimisation of MT1X (a), TF (b) and FTL (c). Each primer set gave similar Ct values, as indicated by the amplification plots, and single PCR products, as indicated by the dissociation curve. The efficiency of the three primers was constant across the range of cDNA concentrations (MT1X 105.9%, TF, 99.5%, FTL 99.8%). The orange line represents the NTC.

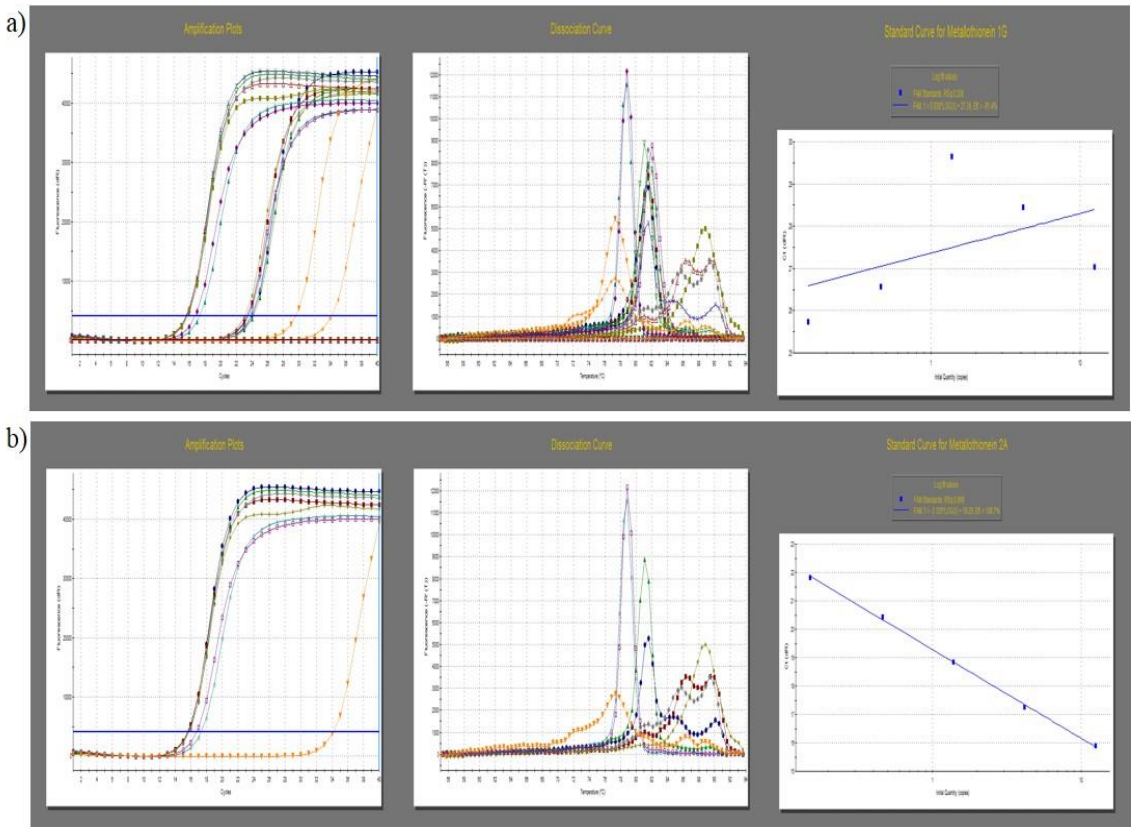

Figure 5.10 Unsuccessful primer pair optimisation for qPCR

Two primer pairs representing MT1G (a) and MT2A (b) were not optimised successfully. The presence of variable Ct values from the amplification plots and multiple PCR product and primer dimers across the range of primer pair combinations is indicative of non-specific primer sets. Also, the efficiency of the two primers was dissimilar to MT1X, TF and FTL (MT1G 91.4%, MT2A 106.7%). The orange line represents the NTC.

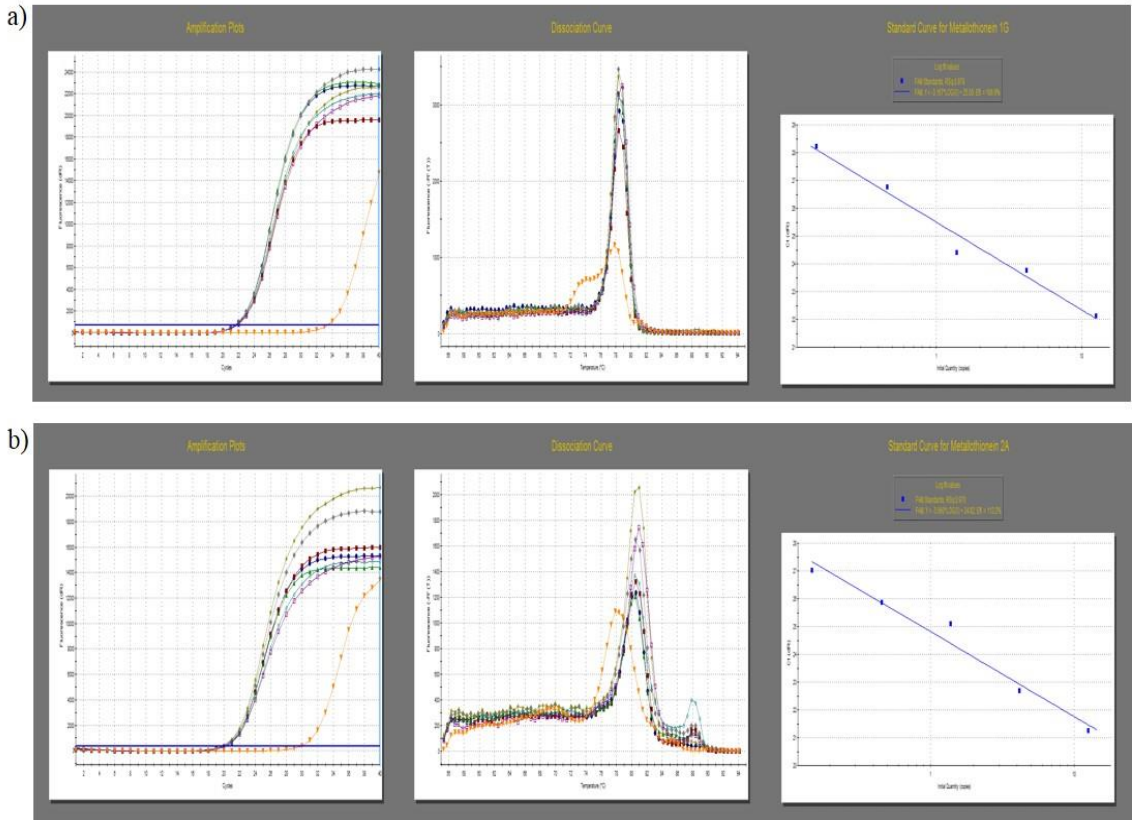

Figure 5.11 Redesigned MT1G and MT2A successful primer pair optimisation for qPCR

Newly designed primer pair sets representing MT1G (a) and MT2A (b) were optimised successfully. The presence of similar Ct values from the amplification plots and single PCR product across the range of primer pair combinations is indicative of more specific primer sets. However, the efficiency of the two primers was higher in comparison to MT1X, TF and FTL (MT1G 106.9%, MT2A 112.9%) which should be considered when analysing the final qPCR data. The orange line represents the NTC.

β-Actin (Probeset ID.)	Mean signal intensity [n=7]	Signal intensity (range)	GAPDH (Probeset ID.)	Mean signal intensity [n=7]	Signal intensity (range)
200801_x_at	5403	(3900-7530)	212581_x_at	2394	(1517-3603)
213867_x_at	5290	(4083-7698)	213453_x_at	1514	(1040-2272)
224594_x_at	5248	(4197-7234)	217398_x_at	1172	(737-1800)

Table 5.8 Housekeeping gene selection for qPCR

A higher signal intensity across all three probe sets was detected for β-actin compared to GAPDH.

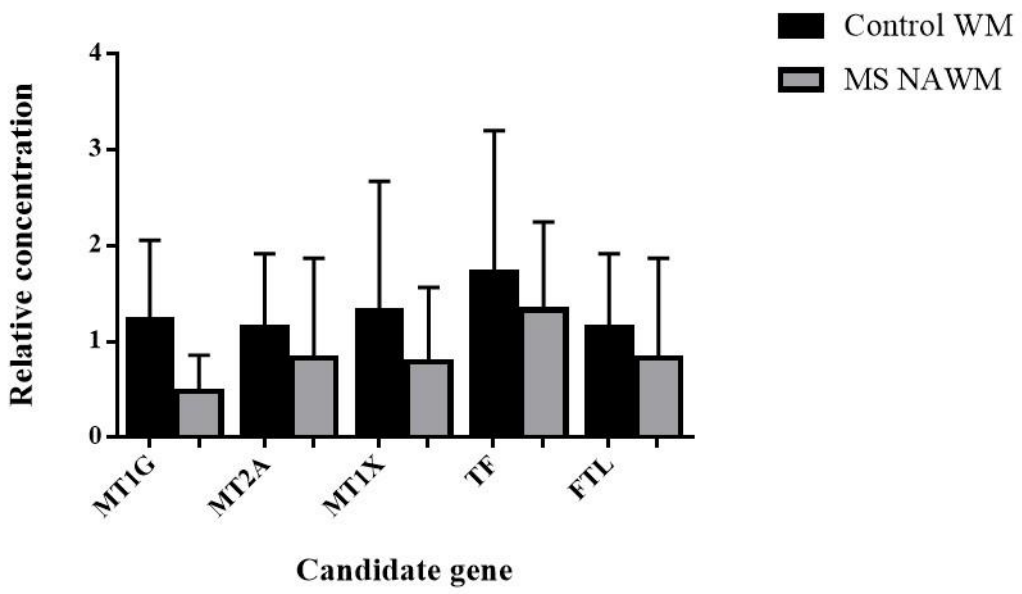

Figure 5.12 qPCR validation of the selected five candidate genes involved in iron homeostasis in an additional validation patient cohort

No significant difference in gene expression was detected between MS NAWM (6 cases) and control WM (6 cases). MT1G p=0.0714, MT2A p= 0.0649, MT1X p=0.2944, TF p= 0.9048, FTL p=0.0649 (Mann-Whitney U test).

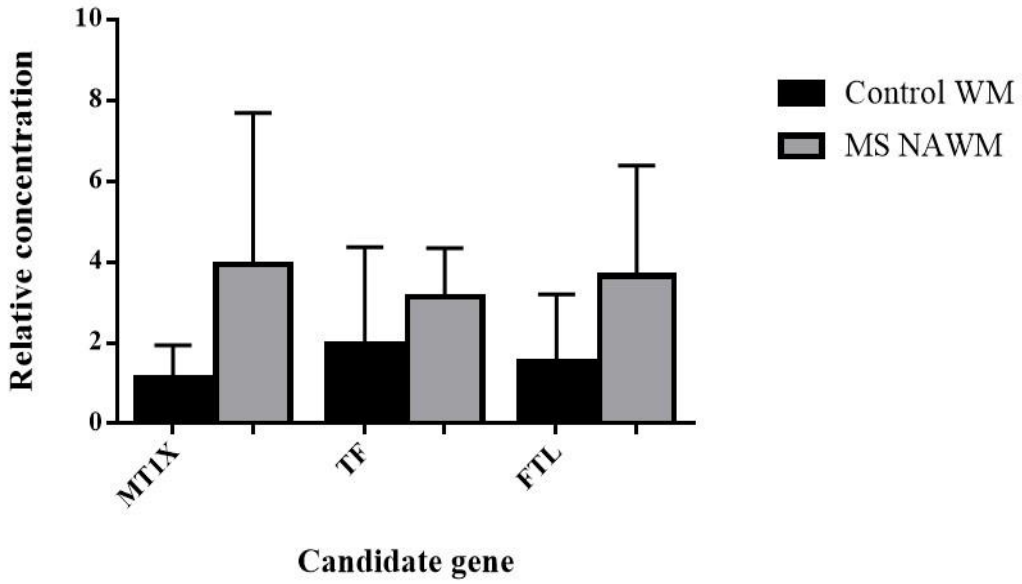

Figure 5.13 qPCR validation for three of the candidate genes in the original microarray patient cohort samples

The same directional upregulatory change for MT1X, TF and FTL was identified in the MS NAWM cases compared to the control WM (p= not significant). (2 MS NAWM and 2 control cases).

5.4.4 Metallothionein immunoreactivity colocalised with GFAP$^+$ astrocytes

Dense MT immunoreactivity was a common feature across all MS NAWM and control cases investigated. In a qualitative assessment, there was a regular distribution of MT throughout the WM, with staining associated with the cell body and extending processes of cells with an astrocytic morphology (Figure 5.14). No apparent differences in the pattern of staining were observed between MS NAWM and control WM, with a regular distribution of positively stained cells throughout both sample groups. MT immunoreactivity colocalised with GFAP$^+$ astrocytes (Figure 5.15, red arrows). However it is worth noting that not all GFAP$^+$ astrocytes were MT$^+$ and not all MT$^+$ cells were GFAP$^+$ (Figure 5.15, blue arrows). MT IHC was completed by Natalie Rounding.

5.4.5 Ferritin light chain immunoreactivity colocalised with GFAP$^+$ astrocytes

FTL immunoreactivity was a common feature across all MS NAWM and control WM investigated. A regular distribution of FTL staining was associated with cell bodies, but was not as extensive as MT immunoreactivity (Figure 5.16a). FTL expression colocalised with GFAP$^+$ astrocytes (Figure 5.16b), but was also associated with small spherical cells morphologically resembling oligodendrocytes. No qualitative differences in staining pattern of FTL was observed between MS NAWM and control WM.

5.4.6 Transferrin immunoreactivity

The pattern of staining observed for TF contrasted with MT and FTL, which was clearly associated with individual cells. TF immunoreactivity aligned in a tract like pattern, suggesting possible associated with axons (Figure 5.17). Upon dual labelling with GFAP, there was not an obvious colocalised pattern of staining between TF and GFAP, however TF expression may be associated with astrocyte end feet where the processes of astrocytes ensheath blood vessels and/or make contact with central synapses within the brain (Ventura & Harris 1999).

5.4.7 Western blot analysis of ferritin light chain in MS NAWM and control WM tissue

Prior to WB, the concentration of each MS and control protein extract was determined via the Bradford assay, a representative standard curve is shown in Figure 5.18. FTL WB detected a single positive protein band in both the MS and control WM at the expected molecular weight of ~20 kDa (Figure 5.19). Densitometric analysis of FTL and β-actin (42 kDa) showed no significant differences in FTL protein expression in NAWM compared to control WM, p=0.944 (Mann-Whitney U test) (Figure 5.20).

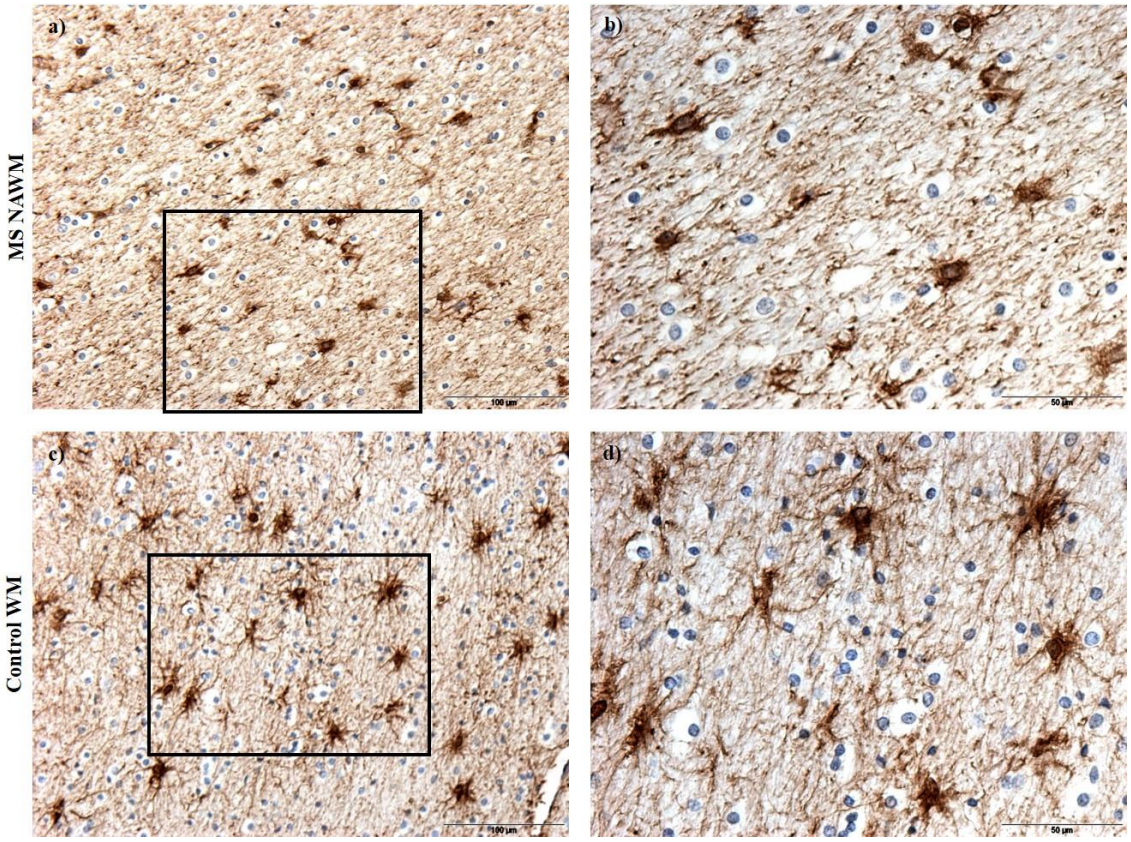

Figure 5.14 Metallothionein protein expression in MS NAWM and control WM
A regular distribution of MT immunoreactivity was detected throughout NAWM (a) and control WM (c), and was associated with cells morphologically resembling astrocytes. (b) and (d) represent a higher magnification of MT immunopositive cells in MS NAWM and control WM respectively, marked with a black box in (a) and (c). *Scale bar represents (a,c)100 µm, (b,d) 50 µm.*

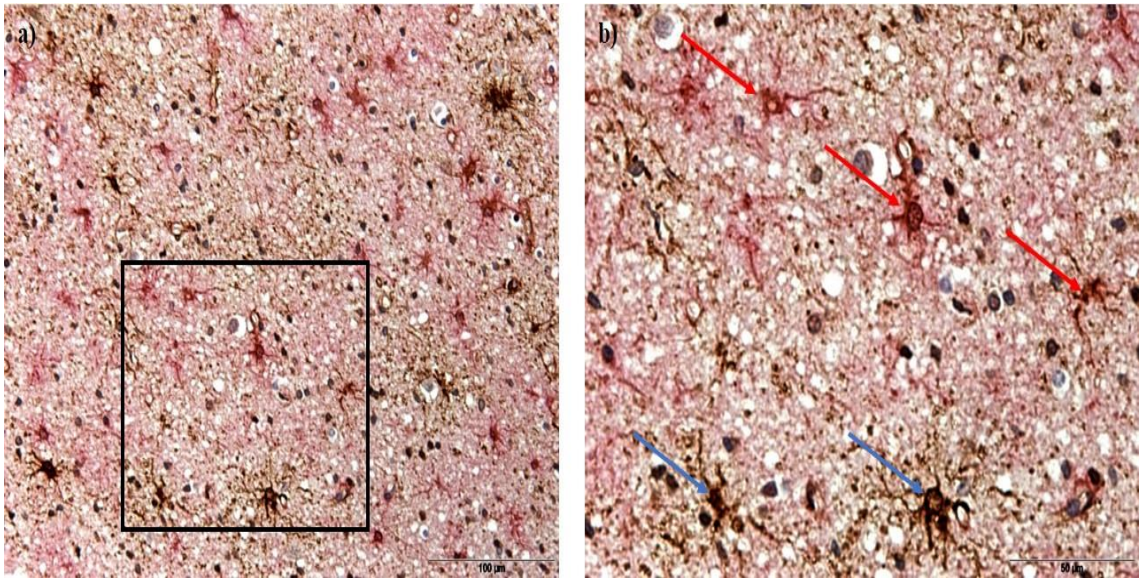

Figure 5.15 Metallothionein immunoreactivity colocalises with GFAP$^+$ astrocytes in MS NAWM

MT (brown) immunoreactivity colocalises with GFAP$^+$ astrocytes (red) (b, red arrows). MT$^+$ GFAP$^-$ cells were also present (b, blue arrows). (b) represents a higher magnification of colocalised MT$^+$ astrocytes marked with a black box in (a). *Scale bar represents: a) 100 µm, b) 50 µm.*

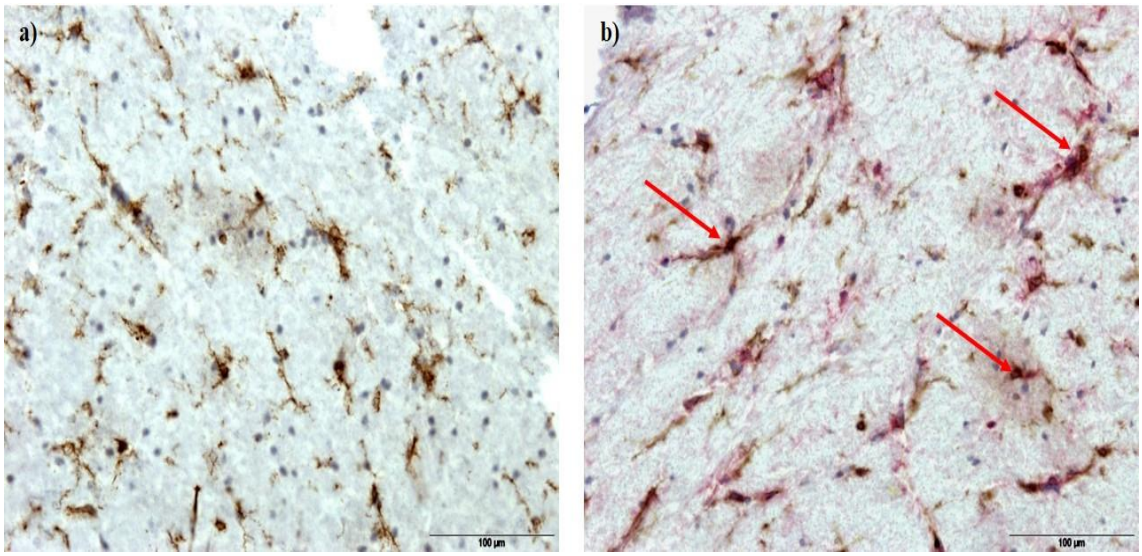

Figure 5.16 Ferritin light chain protein expression in MS NAWM

FTL immunoreactivity visualised using single label IHC (a) and colocalised with GFAP in dual label IHC (b). Colocalised expression of FTL (brown) and GFAP (red) confirm astrocyte expression of FTL (b, red arrows).

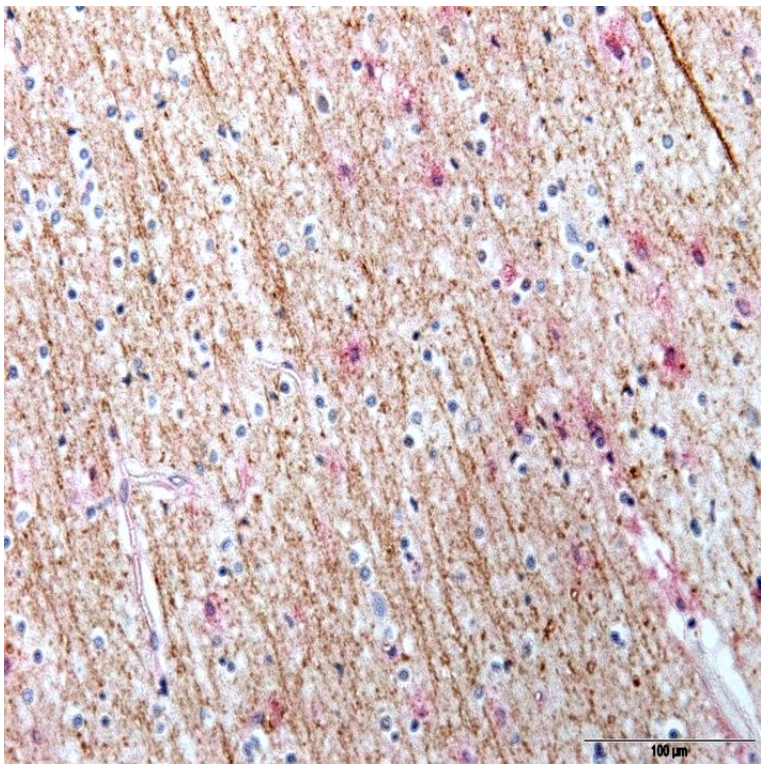

Figure 5.17 Transferrin protein expression in axonal tract like pattern in MS NAWM

The general expression of TF in MS NAWM and control WM was not distinct to individual cell types. The pattern of staining followed a tract like configuration with possible colocalised expression with astrocyte endfeet ensheathing blood vessel and/or contacting axons within the brain. Expression of TF (brown) and GFAP (red) *Scale bar represents 100 µm.*

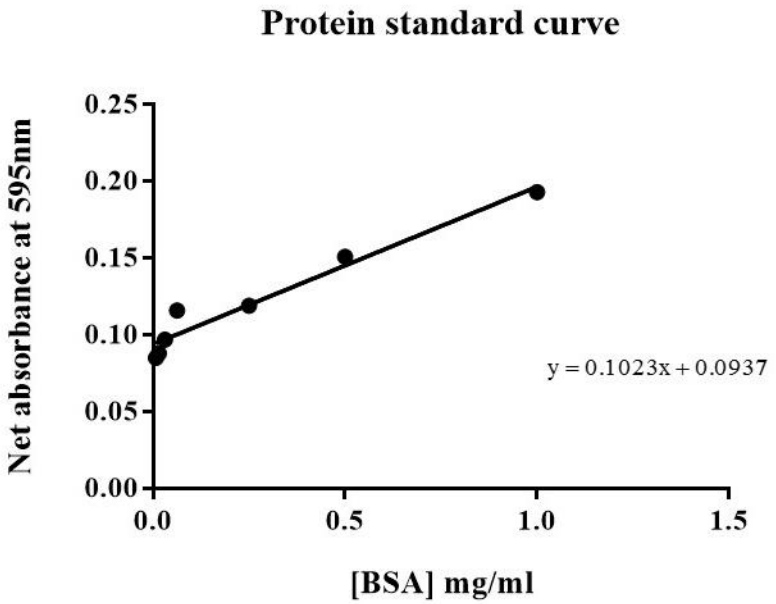

Figure 5.18 A representative standard curve used to determine the protein concentration of the unknown brain extract using the Bradford protein assay

The above data shows the standard curve of known BSA concentration standards and their absorbance at 595nm. The concentration (x) of unknown samples can be determined through the rearrangement of the linear regression formula x= (y-c)/m.

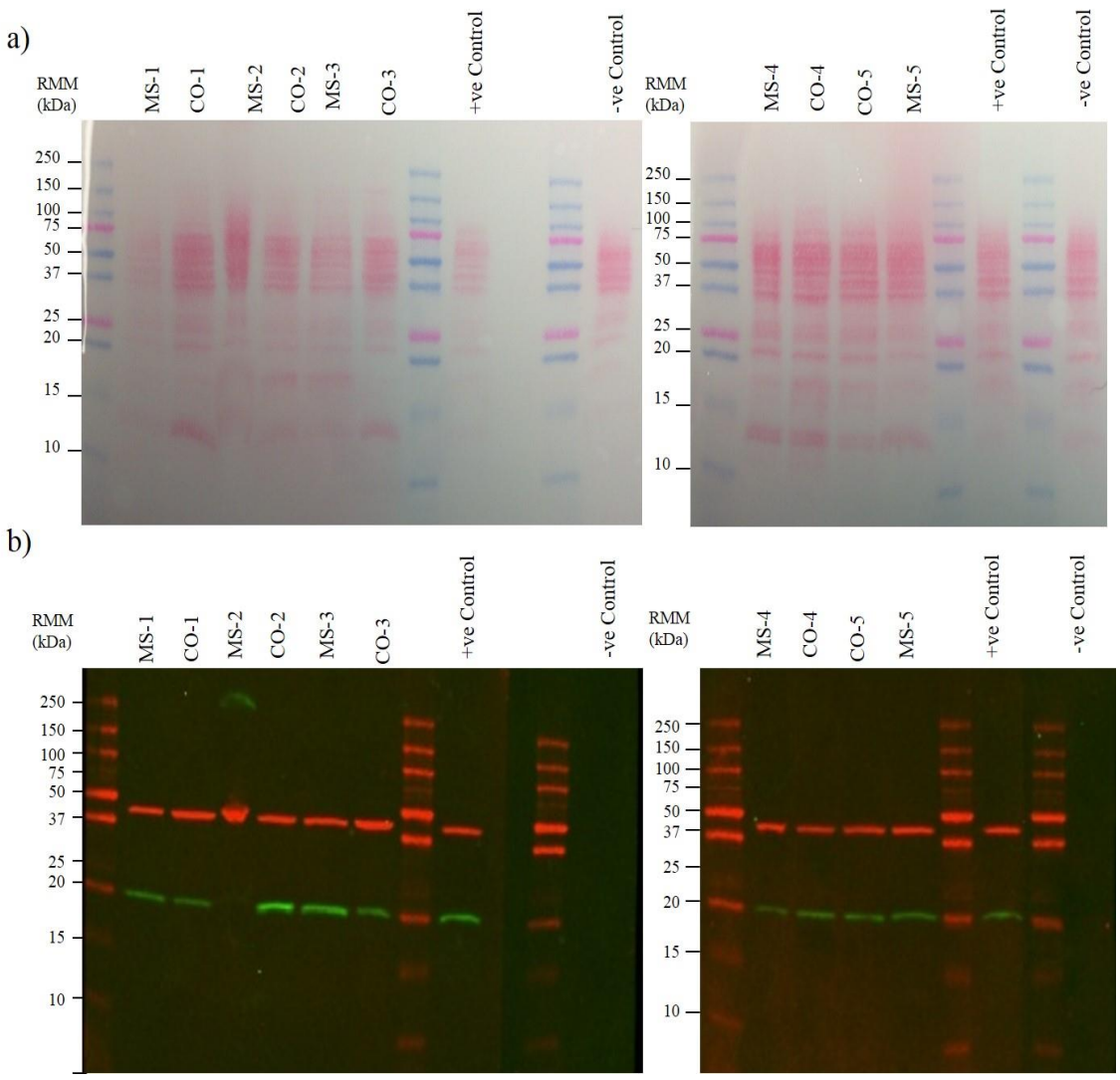

Figure 5.19 Ponceau S red stain and ferritin light chain western blotting from MS and control cases, [30 µg protein/lane]

Ponceau S red indicated the successful transfer of proteins onto the NCM (a). FTL immunoprobed WB of separated brain proteins (green, ~20 kDa) (b). Equal loading was verified by β-actin probing (red, 42 kDa) (b). FTL western blot completed by Ruth Thomas.

Key: MS: multiple sclerosis case, CO: control case, NCM: nitrocellulose membrane, RMM: relative molecular mass, +ve control: positive control, -ve control: negative control.

*MS-2 sample was reanalysed on a separate WB due to sample aggregation in the well.

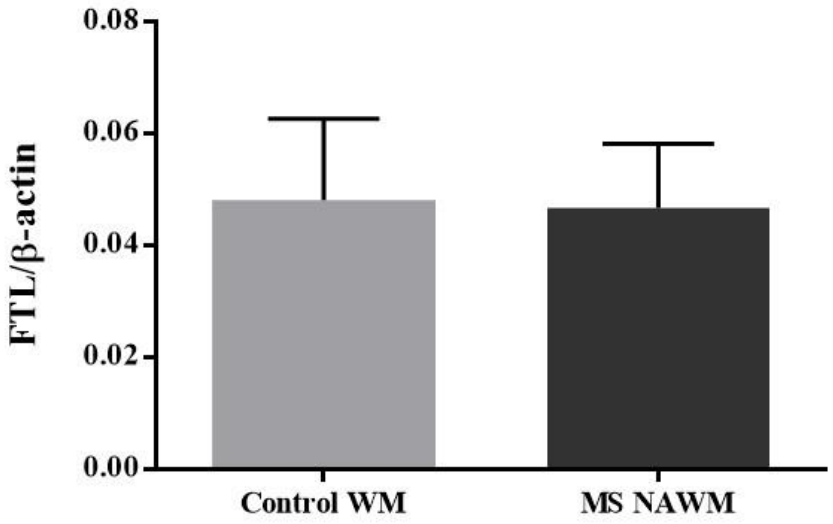

Figure 5.20 Levels of ferritin light chain in MS NAWM and control WM detected by WB

Densitometric analysis values expressed as the density ratio of target (FTL) to loading control (β-actin) in arbitrary units. Data is presented as the mean (n= 5 MS NAWM and 5 control WM cases). No significant differences in the levels of FTL expression were observed between MS NAWM and control WM.

5.4.8 Western blot analysis of metallothionein in MS NAWM and control WM tissue

Numerous optimisation attempts to identify the expression of MT through WB were completed, and included varying the sample protein concentrations applied to the gels, alternative sample buffers, alternative wash steps, varying concentrations of primary and secondary antibody, the use of different secondary antibodies and alterations of antibody incubation times. However no consistent results for MT expression were achieved to enable densitometric analysis to be completed.

However, throughout the optimisation experiments the presence of a protein band at the expected molecular weight of ~12 kDa for MT was consistently identified on the Ponceau S Red stain (Figure 5.21a and Figure 5.22a). Immunoprobing for MT gave inconsistent results. Multiple bands were identified (Figure 5.21b - green), or no positive stain for MT was identified. Due to the high concentration of secondary antibody required to identify MT expression, the α-mouse IR680CW antibody (red) originally used was replaced with the α-mouse IR800CW (green) due to the high background hue from the IR680CW (red) antibody when visualised on the LiCor imaging system.

MT was firstly probed with an α-mouse IR800CW antibody (green) identifying multiple bands as shown in Figure 5.21b, the expected relative molecular mass (RMM) for MT was 12 kDa. β-actin (42 kDa) was probed for with an α-rabbit IR800CW antibody (green), Figure 5.21c. Multiple bands were detected for both MT and β-actin as seen in Figure 5.21b,c, with a particular strong band identified at ~55 kDa in Figure 5.21c.

In another MT WB optimisation experiment, more concentrated protein samples [40 µg/lane] were loaded and alternative secondary antibodies were used. The use of two separate IR labelled secondary antibodies, (α-mouseIR680CW and α-rabbit IR800CW) allowed for the easier distinction between MT (red) and β-actin (green) expression on the membrane. The α-mouse IR680CW antibody did not produce the high background previously seen. In this experiment a single band for MT was present at ~12 kDa, the expected weight for MT, however the bands were unclear and blurred, (Figure 5.22b, red). Equal loading was verified by β-actin probing (Figure 5.22b, green) with the presence of a single band at 42 kDa. However, attempts to repeat this experiment on the full validation cohort failed to reproduce these data and bands at the expected molecular weight for MT were not detected. This experiment was repeated on three separate occasions and therefore no densitometry analysis could be completed for MT expression in MS NAWM and control cases.

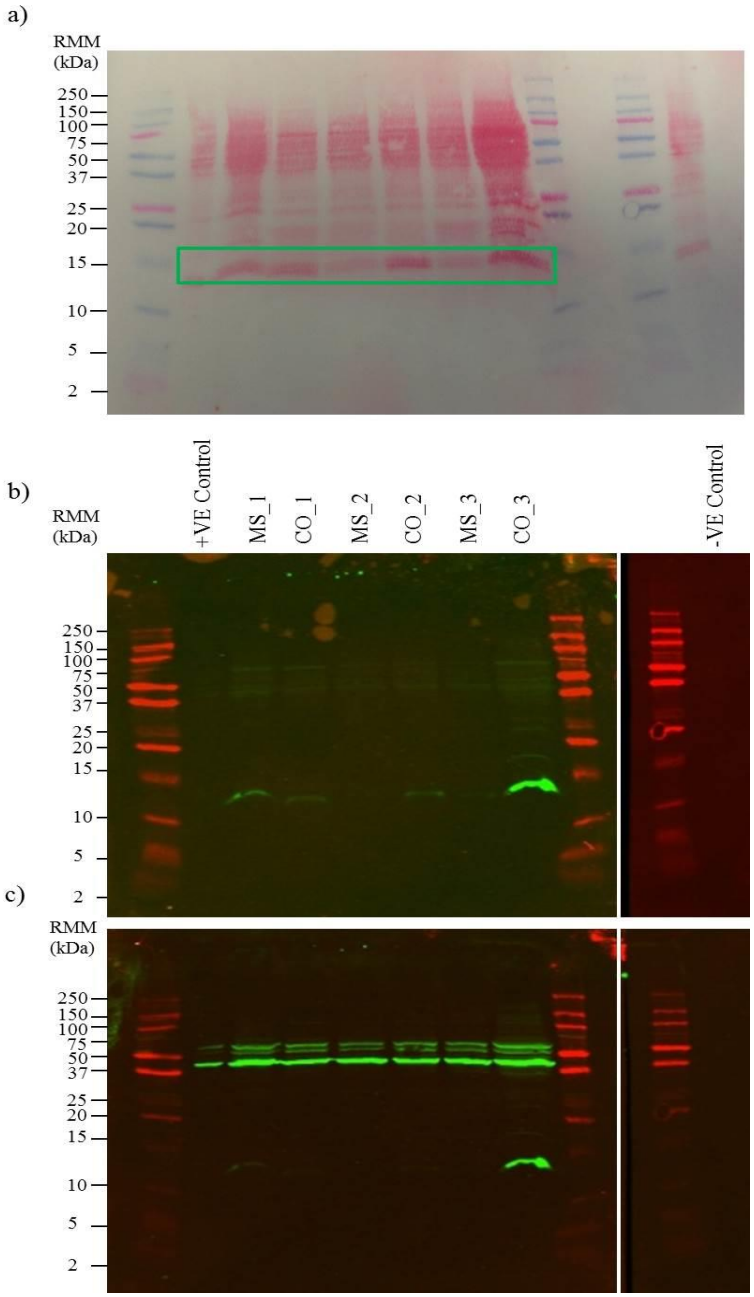

Figure 5.21 Ponceau S red stain and metallothionein western blotting of MS and control cases [20 µg protein/lane]

Ponceau S red indicated the successful transfer of proteins onto the NCM, a protein band at the expected molecular weight (~12 kDa) for MT was present in all samples (a, green box). MT immunoprobed of separated brain proteins, identified multiple bands (b, green). Equal loading was verified by β-actin probing (c, green 42 kDa), yet additional multiple non-specific bands were seen after probing for β-actin in particular a band present at ~55 kDa (c, green).

Key: MS: multiple sclerosis case, CO: control case, NCM: nitrocellulose membrane, RMM: relative molecular mass, +ve control: positive control, -ve control: negative control.

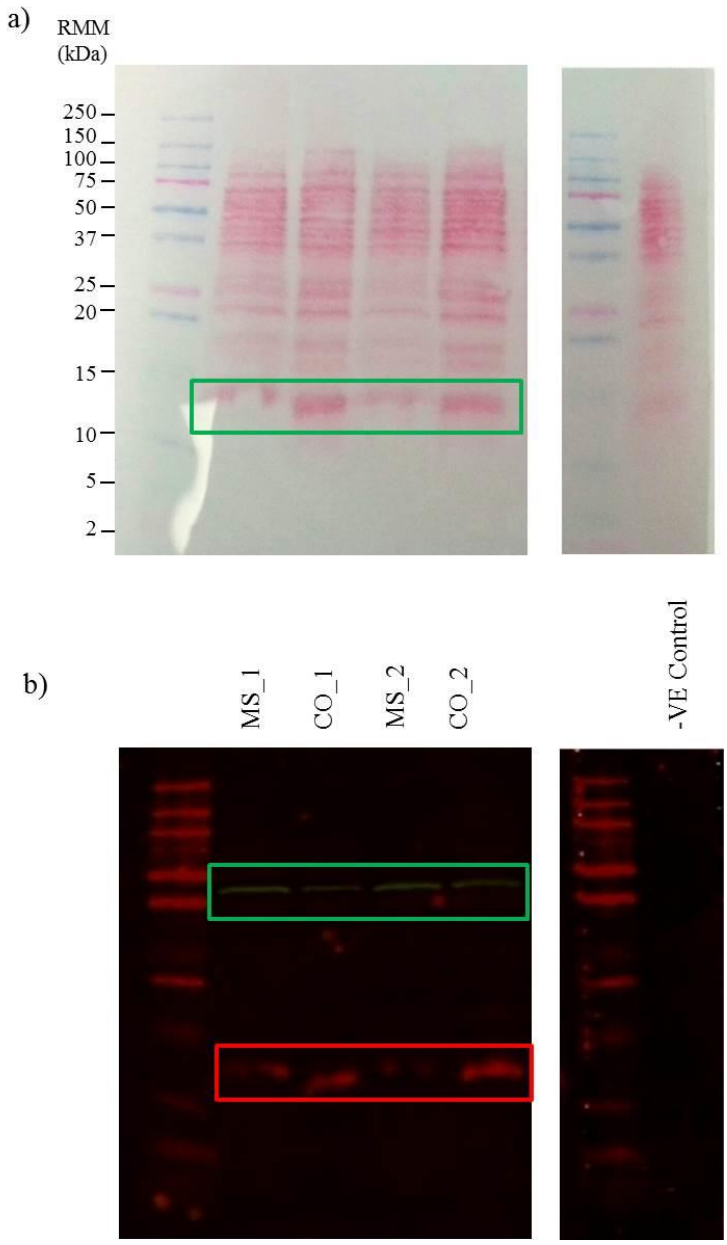

Figure 5.22 Ponceau S red stain and metallothionein western blotting of MS and control cases [40 µg protein/lane]

Ponceau S red stained the successful transfer of proteins onto the NCM, a protein band at the expected molecular weight for MT (~12 kDa) was present in all samples (a, green box). MT immunoprobed WB of separated brain proteins, with a single unclear, blurred band identified (b, red box ~12 kDa). Equal loading was verified by β-actin probing (b, green box 42 kDa).

Key: MS: multiple sclerosis case, CO: control case, NCM: nitrocellulose membrane, RMM: relative molecular mass, +ve control: positive control, -ve control: negative control.

5.4.9 Intact protein profiling (MALDI-MSP)

Direct tissue profiling was carried out on six serial sections (biological repeats) of each MS and control case. Mass spectra were generated from six ROIs (technical repeats) and example spectra are shown in Figure 5.23. Each of the spectra shows the presence of many species represented by the different protein peaks. The detection of particular signals was common to both MS cases and control cases (e.g. the peak at 18.1 kDa, red astericks in Figure 5.23 a-d), while other peaks were specific to a particular MS case over control cases (e.g. the peak at 22.4 kDa, yellow astericks in Figure 5.23 a,b,). Similarly, other peaks were specific to control cases over MS cases (e.g. the peak at 10.5 kDa, purple astericks Figure 5.23 a-d).

5.4.9.1 Principal components analysis – intact protein profiling (MALDI-MSP)

A technically accurate assessment of the differences in protein profiles between control and case samples was carried out by multivariate statistical analysis, principal component analysis (PCA) via MATLAB®, through the Eigen Vector tool box, to produce an unbiased clustering of spectra. PCA turns possibly correlated data linearly into uncorrelated data, and allows an unbiased look at all data to identify any specific groupings between cases. Initially, a non-discriminant PCA was performed on all samples analysed, which included 6 biological repeats of each of the 5 MS NAWM and 5 control cases, with 6 technical repeats per biological repeat to ensure reproducibility of results. From the scores plot, there were no apparent differences between the spectral data sets belonging to MS NAWM and control cases respectively (Figure 5.24a). although there appeared to be *m/z* values that were noticeably distant from the centre of the loadings plot (18056 *m/z*, 14444 *m/z* and 17587*m/z*) (Figure 5.24b) and therefore suggestive as being characteristic of specific cases. However, when the loadings plot was compared to the scores plot, the specific species did not correlate with multiple repeats of particular samples, and therefore cannot be classed as being meaningful and specific to a particular MS or control case.

In order to try and separate the data into disease and control groups, further PCA was carried out on the average spectral data from all biological and technical repeats of each case. Mass spectra representing each of the cases's biological and technical repeats was combined into a single average spectra in SpecAlign, the peak lists from each case's averaged mass spectra was statistically assessed in MATLAB® via PCA. As before, no clear differences between the MS NAWM cases and control cases depicted from the scores plot (Figure 5.25), with no separation or clear groups distinguished.

a)

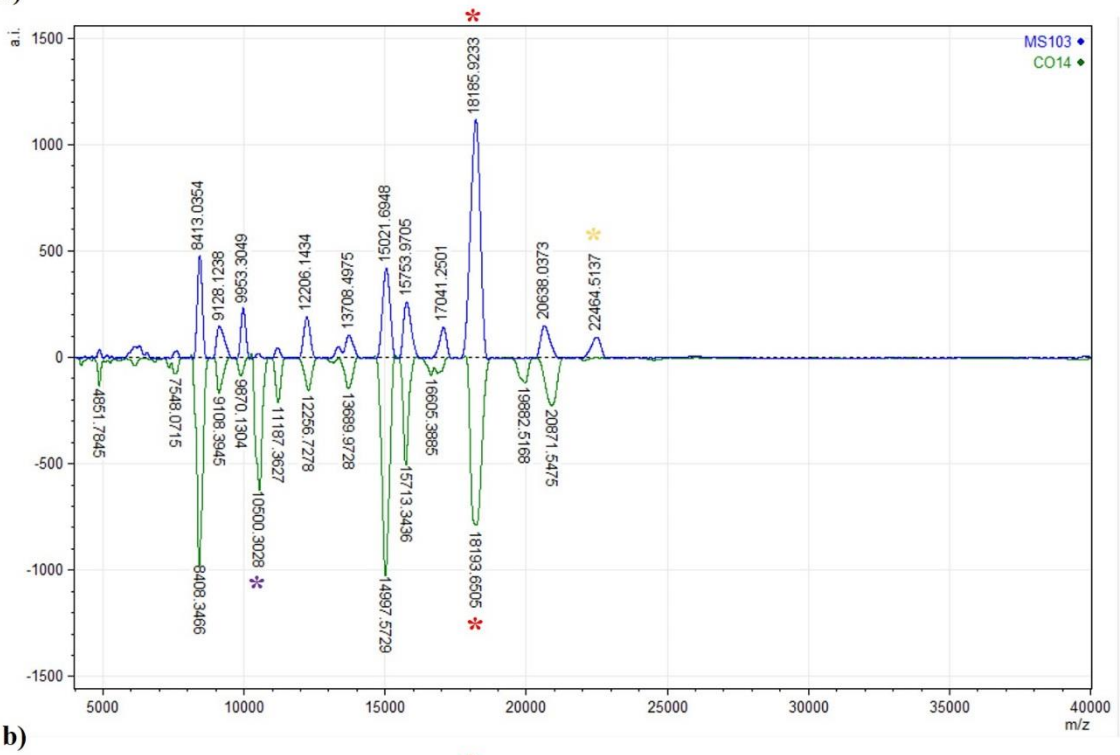
a.i.
MS103
CO14
m/z
4951.7845
7548.0715
8408.3466
9108.3945
9870.1304
10500.3028
11187.3627
12256.7278
13689.6728
14997.5729
15713.3436
16905.3885
18193.6505
18185.9233
19882.5198
20871.5475
20638.0373
22464.5137
8413.0354
9128.1238
9953.3049
12206.1434
13708.4975
15021.6948
15753.9705
17041.2501

b)

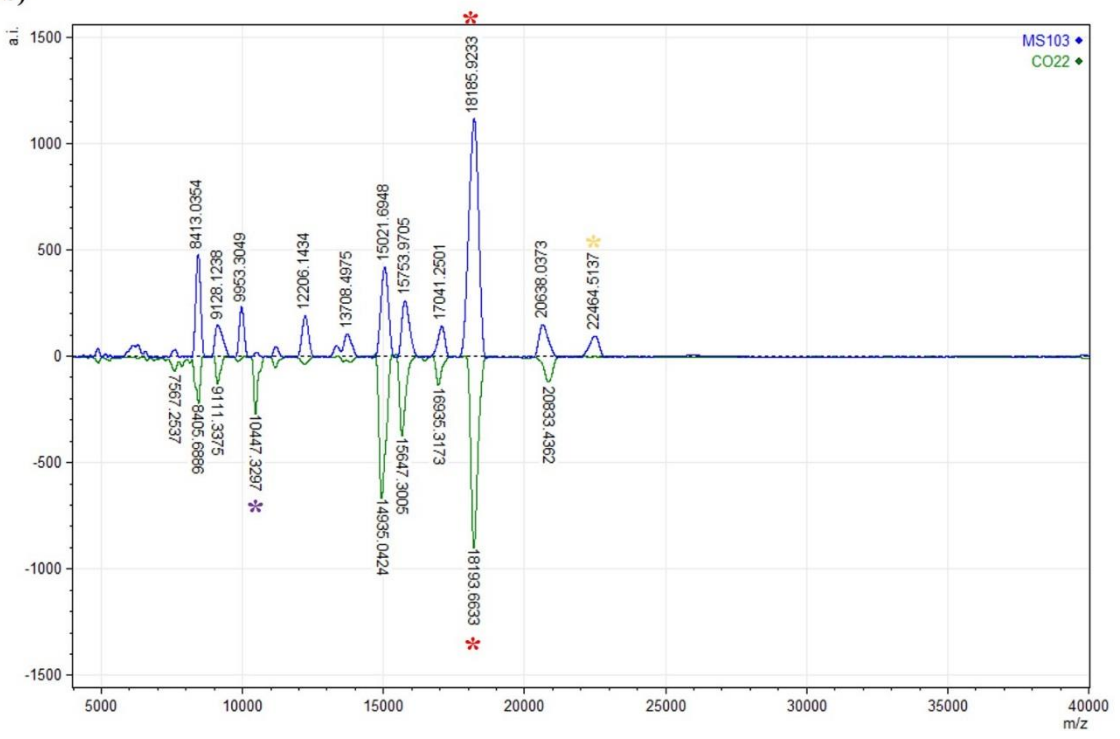
a.i.
MS103
CO22
m/z
7567.2537
8405.6986
9111.3375
10447.3297
14936.0424
15647.3005
16935.3173
18193.6633
18185.9233
20833.4362
20638.0373
22464.5137
8413.0354
9128.1238
9953.3049
12206.1434
13708.4975
15021.6948
15753.9705
17041.2501

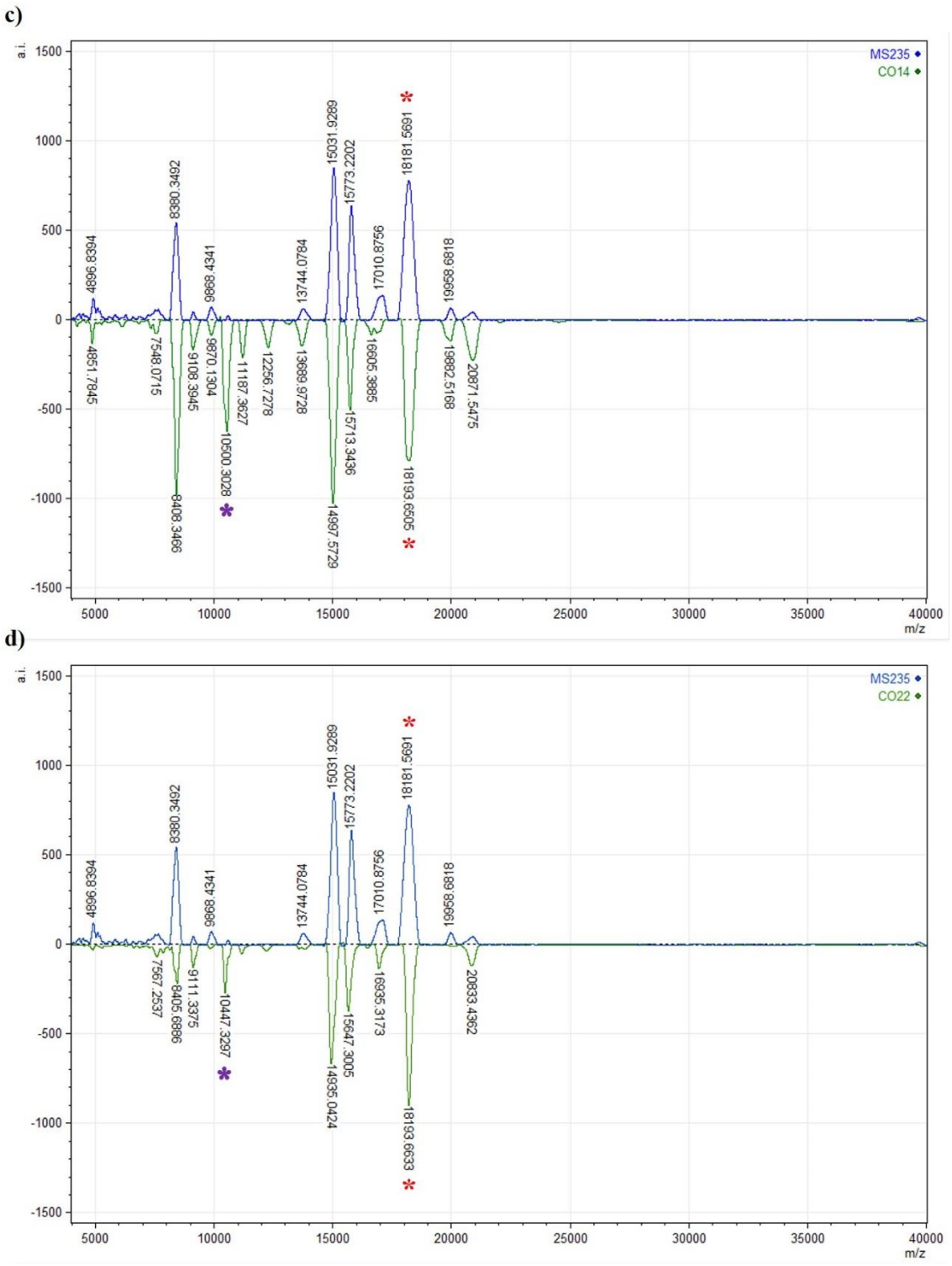

Figure 5.23 Intact protein profiling of MS and control samples

Example mass spectra produced from direct tissue profiling of human PM CNS WM material. MS NAWM vs. control cases; MS103 (blue) vs. CO14 (green) (a), MS103 (blue) vs. CO22 (green) (b), MS235 (blue) vs. CO14 (green) (c), MS235 (blue) vs. CO22 (green) (d). Signals common to both MS and control cases (red astericks at 18.1 kDa, a-d). Signals common to MS103 (yellow astericks at 22.4 kDa, a,b). Signals common to control cases (purple astericks at 10.5 kDa, a-d).

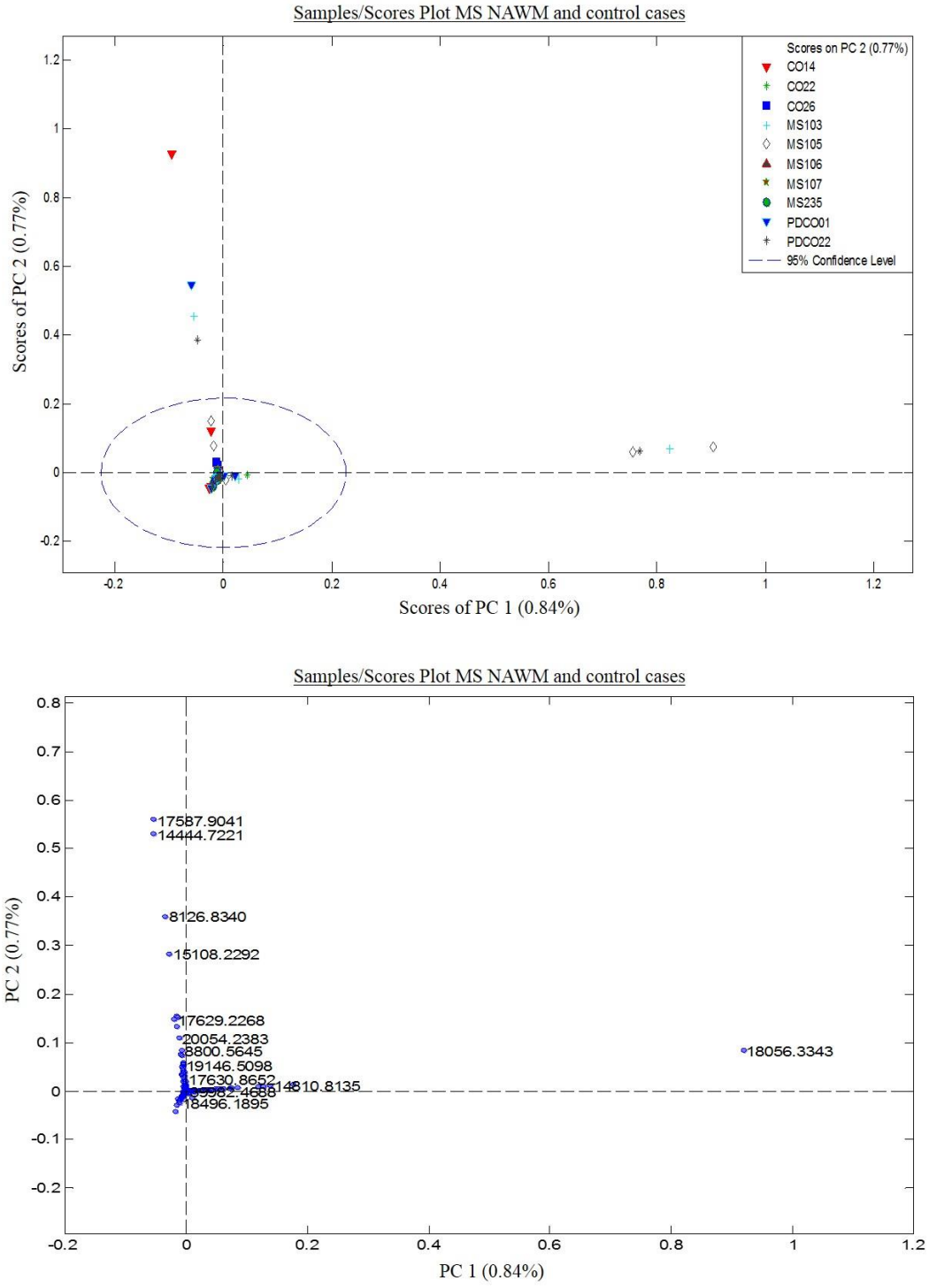

Figure 5.24 PCA score and loadings plot of MS NAWM and control WM tissue from intact protein profiling

There does not appear to be clear separation between MS and control cases from this initial PCA. From the score plot (a) there were no clear groupings of the MS NAWM and control cases, with the loading plot (b) containing peak information that directly correlated with the scores plot in (a).

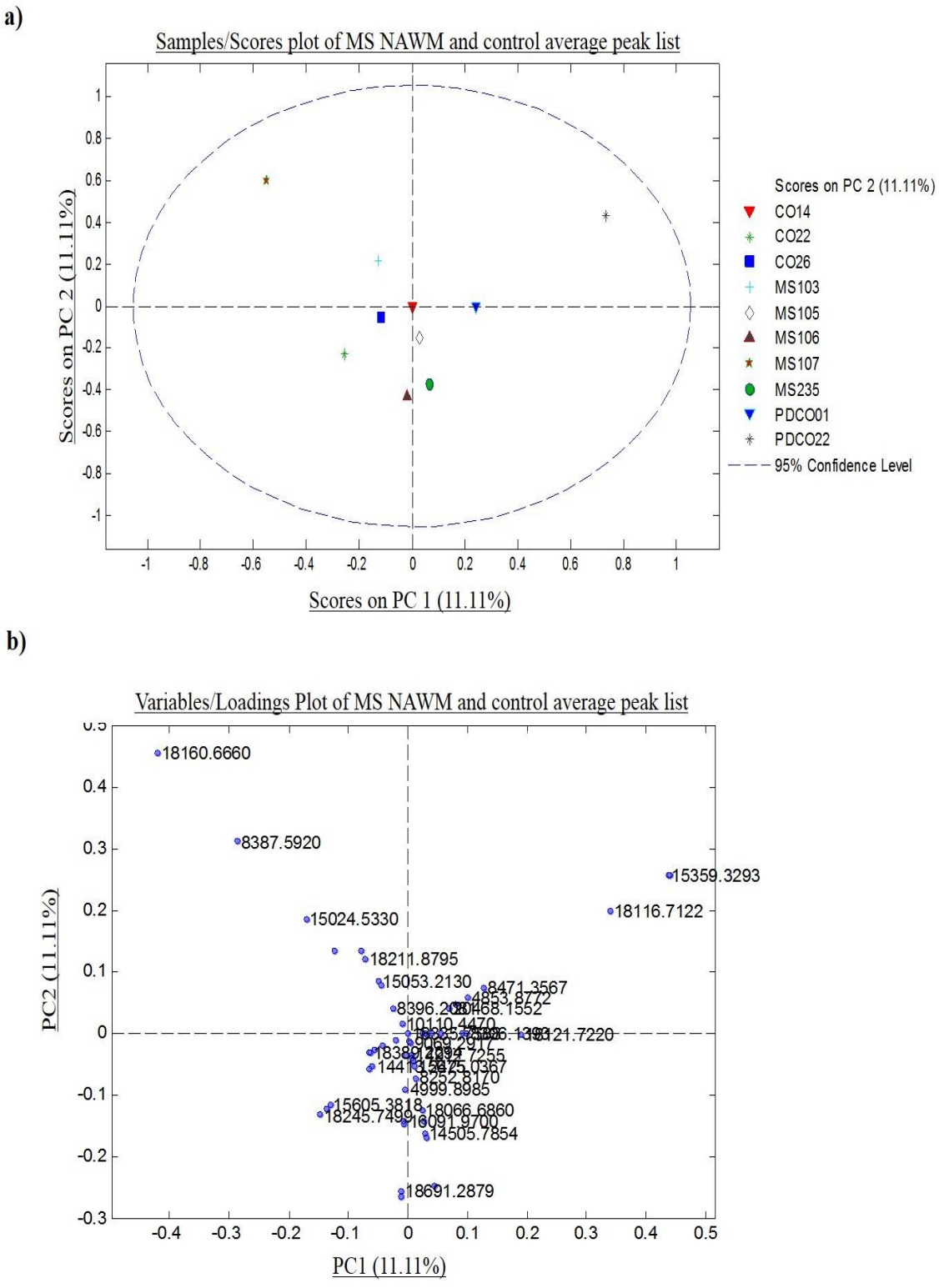

Figure 5.25 PCA score plot of averaged mass spectra

Mass spectra from all biological repeats and technical repeats of each case were combined into an average spectra in SpecAlign. Averaged peak lists of each case were analysed via PCA, the score plot failed to show any groupings between the spectra based on commonalities in *m/z* ratios of peaks (a). The loading plot (b) contains peak information that directly correlates with the scores plot in (a).

5.4.10 Peptide digest imaging (MALDI-MSI)

In situ tryptic digest was carried out on 5 serial sections (biological repeats) of each MS and control case, and MALDI-MSI performed. The data generated was processed in BioMap, where the WM ROIs in each case were isolated and the corresponding mass spectra exported. Example spectra from MS NAWM cases are shown in Figure 5.26, and control cases in Figure 5.27.

Each of the spectra show a range of peptides which can be used to identify corresponding proteins through peptide mass fingerprinting (PMF) which help to identify typically high abundant proteins within MS and control cases. Peak lists from these spectra were used to statistically analyse the data.

Expected proteins within the WM of the brain, such as myelin basic protein (MBP), were identified by manual interpretation according to a targeted approach, in which a theoretical digest of MBP was carried out. In particular MBP peptide (experimental *m/z* 1829.80, monoisotopic theoretical *m/z* 1829.97) was identified within the WM of all cases investigated confirming the specificity of MSI (Figure 5.28). The distribution of *m/z* 1829.80 in the generated mass spectrometric images was restricted to the WM of both MS NAWM and control cases (Figure 5.28a, c, e, g). The localised expression was confirmed by the complementary LFB stained sections clearly showing the different regions of the brain (Figure 5.28b, d, f, h).

5.4.10.1 Principal components analysis – peptide digest (MALDI-MSI)

Statistical analysis of the MS NAWM and control WM tryptic digest spectra was performed using PCA via MATLAB^{TM} through the Eigen Vector tool box. In the same approach as for intact protein profiling, PCA provides an unbiased interpretation of the data spread and attempts to separate groups of data into clusters. Initially PCA was performed on all samples analysed, which included 5 biological repeats of 5 MS NAWM and 5 control cases. From the scores plot, there were no apparent differences between the spectral data sets belonging to MS NAWM and control cases respectively (Figure 5.29a). The scores plot failed to show any firm groupings of MS cases or control cases, also confirmed by the loadings plot, where the majority of the *m/z* values overlap and were within the centre of the plot (Figure 5.29b). However, there were some *m/z* values which were spread away from the centre, yet in relation to the scores plot these were not specific for particular cases.

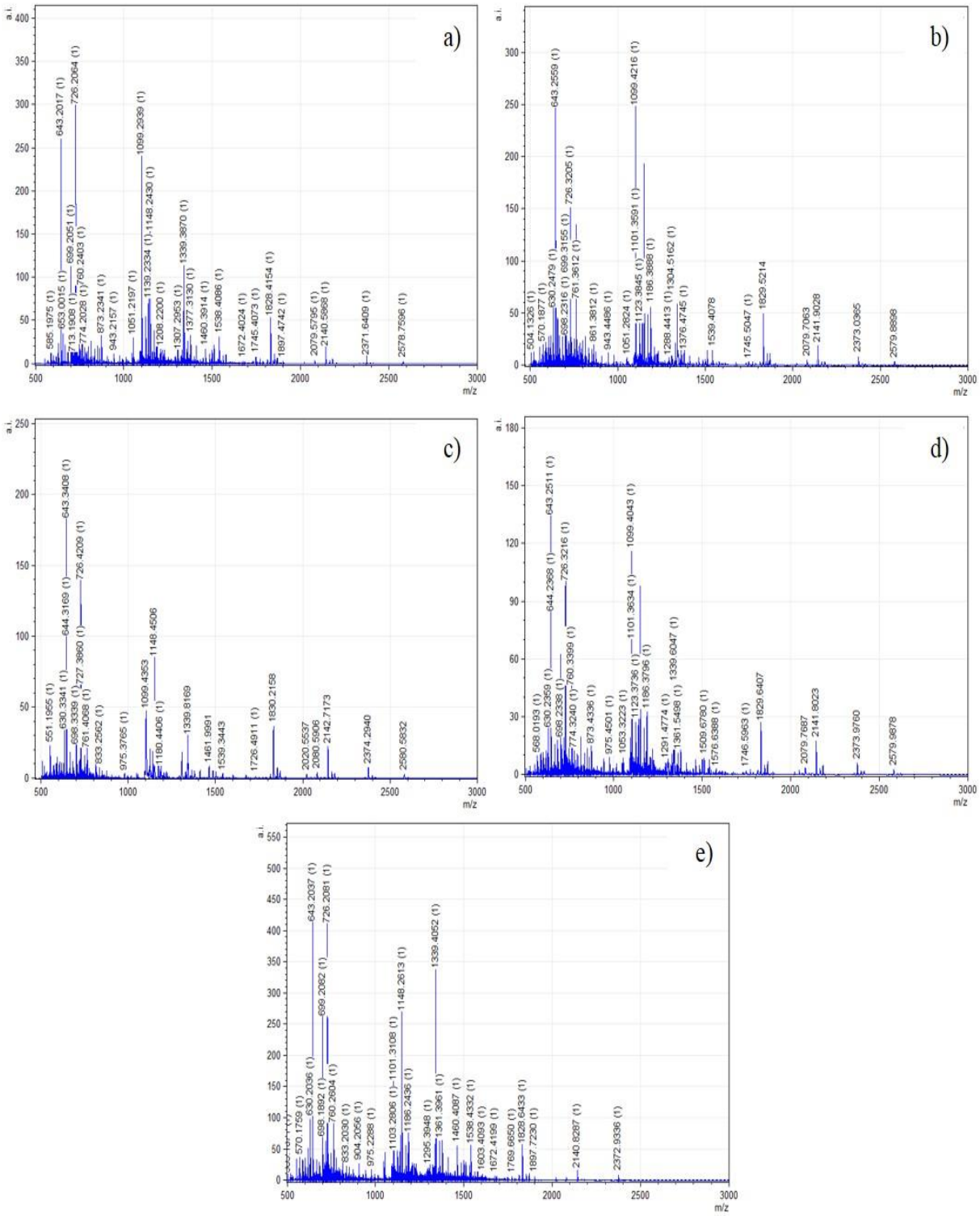

Figure 5.26 Peptide MALDI mass spectra obtained from 5 MS NAWM cases

The mass spectra are representative of WM from each MS case analysed; MS103 (a), MS105 (b), MS106 (c), MS107 (d) and MS235 (e).

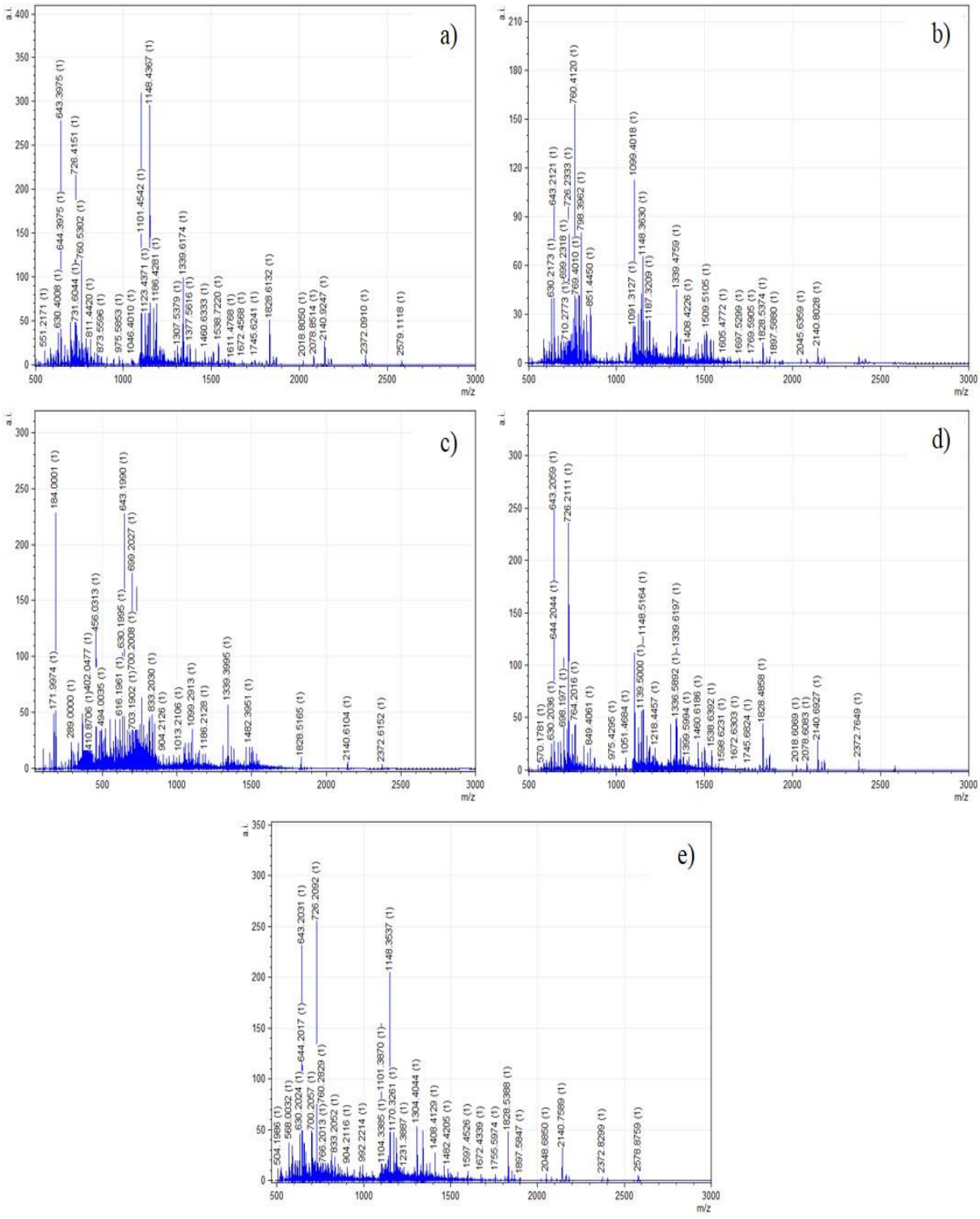

Figure 5.27 Peptide MALDI mass spectra obtained from 5 control cases

The mass spectra are representative of WM from each control case analysed; CO14 (a), CO22 (b), CO26 (c), PDCO01 (d) and PDCO22 (e).

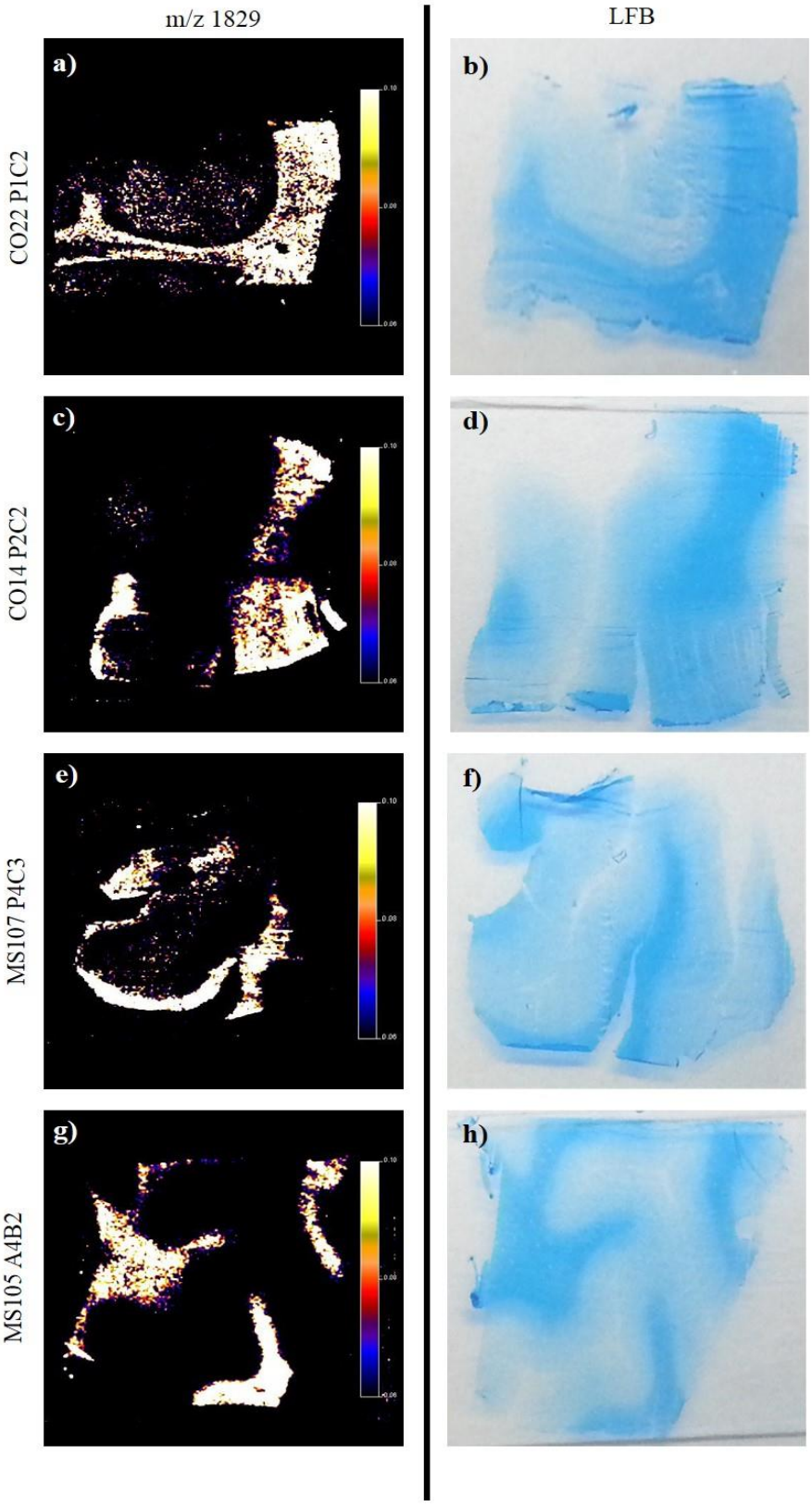

Figure 5.28 MALDI-MS images for the distribution of MBP peptide 1829 *m/z* throughout the WM

The localisation of MBP peptide to the WM of both MS NAWM and control WM (a, c, e, g). This localisation was confirmed by LFB stained corresponding sections (b, d, f, h) that identified the WM (light blue) cortex (dark blue).

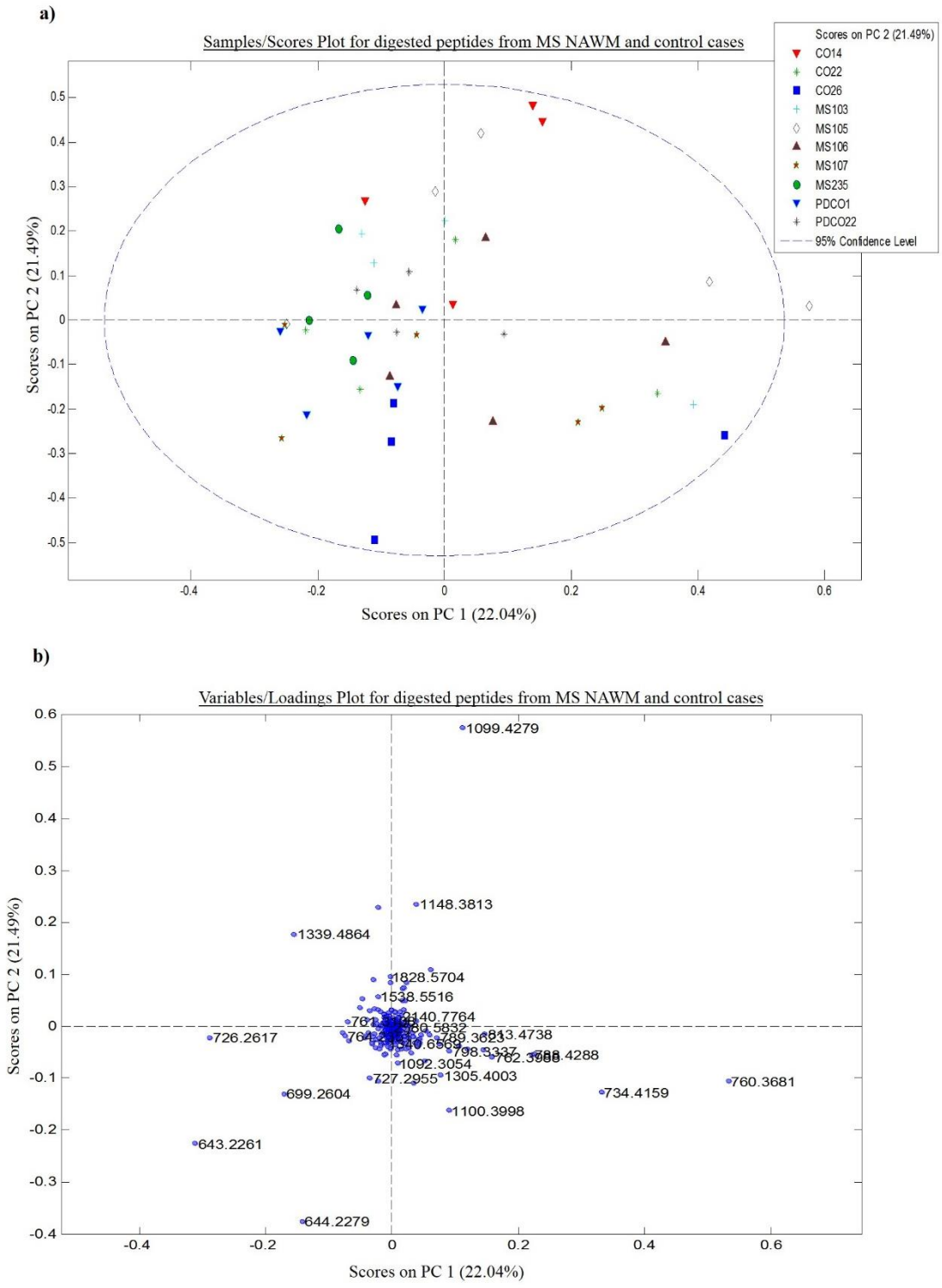

Figure 5.29 PCA score and loadings plot of MS NAWM and control WM tissue from *in situ* peptide digest

From this initial PCA test, there does not appear to be clear separation between MS and control cases. However there is broad separation of some cases, such as CO26 cases localised to the lower half and MS105 cases to the upper half of the PCA plot. The loading plot (b) contains peak information that directly correlates with the scores plot in (a).

An example of potential case groupings is shown between the MS105 samples located in the upper half of the PCA plot and the CO26 samples being grouped in the lower half. With this separation between diseased and control samples established in a non-discriminant manner data was investigated further in a supervised manner.

5.4.10.2 Partial least squares discriminant analysis – peptide digest (MALDI-MSI)

PLSDA was performed to provide classification between two sample groups. This is a discriminant statistical technique that employs the use of pre-selected groups for analysis based on the PCA results. Data was imported into MATLAB to build predictive models, to allow for a greater understanding of complex datasets. Regression vector plots generated via the use of PLSDA showed the presence of ions specific to particular samples. Data imported into MATLAB underwent a range of pre-processing steps, but generally throughout this study the data was linearised and the variables present in the data set were normalised and the data mean centralised (Eigenvector Research Inc. 2012). Choosing a suitable cross validation method when building a PLSDA model was important to determine the complexity of data. In this study 'contiguous blocks' was chosen which assesses predictability between repeat sample spectra. For example, when CO26 and MS105 were analysed through PLSDA the 2 groups modelled were showing differences against each other after cross validation against the rest of the data (the further 8 cases).

A number of specific peaks were determined from the PLSDA regression vector plot (Figure 5.30), 644 *m/z* was specific and the largest peptide peak in CO26 cases, other CO26 specific peptide peaks included 699 *m/z* and 727 *m/z*, which were not identified in MS105 cases. Another peptide ion 1099 *m/z* was increased in MS105 cases when compared to CO26 cases, while 1148 *m/z* peptide was solely present in MS105 and not in CO26.

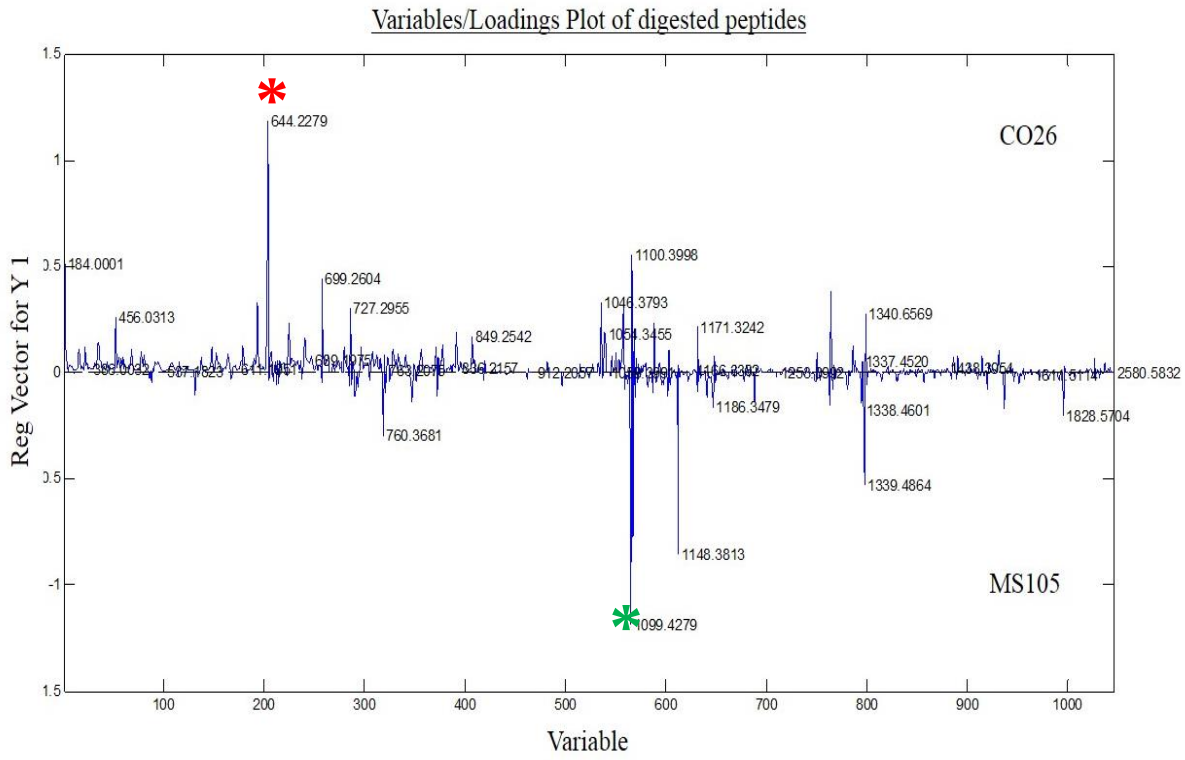

Figure 5.30 PLSDA regression vector plot comparing peptide digest data from MS NAWM and control WM samples

There are differences in peptide abundances, with 644 *m/z* only present in CO26 cases (red asterisk), and conversely 1099 *m/z* was increased in MS105 cases (green asterisk).

5.5 Discussion

5.5.1 Iron regulation by astrocytes in MS NAWM

In this study, four individual experimental approaches were taken, which focussed on attempting to validate a key microarray finding, namely the dysregulation of candidate genes associated with the regulation of iron homeostasis and oxidative stress in astrocytes in MS NAWM. qPCR analysis of the candidate genes performed on patient samples from the original microarray cohort and on an additional validation patient cohort failed to replicate significantly the increased expression of candidate genes. However, qPCR on four of the original microarray samples (2 MS vs. 2 control cases) did show the same directional change as seen in the microarray study, demonstrating a non-significant upregulation of MT1X, FTL and TF in MS NAWM astrocytes compared to control WM astrocytes. Immunohistochemical investigations demonstrated colocalisation of MT, FTL and TF with $GFAP^+$ astrocytes in the WM of an additional cohort of MS and control patients. However, MALDI-MS and WB quantitation of these proteins was unable to demonstrate significant differences in expression between MS NAWM and control WM.

Iron is vitally important in a large number of biological functions including: oxygen transport, DNA synthesis and repair, along with mitochondrial energy production (Crichton *et al* 2011, Todorich *et al* 2009). Within the brain, iron is vital in the synthesis of neurotransmitters and myelin (Levenson & Tassabehji 2004, Moos & Morgan 2004). Increased levels of iron within the brain are associated with the ageing process, and are also linked to several neurodegenerative diseases including AD (Bishop *et al* 2002, Raven *et al* 2013), PD (Gerlach *et al* 2006, Gotz *et al* 2004), epilepsy (Tombini *et al* 2013), stroke (Carbonell & Rama 2007) and MS (Hametner *et al* 2013, Williams *et al* 2012). Increased concentrations of iron participate in the Fenton Reaction ($Fe^{2+} + H_2O_2 \rightarrow Fe^{3+} + OH^{\bullet} + OH^-$) with the formation of hydroxyl radicals and anions (Mills *et al* 2010). Under physiological conditions, ROS are regulated by antioxidant mechanisms that exist in cells to prevent oxidative damage to lipids, proteins and DNA. Antioxidants include catalase and glutathione, which convert H_2O_2 to water (Lillig *et al* 2008). However, in neurodegenerative diseases it is believed that either an increase in ROS production (as a result of iron accumulation), an impairment/overload of antioxidant defence mechanisms, or a combination of the two leads to iron induced oxidative damage (Crichton *et al* 2011, Dringen *et al* 2000, Mills *et al* 2010).

Consequently regulating iron homeostasis in the brain is vitally important and is partially dependent on the BBB, which restricts the exchange of iron and iron related proteins into the CNS thereby controlling the local environment. Iron homeostasis is also controlled by a series of proteins that are expressed in varying amounts depending on the cell type, brain region and iron status. TFR1 and DMT1 are responsible for iron uptake into cells, while iron is imported into the mitochondria by mitoferrin 1 and/or mitoferrin 2 iron importers. FT heavy (H) and light (L) chains store iron, while FPT is responsible for exporting iron out of cells. To date, the precise mechanisms of iron homeostasis in the brain are not fully understood. Regulation of iron is largely controlled by IRPs which control mRNA translation of specific proteins, including TFR1, DMT1, FT and FPT. IRPs are capable of sensing iron levels within the CNS environment, when iron concentration is reduced IRPs bind to stem loops, known as IREs, on mRNAs encoding the regulatory proteins. Binding IRP to IREs located in the 5' UTR region of a gene, for example FT and FPT, prevents mRNA stabilisation and translation. Whereas binding of IRPs to IREs located at the 3' UTR region, eg TRF1 and DMT1, stabilises mRNA resulting in translation and an increased TFR1 and DMT1 expression, leading to iron uptake into cells, and a decrease in iron export. When iron is abundant, IRPs no longer actively bind to IREs thereby stabilising FT and FPT mRNA expression and translation and downregulating TFR1 and DMT1 synthesis leading to an increase in storage and export of iron (Crichton *et al* 2011).

Iron accumulation is variable and not uniform across the CNS. In MS, evidence of iron accumulation has been identified in deep grey matter structures of the brain including the thalamus, caudate and putamen (LeVine *et al* 2013), while accumulation in the WM is associated with areas of inflammation, in particular around venules (Brass *et al* 2006a, Brass *et al* 2006b, Ge *et al* 2007, Khalil *et al* 2009, Khalil *et al* 2011a, Zhang *et al* 2007). A dysregulation of the IRP/IRE regulatory system, resulting in enhanced iron storage, has been suggested to increase deposition of iron in vessels of MS brain tissue (Williams *et al* 2012). Whatever the cause of iron accumulation in MS, it is known to contribute to disease pathogenesis by amplifying the activated state of microglia thereby increasing the production of proinflammatory cytokines (Williams *et al* 2012). Intracellular iron accumulation can also promote mitochondrial dysfunction, whilst insufficient management of iron can lead to the production of ROS resulting in oxidative stress (Hametner *et al* 2013, Khalil *et al* 2011b, Williams *et al* 2012) leading to lipid peroxidation, additional mitochondrial dysfunction, increase in intracellular

free-calcium concentration, and the ability to cause cell dysfunction and death (Halliwell 2006).

Increasing evidence is beginning to indicate the potential roles of astrocytes in MS (Black *et al* 2010, Brosnan & Raine 2013, Holley *et al* 2003, Nair *et al* 2008, Rejdak *et al* 2007, Williams *et al* 2007), yet the exact role(s) astrocytes play in the pathogenesis of the disease remain unknown. The microarray analysis in chapter 3 identified significant upregulation of MT1G, MT1X and MT2A gene expression in MS NAWM astrocytes in comparison to control WM. MTs are low molecular weight, cysteine rich proteins capable of binding metals, in particular zinc, but also other transition metal such as copper, iron, lead etc., (Hidalgo *et al* 2001). In response to injury or pathology within the CNS, increased amounts of MT-I and MT-II, (MT-I+II) mRNA and protein are induced (Hidalgo *et al* 2001, Penkowa *et al* 2001b). In the CNS, MT-I+II proteins are primarily associated with astrocytes, with increased expression forming part of the inflammatory and defence responses associated with many neurodegenerative diseases (Chung *et al* 2004, Espejo *et al* 2005, Penkowa *et al* 2003a, Penkowa *et al* 2003b, Penkowa *et al* 2005). Only one study to date has investigated MT-I+II protein expression by IHC in MS, with the majority of preceding work on MT expression carried out in EAE (Espejo *et al* 2001, Espejo *et al* 2005, Penkowa *et al* 2001a, Penkowa & Hidalgo 2001). In support of the current study's identification of MT-I+II^{+} astrocytes, both of these proteins have previously been linked to astrocytes and activated macrophages in MS active lesions, and a noticeably increased expression with astrocytes in IA lesions (Penkowa *et al* 2003c). Furthermore, a transcriptomic study on lesions from four individuals with MS (two acute lesions, two silent lesions) confirmed this increase in MT gene expression in both lesion types (Lock *et al* 2002).

Astrocytes support CNS recovery by secreting antioxidants, growth factors and trophic factors, possibly reflecting their increased numbers in IA lesions. Therefore increased MT-I+II expression in IA lesions may play an important role in the remission of MS (Penkowa *et al* 2003c). Expression is prolonged even in areas that are relatively dormant in active disease, suggesting the same mechanism may occur in the NAWM where disease pathology is subtle. Increased astrocytic expression of MT-I+II in NAWM may be an attempt to prevent the spread of ROS and ultimately oxidative stress that contribute to disease progression. However, it must be acknowledged that our IHC findings were not quantitative and multiple attempts to quantify MT expression in MS

NAWM by WB proved unsuccessful, most likely reflecting the technical issues and antibody supplier as discussed in this chapter. Nonetheless, the expression of MT in EAE has been shown to peak at the highest clinical score and remain elevated throughout recovery (Espejo *et al* 2005). Again, this implies that MT-I+II protein expression contributes to disease pathogenesis possibly by downregulating inflammation, oxidative stress, demyelination and axonal injury, and/or by upregulating repair processes including growth factors and neurotrophic factors.

The precise function of MT-I+II is currently unknown. The literature suggests that MT-I+II act intracellularly, with increased MT expression in the cytoplasm of astrocytes observed following neuronal injury (Chung *et al* 2004). MT-I+II enable astrocytes to handle free radicals and ROS (Chung *et al* 2008b) and their expression is known to help regulate metal homeostasis and promote neuroregeneration (Hidalgo *et al* 2001). Increasing evidence demonstrates MT-I+II may also have extracellular effects on neuronal regeneration: injured neuronal cultures treated with MT-I+II display regenerative capabilities (Chung *et al* 2003, Kohler *et al* 2003). Administered MT-II protein *in vivo* has also been shown to improve clinical symptoms of EAE (Penkowa & Hidalgo 2000, Penkowa & Hidalgo 2003) while animals lacking MT-I+II expression go on to develop a more severe disease course (Penkowa & Hidalgo 2001). In addition to the release of MT-I+II, astrocytes produce an array of other protective proteins in response to injury including increased expression of S100B (Businaro *et al* 2006) (refer to Chapter 2). Astrocytes respond to insult/injury with changes in their morphology, phenotype and gene expression (West *et al* 2008), suggesting they are able to respond to and reduce the detrimental environment that occurs in MS lesions and in areas immediately surrounding lesions, thereby increasing neuronal and oligodendrocyte survival supporting remyelination and regeneration (Chung *et al* 2004, Chung *et al* 2008a).

It has been suggested that MT-I+II may promote astrocyte proliferation, or act directly as an antioxidant, or indirectly by decreasing oxidative stress by reducing ROS production by activated microglia/macrophage (Figure 5.31) (Penkowa 2006). The increase in MT expression by astrocytes has been shown to reduce the microglial response, reduce neuronal apoptosis and inhibit the apoptosis of autoreactive T cells, which are known to be detrimental in MS pathogenesis. These studies, however, failed to acknowledge the potential dual role of astrocytes in the CNS, which has only been

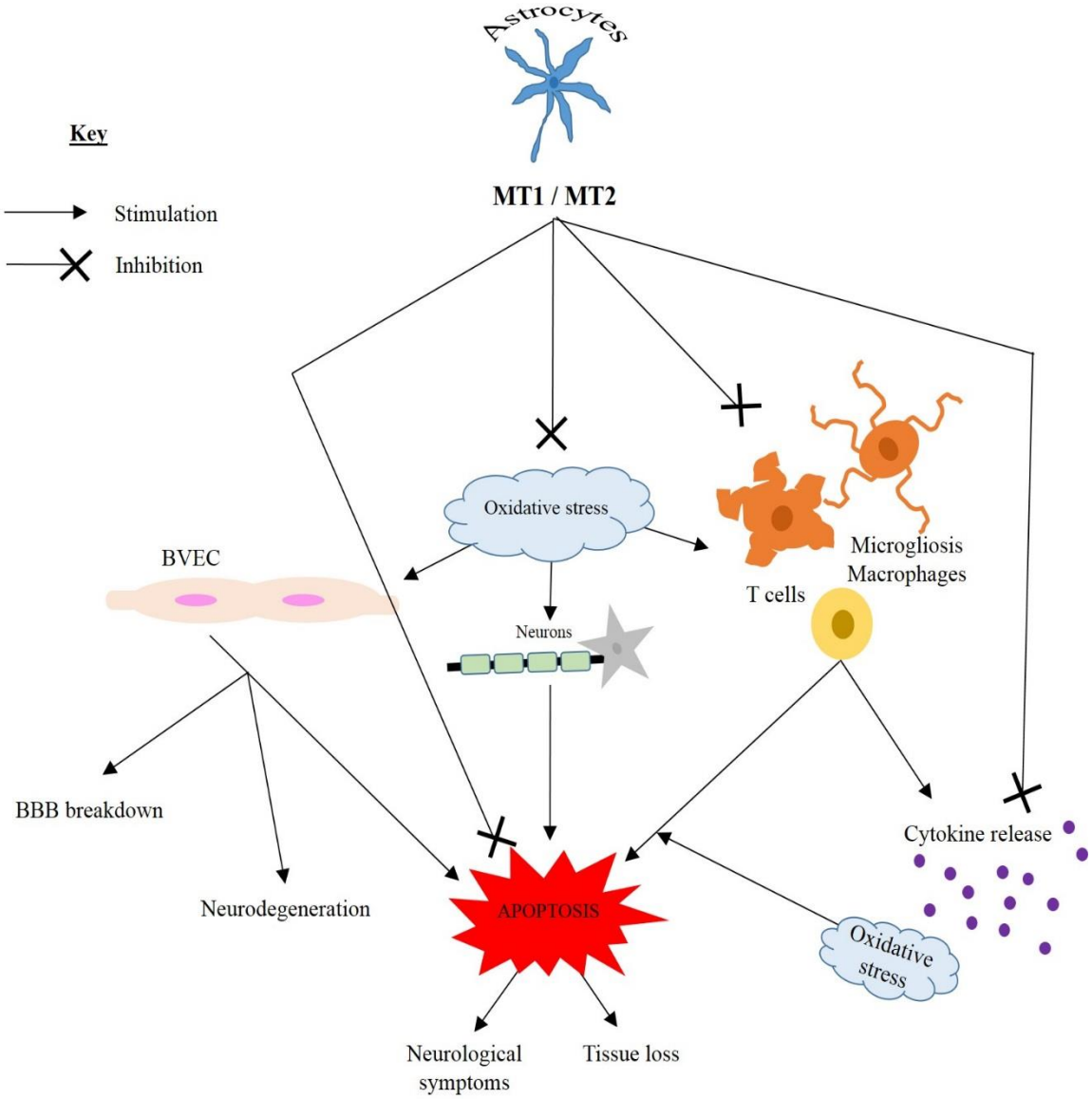

Figure 5.31 Metallothionein-I+II actions in the brain

During pathology an increased MT-I+II expression by astrocytes leads to the inhibition of apoptosis, oxidative stress, inflammation and cytokine release with downstream actions. MT-I+II are involved in anti-inflammatory, antioxidant and anti-apoptotic pathways that lead to neuroregeneration, angiogenesis and repair. Figure adapted from Penkowa 2006.

Key: BVEC: blood vessel endothelial cells.

recognised through more recent studies (Brosnan & Raine 2013, Nash *et al* 2011b, Sofroniew & Vinters 2010, Williams *et al* 2007).

Clearly achieving a balance of the astrocyte expression of MT and the beneficial anti-inflammatory, antioxidant and anti-apoptotic properties of these proteins is crucial. However, due to MS heterogeneity and the nature and plasticity of astrocytes, a current lack of understanding of MT regulation and its role in MS disease is evident, hence a need for further work to elucidate the detailed mechanisms and role in MS are essential.

In general, the physiological level of iron present in astrocytes is relatively low; 10nmol/mg of cellular protein (Hoepken *et al* 2004) consistent with the majority of research reporting astrocytes *in vivo* lacking the expression of TF or TFR (Leitner & Connor 2012). However, one report demonstrated TF expression associated with $GFAP^+$ astrocytes in the aged human brain (Connor *et al* 1990). Despite the proposed lack of TF and TFR expression by astrocytes *in vivo*, continuing research has investigated expression of TFRs by astrocytes *in vitro*, and their involvement in iron metabolism in the brain. This may be a factor that has confounded the understanding of iron metabolism within the human brain.

Astrocytes *in vitro* are capable of binding TF-bound iron (Hoepken *et al* 2004, Qian *et al* 2000, Qian *et al* 1999) through their expression of TFR, but also synthesise and secrete TF (Espinosa de los Monteros *et al* 1990), as well as storing large amounts of iron as FT (Dringen *et al* 2007). Due to the lack of convincing *in vivo* research demonstrating TF and TFR expression by astrocytes it has been suggested that most iron uptake by astrocytes is not bound to TF, with evidence demonstrating that the main mechanism of iron uptake in astrocytes involving DMT-1 expression on astrocyte end feet (Burdo *et al* 2003, Dringen *et al* 2007). However in the current study we failed to identify significant expression of DMT-1, instead a significant increase in the iron transporter TF was identified in MS NAWM astrocytes.

Whatever the uptake mechanism of iron into astrocytes, iron metabolism involves Cp, a ferroxidase enzyme, and FPT, the only known iron exporter in mammalian cells (Crichton *et al* 2011). Cp expression by astrocytes allows the oxidation of ferrous iron that enters the brain at the abluminal side of the BBB, while FPT allows the exportation of ferric iron from the astrocyte into the extracellular space where it can become bound

to TF in the brain and be taken up by TFR1 expressing cells (Moos *et al* 2007, Rouault & Cooperman 2006). However, in the current microarray study mRNA levels of Cp and FPT were not significantly differentially expressed in astrocytes isolated from MS NAWM, suggesting the cells attempt to prevent the release of free iron into the CNS. In contrast, the current microarray study identified both TF and FTL mRNA expression was increased in isolated astrocytes from MS NAWM, and the astrocytic association of these candidates with $GFAP^+$ astrocytes demonstrated by IHC. Therefore, based on these findings it can be suggested that in response to the depletion of oligodendrocytes in MS lesions and the resulting increase in local iron levels, astrocytes in the surrounding NAWM increase expression of TF and FTL. Oligodendrocytes are the major cell type in the brain that express TF and FT (Hulet *et al* 1999, Leitner & Connor 2012). Yet, within MS lesions the loss of oligodendrocytes would lead to a decrease in FT causing increased levels of free iron within the CNS (Bagnato *et al* 2011, LeVine *et al* 1999, van Rensburg *et al* 2012). Furthermore, oligodendrocyte depletion would result in the decreased expression of TF, which is essential in OPC differentiation and myelin formation (Hulet *et al* 1999, Izawa *et al* 2010b). Increased TF expression in astrocytes, would enable the transport of excess iron to OPC, supporting their differentiation into mature oligodendrocytes capable of remyelinating areas of demyelination (Hulet *et al* 1999). An increase in FTL expression by NAWM astrocytes could also sequester excess iron, with FT known to be more efficient at accommodating iron than TF (Harrison & Arosio 1996), thereby limiting further ROS production and reducing oxidative stress. An increase in FT expression in astrocytes has previously been seen as a response to increasing iron toxicity (Izawa *et al* 2010a). This proposed protective role of NAWM astrocytes is also complemented by the astrocyte's increased expression of antioxidants including MT as discussed earlier (Pedersen *et al* 2009).

Significant upregulation in the expression of FTL in the current microarray study is supported by evidence that FTL is the predominant FT subtype in astrocytes in the rat brain (Han *et al* 2002). *In vitro* studies have shown that FTL has a greater capacity to store iron than FTH (Levi *et al* 1994) which functions as the major ferroxidase component of FT. Therefore, in response to the iron accumulation associated with MS, astrocytes may increase their expression of FTL to offer an alternative to oligodendrocyte storage of iron. The synthesis of FT is controlled by both transcriptional and post transcriptional mechanisms, with FT mRNA translation increased when iron levels are abundant and repressed when iron levels are depleted

(Orino *et al* 2001). Additional work on the cellular expression, distribution and regulation of IRPs in MS is required to identify whether there is a dysregulation of the system with respect to iron accumulation in the brain resulting in disease progression. To date, very few studies investigating IRPs in the brain have been reported (Connor *et al* 2001). However, improving understanding of IRPs in relation to iron homeostasis in the brain is fundamental to understand the impact of dysregulation of these processes in neurological diseases, including MS.

Specific cellular responses to oxidative stress are likely the result of several processes. For example, at the time of an insult the cellular outcome may depend on FT levels in the cell, level of ascorbate (shown to enhance FT translation) and the availability of other antioxidant mechanisms such as glutathione, catalase, or MT (Orino *et al* 2001). The current microarray study identified the upregulation of FTL by NAWM astrocytes, likely in response to oxidative stress within the WML. Over a period of time this FTL expression by astrocytes, as well as other cell types, becomes insufficient at preventing ROS formation, thereby contributing to lesion spread. Alternatively, FTL induction by astrocytes may be one component of a larger multi-cellular, multi-component anti-oxidant response, with ultimate limits to their buffering capacity. Conflicting literature on FT expression in response to oxidative insults is probably due to cell-type specific responses. As already identified, oligodendrocytes are primarily associated with FT and iron storage, yet contain limited antioxidant mechanisms, thereby making these cells more susceptible to oxidative damage (Juurlink *et al* 1998). In comparison astrocytes, which generally do not store iron, readily metabolise and traffic iron between cells (Dringen *et al* 2007) while containing high levels of antioxidants including glutathione, catalase and MT (Liddell *et al* 2006a, Liddell *et al* 2006b, Pedersen *et al* 2009). Consequently astrocytes are highly resistant to ROS and metal induced toxicity in the brain.

Further work into the long-term consequences of iron accumulation in astrocytes in MS NAWM is required. Studies using genetically modified mice suggest that the sustained upregulation of FT in astrocytes may be toxic, although precise mechanisms have yet to be identified (Li *et al* 2009). FT-bound iron in astrocytes in the ageing Cp KO mouse are associated with cell loss (Jeong & David 2006). Investigating the effect of increasing and prolonged iron accumulation in astrocytes in MS and their subsequent expression of antioxidant molecules would enable the extent of the astrocytes' ability to

maintain a neuroprotective role in response to iron accumulation in MS to be determined.

During iron accumulation, astrocytes are stimulated to produce FT (Regan *et al* 2002) increasing iron storage in the cells, while TFR is downregulated reducing TF-bound iron uptake (Hoepken *et al* 2004). However, from the current microarray study both TF and FTL expression was increased by astrocytes isolated from MS patients, suggesting that in response to iron accumulation associated with the disease, astrocytes not only increase their iron storage capacity but also transport mechanisms to sequester excess iron. It has been suggested that astrocytes *in vivo* do not express TFR (Leitner & Connor 2012), therefore further work is required to demonstrate the expression of TFR by astrocytes in MS NAWM as a means of iron entry into the cell. Otherwise, an alternative as yet unidentified receptor for TF-bound iron may account for the uptake and entry of TF-bound iron into these cells. Alternatively, astrocytes may express TF as a means of transporting iron within the cell itself or as a storage molecule for iron which has been imported into the cell by other means, such as by DMT-1 or other transporter ligands. However, DMT-1 was not significantly expressed in WM astrocytes in the current study, reinforcing the possibility that unknown specialised iron regulatory mechanism(s) may be occurring in the brain.

5.5.1.1 Conclusion

In conclusion, the significant increased mRNA expression of TF, FTL and the different isoforms of MT in MS NAWM astrocytes in comparison to control astrocytes was not validated in additional qPCR studies. Despite this, through IHC the candidate genes showed colocalisation with $GFAP^+$ astrocytes. Even with the lack of validating quantitative investigations, the significance of the initial microarray findings and corroboration from current literature helps to support the hypothesis that astrocytes in MS NAWM are neuroprotective, both in terms of their role in regulating iron homeostasis in the CNS and in reducing the spread of oxidative damage associated with the disease (Figure 5.32). Expansion of the current study to investigate more MS patient samples along with additional iron regulatory proteins would add further weight to these findings. This study highlights the complexity and current lack of understanding of iron regulation within the brain. Conflicting *in vitro* and *in vivo* published research with respects to the role of astrocytes in iron regulation adds to this complexity, which must be challenged if a better understanding of disease processes with regard to iron and oxidative stress are to be resolved.

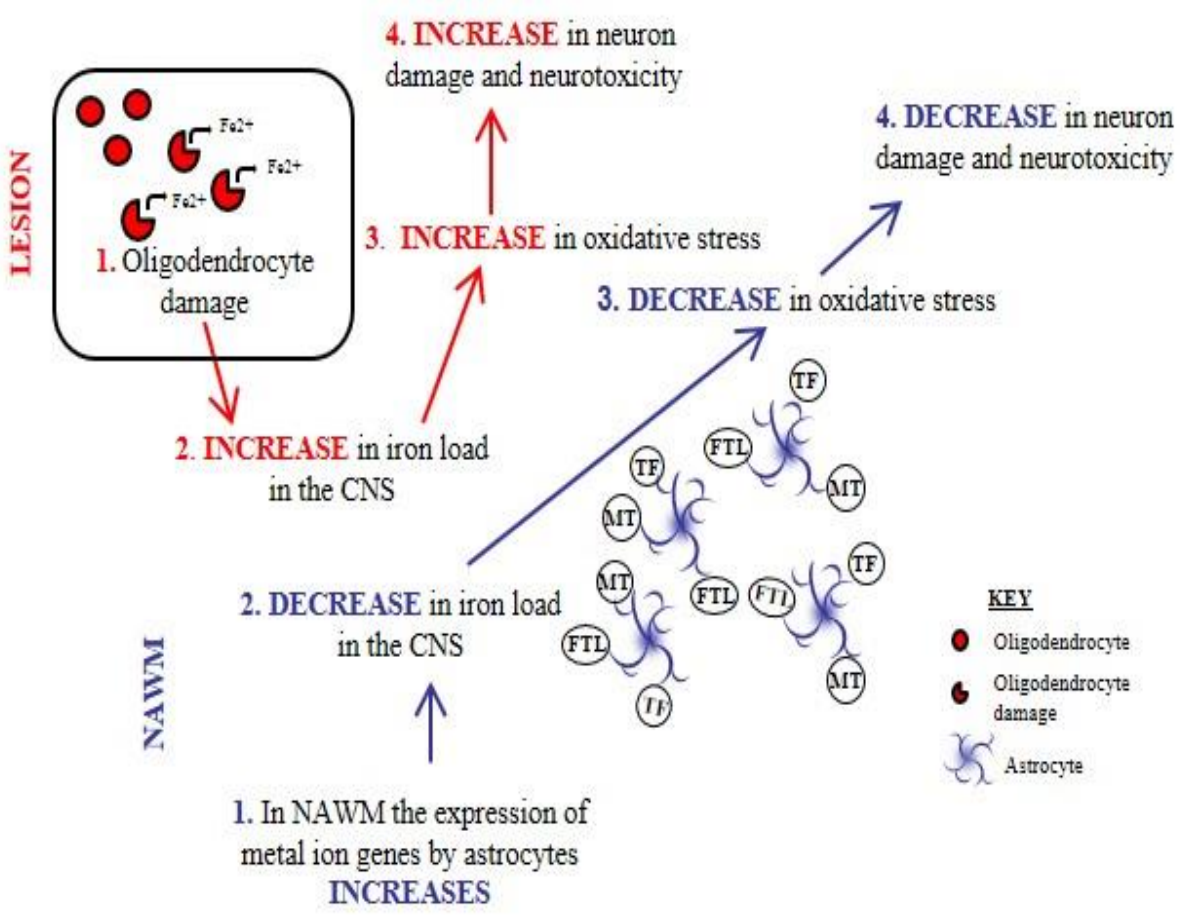

Figure 5.32 The proposed role of astrocytes in regulating iron load and oxidative stress in MS

An increase in iron load in the CNS as a result of oligodendrocyte damage in MS lesions leads to an increased release of iron and subsequent increase in oxidative stress and neurotoxicity, 1-4 (red). Astrocytes in NAWM increase their expression of iron regulatory and antioxidant genes/proteins to decrease iron load, oxidative stress and neurotoxicity, acting in a neuroprotective manner 1-4 (blue).

5.5.2 The current advantages and disadvantages of protein identification in neurological disease using MALDI-MS

To date a very limited number of studies have used MALDI-MS to investigate the proteome of MS, and no MALDI-MSI study has been conducted on tissue derived from MS patients. Although the potential for studying human neurological disease using MALDI-MSI is evident from the investigations on peptide and protein expression in animal models of PD (Hanrieder *et al* 2012, Skold *et al* 2006, Stauber *et al* 2008) and AD (Rohner *et al* 2005, Stoeckli *et al* 2006, Stoeckli *et al* 2002) the use of this technique in neuroscience particularly in relation to human CNS tissue is very limited (Hanrieder *et al* 2013b). Only one study to our knowledge has shown the use of MALDI-MSI to investigate the protein expression profile of human spinal cord to gain an insight into the molecular mechanisms underlying ALS (Hanrieder *et al* 2013a).

In the current study MALDI-MSP was employed to determine the expression and abundance of intact proteins encoded by the candidate genes identified in the microarray study, in MS NAWM compared to control WM samples. While MALDI-MSI was used to investigate the molecular distribution of trypsin-digested peptides in MS NAWM compared to control WM.

Profiling intact proteins in whole tissue sections was carried out for a number of reasons: firstly in order to gain an initial insight into the intact protein profile in MS NAWM and control WM, secondly, MSP of intact proteins generated data more quickly than MSI, which required a considerable amount of instrument time using the Voyager De Pro MALDI-TOF to acquire full images of brains sections (~2 days per section). In order to help verify the intact proteins identified through MSP, MSI of digested peptides was performed in parallel using the Q-Star Pulsar/Q-TOF mass spectrometer. MSI using the Q-Star Pulsar/Q-TOF mass spectrometer acquired images at a faster rate (~4 hours per section) while also allowing for the distribution of peptides to be distinguished with respect to histological features. Overall the two approaches, MSP of intact proteins and MSI of digested peptides was designed to complement one another working with the currently available instrumentation, resources and time permitted. Additional work is needed to confirm exact protein identification using MALDI.

A factor to address in the current study was the choice of matrix and the method of matrix application employed. In any MALDI experiment, the choice of matrix depends

largely on the targeted substance. A recent study showed that the application of FA on a range of tissue samples allowed the detection of proteins upto 125 kDa when implementing MALDI-MS (Mainini *et al* 2013). From the optimisation studies carried out investigating varying matrices, along with the desire to acquire high molecular weight protein profiles due to our candidate proteins ranging from 6 kDa (MT) to 75 kDa (TF), FA was chosen as the matrix for use in the current study for MALDI-MSP of intact proteins. There are limitations in the different matrices used in MALDI including the crystal size, reproducibility, interfering matrix clusters, mass range and signal quality (Hanrieder *et al* 2013b). With FA manual spotting and spraying led to huge variability in crystal size and analyte extraction efficiency, resulting in fluctuating signal quality/intensity from the analysed samples. However, when using the TM sprayer, which provided heat to the matrix solution to accelerate adsorption into the tissue, as well as a controlled flow of dry air to focus the spray and control drying time the matrix/analyte co-crystallisation proved to be more uniform and homogenous compared to manual spotting, which improved reproducibility and signal quality. Worth noting despite published literature on the proposed capabilities of profiling proteins up to 125 kDa and imaging proteins upto 70 kDa with the use of FA (Mainini *et al* 2013), none of the samples investigated in this study using the instrumentation and methods described in this chapter detected signals above 25 kDa, a common drawback in many MALDI-MS systems (Wenzel *et al* 2005). This has previously been shown to be overcome by altering the matrix deposition method from spraying to spotting with proteins upto 200 kDa being detected in this way (Chaurand *et al* 2002). Yet with the characteristics of FA as a matrix this was shown not to be possible. High molecular weight proteins have been identified as failing to reach common mass spectrometry detectors resulting in an overall poor representation of high molecular weight species. This has shown to be helped in other studies by using an alternative cryogenic detector (Frank *et al* 1999). Clearly, additional work is needed to elucidate exact protein identification using MALDI.

To move forward with the current mass spectrometry work would involve specifically identifying particular peptide peaks using fragmentation of candidate peptides via MS/MS. MS/MS is a routinely used method for peptide sequencing and could be used in parallel with MALDI to support protein identification from the *in situ* tissue sample surface. Ions are produced during MS/MS by the breaking of amide bonds along the backbone of the peptide. The mass differences between these fragmented ions in the

spectra are representative of the amino acid residues within the peptide. Subsequent peptide sequences and MS/MS spectra can be entered into bioinformatics programmes i.e. MASCOT, allowing for protein identification to be made through searches performed against protein databases such as Swiss-Prot and UniProt KB. For example, the peptide ion at 1829.80 Da detected in the WM of all the cases investigated could be subjected to MS/MS in order to verify the amino acid sequence provided by the database when carrying out the peptide mass fingerprinting, leading to the identification of MBP; this in turn would confirm the initial MBP identification. MS/MS could therefore be used to confirm the identification of species discriminating the MS NAWM and control WM cases. However, the current study was unsuccessful at identifying discriminative proteins/peptides between MS and control cases. It is thought that to improve statistical significance, additional samples, or technical repeats are needed to try and identify any differences between the two groups. As seen in other techniques, biomarker discovery in MALDI is hindered by the presence of abundant proteins, which may prevent detection of much less abundant species (typically those of interest). For example, due to the heterogeneity of whole tissue sections, the expression of candidate proteins may be masked by more dominant proteins such as MBP, which would be highly abundant in MS NAWM and control WM.

Evidently a need for the implementation of LCM-ed based techniques to isolate cells or ROI from whole tissue sections prior to MALDI-MS would be beneficial at associating protein expression to cell type, as was done in the original microarray study investigating the astrocyte transcriptome. LCM coupled with MALDI-MS has been used to investigate biomolecules specific to cancer cells compared to non-cancerous cells. One study identified differences in biomolecules between LCM-ed invasive mammary carcinoma and control human breast epithelium cells, (Sanders *et al* 2008, Xu *et al* 2002). Also in lung cancer, squamous cell carcinoma/adenocarcinoma cells were isolated from tissue using LCM and specific biomolecules identified through MALDI-MS to differentiate between the two cancers (Bhattacharya *et al* 2003). With this in mind, MALDI-MS could be used to extend the current study to identify particular protein peaks that are indicative of isolated MS NAWM astrocytes compared to isolated control WM that could be used as a fingerprint that identifies the astrocyte's role in MS development.

Overall, from the current mass spectrometry work consistent, statistically significant differences in the protein profile of MS NAWM and control WM cases used in this

study based on the conditions/methods and instrumentation documented in this chapter were not detected. That said, with further method development and increasing the number of samples investigated, the method of MALDI-MSP and -MSI are promising tools for proteomic investigations that have many advantages over traditional proteomic approaches such as WB and IHC.

Development of soft ionisation techniques, such as MALDI has enabled the detection and analysis of large biomolecules such as peptides and proteins by mass spectrometry. Proteomics has developed significantly in the area of mass spectrometry due to its capacity to provide information on the protein profile of biological samples, such as body fluids and tissue biopsies (Aebersold & Mann 2003, Domon & Aebersold 2006) Studies to date investigating the proteomics of MS using mass spectrometry have concentrated mainly on patient serum samples (Pieragostino *et al* 2010) or CSF samples (Liu *et al* 2009, Rajalahti *et al* 2010, Stoop *et al* 2008). Due to the heterogeneity of MS and complexity of disease mechanisms, there is probably not one specific gene, or protein that can act as a biomarker for the disease. However MS patients may express different peptides/proteins in comparison to healthy control subjects, which could be exploited as a potential biomarker of disease (Stoop *et al* 2008). Analysis of the proteins in CSF samples from patients enables the disease activity to be monitored through life, which may help in identifying disease pathways as well as in identifying potential biomarkers of disease (Stoop *et al* 2008). The limitations with using CSF to identify peptides/proteins associated with MS is that other factors could be affecting the composition of CSF that are not directly related to the disease process, these may be a result of some other pathology or therapy and not directly related to MS. Protein profiling studies on CSF are carried out using MALDI-TOF-MS with the technique used in an array of diseases to identify protein expression without the need for tissue localisation (Mikkat *et al* 2010).

MALDI-TOF-MS studies investigating the proteome of CSF from MS patients identified specific proteins compared with CSF taken from patients with other neurological disease (Stoop *et al* 2008). Another MALDI-TOF-MS study detected MS specific proteins including a variety of cytokines, chemokines and hormones in CSF samples from MS patients compared to control patients (Rajalahti *et al* 2010). This study was the first to use a novel multivariative data modelling approach of sample grouping using *m/z* values collated from the overlap of MALDI peaks, enabling

identification patterns that distinguished between MS patients and controls. Further work is needed to identify particular proteins/biomarkers of interest found in this study. Investigating peptides/proteins in tissue using MALDI-MSP and -MSI is advantageous because of the ability to investigate multiple peptides/proteins without the need for antibodies as in IHC and WB (Elkabes & Li 2007), while MALDI-MSI maintains spatial information within the tissue section. IHC and WB have a limited throughput only allowing the detection of one or two proteins per sample, and quantification can pose challenging with regards to antibody signal intensity, all fundamental flaws in such proteomic techniques which is overcome by using MALDI-MS. Yet to date, no study has used MALDI-MSP or -MSI directly on human MS tissue samples due to a number of limiting factors. Identifying human material suitable for MALDI-MSP and -MSI is difficult due to the uncontrollable practical issues that affect sample quality, a major factor determining the success of MALDI-MS. These limiting factors include the method of tissue collection and storage, PMI, along with the inevitable inter patient variability (Hanrieder *et al* 2013b). In a neurobiological setting the use of MALDI-MSI is somewhat limited, mainly due to the limited access to the technology, difficulty in sample preparation and huge workload to achieve a generally low throughput of meaningful data (Hanrieder *et al* 2013b). In a typical MALDI-MSI study, initial work needs to be carried out to optimise and standardise methods for sample preparation, choice of suitable matrix, dependant on intended outcome, along with the matrix deposition method. With the ability to investigate hundreds of potential peptides/proteins by MALDI-MSI the balance regarding the appropriate number of biological and technical repeats needs to be considered and the interpretation of the vast array of datasets taken into account. These issues are currently the main focus of MALDI-MSI research, with a desire to obtain a more standardised uniform approach to allow study comparability. As technology is improving with increasing resolution and sensitivity, the implementation of MALDI-MSI to investigate single cell types will be made possible. Nonetheless, to date the majority of MADLI-MS studies in neurological research have been concluded on whole brain tissue (Hanrieder *et al* 2013b) with the technique still relatively in it's infancy within this field.

5.5.2.1 Conclusion

As a result of carrying out the current MALDI study in reflection of the study aims no specific iron regulatory proteins were detected, however there is huge potential in the technique especially in relation to MSI with many advantages over the current proteomic approaches as discussed. Yet with any developing technologies, a lot of

challenges are put forward that need to be addressed in order for MALDI-MS to be regularly used in the biological setting, not just in scientific research but also clinically. A need for better sample preparation is apparent, standardised protocols according to the tissue, molecule, and instrumentation need to be addressed if the technology is to be implemented more routinely. As well, the overall workflow from the preparation of samples, data acquisition, through to data analysis needs to be more streamlined. The development of analysis software that is reliable and able to reduce and filter the vast array of MSI data while not jeopardising results is a necessity. A step forward for research using MALDI-MS would be to develop databases in which not just standardised protocols are stored but also raw data is held, made accessible to researchers and clinicians, as is done for transcriptomic microarray data with the gene expression omnibus (GEO), a database repository of gene expression data. With continuing development, MALDI-MSP and -MSI has the ability to uncover an array of proteomic information with regards to diseased tissue compared to healthy tissue, which could unveil potential disease mechanisms and processes faster than any traditional pathological investigation.

CHAPTER 6

CONCLUSIONS AND FUTURE WORK

MS is a chronic, neuroinflammatory, demyelinating disease of the CNS characterised by the infiltration of inflammatory cells, myelin loss, axonal injury and astrogliosis. The current project aimed to define the specific astroglial changes that exist in MS NAWM compared to control WM that are contributing to the overall WM pathology in MS. This involved analysing astrocytes in MS NAWM, areas of WM from which pathology is apparently absent, to determine whether specific gene expression and proteomic changes exist, which either support lesion development and disease progression or inhibit tissue damage, lesion expansion and disease development. In order to establish an understanding of astrocyte behaviour and function(s) in MS, initially this project characterised the astrocyte phenotype in MS by immunohistologically investigating a panel of established astrocyte markers. The study also developed a robust method to isolate distinct glial cells from PM CNS tissue combining rapid IHC with LCM to enable enriched populations of specific glia to be investigated in downstream transcriptomic and proteomic studies. Using this technique, the study employed microarray technology to identify significantly differentially expressed genes in astrocytes from MS NAWM compared to control WM astrocytes, thereby contributing to understanding of the role of astrocytes in MS pathology. The final part of the study involved a four-pronged approach to attempt to validate the microarray findings, applying qPCR, IHC, WB and MALDI-MS techniques to explore the potential neuroprotective role of astrocytes in the regulation of iron and reduction of oxidative stress associated with MS.

Previous studies have discussed the complexity of astrocytes in MS (Brosnan & Raine 2013, Nair *et al* 2008, Williams *et al* 2007) with much emphasis on their dual function: on the one hand astrocytes have the ability to enhance immune responses, increase BBB permeability and inhibit myelin repair; while on the other these glia have the ability to be neuroprotective, supporting oligodendrocyte remyelination and axonal regeneration. Astrocytes are dynamic cells capable of adapting to their environment by becoming reactive and undergoing astrogliosis with changes in their molecular expression, phenotype and function in response to injury or insult (Sofroniew & Vinters 2010). Previous studies have identified the upregulation of GFAP within MS lesions as a hallmark of reactive astrogliosis, which was also apparent in the current study. Similarly an increased expression of S100B, an established marker for astrocyte metabolism and suggested indicator of activated astrocytes, was also apparent within MS lesions (Rothermundt *et al* 2003, Sen & Belli 2007). Despite the majority of studies reporting a dysregulation of glutamate signalling in MS lesion as indicated by a decreased

expression of glutamate transporters and regulatory enzymes (Pampliega *et al* 2008, Vercellino *et al* 2007). In contrast, in the current study a non-significant increased expression of the glutamate transporters EAAT1 and EAAT2 and regulatory enzyme GS was identified, despite contrasting qualitative findings. However, overall differences in astrocyte morphology and phenotype in MS are clearly demonstrated by each marker, indicating that astrocytes consist of a heterogeneous population of cells with many different subclasses and possible functions. The need for a specific antibody that labels all astrocytes is vital, however, a pan-astrocyte marker is yet to be established, but is vitally important to enable the true identity of the astrocyte role to be defined.

The ability to isolate enriched, specific cell types from human tissue is fundamental to defining a particular cell's role in disease pathogenesis. LCM allows for the accurate isolation of a particular ROI or cell(s) from tissue sections and has been commonly used to investigate gene expression profiles in both human and animal models of neurological disease (Boone *et al* 2013, Chu *et al* 2009, Ferraiuolo *et al* 2011, Pietersen *et al* 2009, Simpson *et al* 2011, Torres-Munoz *et al* 2004). With respect to MS, currently LCM has only been used to isolate ROI and has not been employed to rigorously investigate transcriptomic changes in specific cell types. A combined rapid immuno-LCM method was developed in the current study to isolate enriched glial cell populations suitable for transcriptomic and proteomic investigations, the enrichment being confirmed by RT-PCR. There are many advantages associated with working with enriched cell populations over the use of heterogeneous cell populations present in whole tissue extracts. Studies on whole tissue may mask important pathological mechanisms and prevent mechanisms/functions being linked to specific cell types (Waller *et al* 2012). However it should be noted that not all PM human tissue can be considered suitable for LCM to isolate ROI/cells for transcriptomic studies, in particular relating to the unavoidable poor RNA quality of human PM material. Factors that have been shown to affect RNA integrity include the agonal state of the patient, PMI and brain pH (Harrison *et al* 1991, Kingsbury *et al* 1995). The additional steps involving immunostaining tissue sections and the LCM procedure itself can further affect the integrity of RNA (Waller *et al* 2012). Despite the potential limitations of immuno-LCM on PM CNS tissue, the downstream studies completed on isolated cells from human tissue are more complementary than working with cell lines or animal models that lack full replication of human disease. As long as strict guidelines are in place for selecting suitable cases, then immuno-LCM could pave the way in identifying the role of a variety of cells in a range of neurodegenerative disorders.

Microarray analysis enables changes in functional pathways and molecular functions to be determined between disease and control samples. The majority of current MS microarray studies have been completed on either whole tissue (Dutta & Trapp 2010), EAE models or PBMC isolated from MS patients. To date, only two microarray studies of MS have utilised the use of LCM to isolate ROI prior to microarray analysis (Cunnea *et al* 2010, Mycko *et al* 2012). In the current study astrocytes were isolated from MS NAWM and control WM using immuno-LCM and microarray analysis to interrogate changes in the astrocyte transcriptome. Significant differentially expressed genes in NAWM astrocytes were associated with the immune response, cell signaling, cytoskeletal changes and in the regulation of homeostasis, all classical roles of astrocytes (Sofroniew & Vinters 2010). The most significantly upregulated genes in MS NAWM astrocytes were related to the regulation of iron and oxidative stress, and included the differential expression of *FT, TF* and varying isoforms of *MT*, suggesting the hypothesis that astrocytes maintain homeostasis in the NAWM by responding to increasing iron levels and subsequent oxidative stress (Bagnato *et al* 2011, Lassmann *et al* 2012). The upregulated expression of iron regulatory mechanisms is most likely one aspect of the astrocyte neuroprotective response against accumulating damage within MS lesions, whereby astrocytes adapt to protect the NAWM from widespread iron induced oxidative damage. Dual labelling IHC confirmed colocalisation of FT, TF and MT with $GFAP^+$ astrocytes. Previous studies have shown that MT (Hidalgo *et al* 2001, Penkowa *et al* 2001a), FT (Dringen *et al* 2007) and to an extent TF (Connor *et al* 1990, Espinosa de los Monteros *et al* 1990) are increased in astrocytes in response to insult.

The increased expression of iron regulatory genes identified in the microarray study was not validated in an additional cohort of patients by qPCR. This likely reflects both patient variation and limited access to high quality NAWM tissue. The criteria for case selection for the validation cohort was based on the histological profile of each case and did not follow as stringent criteria as in the original microarray study: measures for controlling for age, sex, anatomical location as well as the RNA integrity of each sample were not as strictly observed. These cases used in this study had a well-established disease phenotype, but had no detailed patient history of drug therapy, or knowledge of disease activity at time of death. PM samples provide a single snap shot of the individuals' disease, but do not provide an insight into the disease in the years before death. Without a thorough history of MRI brain scans for each individual patient and regular blood/CSF examinations throughout life, the limitations of working with PM CNS material will always be apparent. Nonetheless, as identified throughout this

thesis, the clear advantages of working with this valuable resource are enormous, which when working with cell lines and animal models will never be able to fully replicate actual human disease mechanisms or processes.

To determine protein expression quantitatively, WB was employed but failed to identify any significant differences in the expression levels of FTL in MS NAWM and control WM, likely reflecting the cohort size and human variation, as already discussed. MT WB proved very challenging with variable, unreliable results despite numerous attempts of optimisation. Obtaining an alternative MT antibody would be the next step, or carrying out immunoprecipitation using the MT antibody to isolate the protein from the whole tissue protein extracts, prior to analysis via gel electrophoresis, mass spectrometry or WB could help. WB was performed on whole tissue extracts, therefore relating the expression of any protein to specific cell type(s) was hindered. Any slight fold change at the mRNA level, as shown by the candidate genes investigated in this study, may not directly relate to proteomic changes. With additional work, LCM could be used to isolate astrocytes for proteomic studies, including MALDI-MS and WB. Using LCM-ed isolated astrocytes in proteomic studies would also link the expression of the candidate proteins or other novel proteins to astrocytes rather than a whole tissue extract, as attempted in the current study. Similar approaches using LCM coupled with WB have been completed (Koob *et al* 2012, Martinet *et al* 2004, Mu *et al* 2013), but without the equivalent protein amplification methods as for RNA, acquiring enough protein for WB via LCM may prove challenging (Mu *et al* 2013).

In the same way that microarray analysis allows for a non-candidate approach when investigating transcriptomic changes between disease and control cases, MALDI is also capable of demonstrating the same non-candidate approach when investigating protein expression, without the need for specific antibodies. The technique can also be used to image the localisation of molecules across a tissue section using MSI, as seen in previous investigations on peptide and protein expression in animal models of PD (Hanrieder *et al* 2012, Skold *et al* 2006, Stauber *et al* 2008) and AD (Rohner *et al* 2005, Stoeckli *et al* 2006, Stoeckli *et al* 2002). In the current study, the identification of candidate proteins through MALDI-MS due to time restraints and instrumentation issues was not achieved. Conclusions drawn from the mass spectrometry work completed, identified no significant differences in the peptide/proteins profiles between the MS NAWM and control WM cases used in the current study. Yet with further optimisation of techniques, sample preparation and increased number of biological and

technical repeats MALDI-MS is a promising tool in proteomic research with many advantages. MALDI-MS has also been employed previously to look at the protein expression of LCM-ed isolated cells (Bhattacharya *et al* 2003, Sanders *et al* 2008, Xu *et al* 2002), which with additional work and optimisation could be employed to extend the current study to relate protein expression directly to astrocytes.

In vitro studies could help to gain a better understanding of the effect of increasing iron concentration on astrocytes overtime, and whether increased astrocytic expression of FT, TF and MT occurs with increasing levels of iron and oxidative stress. *In vitro* time course experiments could be carried out to see how astrocytes respond to prolonged exposure to increased iron and oxidative stress to identify the extent of their iron regulating homeostasis capabilities. While the introduction of various metal chelators and their effects on levels of iron and oxidative stress in culture could be monitored, along with the effects of any potential therapeutic approach on the overall astrocytes behaviour. Investigating co-culture systems of astrocytes, neurons and other glial cells may further enhance the knowledge of the role of astrocytes in response to increasing iron levels, and the effects on surrounding cell types, and is more similar to the *in vivo* setting than studies carried out on pure astrocyte cultures. As well studies investigating induced pluripotent stem cells (iPSC) derived from MS and control patients could enable researchers to gain a better understanding of iPSC derived glial cells and their association and possible role in iron metabolism and oxidative stress in MS pathogenesis. These studies must be considered carefully in light of the current lack of understanding about iron metabolism and regulation within the CNS and based on the current conflicting results of TF/TFR expression in astrocytes *in vitro* compared to *in vivo*.

Microarray studies, including those carried out in this thesis are non-hypothesis driven approaches to research which lead to the generation of specific scientific questions, hypotheses and lines of investigation. Along with the proposed role of astrocytes in regulating iron and oxidative stress in MS, other potential areas for further research have been postulated. Additional candidate groups of genes derived from the current study include the astrocyte's role in the immune response, regularly associated with MS, along with the changes in cytoskeletal genes associated with MS NAWM astrocytes, all avenues worthy of further investigation. Additional studies isolating astrocytes by immuno-LCM using an alternative astrocyte marker may provide an additional insight into the role of astrocytes in the pathogenesis of MS. Again, the necessity for a pan-

astrocyte marker to gain a more thorough understanding of astrocytes in relation to disease is paramount. Furthermore extending the study to isolate other glial populations from PM MS NAWM, including microglia and oligodendrocytes, would enable the comparison of their transcriptome to decipher how these cells interact and what role(s) they play in driving and/or preventing lesion pathogenesis. Comparison of the current gene expression profile of astrocytes in MS to the astrocyte transcriptome in other neurological diseases such as AD, ALS and PD would enable identification of any common genes and disease specific genes across diverse neurological pathologies.

6.1 Potential therapeutics

Developing a clearer understanding of the mechanisms involved in iron-induced oxidative stress within the brain in MS is essential in designing novel therapeutic agents. Iron dysregulation has been linked to several neurodegenerative diseases such as PD, AD and ALS, with current iron chelating therapeutics designed to block the redox-activity of iron, and its contribution in disease progression (Farina *et al* 2013). Ultimately these types of therapeutics could also help in MS, where increasing evidence has identified iron as having a key role in disease pathogenesis (Hametner *et al* 2013, Lassmann *et al* 2012, Williams *et al* 2012). There are three currently developed types of metal chelator, the chemical iron chelators, natural iron chelators and endogenous iron chelators with increasing evidence of their neuroprotective effects in neurodegenerative disease (Li *et al* 2011). For example, the chemical iron chelator desferrioxamine (DFO) has been shown to prevent neuronal degeneration in the 6-hydroxydopamine (6-OHDA)-induced rat experimental model of PD (Zhang *et al* 2005). Natural iron chelators are found in plant material such as epigallocatechin gallate (EGCG) and curcumin. In addition, phenols such as quercetin, a key antioxidant and present in a variety of Chinese medicines have demonstrated strong iron chelation properties (Perez *et al* 2008). Endogenous iron chelators, such as FT have shown to not only to sequester free iron but also convert it into non-toxic ferric iron due to the ferroxidase function of such chelators.

The neuroprotective function of iron chelation may derive from the reduction of oxidative stress, alongside iron chelator treatment, therefore antioxidant therapies could also help prevent widespread damage caused by oxidative species in MS. Endogenous antioxidants include glutathione peroxidase, catalase and SOD, which directly eliminate ROS including hydroxyl radicals, superoxide radical and hydrogen peroxide (Guerra-Araiza *et al* 2013). The levels of endogenous antioxidants are said to decline in a

number of neurodegenerative diseases and with age (Finkel & Holbrook 2000). The most widely studied antioxidants are the common dietary type including vitamin C and vitamin E (Guerra-Araiza *et al* 2013). Alongside the traditional vitamins are the phytochemicals including flavonoids, which are found in fruits, flowers, seeds, medicinal plants and olive oil holding a number of beneficial properties including anti-inflammatory, anticarcinogenic, antibacterial and antiviral properties (Joseph *et al* 2007, Rossi *et al* 2008). Flavonoids are also capable of scavenging free radicals and modulating intracellular signals to promote cell survival, acting in a neuroprotective manner against oxidative stress (Joseph *et al* 2007, Mercer *et al* 2005, Rossi *et al* 2008). The most potent flavonoid antioxidant is quercetin capable of scavenging ROS and binding transition metal irons, including iron along with its strong anti-inflammatory function (Georgetti *et al* 2003, Nijveldt *et al* 2001) making it a key potential therapeutic in regulating iron toxicity and oxidative damage in MS. Consequently, therapy established to limit iron induced oxidative damage in PD, AD and ALS should be contemplated in MS, where an increase in iron induced oxidative stress is also apparent.

6.2 Overall conclusions

Although the results from this thesis are not entirely conclusive, from the top 20 significantly upregulated genes observed in the microarray study comparing the transcriptome of MS NAWM astrocytes and control WM astrocytes, six were related to the regulation of iron and oxidative stress. The role of oxidative stress is widely acknowledged in MS (Hametner *et al* 2013, Lassmann *et al* 2012, LeVine *et al* 2013, Williams *et al* 2012) and also in other neurological disorders (Crichton *et al* 2011, Johnstone & Milward 2010, Mills *et al* 2010, Skjorringe *et al* 2012) and warrants further investigation. Evidently a clear alteration in astrocyte phenotype in MS suggests a change in their normal function, with this study demonstrating the protein expression of the candidate genes colocalised with $GFAP^+$ astrocytes in MS NAWM. Studying and debating the function/role of astrocytes in the different MS lesion types is important but fails to address the underlying cause of lesion pathogenesis and the processes by which these lesions spread. No other study to date has investigated in detail the role of astrocytes with respect to MS NAWM. It is however, extremely important that future research focusses on the NAWM and astrocytes to determine the mechanisms/processes responsible for driving and/or preventing disease progression.

REFERENCES

Abbott NJ, Patabendige AA, Dolman DE, Yusof SR, Begley DJ. (2010). Structure and function of the blood-brain barrier. *Neurobiol Dis* 37(1): 13-25.

Abbott NJ, Ronnback L, Hansson E. (2006). Astrocyte-endothelial interactions at the blood-brain barrier. *Nature Reviews Neuroscience* 7(1): 41-53.

Aboul-Enein F, Krssak M, Hoftberger R, Prayer D, Kristoferitsch W. (2010). Reduced NAA-levels in the NAWM of patients with MS is a feature of progression. A study with quantitative magnetic resonance spectroscopy at 3 Tesla. *PLoS One* 5:e11625.

Achiron A, Grotto I, Balicer R, Magalashvili D, Feldman A, Gurevich M. (2010). Microarray analysis identifies altered regulation of nuclear receptor family members in the pre-disease state of multiple sclerosis. *Neurobiology of Disease* 38(2): 201-9.

Adams AB, Williams MA, Jones TR, Shirasugi N, Durham MM, *et al*. (2003). Heterologous immunity provides a potent barrier to transplantation tolerance. *J Clin Invest* 111(12): 1887-95.

Aebersold R, Mann M. (2003). Mass spectrometry-based proteomics. *Nature* 422(6928): 198-207.

Aerni HR, Cornett DS, Caprioli RM. (2006). Automated acoustic matrix deposition for MALDI sample preparation. *Analytical Chemistry* 78(3): 827-34.

Affymetrix. 2009. GeneChip Human Genome U133 Plus 2.0 Array. Product Description: Affymetrix.

Agilent Technologies. (2012). Introduction to Quantitative PCR - Methods and Applications Guide. Germany - IN 70200 D: © Agilent Technologies, Inc.

Akiyama H, Tooyama I, Kawamata T, Ikeda K, McGeer PL. (1993). Morphological diversities of CD44 positive astrocytes in the cerebral cortex of normal subjects and patients with Alzheimer's disease. *Brain Research* 632(1-2): 249-59.

Al'Qteishat A, Gaffney J, Krupinski J, Rubio F, West D, *et al*. (2006). Changes in hyaluronan production and metabolism following ischaemic stroke in man. *Brain* 129(8): 2158-76.

Al-Radaideh AM, Wharton SJ, Lim SY, Tench CR, Morgan PS, *et al*. (2013). Increased iron accumulation occurs in the earliest stages of demyelinating disease: an ultra-high field susceptibility mapping study in Clinically Isolated Syndrome. *Multiple Sclerosis* 19(7): 896-903.

Alcina A, Fedetz M, Fernandez O, Saiz A, Izquierdo G, *et al*. (2013). Identification of a functional variant in the KIF5A-CYP27B1-METTL1-FAM119B locus associated with multiple sclerosis. *Journal of Medical Genetics* 50(1): 25-33.

Allen IV, McKeown SR. (1979). A histological, histochemical and biochemical study of the macroscopically normal white matter in multiple sclerosis. *J Neurol Sci* 41(1): 81-91.

Allen IV, McQuaid S, Mirakhur M, Nevin G. (2001). Pathological abnormalities in the normal-appearing white matter in multiple sclerosis. *Neurological Sciences : official journal of the Italian Neurological Society and of the Italian Society of Clinical Neurophysiology* 22(2): 141-4.

Aloisi F, Ria F, Columba-Cabezas S, Hess H, Penna G, Adorini L. (1999). Relative efficiency of microglia, astrocytes, dendritic cells and B cells in naive CD4+ T

cell priming and Th1/Th2 cell restimulation. *European Journal of Immunology* 29(9): 2705-14.

Aloisi F, Ria F, Penna G, Adorini L. (1998). Microglia are more efficient than astrocytes in antigen processing and in Th1 but not Th2 cell activation. *Journal of Immunology* 160(10): 4671-80.

Alvarez JI, Cayrol R, Prat A. (2011a). Disruption of central nervous system barriers in multiple sclerosis. *Biochimica et Biophysica Acta* 1812(2): 252-64.

Alvarez JI, Dodelet-Devillers A, Kebir H, Ifergan I, Fabre PJ, *et al*. (2011b). The Hedgehog pathway promotes blood-brain barrier integrity and CNS immune quiescence. *Science* 334(6063): 1727-31.

Andersson M, Andren P, Caprioli RM (2010). MALDI Imaging and Profiling Mass Spectrometry in Neuroproteomics. In: *Neuroproteomics* (Alzate, O., ed) Boca Raton (FL).

Antel J, Antel S, Caramanos Z, Arnold DL, Kuhlmann T. (2012). Primary progressive multiple sclerosis: part of the MS disease spectrum or separate disease entity? *Acta Neuropathol* 123(5): 627-38.

Anthony TE, Heintz N. (2007). The folate metabolic enzyme ALDH1L1 is restricted to the midline of the early CNS, suggesting a role in human neural tube defects. *The Journal of Comparative Neurology* 500(2): 368-83.

Arai Y, Takashima S, Becker LE. (2000). CD44 expression in tuberous sclerosis. *Pathobiology* 68(2): 87-92.

Arber DA. (2002). Effect of prolonged formalin fixation on the immunohistochemical reactivity of breast markers. *Applied Immunohistochemistry & Molecular Morphology* 10(2): 183-6.

Argaw AT, Asp L, Zhang J, Navrazhina K, Pham T, *et al*. (2012). Astrocyte-derived VEGF-A drives blood-brain barrier disruption in CNS inflammatory disease. *J Clin Invest* 122(7): 2454-68.

Argaw AT, Gurfein BT, Zhang Y, Zameer A, John GR. (2009). VEGF-mediated disruption of endothelial CLN-5 promotes blood-brain barrier breakdown. *Proceedings of the National Academy of Sciences of the United States of America* 106(6): 1977-82.

Argaw AT, Zhang Y, Snyder BJ, Zhao ML, Kopp N, *et al*. (2006). IL-1beta regulates blood-brain barrier permeability via reactivation of the hypoxia-angiogenesis program. *Journal of Immunology* 177(8): 5574-84.

Aritake K, Koh CS, Inoue A, Yabuuchi F, Kitagaki K, *et al*. (2010). Effects of human recombinant-interferon beta in experimental autoimmune encephalomyelitis in guinea pigs. *Pharmaceutical Biology* 48(11): 1273-9.

Ascherio A, Munger KL, Simon KC. (2010). Vitamin D and multiple sclerosis. *Lancet Neurology* 9(6): 599-612.

Axelsson M, Malmestrom C, Nilsson S, Haghighi S, Rosengren L, Lycke J. (2011). Glial fibrillary acidic protein: a potential biomarker for progression in multiple sclerosis. *J Neurol* 258(5): 882-828.

Azami Tameh A, Clarner T, Beyer C, Atlasi MA, Hassanzadeh G, Naderian H. (2013). Regional regulation of glutamate signaling during cuprizone-induced demyelination in the brain. *Annals of anatomy = Anatomischer Anzeiger* 196(6): 416-423.

Babbe H, Roers A, Waisman A, Lassmann H, Goebels N, *et al*. (2000). Clonal expansions of CD8(+) T cells dominate the T cell infiltrate in active multiple sclerosis lesions as shown by micromanipulation and single cell polymerase chain reaction. *The Journal of Experimental Medicine* 192(3): 393-404.

Back SA, Tuohy TM, Chen H, Wallingford N, Craig A, *et al*. (2005). Hyaluronan accumulates in demyelinated lesions and inhibits oligodendrocyte progenitor maturation. *Nature Medicine* 11(9): 966-72.

Bagnato F, Hametner S, Yao B, van Gelderen P, Merkle H, *et al*. (2011). Tracking iron in multiple sclerosis: a combined imaging and histopathological study at 7 Tesla. *Brain* 134(12): 3602-15.

Bahn S, Augood SJ, Ryan M, Standaert DG, Starkey M, Emson PC. (2001). Gene expression profiling in the post-mortem human brain--no cause for dismay In *Journal of Chemical Neuroanatomy* 22(1-2): 79-94.

Baker D, O'Neill JK, Gschmeissner SE, Wilcox CE, Butter C, Turk JL. (1990). Induction of chronic relapsing experimental allergic encephalomyelitis in Biozzi mice. *J Neuroimmunol* 28(3): 261-70.

Baker D, Gerritsen W, Rundle J, Amor S. (2011). Critical appraisal of animal models of multiple sclerosis. *Multiple Sclerosis* 17(6): 647-57.

Baker H, Patel V, Molinolo AA, Shillitoe EJ, Ensley JF, *et al*. (2005). Proteome-wide analysis of head and neck squamous cell carcinomas using laser-capture microdissection and tandem mass spectrometry. *Oral Oncology* 41(2): 183-99.

Banisor I, Kalman B. (2004). Bcl-2 and its homologues in the brain of patients with multiple sclerosis. *Multiple Sclerosis* 10(2): 176-81.

Bar-Or A. (2008). The immunology of multiple sclerosis. *Seminars in Neurology* 28(1): 29-45.

Baranzini SE, Bernard CC, Oksenberg JR. (2005). Modular transcriptional activity characterizes the initiation and progression of autoimmune encephalomyelitis. *Journal of Immunology* 174(11): 7412-22.

Baranzini SE, Wang J, Gibson RA, Galwey N, Naegelin Y, *et al*. (2009). Genome-wide association analysis of susceptibility and clinical phenotype in multiple sclerosis. *Human Molecular Genetics* 18(4): 767-78.

Barley K, Dracheva S, Byne W. (2009). Subcortical oligodendrocyte- and astrocyte-associated gene expression in subjects with schizophrenia, major depression and bipolar disorder. *Schizophr Res* 112(1-3): 54-64.

Barna BP, Pettay J, Barnett GH, Zhou P, Iwasaki K, Estes ML. (1994). Regulation of monocyte chemoattractant protein-1 expression in adult human non-neoplastic astrocytes is sensitive to tumor necrosis factor (TNF) or antibody to the 55-kDa TNF receptor. *J Neuroimmunol* 50(1): 101-7.

Barnett MH, Parratt JD, Cho ES, Prineas JW. (2009a). Immunoglobulins and complement in postmortem multiple sclerosis tissue. *Annals of Neurology* 65(1): 32-46.

Barnett MH, Parratt JDE, Pollard JD, Prineas JW. (2009b). MS: is it one disease? *International MS Journal* 16(2): 57-65.

Barnham KJ, Bush AI. (2008). Metals in Alzheimer's and Parkinson's diseases. *Current Opinion in Chemical Biology* 12(2): 222-8.

Barnum SR. (2002). Complement in central nervous system inflammation. *Immunologic Research* 26(1-3): 7-13.

Barrere C, Chendo C, Phan TN, Monnier V, Trimaille T, *et al*. (2012). Successful MALDI-MS analysis of synthetic polymers with labile end-groups: the case of nitroxide-mediated polymerization using the MAMA-SG1 alkoxyamine. *Chemistry* 18(25): 7916-24.

Barreto GE, Sun X, Xu L, Giffard RG. (2011). Astrocyte proliferation following stroke in the mouse depends on distance from the infarct In *PLoS One* e27881.

Bartosik-Psujek H, Psujek M, Jaworski J, Stelmasiak Z. (2011). Total tau and S100b proteins in different types of multiple sclerosis and during immunosuppressive treatment with mitoxantrone. *Acta Neurologica Scandinavica* 123(4): 252-6.

Barun B, Bar-Or A. (2012). Treatment of multiple sclerosis with anti-CD20 antibodies. *Clinical Immunology* 142(1): 31-7.

Basso AS, Frenkel D, Quintana FJ, Costa-Pinto FA, Petrovic-Stojkovic S, *et al*. (2008). Reversal of axonal loss and disability in a mouse model of progressive multiple sclerosis. *J Clin Invest* 118(4): 1532-43.

Basta G, Lazzerini G, Massaro M, Simoncini T, Tanganelli P, *et al*. (2002). Advanced glycation end products activate endothelium through signal-transduction receptor RAGE: a mechanism for amplification of inflammatory responses. *Circulation* 105(7): 816-22.

Beaty MW, Fetsch P, Wilder AM, Marincola F, Abati A. (1997). Effusion cytology of malignant melanoma. A morphologic and immunocytochemical analysis including application of the MART-1 antibody. *Cancer* 81(1): 57-63.

Becher B, Durell BG, Noelle RJ. (2002). Experimental autoimmune encephalitis and inflammation in the absence of interleukin-12. *J Clin Invest* 110(4): 493-7.

Begley DJ. (2003). Understanding and circumventing the blood-brain barrier. *Acta Paediatr Suppl* 92(443): 83-91.

Bergmann CC, Lane TE, Stohlman SA. (2006). Coronavirus infection of the central nervous system: host-virus stand-off. *Nature Reviews. Microbiology* 4(2): 121-32.

Bernard R, Burke S, Kerman IA. (2011). Region-specific in situ hybridization-guided laser-capture microdissection on postmortem human brain tissue coupled with gene expression quantification. *Methods in Molecular Biology* 755: 345-61.

Berridge MJ. (2012). *Cell Signalling Biology* 10.1042/csb0001002.

Bhattacharya SH, Gal AA, Murray KK. (2003). Laser capture microdissection MALDI for direct analysis of archival tissue. *J Proteome Res* 2(1): 95-8.

Bi WL, Keller-McGandy C, Standaert DG, Augood SJ. (2002). Identification of nitric oxide synthase neurons for laser capture microdissection and mRNA quantification. *BioTechniques* 33(6): 1274-83.

Bianchi R, Adami C, Giambanco I, Donato R. (2007). S100B binding to RAGE in microglia stimulates COX-2 expression. *Journal of Leukocyte Biology* 81(1): 108-18.

Bianchi R, Kastrisianaki E, Giambanco I, Donato R. (2011). S100B protein stimulates microglia migration via RAGE-dependent up-regulation of chemokine expression and release. *The Journal of Biological Chemistry* 286(9): 7214-26.

Bishop GM, Robinson SR, Liu Q, Perry G, Atwood CS, Smith MA. (2002). Iron: a pathological mediator of Alzheimer disease? *Developmental Neuroscience* 24(2-3): 184-7.

Bitsch A, Kuhlmann T, Da Costa C, Bunkowski S, Polak T, Bruck W. (2000). Tumour necrosis factor alpha mRNA expression in early multiple sclerosis lesions: correlation with demyelinating activity and oligodendrocyte pathology. *Glia* 29(4): 366-75.

Black JA, Newcombe J, Waxman SG. (2010). Astrocytes within multiple sclerosis lesions upregulate sodium channel Nav1.5. *Brain* 133(3):835-46.

Boche D, Perry VH, Nicoll JA. (2013). Review: Activation patterns of microglia and their identification in the human brain. *Neuropathology and Applied Neurobiology* 39(1): 3-18.

Boenisch T. (2005). Effect of heat-induced antigen retrieval following inconsistent formalin fixation. *Applied Immunohistochemistry & Molecular Morphology* 13(3): 283-6.

Bomprezzi R, Ringner M, Kim S, Bittner ML, Khan J, *et al*. (2003). Gene expression profile in multiple sclerosis patients and healthy controls: identifying pathways relevant to disease. *Human Molecular Genetics* 12(17): 2191-9.

Boone DR, Sell SL, Hellmich HL. (2013). Laser capture microdissection of enriched populations of neurons or single neurons for gene expression analysis after traumatic brain injury. *Journal of Visualized Experiments* 10(17):1-7.

Borjabad A, Volsky DJ. (2012). Common transcriptional signatures in brain tissue from patients with HIV-associated neurocognitive disorders, Alzheimer's disease, and Multiple Sclerosis. *Journal of Neuroimmune Pharmacology* 7(4): 914-26.

Bossers K, Meerhoff G, Balesar R, van Dongen JW, Kruse CG, *et al*. (2009). Analysis of gene expression in Parkinson's disease: possible involvement of neurotrophic support and axon guidance in dopaminergic cell death. *Brain Pathology* 19(1): 91-107.

Boyd-Kimball D, Sultana R, Poon HF, Lynn BC, Casamenti F, *et al*. (2005). Proteomic identification of proteins specifically oxidized by intracerebral injection of amyloid beta-peptide (1-42) into rat brain: implications for Alzheimer's disease. *Neuroscience* 132(2): 313-24.

Bradford MM. (1976). A rapid and sensitive method for the quantitation of microgram quantities of protein utilizing the principle of protein-dye binding. *Analytical Biochemistry* 72: 248-54.

Bradl M, Lassmann H. (2012). Microarray analysis on archival multiple sclerosis tissue: pathogenic authenticity outweighs technical obstacles. *Neuropathology* 32(4): 463-6.

Bradley LM, Watson SR. (1996). Lymphocyte migration into tissue: the paradigm derived from CD4 subsets. *Curr Opin Immunol* 8(3): 312-20.

Brambilla R, Bracchi-Ricard V, Hu WH, Frydel B, Bramwell A, *et al*. (2005). Inhibition of astroglial nuclear factor kappaB reduces inflammation and improves functional recovery after spinal cord injury. *The Journal of Experimental Medicine* 202(1): 145-56.

Brand-Schieber E, Werner P, Iacobas DA, Iacobas S, Beelitz M, *et al*. (2005). Connexin43, the major gap junction protein of astrocytes, is down-regulated in inflamed white matter in an animal model of multiple sclerosis. *J Neurosci Res* 80(6): 798-808.

Brass SD, Benedict RH, Weinstock-Guttman B, Munschauer F, Bakshi R. (2006a). Cognitive impairment is associated with subcortical magnetic resonance imaging grey matter T2 hypointensity in multiple sclerosis. *Multiple Sclerosis* 12(4): 437-44.

Brass SD, Chen NK, Mulkern RV, Bakshi R. (2006b). Magnetic resonance imaging of iron deposition in neurological disorders. *Topics in Magnetic Resonance Imaging* 17(1): 31-40.

Brennan FR, O'Neill JK, Allen SJ, Butter C, Nuki G, Baker D. (1999). CD44 is involved in selective leucocyte extravasation during inflammatory central nervous system disease. *Immunology* 98(3): 427-35.

Brilot F, Dale RC, Selter RC, Grummel V, Kalluri SR, *et al*. (2009). Antibodies to native myelin oligodendrocyte glycoprotein in children with inflammatory demyelinating central nervous system disease. *Annals of Neurology* 66(6): 833-42.

Brink BP, Veerhuis R, Breij EC, van der Valk P, Dijkstra CD, Bo L. (2005). The pathology of multiple sclerosis is location-dependent: no significant complement activation is detected in purely cortical lesions. *Journal of Neuropathology and Experimental Neurology* 64(2): 147-55.

Brochu C, Cabrita MA, Melanson BD, Hamill JD, Lau R, *et al*. (2013). NF-kappaB-dependent role for cold-inducible RNA binding protein in regulating interleukin 1beta. *PLoS One* 8(2): e57426.

Brocke S, Gaur A, Piercy C, Gautam A, Gijbels K, *et al*. (1993). Induction of relapsing paralysis in experimental autoimmune encephalomyelitis by bacterial superantigen. *Nature* 365(6447): 642-4.

Brocke S, Piercy C, Steinman L, Weissman IL, Veromaa T. (1999). Antibodies to CD44 and integrin alpha4, but not L-selectin, prevent central. *Proceedings of the National Academy of Sciences of the United States of America* 96(12): 6896-901.

Brockington A, Ning K, Heath PR, Wood E, Kirby J, *et al*. (2013). Unravelling the enigma of selective vulnerability in neurodegeneration: motor neurons resistant to degeneration in ALS show distinct gene expression characteristics and decreased susceptibility to excitotoxicity. *Acta Neuropathol* 125(1): 95-109.

Brodel P. (2010). The central nervous system: structure and function. 4th edition, New York: Oxford University Press.

Brosnan CF, Raine CS. (2013). The astrocyte in multiple sclerosis revisited. *Glia* 61(4): 453-65.

Bruck W, Porada P, Poser S, Rieckmann P, Hanefeld F, *et al*. (1995). Monocyte/macrophage differentiation in early multiple sclerosis lesions. *Annals of Neurology* 38(5): 788-96.

Bsibsi M, Persoon-Deen C, Verwer RW, Meeuwsen S, Ravid R, Van Noort JM. (2006). Toll-like receptor 3 on adult human astrocytes triggers production of neuroprotective mediators. *Glia* 53(7): 688-95.

Buckley CE, Goldsmith P, Franklin RJ. (2008). Zebrafish myelination: a transparent model for remyelination? *Disease Models & Mechanisms* 1(4-5): 221-8.

Buckley CE, Marguerie A, Roach AG, Goldsmith P, Fleming A, *et al*. (2010). Drug reprofiling using zebrafish identifies novel compounds with potential pro-myelination effects. *Neuropharmacology* 59(3): 149-59.

Budd RC, Cerottini JC, Horvath C, Bron C, Pedrazzini T, *et al*. (1987). Distinction of virgin and memory T lymphocytes. Stable acquisition of the Pgp-1 glycoprotein concomitant with antigenic stimulation. *Journal of Immunology* 138(10): 3120-9.

Bugiani M, Postma N, Polder E, Dieleman N, Scheffer PG, *et al*. (2013). Hyaluronan accumulation and arrested oligodendrocyte progenitor maturation in vanishing white matter disease. *Brain* 136(1): 209-22.

Bundgaard M, Abbott NJ. (2008). All vertebrates started out with a glial blood-brain barrier 4-500 million years ago. *Glia* 56(7): 699-708.

Burdo JR, Antonetti DA, Wolpert EB, Connor JR. (2003). Mechanisms and regulation of transferrin and iron transport in a model blood-brain barrier system. *Neuroscience* 121(4): 883-90.

Burdo JR, Connor JR. (2003). Brain iron uptake and homeostatic mechanisms: an overview. *Biometals* 16(1): 63-75.

Burgemeister R. (2011). Laser capture microdissection of FFPE tissue sections bridging the gap between microscopy and molecular analysis. *Methods in Molecular Biology* 724: 105-15.

Burgess JK, McParland BE. (2002). Analysis of gene expression. *Methods in Enzymology* 356: 259-70.

Bush WS, McCauley JL, DeJager PL, Dudek SM, Hafler DA, *et al*. (2011). A knowledge-driven interaction analysis reveals potential neurodegenerative mechanism of multiple sclerosis susceptibility. *Genes and immunity* 12(5): 335-40.

Businaro R, Leone S, Fabrizi C, Sorci G, Donato R, *et al*. (2006). S100B protects LAN-5 neuroblastoma cells against Abeta amyloid-induced neurotoxicity via RAGE engagement at low doses but increases Abeta amyloid neurotoxicity at high doses. *J Neurosci Res* 83(5): 897-906.

Butterfield DA, Poon HF, St Clair D, Keller JN, Pierce WM, *et al*. (2006). Redox proteomics identification of oxidatively modified hippocampal proteins in mild cognitive impairment: insights into the development of Alzheimer's disease. *Neurobiol Dis* 22(2): 223-32.

Cahoy JD, Emery B, Kaushal A, Foo LC, Zamanian JL, *et al*. (2008). A transcriptome database for astrocytes, neurons, and oligodendrocytes: a new resource for understanding brain development and function. *Journal of Neuroscience* 28(1): 264-78.

Cairns NJ, Lee VM, Trojanowski JQ. (2004). The cytoskeleton in neurodegenerative diseases. *The Journal of Pathology* 204(4): 438-49.

Calderon TM, Eugenin EA, Lopez L, Kumar SS, Hesselgesser J, *et al*. (2006). A role for CXCL12 (SDF-1alpha) in the pathogenesis of multiple sclerosis: regulation of CXCL12 expression in astrocytes by soluble myelin basic protein. *J Neuroimmunol* 177(1-2): 27-39.

Cammer W. (2000). Effects of TNFalpha on immature and mature oligodendrocytes and their progenitors in vitro. *Brain Res* 864(2): 213-9.

Campbell GR, Kraytsberg Y, Krishnan KJ, Ohno N, Ziabreva I, *et al*. (2012). Clonally expanded mitochondrial DNA deletions within the choroid plexus in multiple sclerosis. *Acta Neuropathol* 124(2): 209-20.

Caprioli RM, Farmer TB, Gile J. (1997). Molecular imaging of biological samples: localization of peptides and proteins using MALDI-TOF MS. *Analytical Chemistry* 69(23): 4751-60.

Carbonell T, Rama R. (2007). Iron, oxidative stress and early neurological deterioration in ischemic stroke. *Current Medicinal Chemistry* 14(8): 857-74.

Carmody RJ, Hilliard B, Maguschak K, Chodosh LA, Chen YH. (2002). Genomic scale profiling of autoimmune inflammation in the central nervous system: the nervous response to inflammation. *J Neuroimmunol* 133(1-2): 95-107.

Carter CL, McLeod CW, Bunch J. (2011). Imaging of phospholipids in formalin fixed rat brain sections by matrix assisted. *J Am Soc Mass Spectrom* 22(11): 1991-8.

Castegna A, Palmieri L, Spera I, Porcelli V, Palmieri F, *et al*. (2011). Oxidative stress and reduced glutamine synthetase activity in the absence of inflammation in the cortex of mice with experimental allergic encephalomyelitis. *Neuroscience* 185: 97-105.

Cecchelli R, Berezowski V, Lundquist S, Culot M, Renftel M, *et al*. (2007). Modelling of the blood-brain barrier in drug discovery and development. *Nature reviews. Drug Discovery* 6(8): 650-61.

Cepok S, Zhou D, Srivastava R, Nessler S, Stei S, et al. (2005). Identification of Epstein-Barr virus proteins as putative targets of the immune response in multiple sclerosis. *J Clin Invest* 115(5): 1352-60.

Cha S, Imielinski MB, Rejtar T, Richardson EA, Thakur D, *et al*. (2010). In situ proteomic analysis of human breast cancer epithelial cells using laser capture microdissection: annotation by protein set enrichment analysis and gene ontology. *Molecular & Cellular Proteomics* 9(11): 2529-44.

Chabas D, Baranzini SE, Mitchell D, Bernard CC, Rittling SR, *et al*. (2001). The influence of the proinflammatory cytokine, osteopontin, on autoimmune demyelinating disease. *Science* 294(5547): 1731-5.

Chaudhuri A. (2013). Multiple sclerosis is primarily a neurodegenerative disease. *J Neural Transm* 120(10): 1463-6.

Chaurand P, Norris JL, Cornett DS, Mobley JA, Caprioli RM. (2006). New developments in profiling and imaging of proteins from tissue sections by MALDI mass spectrometry. *J Proteome Res* 5(11): 2889-900.
Chaurand P, Schwartz SA, Caprioli RM. (2002). Imaging mass spectrometry: a new tool to investigate the spatial organization of peptides and proteins in mammalian tissue sections. *Current Opinion in Chemical Biology* 6(5): 676-81.
Chen CH, Jiang Z, Yan JH, Yang L, Wang K, *et al*. (2013a). The involvement of programmed cell death 5 (PDCD5) in the regulation of apoptosis in cerebral ischemia/reperfusion injury. *CNS Neuroscience & Therapeutics* 19(8): 566-76.
Chen J, Marks E, Lai B, Zhang Z, Duce JA, *et al*. (2013b). Iron Accumulates in Huntington's Disease Neurons: Protection by Deferoxamine. *PLoS One* 8(10): e77023.
Chevalier-Larsen E, Holzbaur EL. (2006). Axonal transport and neurodegenerative disease. *Biochimica et Biophysica Acta* 1762(11-12): 1094-108.
Choi SR, Howell OW, Carassiti D, Magliozzi R, Gveric D, *et al*. (2012). Meningeal inflammation plays a role in the pathology of primary progressive multiple sclerosis. *Brain* 135(10): 2925-37.
Chorna NE, Santiago-Perez LI, Erb L, Seye CI, Neary JT, *et al*. (2004). P2Y receptors activate neuroprotective mechanisms in astrocytic cells. *Journal of Neurochemistry* 91(1): 119-32.
Chu TT, Liu Y, Kemether E. (2009). Thalamic transcriptome screening in three psychiatric states. *Journal of Human Genetics* 54(11): 665-75.
Chung AY, Kim PS, Kim S, Kim E, Kim D, *et al*. (2013). Generation of demyelination models by targeted ablation of oligodendrocytes in the zebrafish CNS. *Molecules and Cells* 36(1): 82-7.
Chung RS, Adlard PA, Dittmann J, Vickers JC, Chuah MI, West AK. (2004). Neuron-glia communication: metallothionein expression is specifically up-regulated by astrocytes in response to neuronal injury. *Journal of Neurochemistry* 88(2): 454-61.
Chung RS, Hidalgo J, West AK. (2008a). New insight into the molecular pathways of metallothionein-mediated neuroprotection and regeneration. *Journal of Neurochemistry* 104(1): 14-20.
Chung RS, Penkowa M, Dittmann J, King CE, Bartlett C, *et al*. (2008b). Redefining the role of metallothionein within the injured brain: extracellular metallothioneins play an important role in the astrocyte-neuron response to injury. *The Journal of Biological Chemistry* 283(22): 15349-58.
Chung RS, Vickers JC, Chuah MI, West AK. (2003). Metallothionein-IIA promotes initial neurite elongation and postinjury reactive neurite growth and facilitates healing after focal cortical brain injury. *The Journal of Neuroscience* 23(8): 3336-42.
Clapham DE. (2007). Calcium signaling. *Cell* 131(6): 1047-58
Clarner T, Diederichs F, Berger K, Denecke B, Gan L, *et al*. (2012). Myelin debris regulates inflammatory responses in an experimental demyelination animal model and multiple sclerosis lesions. *Glia* 60(10): 1468-80.
Colombo E, Cordiglieri C, Melli G, Newcombe J, Krumbholz M, *et al*. (2012). Stimulation of the neurotrophin receptor TrkB on astrocytes drives nitric oxide production and neurodegeneration. *The Journal of Experimental Medicine* 209(3): 521-35.
Comabella M, Martin R. (2007). Genomics in multiple sclerosis--current state and future directions. *J Neuroimmunol* 187(1-2): 1-8.
Compston A. (2006). Making progress on the natural history of multiple sclerosis. *Brain* 129(3): 561-3.

Compston A, Coles A. (2008). Multiple sclerosis. *Lancet* 372: 1502-17.
Connor JR, Menzies SL, Burdo JR, Boyer PJ. (2001). Iron and iron management proteins in neurobiology. *Pediatric Neurology* 25(2): 118-29.
Connor JR, Menzies SL, St Martin SM, Mufson EJ. (1990). Cellular distribution of transferrin, ferritin, and iron in normal and aged human brains. *J Neurosci Res* 27(4): 595-611.
Constantinescu CS, Farooqi N, O'Brien K, Gran B. (2011). Experimental autoimmune encephalomyelitis (EAE) as a model for multiple sclerosis (MS). *British Journal of Pharmacology* 164(4): 1079-106.
Constantinescu CS, Tani M, Ransohoff RM, Wysocka M, Hilliard B, *et al*. (2005). Astrocytes as antigen-presenting cells: expression of IL-12/IL-23. *Journal of Neurochemistry* 95: 331-40.
Correale J, Balbuena Aguirre ME, Farez MF. (2013). Sex-specific environmental influences affecting MS development. *Clinical Immunology* 149(2): 176-81.
Correale J, Villa A. (2007). The blood-brain-barrier in multiple sclerosis: functional roles and therapeutic targeting. *Autoimmunity* 40(2): 148-60.
Correale J, Ysrraelit MC, Gaitan MI. (2009). Immunomodulatory effects of Vitamin D in multiple sclerosis. *Brain* 132(5): 1146-60.
Coudry RA, Meireles SI, Stoyanova R, Cooper HS, Carpino A, *et al*. (2007). Successful application of microarray technology to microdissected formalin-fixed, paraffin-embedded tissue. *The Journal of Molecular Diagnostics* 9(1): 70-9.
Coulter DA, Eid T. (2012). Astrocytic regulation of glutamate homeostasis in epilepsy. *Glia* 60(8): 1215-26.
Courtney E, Kornfeld S, Janitz K, Janitz M. (2010). Transcriptome profiling in neurodegenerative disease. *J Neurosci Methods* 193(2): 189-202.
Crichton RR, Dexter DT, Ward RJ. (2011). Brain iron metabolism and its perturbation in neurological diseases. *J Neural Transm* 118(3): 301-14.
Crocker SJ, Whitmire JK, Frausto RF, Chertboonmuang P, Soloway PD, *et al*. (2006). Persistent macrophage/microglial activation and myelin disruption after experimental autoimmune encephalomyelitis in tissue inhibitor of metalloproteinase-1-deficient mice. *The American Journal of Pathology* 169: 2104-16.
Cross AH, Ku G. (2000). Astrocytes and central nervous system endothelial cells do not express B7-1 (CD80) or B7-2 (CD86) immunoreactivity during experimental autoimmune encephalomyelitis. *J Neuroimmunol* 110(1-2): 76-82.
Cruz TF, Quackenbush EJ, Letarte M, Moscarello MA. (1985). Effects of development and aging on the concentration of a human brain antigen. *Neuroscience Letters*, 59: 253-7.
Cua DJ, Sherlock J, Chen Y, Murphy CA, Joyce B, *et al*. (2003). Interleukin-23 rather than interleukin-12 is the critical cytokine for autoimmune inflammation of the brain. *Nature* 421(6924): 744-8.
Cunnea P, McMahon J, O'Connell E, Mashayekhi K, Fitzgerald U, McQuaid S. (2010). Gene expression analysis of the microvascular compartment in multiple sclerosis using laser microdissected blood vessels. *Acta Neuropathologica* 119(5): 601-15.
Cunnea P, Mhaille AN, McQuaid S, Farrell M, McMahon J, FitzGerald U. (2011). Expression profiles of endoplasmic reticulum stress-related molecules in demyelinating lesions and multiple sclerosis. *Multiple Sclerosis* 17(7): 808-18.
D'Amico F, Skarmoutsou E, Stivala F. (2009). State of the art in antigen retrieval for immunohistochemistry. *Journal of Immunological Methods* 341(1-2): 1-18.
Daginakatte GC, Gadzinski A, Emnett RJ, Stark JL, Gonzales ER, *et al*. (2008). Expression profiling identifies a molecular signature of reactive astrocytes

stimulated by cyclic AMP or proinflammatory cytokines. *Exp Neurol* 210(1): 261-7.
Dalle-Donne I, Rossi R, Milzani A, Di Simplicio P, Colombo R. (2001). The actin cytoskeleton response to oxidants: from small heat shock protein phosphorylation to changes in the redox state of actin itself. *Free Radical Biology & Medicine* 31(12): 1624-32.
Danbolt NC. (2001). Glutamate uptake. *Progress in Neurobiology* 65(1): 1-105.
Daneman R. (2012). The blood-brain barrier in health and disease. *Annals of Neurology* 72(5): 648-72.
Davies GR, Altmann DR, Hadjiprocopis A, Rashid W, Chard DT, *et al*. (2005). Increasing normal-appearing grey and white matter magnetisation transfer ratio abnormality in early relapsing-remitting multiple sclerosis. *J Neurol* 252(9): 1037-44.
De Keyser J, Laureys G, Demol F, Wilczak N, Mostert J, Clinckers R. (2010). Astrocytes as potential targets to suppress inflammatory demyelinating lesions in multiple sclerosis. *Neurochemistry International* 57(4): 446-50.
de Pablos RM, Espinosa-Oliva AM, Herrera AJ. (2013). Immunohistochemical detection of microglia. *Methods in Molecular Biology* 1041: 281-9.
De Rosa V, Procaccini C, Cali G, Pirozzi G, Fontana S, *et al*. (2007). A key role of leptin in the control of regulatory T cell proliferation. *Immunity* 26(2): 241-55.
De Santi L, Annunziata P, Sessa E, Bramanti P. (2009). Brain-derived neurotrophic factor and TrkB receptor in experimental autoimmune encephalomyelitis and multiple sclerosis. *J Neurol Sci* 287(1-2): 17-26.
Deane R, Zheng W, Zlokovic BV. (2004). Brain capillary endothelium and choroid plexus epithelium regulate transport of transferrin-bound and free iron into the rat brain. *Journal of Neurochemistry* 88(4): 813-20.
Deitmer JW, Broer A, Broer S. (2003). Glutamine efflux from astrocytes is mediated by multiple pathways. *Journal of Neurochemistry* 87(1): 127-35.
deLuca LE, Pikor NB, O'Leary J, Galicia-Rosas G, Ward LA, *et al*. (2010). Substrain differences reveal novel disease-modifying gene candidates that alter the clinical course of a rodent model of multiple sclerosis. *Journal of Immunology* 184(6): 3174-85.
Derouiche A, Rauen T. (1995). Coincidence of L-glutamate/L-aspartate transporter (GLAST) and glutamine synthetase (GS) immunoreactions in retinal glia: evidence for coupling of GLAST and GS in transmitter clearance. *J Neurosci Res* 42(1): 131-43.
Domercq M, Sanchez-Gomez MV, Areso P, Matute C. (1999). Expression of glutamate transporters in rat optic nerve oligodendrocytes. *The European Journal of Neuroscience* 11(7): 2226-36.
Domingues HS, Mues M, Lassmann H, Wekerle H, Krishnamoorthy G. (2010). Functional and pathogenic differences of Th1 and Th17 cells in experimental autoimmune encephalomyelitis. *PLoS One* 5(11): e15531.
Domon B, Aebersold R. (2006). Mass spectrometry and protein analysis. *Science* 312(5771): 212-7.
Donato R. (2001). S100: a multigenic family of calcium-modulated proteins of the EF-hand type with intracellular and extracellular functional roles. *The International Journal of Biochemistry & Cell Biology* 33(7): 637-68.
Donato R, Sorci G, Riuzzi F, Arcuri C, Bianchi R, *et al*. (2009). S100B's double life: intracellular regulator and extracellular signal. *Biochimica et Biophysica Acta* 1793(6): 1008-22.
Dong X, Cheng J, Li J, Wang Y. (2010). Graphene as a novel matrix for the analysis of small molecules by MALDI-TOF MS. *Analytical Chemistry* 82(14): 6208-14.

Dougherty JD, Zhang J, Feng H, Gong S, Heintz N. (2012). Mouse transgenesis in a single locus with independent regulation for multiple fluorophores. *PLoS ONE* 7(7): e40511.

Doyle JP, Dougherty JD, Heiman M, Schmidt EF, Stevens TR, *et al*. (2008). Application of a translational profiling approach for the comparative analysis of CNS cell types. *Cell* 135(4): 749-62.

Dringen R, Bishop GM, Koeppe M, Dang TN, Robinson SR. (2007). The pivotal role of astrocytes in the metabolism of iron in the brain. *Neurochemical Research* 32(11): 1884-90.

Dringen R, Gutterer JM, Hirrlinger J. (2000). Glutathione metabolism in brain metabolic interaction between astrocytes and neurons in the defense against reactive oxygen species. *European Journal of Biochemistry* 267(16): 4912-6.

Du YJ, Xiong L, Lou Y, Tan WL, Zheng SB. (2009). Reduced expression of programmed cell death 5 protein in tissue of human prostate cancer. *Chinese Medical Sciences Journal* 24(4): 241-5.

Dunn SE, Steinman L. (2013). The gender gap in multiple sclerosis: intersection of science and society. *JAMA Neurology* 70(5): 634-5.

Dunstan RW, Wharton KA, Quigley C, Lowe A. (2011). The use of immunohistochemistry for biomarker assessment - Can it compete with other technologies? *Toxicol Pathol* 39:988-1002.

Dupree JL, Girault JA, Popko B. (1999). Axo-glial interactions regulate the localization of axonal paranodal proteins. *The Journal of Cell Biology* 147(6): 1145-52.

Durrenberger PF, Fernando S, Kashefi SN, Ferrer I, Hauw JJ, *et al*. (2010). Effects of antemortem and postmortem variables on human brain mRNA quality: a BrainNet Europe study. *Journal of Neuropathology and Experimental Neurology* 69(1): 70-81.

Dutta R. (2013). Gene expression changes underlying cortical pathology: clues to understanding neurological disability in multiple sclerosis. *Multiple Sclerosis* 19(10): 1249-54.

Dutta R, Chang A, Doud MK, Kidd GJ, Ribaudo MV, *et al*. (2011). Demyelination causes synaptic alterations in hippocampi from multiple sclerosis patients. *Annals of Neurology* 69(3): 445-54.

Dutta R, McDonough J, Chang A, Swamy L, Siu A, *et al*. (2007). Activation of the ciliary neurotrophic factor (CNTF) signalling pathway in cortical neurons of multiple sclerosis patients. *Brain* 130(10): 2566-76.

Dutta R, McDonough J, Yin X, Peterson J, Chang A, *et al*. (2006). Mitochondrial dysfunction as a cause of axonal degeneration in multiple sclerosis patients. *Annals of Neurology* 59(3): 478-89.

Dutta R, Trapp BD. (2010). Gene expression profiling in multiple sclerosis brain. *Neurobiol Dis*: A 2010 Elsevier Inc.

Dutta R, Trapp BD. (2012). Gene expression profiling in multiple sclerosis brain. *Neurobiol Dis* 45(1): 108-14.

Eberlin LS, Liu X, Ferreira CR, Santagata S, Agar NY, Cooks RG. (2011). Desorption electrospray ionization then MALDI mass spectrometry imaging of lipid and protein distributions in single tissue sections. *Analytical Chemistry* 83(22): 8366-71.

Eid T, Thomas MJ, Spencer DD, Runden-Pran E, Lai JC, *et al*. (2004). Loss of glutamine synthetase in the human epileptogenic hippocampus: possible mechanism for raised extracellular glutamate in mesial temporal lobe epilepsy. *Lancet* 363(9402): 28-37.

Eid T, Tu N, Lee TS, Lai JC. (2013). Regulation of Astrocyte Glutamine Synthetase in Epilepsy. *Neurochem Int* 63(7): 670-681.

Elkabes S, Li H. (2007). Proteomic strategies in multiple sclerosis and its animal models. *Proteomics. Clinical applications* 1(11): 1393-405.
Emmert-Buck MR, Bonner RF, Smith PD, Chuaqui RF, Zhuang Z, *et al*. (1996). Laser capture microdissection. *Science* 274(5289): 998-1001.
Eng LF, Ghirnikar RS. (1994). GFAP and astrogliosis. *Brain Pathology* 4(3): 229-37.
Eng LF, Vanderhaeghen JJ, Bignami A, Gerstl B. (1971). An acidic protein isolated from fibrous astrocytes *Brain Res* 28: 351-4.
Engel KB, Moore HM. (2011). Effects of preanalytical variables on the detection of proteins by immunohistochemistry in formalin-fixed, paraffin-embedded tissue. *Archives of Pathology & Laboratory Medicine* 135(5): 537-43.
Espejo C, Carrasco J, Hidalgo J, Penkowa M, Garcia A, *et al*. (2001). Differential expression of metallothioneins in the CNS of mice with experimental autoimmune encephalomyelitis. *Neuroscience* 105(4): 1055-65.
Espejo C, Penkowa M, Demestre M, Montalban X, Martinez-Caceres EM. (2005). Time-course expression of CNS inflammatory, neurodegenerative tissue repair markers and metallothioneins during experimental autoimmune encephalomyelitis. *Neuroscience* 132(4): 1135-49.
Espinosa de los Monteros A, Kumar S, Scully S, Cole R, de Vellis J. (1990). Transferrin gene expression and secretion by rat brain cells in vitro. *J Neurosci Res* 25(4): 576-80.
Farina M, Avila DS, da Rocha JB, Aschner M. (2013). Metals, oxidative stress and neurodegeneration: a focus on iron, manganese and mercury. *Neurochem Int* 62(5): 575-94.
Farrell M. (2013). Relapsing-remitting and primary progressive MS have the same cause(s)--the neuropathologist's view: commentary. *Multiple Sclerosis* 19(3): 270.
Fawcett JW, Asher RA. (1999). The glial scar and central nervous system repair. *Brain Research Bulletin* 49(6): 377-91.
Fellin T. (2009). Communication between neurons and astrocytes: relevance to the modulation of synaptic and network activity. *Journal of Neurochemistry* 108: 533-44.
Fellner L, Stefanova N. (2013). The role of glia in alpha-synucleinopathies. *Mol Neurobiol* 47(2): 575-86.
Fend F, Emmert-Buck MR, Chuaqui R, Cole K, Lee J, *et al*. (1999). Immuno-LCM: laser capture microdissection of immunostained frozen sections for mRNA analysis. *The American Journal of Pathology* 154: 61-6.
Fend F, Kremer M, Quintanilla-Martinez L. (2000). Laser capture microdissection: methodical aspects and applications with emphasis on immuno-laser capture microdissection. *Pathobiology : Journal of Immunopathology, Molecular and Cellular Biology* 68: 209-14.
Fenn JB, Mann M, Meng CK, Wong SF, Whitehouse CM. (1989). Electrospray ionization for mass spectrometry of large biomolecules. *Science* 246(4926): 64-71.
Fernandes SP, Dringen R, Lawen A, Robinson SR. (2011). Inactivation of astrocytic glutamine synthetase by hydrogen peroxide requires iron. *Neuroscience Letters* 490(1): 27-30.
Fernando MM, Stevens CR, Walsh EC, De Jager PL, Goyette P, *et al*. (2008). Defining the role of the MHC in autoimmunity: a review and pooled analysis. *PLoS genetics* 4(4): e1000024.
Ferraiuolo L, Higginbottom A, Heath PR, Barber S, Greenald D, *et al*. (2011). Dysregulation of astrocyte-motoneuron cross-talk in mutant superoxide dismutase 1-related amyotrophic lateral sclerosis. *Brain* 134(9): 2627-41.

Filippi M, Rocca MA, Martino G, Horsfield MA, Comi G. (1998). Magnetization transfer changes in the normal appearing white matter precede the appearance of enhancing lesions in patients with multiple sclerosis. *Annals of Neurology* 43(6): 809-14.

Finkel T, Holbrook NJ. (2000). Oxidants, oxidative stress and the biology of ageing. *Nature* 408(6809): 239-47.

Fischer MT, Wimmer I, Hoftberger R, Gerlach S, Haider L, *et al*. (2013). Disease-specific molecular events in cortical multiple sclerosis lesions. *Brain* 136(6): 1799-815.

Fishman JB, Rubin JB, Handrahan JV, Connor JR, Fine RE. (1987). Receptor-mediated transcytosis of transferrin across the blood-brain barrier. *J Neurosci Res* 18(2): 299-304.

Fitch MT, Silver J. (2008). CNS injury, glial scars, and inflammation: Inhibitory extracellular matrices and regeneration failure. *Exp Neurol* 209(2): 294-301.

Fletcher JM, Lalor SJ, Sweeney CM, Tubridy N, Mills KH. (2010). T cells in multiple sclerosis and experimental autoimmune encephalomyelitis. *Clinical and Experimental Immunology* 162(1): 1-11.

Flynn KM, Michaud M, Madri JA. (2013). CD44 deficiency contributes to enhanced experimental autoimmune encephalomyelitis: a role in immune cells and vascular cells of the blood-brain barrier. *The American Journal of Pathology* 182(4): 1322-36.

Foo LC, Dougherty JD. (2013). Aldh1L1 is expressed by postnatal neural stem cells in vivo. *Glia* 61(9): 1533-41.

Frank M, Labov SE, Westmacott G, Benner WH. (1999). Energy-sensitive cryogenic detectors for high-mass biomolecule mass spectrometry. *Mass spectrometry Reviews* 18(3-4): 155-86.

Fressinaud C, Berges R, Eyer J. (2012). Axon cytoskeleton proteins specifically modulate oligodendrocyte growth and differentiation in vitro. *Neurochem Int* 60(1): 78-90.

Frigo M, Cogo MG, Fusco ML, Gardinetti M, Frigeni B. (2012). Glutamate and multiple sclerosis. *Current Medicinal Chemistry* 19(9): 1295-9.

Frischer JM, Bramow S, Dal-Bianco A, Lucchinetti CF, Rauschka H, *et al*. (2009). The relation between inflammation and neurodegeneration in multiple sclerosis brains. *Brain* 132(5): 1175-89.

Frisen J, Verge VM, Fried K, Risling M, Persson H, *et al*. (1993). Characterization of glial trkB receptors: differential response to injury in the central and peripheral nervous systems. *Proceedings of the National Academy of Sciences of the United States of America* 90(11): 4971-5.

Funfschilling U, Supplie LM, Mahad D, Boretius S, Saab AS, *et al*. (2012). Glycolytic oligodendrocytes maintain myelin and long-term axonal integrity. *Nature* 485(7399): 517-21.

Fusby JS, Kassmeier MD, Palmer VL, Perry GA, Anderson DK, *et al*. (2010). Cigarette smoke-induced effects on bone marrow B-cell subsets and CD4+:CD8+ T-cell ratios are reversed by smoking cessation: influence of bone mass on immune cell response to and recovery from smoke exposure. *Inhalation Toxicology* 22(9): 785-96.

Gaasch JA, Lockman PR, Geldenhuys WJ, Allen DD, Van der Schyf CJ. (2007). Brain iron toxicity: differential responses of astrocytes, neurons, and endothelial cells. *Neurochemical Research* 32(7): 1196-208.

Galano E, Fidani M, Baia F, Palomba L, Marino G, Amoresano A. (2012). Qualitative screening in doping control by MALDI-TOF/TOF mass spectrometry: a proof-of-evidence. *Journal of Pharmaceutical and Biomedical Analysis* 71: 193-7.

Gardner C, Magliozzi R, Durrenberger PF, Howell OW, Rundle J, Reynolds R. (2013). Cortical grey matter demyelination can be induced by elevated pro-inflammatory cytokines in the subarachnoid space of MOG-immunized rats. *Brain* 136(12): 3596-608.

Ge Y, Jensen JH, Lu H, Helpern JA, Miles L, *et al*. (2007). Quantitative assessment of iron accumulation in the deep gray matter of multiple sclerosis by magnetic field correlation imaging. *AJNR. American Journal of Neuroradiology* 28(9): 1639-44.

Gebril OH, Simpson JE, Kirby J, Brayne C, Ince PG. (2011). Brain iron dysregulation and the risk of ageing white matter lesions. *Neuromolecular Medicine* 13(4): 289-99.

Georgetti SR, Casagrande R, Di Mambro VM, Azzolini AE, Fonseca MJ. (2003). Evaluation of the antioxidant activity of different flavonoids by the chemiluminescence method. *AAPS PharmSci* 5(2): E20.

Gerlach M, Double KL, Youdim MB, Riederer P. (2006). Potential sources of increased iron in the substantia nigra of parkinsonian patients. *Journal of Neural Transmission. Supplementum* (70): 133-42.

Gilgun-Sherki Y, Barhum Y, Atlas D, Melamed E, Offen D. (2005). Analysis of gene expression in MOG-induced experimental autoimmune encephalomyelitis after treatment with a novel brain-penetrating antioxidant. *Journal of Molecular Neuroscience* 27(1): 125-35.

Giovannoni G. (2006). Multiple sclerosis cerebrospinal fluid biomarkers. *Disease Markers* 22(4): 187-96.

Girgrah N, Letarte M, Becker LE, Cruz TF, Theriault E, Moscarello MA. (1991). Localization of the CD44 glycoprotein to fibrous astrocytes in normal white matter and to reactive astrocytes in active lesions in multiple sclerosis. *Journal of Neuropathology and Experimental Neurology* 50(6): 779-92.

Glish GL, Vachet RW. (2003). The basics of mass spectrometry in the twenty-first century. *Nature Reviews. Drug discovery* 2(2): 140-50.

Goddard DR, Berry M, Butt AM. (1999). In vivo actions of fibroblast growth factor-2 and insulin-like growth factor-I on oligodendrocyte development and myelination in the central nervous system. *J Neurosci Res 57:* 74-85.

Goertsches R, Zettl UK. (2007). MS therapy research applying genome-wide RNA profiling of peripheral blood. *Int MS J* 14(3): 98-107.

Going JJ, Lamb RF. (1996). Practical histological microdissection for PCR analysis. *The Journal of Pathology* 179: 121-4.

Goldacre MJ, Seagroatt V, Yeates D, Acheson ED. (2004). Skin cancer in people with multiple sclerosis: a record linkage study. *Journal of Epidemiology and Community Health* 58(2): 142-4.

Goncalves CA, Leite MC, Nardin P. (2008). Biological and methodological features of the measurement of S100B, a putative marker of brain injury. *Clin Biochem* 41: 755-63.

Goodwin RJ, Pennington SR, Pitt AR. (2008). Protein and peptides in pictures: imaging with MALDI mass spectrometry. *Proteomics* 8(18): 3785-800.

Goris A, Boonen S, D'Hooghe M B, Dubois B. (2010). Replication of KIF21B as a susceptibility locus for multiple sclerosis. *Journal of Medical Genetics* 47(11): 775-6.

Gotz ME, Double K, Gerlach M, Youdim MB, Riederer P. (2004). The relevance of iron in the pathogenesis of Parkinson's disease. *Annals of the New York Academy of Sciences* 1012: 193-208.

Goudriaan A, de Leeuw C, Ripke S, Hultman CM, Sklar P, *et al*. (2013). Specific Glial Functions Contribute to Schizophrenia Susceptibility. *Schizophrenia Bulletin* (Ahead of print).

Gozal YM, Dammer EB, Duong DM, Cheng D, Gearing M, *et al*. (2011). Proteomic analysis of hippocampal dentate granule cells in frontotemporal lobar degeneration: application of laser capture technology. *Frontiers in Neurology* 2(24): 1-11.

Graumann U, Reynolds R, Steck AJ, Schaeren-Wiemers N. (2003). Molecular changes in normal appearing white matter in multiple sclerosis are characteristic of neuroprotective mechanisms against hypoxic insult. *Brain Pathology* 13(4): 554-73.

Gravano DM, Hoyer KK. (2013). Promotion and prevention of autoimmune disease by CD8+ T cells. *Journal of Autoimmunity* 45: 68-79.

Greene JG, Dingledine R, Greenamyre JT. (2010). Neuron-selective changes in RNA transcripts related to energy metabolism in toxic models of parkinsonism in rodents. *Neurobiol Dis* 38: 476-81.

Grenier J, Tomkiewicz C, Trousson A, Rajkowski KM, Schumacher M, Massaad C. (2005). Identification by microarray analysis of aspartate aminotransferase and glutamine synthetase as glucocorticoid target genes in a mouse Schwann cell line. *J Steroid Biochem Mol Biol* 97: 342-52.

Grunblatt E, Zander N, Bartl J, Jie L, Monoranu CM, *et al*. (2007). Comparison analysis of gene expression patterns between sporadic Alzheimer's and Parkinson's disease. *Journal of Alzheimer's Disease* 12(4): 291-311.

Guan H, Nagarkatti PS, Nagarkatti M. (2011). CD44 Reciprocally regulates the differentiation of encephalitogenic Th1/Th17 and Th2/regulatory T cells through epigenetic modulation involving DNA methylation of cytokine gene promoters, thereby controlling the development of experimental autoimmune encephalomyelitis. *Journal of Immunology* 186(12): 6955-64.

Guazzo EP. (2005). A technique for producing demyelination of the rat optic nerves. *Journal of Clinical Neuroscience* 12(1): 54-8.

Guerra-Araiza C, Alvarez-Mejia AL, Sanchez-Torres S, Farfan-Garcia E, Mondragon-Lozano R, *et al*. (2013). Effect of natural exogenous antioxidants on aging and on neurodegenerative diseases. *Free Radical Research* 47(6-7): 451-62.

Haanstra KG, Jagessar SA, Bauch*et al*, Doussau M, Fovet CM, *et al*. (2013). Induction of Experimental Autoimmune Encephalomyelitis With Recombinant Human Myelin Oligodendrocyte Glycoprotein in Incomplete Freund's Adjuvant in Three Non-human Primate Species. *Journal of Neuroimmune Pharmacology* 8(5): 1251-64.

Haegel H, Tolg C, Hofmann M, Ceredig R. (1993). Activated mouse astrocytes and T cells express similar CD44 variants. Role of CD44 in astrocyte/T cell binding. *The Journal of Cell Biology* 122(5): 1067-77.

Hagel C, Stavrou DK. (1999). CD44 expression in primary and recurrent oligodendrogliomas and in adjacent gliotic brain tissue. *Neuropathology and Applied Neurobiology* 25: 313-8.

Haider L, Fischer MT, Frischer JM, Bauer J, Hoftberger R, *et al*. (2011). Oxidative damage in multiple sclerosis lesions. *Brain* 134(7): 1914-24.

Halinski LP, Stepnowski P. (2013). GC-MS and MALDI-TOF MS profiling of sucrose esters from Nicotiana tabacum and N. rustica. *Zeitschrift fur Naturforschung. C, Journal of Biosciences* 68(5-6): 210-22.

Halliday GM, Stevens CH. (2011). Glia: initiators and progressors of pathology in Parkinson's disease. *Movement Disorders* 26(1): 6-17.

Halliwell B. (2006). Oxidative stress and neurodegeneration: where are we now? *Journal of Neurochemistry* 97(6): 1634-58.
Hametner S, Wimmer I, Haider L, Pfeifenbring S, Bruck W, Lassmann H. (2013). Iron and neurodegeneration in the multiple sclerosis brain. *Annals of Neurology* (Ahead of print).
Hampton DW, Anderson J, Pryce G, Irvine KA, Giovannoni G, *et al*. (2008). An experimental model of secondary progressive multiple sclerosis that shows regional variation in gliosis, remyelination, axonal and neuronal loss. *J Neuroimmunol* 201-202: 200-11.
Han J, Day JR, Connor JR, Beard JL. (2002). H and L ferritin subunit mRNA expression differs in brains of control and iron-deficient rats. *The Journal of Nutrition* 132(9): 2769-74.
Han MH, Hwang SI, Roy DB, Lundgren DH, Price JV, *et al*. (2008). Proteomic analysis of active multiple sclerosis lesions reveals therapeutic targets. *Nature* 451: 1076-81.
Handel AE, Giovannoni G, Ebers GC, Ramagopalan SV. (2010a). Environmental factors and their timing in adult-onset multiple sclerosis. *Nature Reviews. Neurology* 6(3): 156-66.
Handel AE, Handunnetthi L, Giovannoni G, Ebers GC, Ramagopalan SV. (2010b). Genetic and environmental factors and the distribution of multiple sclerosis in Europe. *European Journal of Neurology* 17(9): 1210-4.
Hanrieder J, Ekegren T, Andersson M, Bergquist J. 2013a. MALDI imaging of post-mortem human spinal cord in amyotrophic lateral sclerosis. *Journal of neurochemistry* 124(5): 695-707.
Hanrieder J, Ljungdahl A, Andersson M. (2012). MALDI imaging mass spectrometry of neuropeptides in Parkinson's disease. *Journal of Visualized Experiments* (60):e3445.
Hanrieder J, Phan NT, Kurczy ME, Ewing AG. (2013b). Imaging mass spectrometry in neuroscience. *ACS Chemical Neuroscience* 4(5): 666-79.
Hardin-Pouzet H, Krakowski M, Bourbonniere L, Didier-Bazes M, Tran E, Owens T. (1997). Glutamate metabolism is down-regulated in astrocytes during experimental allergic encephalomyelitis. *Glia* 20(1): 79-85.
Harper S, Speicher DW. (2001). Detection of proteins on blot membranes. *Current Protocols in Protein Science* 10(10.8).
Harrison PJ, Procter AW, Barton AJ, Lowe SL, Najlerahim A, *et al*. (1991). Terminal coma affects messenger RNA detection in post mortem human temporal cortex. *Brain research. Molecular Brain Research* 9(1-2): 161-4.
Harrison PM, Arosio P. 1996. The ferritins: molecular properties, iron storage function and cellular regulation. *Biochimica et Biophysica Acta* 1275(3): 161-203.
Hauser SL, Oksenberg JR. (2006). The Neurobiology of Multiple Sclerosis: Genes, Inflammation, and Neurodegeneration. *Neuron* 52(1): 61-76.
Hawkes CH, Macgregor AJ. (2009). Twin studies and the heritability of MS: a conclusion. *Multiple Sclerosis* 15:661-7.
He F, Sun YE. (2007). Glial cells more than support cells? *The International Journal of Biochemistry & Cell Biology* 39: 661-5.
Hearst SM, Walker LR, Shao Q, Lopez M, Raucher D, Vig PJ. (2011). The design and delivery of a thermally responsive peptide to inhibit S100B-mediated neurodegeneration. *Neuroscience* 197: 369-80.
Hedstrom AK, Hillert J, Olsson T, Alfredsson L. (2013). Smoking and multiple sclerosis susceptibility. *European Journal of Epidemiology* 28(11): 867-74.

Hedstrom AK, Olsson T, Alfredsson L. (2012). High body mass index before age 20 is associated with increased risk for multiple sclerosis in both men and women. *Multiple Sclerosis* 18(9): 1334-6.
Heizmann CW, Fritz G, Schafer BW. (2002). S100 proteins: structure, functions and pathology. *Frontiers in Bioscience : a journal and virtual library* 7: d1356-68.
Hernandez S, Lloreta J. (2006). Manual versus laser micro-dissection in molecular biology. *Ultrastructural Pathology* 30: 221-8.
Herrmann JE, Imura T, Song B, Qi J, Ao Y, *et al*. (2008). STAT3 is a critical regulator of astrogliosis and scar formation after spinal cord injury. *The Journal of Neuroscience 28:* 7231-43.
Hertz L. (2004). Intercellular metabolic compartmentation in the brain: past, present and future. *Neurochem Int* 45: 285-96.
Hibbits N, Yoshino J, Le TQ, Armstrong RC. (2012). Astrogliosis during acute and chronic cuprizone demyelination and implications for remyelination. *ASN Neuro* 4(6): 393-408.
Hidalgo J, Aschner M, Zatta P, Vasak M. (2001). Roles of the metallothionein family of proteins in the central nervous system. *Brain Research Bulletin* 55(2): 133-45.
Hillenkamp F, Karas M, Beavis RC, Chait BT. (1991). Matrix-assisted laser desorption/ionization mass spectrometry of biopolymers. *Analytical Chemistry* 63(24): 1193A-203A.
Hinz B, Brune K. (2002). Cyclooxygenase-2--10 years later. *The Journal of Pharmacology and Experimental Therapeutics* 300(2): 367-75.
Hitzemann R, Bottomly D, Darakjian P, Walter N, Iancu O, *et al*. (2013). Genes, behavior and next-generation RNA sequencing. *Genes, Brain, and Behavior* 12(1): 1-12.
Hoepken HH, Korten T, Robinson SR, Dringen R. (2004). Iron accumulation, iron-mediated toxicity and altered levels of ferritin and transferrin receptor in cultured astrocytes during incubation with ferric ammonium citrate. *Journal of Neurochemistry* 88(5): 1194-202.
Hoffmann EdS, V. (2007). *Mass Spectrometry: Principles and Applications*. Chichester, UK: John Wiley & Sons.
Holley JE, Gveric D, Newcombe J, Cuzner ML, Gutowski NJ. (2003). Astrocyte characterization in the multiple sclerosis glial scar. *Neuropathology and Applied Neurobiology* 29: 434-44.
Honig LS, Chambliss DD, Bigio EH, Carroll SL, Elliott JL. (2000). Glutamate transporter EAAT2 splice variants occur not only in ALS, but also in AD and controls. *Neurology* 55(8): 1082-8.
Hori M, Nakamachi T, Rakwal R, Shibato J, Ogawa T, *et al*. (2012). Transcriptomics and proteomics analyses of the PACAP38 influenced ischemic brain in permanent middle cerebral artery occlusion model mice. *Journal of Neuroinflammation* 9: 256.
Hsiao HY, Chern Y. (2010). Targeting glial cells to elucidate the pathogenesis of Huntington's disease. *Mol Neurobiol* 41(2-3): 248-55.
Hu J, Ferreira A, Van Eldik LJ. (1997). S100beta induces neuronal cell death through nitric oxide release from astrocytes. *Journal of Neurochemistry* 69(6): 2294-301.
Huang da W, Sherman BT, Lempicki RA. (2009a). Bioinformatics enrichment tools: paths toward the comprehensive functional analysis of large gene lists. *Nucleic Acids Research* 37(1): 1-13.
Huang da W, Sherman BT, Lempicki RA. (2009b). Systematic and integrative analysis of large gene lists using DAVID bioinformatics resources. *Nature Protocols* 4(1): 44-57.

Hulet SW, Powers S, Connor JR. (1999). Distribution of transferrin and ferritin binding in normal and multiple sclerotic human brains. *J Neurol Sci* 165(1): 48-55.
Ibrahim SM, Mix E, Bottcher T, Koczan D, Gold R, *et al*. (2001). Gene expression profiling of the nervous system in murine experimental autoimmune encephalomyelitis. *Brain* 124(10): 1927-38.
Inglis HR, Greer JM, McCombe PA. (2012). Gene expression in the spinal cord in female lewis rats with experimental autoimmune encephalomyelitis induced with myelin basic protein. *PLoS One* 7(11): e48555.
Ingram G, Hakobyan S, Hirst CL, Harris CL, Loveless S, *et al*. (2012). Systemic complement profiling in multiple sclerosis as a biomarker of disease state. *Multiple Sclerosis* 18(10): 1401-11.
International Multiple Sclerosis Genetics C, Wellcome Trust Case Control C, Sawcer S, Hellenthal G, Pirinen M, *et al*. (2011). Genetic risk and a primary role for cell-mediated immune mechanisms in multiple sclerosis. *Nature* 476(7359): 214-9.
Iuvone T, Esposito G, De Filippis D, Bisogno T, Petrosino S, *et al*. (2007). Cannabinoid CB1 receptor stimulation affords neuroprotection in MPTP-induced neurotoxicity by attenuating S100B up-regulation in vitro. *Journal of Molecular Medicine* 85(12): 1379-92.
Izawa T, Yamate J, Franklin RJ, Kuwamura M. (2010a). Abnormal iron accumulation is involved in the pathogenesis of the demyelinating dmy rat but not in the hypomyelinating mv rat. *Brain Res* 1349: 105-14.
Izawa T, Yamate J, Franklin RJ, Kuwamura M. (2010b). Abnormal myelinogenesis both in the white and gray matter of the attractin-deficient mv rat. *Brain Res* 1312: 145-55.
Jack C, Ruffini F, Bar-Or A, Antel JP. (2005). Microglia and multiple sclerosis. *J Neurosci Res* 81(3): 363-73.
Jager A, Dardalhon V, Sobel RA, Bettelli E, Kuchroo VK. (2009). Th1, Th17, and Th9 effector cells induce experimental autoimmune encephalomyelitis with different pathological phenotypes. *Journal of Immunology* 183(11): 7169-77.
Jelinsky SA, Miyashiro JS, Saraf KA, Tunkey C, Reddy P, *et al*. (2005). Exploiting genotypic differences to identify genes important for EAE development. *J Neurol Sci* 239(1): 81-93.
Jensen CJ, Massie A, De Keyser J. (2013). Immune Players in the CNS: The Astrocyte. *Journal of Neuroimmune Pharmacology* 8(4): 824-39.
Jeong SY, David S. (2006). Age-related changes in iron homeostasis and cell death in the cerebellum of ceruloplasmin-deficient mice. *The Journal of Neuroscience* 26(38): 9810-9.
Jersild C, Svejgaard A, Fog T. (1972). HL-A antigens and multiple sclerosis. *Lancet* 1(7762): 1240-1.
John GR, Shankar SL, Shafit-Zagardo B, Massimi A, Lee SC, *et al*. (2002). Multiple sclerosis: re-expression of a developmental pathway that restricts oligodendrocyte maturation. *Nature Medicine* 8(10): 1115-21.
Johnstone D, Milward EA. (2010). Molecular genetic approaches to understanding the roles and regulation of iron in brain health and disease. *Journal of Neurochemistry* 113(6): 1387-402.
Jomova K, Valko M. (2011). Importance of iron chelation in free radical-induced oxidative stress and human disease. *Current Pharmaceutical Design* 17(31): 3460-73.
Joseph A, Gnanapragasam VJ. (2011). Laser-capture microdissection and transcriptional profiling in archival FFPE tissue in prostate cancer. *Methods in Molecular Biology* 755: 291-300.

Joseph JA, Shukitt-Hale B, Lau FC. (2007). Fruit polyphenols and their effects on neuronal signaling and behavior in senescence. *Annals of the New York Academy of Sciences* 1100: 470-85.
Joyner JC, Keuper KD, Cowan JA. (2013). Analysis of RNA cleavage by MALDI-TOF mass spectrometry. *Nucleic Acids Research* 41(1): e2.
Jucker M. (2010). The benefits and limitations of animal models for translational research in neurodegenerative diseases. *Nature Medicine* 16: 1210-4.
Juurlink BH, Schousboe A, Jorgensen OS, Hertz L. (1981). Induction by hydrocortisone of glutamine synthetase in mouse primary astrocyte cultures. *Journal of Neurochemistry* 36(1): 136-42.
Juurlink BH, Thorburne SK, Hertz L. (1998). Peroxide-scavenging deficit underlies oligodendrocyte susceptibility to oxidative stress. *Glia* 22(4): 371-8.
Kafka AP, Kleffmann T, Rades T, McDowell A. (2011). The application of MALDI TOF MS in biopharmaceutical research. *International Journal of Pharmaceutics* 417(1-2): 70-82.
Kap YS, Laman JD, t Hart BA. (2010). Experimental autoimmune encephalomyelitis in the common marmoset, a bridge between rodent EAE and multiple sclerosis for immunotherapy development. *Journal of Neuroimmune Pharmacology* 5(2): 220-30.
Ke Y, Qian ZM. (2007). Brain iron metabolism: neurobiology and neurochemistry. *Progress in Neurobiology* 83(3): 149-73.
Keays KM, Owens GP, Ritchie AM, Gilden DH, Burgoon MP. (2005). Laser capture microdissection and single-cell RT-PCR without RNA purification. *Journal of Immunological Methods* 302(1-2): 90-8.
Kettenmann H, Verkhratsky A. (2008). Neuroglia: the 150 years after. *Trends Neurosci* 31(12): 653-9.
Khalil M, Enzinger C, Langkammer C, Tscherner M, Wallner-Blazek M, *et al*. (2009). Quantitative assessment of brain iron by R(2)* relaxometry in patients with clinically isolated syndrome and relapsing-remitting multiple sclerosis. *Multiple Sclerosis* 15(9): 1048-54.
Khalil M, Langkammer C, Ropele S, Petrovic K, Wallner-Blazek M, *et al*. (2011a). Determinants of brain iron in multiple sclerosis: a quantitative 3T MRI study. *Neurology* 77(18): 1691-7.
Khalil M, Teunissen C, Langkammer C. (2011b). Iron and neurodegeneration in multiple sclerosis. *Multiple Sclerosis International* 2011(4): 1-6.
Kihara Y, Ishii S, Kita Y, Toda A, Shimada A, Shimizu T. (2005). Dual phase regulation of experimental allergic encephalomyelitis by platelet-activating factor. *The Journal of Experimental Medicine* 202(6): 853-63.
Kim MD, Cho HJ, Shin T. (2004). Expression of osteopontin and its ligand, CD44, in the spinal cords of Lewis rats with experimental autoimmune encephalomyelitis. *J Neuroimmunol* 18(3): 78-84.
Kimura H, Tooyama I, McGeer PL. (1994). Acidic FGF expression in the surroundings of senile plaques. *The Tohoku Journal of Experimental Medicine* 174(3): 279-93.
Kingsbury AE, Foster OJ, Nisbet AP, Cairns N, Bray L, *et al*. (1995). Tissue pH as an indicator of mRNA preservation in human post-mortem brain. *Brain Research. Molecular Brain Research* 28: 311-8.
Kinter J, Zeis T, Schaeren-Wiemers N. (2008). RNA profiling of MS brain tissues. *International MS Journal* 15(2): 51-8.
Kipp M, Gingele S, Pott F, Clarner T, van der Valk P, *et al*. (2011). BLBP-expression in astrocytes during experimental demyelination and in human multiple sclerosis lesions. *Brain, Behavior, and Immunity* 25(8): 1554-68.

Kirby J, Ning K, Ferraiuolo L, Heath PR, Ismail A, *et al*. (2011). Phosphatase and tensin homologue/protein kinase B pathway linked to motor neuron survival in human superoxide dismutase 1-related amyotrophic lateral sclerosis. *Brain* 134(2): 506-17.

Klegeris A, McGeer PL. (2005). Non-steroidal anti-inflammatory drugs (NSAIDs) and other anti-inflammatory agents in the treatment of neurodegenerative disease. *Curr Alzheimer Res* 2(3): 355-65.

Koch M, Mostert J, Heersema D, Teelken A, De Keyser J. (2007). Plasma S100beta and NSE levels and progression in multiple sclerosis. *J Neurol Sci* 252(2): 154-8.

Koeppen AH. (1995). The history of iron in the brain. *J Neurol Sci* 134: Suppl: 1-9.

Kohler LB, Berezin V, Bock E, Penkowa M. (2003). The role of metallothionein II in neuronal differentiation and survival. *Brain Res* 992(1): 128-36.

Kondo H, Takahashi H, Takahashi Y. (1984). Immunohistochemical study of S-100 protein in the postnatal development of Muller cells and astrocytes in the rat retina. *Cell and Tissue Research* 238(3): 503-8.

Koning N, Bo L, Hoek RM, Huitinga I. (2007). Downregulation of macrophage inhibitory molecules in multiple sclerosis lesions. *Annals of Neurology* 62(5): 504-14.

Koob AO, Bruns L, Prassler C, Masliah E, Klopstock T, Bender A. (2012). Protein analysis through Western blot of cells excised individually from human brain and muscle tissue. *Analytical Biochemistry* 425(2): 120-4.

Koppelkamm A, Vennemann B, Lutz-Bonengel S, Fracasso T, Vennemann M. (2011). RNA integrity in post-mortem samples: influencing parameters and implications on RT-qPCR assays. *International Journal of Legal Medicine* 125(4): 573-80.

Korn T, Magnus T, Jung S. (2005). Autoantigen specific T cells inhibit glutamate uptake in astrocytes by decreasing expression of astrocytic glutamate transporter GLAST: a mechanism mediated by tumor necrosis factor-alpha. *FASEB Journal* 19(13): 1878-80.

Kort JJ, Kawamura K, Fugger L, Weissert R, Forsthuber TG. (2006). Efficient presentation of myelin oligodendrocyte glycoprotein peptides but not protein by astrocytes from HLA-DR2 and HLA-DR4 transgenic mice. *J Neuroimmunol* 173(1-2): 23-34.

Kostic M, Zivkovic N, Stojanovic I. (2012). Multiple sclerosis and glutamate excitotoxicity. *Reviews in the Neurosciences* 24(1): 1-18.

Koyama Y, Kimura Y, Baba A. (1997). Induction of glutamine synthetase by L-alpha-aminoadipate in developmental stages of cultured astrocytes. *Neuroscience Letters 223:* 65-8.

Kremenchutzky M, Rice GP, Baskerville J, Wingerchuk DM, Ebers GC. (2006). The natural history of multiple sclerosis: a geographically based study 9: observations on the progressive phase of the disease. *Brain* 129(3): 584-94.

Krementsov DN, Thornton TM, Teuscher C, Rincon M. (2013). The Emerging Role of p38 Mitogen-Activated Protein Kinase in Multiple Sclerosis and Its Models. *Molecular and Cellular Biology* 33(19): 3728-34.

Kress-Bennett JM, Ehrlich GD, Bruno A, Post JC, Hu FZ, Scott TF. (2011). Preliminary study: treatment with intramuscular interferon beta-1a results in increased levels of IL-12Rbeta2+ and decreased levels of IL23R+ CD4+ T - Lymphocytes in multiple sclerosis. *BMC Neurology* 11(155): 1-7.

Krieglstein K, Strelau J, Schober A, Sullivan A, Unsicker K. (2002). TGF-beta and the regulation of neuron survival and death. *Journal of Physiology* 96(1-2): 25-30.

Krupenko SA. (2009). FDH: an aldehyde dehydrogenase fusion enzyme in folate metabolism. *Chem Biol Interact* 178: 84-93.

Krupenko SA, Oleinik NV. (2002). 10-formyltetrahydrofolate dehydrogenase, one of the major folate enzymes, is down-regulated in tumor tissues and possesses suppressor effects on cancer cells. *Cell Growth & Differentiation* 13(5): 227-36.
Kuhlmann T, Goldschmidt T, Antel J, Wegner C, König F, *et al*. (2009). Gender differences in the histopathology of MS? *Journal of the Neurological Sciences* 286(1-2): 86-91.
Kuhlmann T, Lingfeld G, Bitsch A, Schuchardt J, Bruck W. (2002). Acute axonal damage in multiple sclerosis is most extensive in early disease stages and decreases over time. *Brain* 125(10): 2202-12.
Kuhn A, Kumar A, Beilina A, Dillman A, Cookson MR, Singleton AB. (2012). Cell population-specific expression analysis of human cerebellum. *BMC Genomics* 13(1): 1-15.
Kumar A, Gibbs JR, Beilina A, Dillman A, Kumaran R, *et al*. (2013). Age-associated changes in gene expression in human brain and isolated neurons. *Neurobiol Aging* 34(4): 1199-209.
Kurnellas MP, Donahue KC, Elkabes S. (2007). Mechanisms of neuronal damage in multiple sclerosis and its animal models: role of calcium pumps and exchangers. *Biochemical Society Transactions* 35(5): 923-6.
Kutzelnigg A, Lucchinetti CF, Stadelmann C, Bruck W, Rauschka H, *et al*. (2005). Cortical demyelination and diffuse white matter injury in multiple sclerosis. *Brain* 128(11): 2705-12.
Langrish CL, Chen Y, Blumenschein WM, Mattson J, Basham B, *et al*. (2005). IL-23 drives a pathogenic T cell population that induces autoimmune inflammation. *The Journal of Experimental Medicine* 201(2): 233-40.
Larochelle C, Alvarez JI, Prat A. (2011). How do immune cells overcome the blood-brain barrier in multiple sclerosis? *FEBS Letters* 585(23): 3770-80.
Larsen PH, Wells JE, Stallcup WB, Opdenakker G, Yong VW. (2003). Matrix metalloproteinase-9 facilitates remyelination in part by processing the inhibitory NG2 proteoglycan. *The Journal of Neuroscience 23:* 11127-35.
Lasiene J, Yamanaka K. (2011). Glial cells in amyotrophic lateral sclerosis. *Neurology Research International* 2011: 1-7.
Lassmann H. (1999). Mechanisms of demyelination and tissue damage in multiple sclerosis. *Acta Neurol Belg* 99(1): 6-10.
Lassmann H. (2011). Review: the architecture of inflammatory demyelinating lesions: implications for studies on pathogenesis. *Neuropathology and Applied Neurobiology* 37(7): 698-710.
Lassmann H, Ransohoff RM. (2004). The CD4-Th1 model for multiple sclerosis: a critical [correction of crucial] re-appraisal. *Trends in Immunology* 25(3): 132-7.
Lassmann H, van Horssen J. (2011). The molecular basis of neurodegeneration in multiple sclerosis. *FEBS Letters* 585(23): 3715-23.
Lassmann H, van Horssen J, Mahad D. (2012). Progressive multiple sclerosis: pathology and pathogenesis. *Nature Reviews. Neurology* 8(11): 647-56.
Lau A, Tymianski M. 2010. Glutamate receptors, neurotoxicity and neurodegeneration. *Pflugers Archiv : European Journal of Physiology* 460(2): 525-42.
Lau CL, Perreau VM, Chen MJ, Cate HS, Merlo D, *et al*. (2012). Transcriptomic profiling of astrocytes treated with the Rho kinase inhibitor fasudil reveals cytoskeletal and pro-survival responses. *Journal of Cellular Physiology* 227(3): 1199-211.
Lavrnja I, Savic D, Bjelobaba I, Dacic S, Bozic I, *et al*. (2012). The effect of ribavirin on reactive astrogliosis in experimental autoimmune encephalomyelitis. *Journal of Pharmacological Sciences* 119(3): 221-32.

Leitner DF, Connor JR. (2012). Functional roles of transferrin in the brain. *Biochimica et Biophysica Acta* 1820(3): 393-402.
Lesley J, Hyman R, Kincade PW. (1993). CD44 and its interaction with extracellular matrix. *Advances in Immunology* 54: 271-335.
Levenson CW, Tassabehji NM. (2004). Iron and ageing: an introduction to iron regulatory mechanisms. *Ageing Rresearch Reviews* 3(3): 251-63.
Leverenz JB, Umar I, Wang Q, Montine TJ, McMillan PJ, *et al*. (2007). Proteomic identification of novel proteins in cortical lewy bodies. *Brain Pathology* 17(2): 139-45.
Levi S, Santambrogio P, Cozzi A, Rovida E, Corsi B, *et al*. (1994). The role of the L-chain in ferritin iron incorporation. Studies of homo and heteropolymers. *Journal of Molecular Biology* 238(5): 649-54.
LeVine SM, Bilgen M, Lynch SG. (2013). Iron accumulation in multiple sclerosis: an early pathogenic event. *Expert Review of Neurotherapeutics* 13(3): 247-50.
LeVine SM, Lynch SG, Ou CN, Wulser MJ, Tam E, Boo N. (1999). Ferritin, transferrin and iron concentrations in the cerebrospinal fluid of multiple sclerosis patients. *Brain Res* 821(2): 511-5.
Li H, Newcombe J, Groome NP, Cuzner ML. (1993). Characterization and distribution of phagocytic macrophages in multiple sclerosis plaques. *Neuropathology and Applied Neurobiology* 19(3): 214-23.
Li H, Wang Q, Gao F, Zhu F, Wang X, *et al*. (2008a). Reduced expression of PDCD5 is associated with high-grade astrocytic gliomas. *Oncology Reports* 20(3): 573-9.
Li L, Lundkvist A, Andersson D, Wilhelmsson U, Nagai N, *et al*. (2008b). Protective role of reactive astrocytes in brain ischemia. *Journal of Cerebral Blood Flow and Metabolism* 28(3): 468-81.
Li X, Jankovic J, Le W. (2011). Iron chelation and neuroprotection in neurodegenerative diseases. *J Neural Transm* 118(3): 473-7.
Li Z, Chen-Roetling J, Regan RF. (2009). Increasing expression of H- or L-ferritin protects cortical astrocytes from hemin toxicity. *Free Radical Research* 43(6): 613-21.
Liang AL, Vavasour IM, Madler B, Traboulsee AL, Lang DJ, *et al*. (2012). Short-term stability of T1 and T2 relaxation measures in multiple sclerosis normal appearing white matter. *J Neurol* 259(6): 1151-8.
Liddell JR, Dringen R, Crack PJ, Robinson SR. (2006a). Glutathione peroxidase 1 and a high cellular glutathione concentration are essential for effective organic hydroperoxide detoxification in astrocytes. *Glia* 54(8): 873-9.
Liddell JR, Hoepken HH, Crack PJ, Robinson SR, Dringen R. (2006b). Glutathione peroxidase 1 and glutathione are required to protect mouse astrocytes from iron-mediated hydrogen peroxide toxicity. *J Neurosci Res* 84(3): 578-86.
Liedtke W, Edelmann W, Bieri PL, Chiu FC, Cowan NJ, *et al*. (1996). GFAP is necessary for the integrity of CNS white matter architecture and long-term maintenance of myelination. *Neuron* 17(4): 607-15.
Lillig CH, Berndt C, Holmgren A. 2008. Glutaredoxin systems. *Biochimica et Biophysica Acta* 1780(11): 1304-17.
Lim ET, Grant D, Pashenkov M, Keir G, Thompson EJ, *et al*. (2004). Cerebrospinal fluid levels of brain specific proteins in optic neuritis. *Multiple Sclerosis* 10(3): 261-5.
Lindberg RL, De Groot CJ, Certa U, Ravid R, Hoffmann F, *et al*. (2004). Multiple sclerosis as a generalized CNS disease--comparative microarray analysis of normal appearing white matter and lesions in secondary progressive MS. *J Neuroimmunol* 152: 154-67.

Linker RA, Brechlin P, Jesse S, Steinacker P, Lee DH, *et al*. (2009). Proteome profiling in murine models of multiple sclerosis: identification of stage specific markers and culprits for tissue damage. *PLoS ONE* 4(10): e7624.

Lipman NS, Jackson LR, Trudel LJ, Weis-Garcia F. (2005). Monoclonal versus polyclonal antibodies: distinguishing characteristics, applications, and information resources. *ILAR Journal* 46(3): 258-68.

Lisak RP, Benjamins JA, Bealmear B, Nedelkoska L, Studzinski D, *et al*. (2009). Differential effects of Th1, monocyte/macrophage and Th2 cytokine mixtures on early gene expression for molecules associated with metabolism, signaling and regulation in central nervous system mixed glial cell cultures. *Journal of Neuroinflammation* 6:4.

Lisak RP, Benjamins JA, Bealmear B, Nedelkoska L, Yao B, *et al*. (2007). Differential effects of Th1, monocyte/macrophage and Th2 cytokine mixtures on early gene expression for glial and neural-related molecules in central nervous system mixed glial cell cultures: neurotrophins, growth factors and structural proteins. *Journal of Neuroinflammation* 4:30.

Lisak RP, Benjamins JA, Bealmear B, Yao B, Land S, *et al*. (2006). Differential effects of Th1, monocyte/macrophage and Th2 cytokine mixtures on early gene expression for immune-related molecules by central nervous system mixed glial cell cultures. *Multiple Sclerosis* 12(2): 149-68.

Liu MT, Keirstead HS, Lane TE. (2001). Neutralization of the chemokine CXCL10 reduces inflammatory cell invasion and demyelination and improves neurological function in a viral model of multiple sclerosis. *Journal of Immunology* 167(7): 4091-7.

Liu NQ, Braakman RB, Stingl C, Luider TM, Martens JW, *et al*. (2012). Proteomics pipeline for biomarker discovery of laser capture microdissected breast cancer tissue. *Journal of Mammary Gland Biology and Neoplasia* 17(2): 155-64.

Liu S, Bai S, Qin Z, Yang Y, Cui Y, Qin Y. (2009). Quantitative proteomic analysis of the cerebrospinal fluid of patients with multiple sclerosis. *J Cell Mol Med* 13(8A): 1586-603.

Liu X, Lindberg R, Xiao BG, Steffensen KR, Leppert D, *et al*. (2006). CD24 and myosin light polypeptide 2 are involved in prevention of experimental autoimmune encephalomyelitis by myelin basic protein-pulsed dendritic cells. *J Neuroimmunol* 172(1-2): 137-44.

Lleo A, Galea E, Sastre M. (2007). Molecular targets of non-steroidal anti-inflammatory drugs in neurodegenerative diseases. *Cellular and Molecular Life Sciences* 64(11): 1403-18.

Loboda AV, Krutchinsky AN, Bromirski M, Ens W, Standing KG. (2000). A tandem quadrupole/time-of-flight mass spectrometer with a matrix-assisted laser desorption/ionization source: design and performance. *Rapid Communications in Mass Spectrometry* 14(12): 1047-57.

Lock C, Hermans G, Pedotti R, Brendolan A, Schadt E, *et al*. (2002). Gene-microarray analysis of multiple sclerosis lesions yields new targets validated in autoimmune encephalomyelitis. *Nature Medicine* 8(5): 500-8.

Lock CB, Heller RA. (2003). Gene microarray analysis of multiple sclerosis lesions. *Trends in Molecular Medicine* 9(12): 535-41.

Lord GM, Matarese G, Howard JK, Baker RJ, Bloom SR, Lechler RI. (1998). Leptin modulates the T-cell immune response and reverses starvation-induced immunosuppression. *Nature* 394(6696): 897-901.

Lucchinetti C, Bruck W, Parisi J, Scheithauer B, Rodriguez M, Lassmann H. (2000). Heterogeneity of multiple sclerosis lesions: implications for the pathogenesis of demyelination. *Annals of Neurology* 47(6): 707-17.

Ludwin SK. (2006). The pathogenesis of multiple sclerosis: relating human pathology to experimental studies. *Journal of Neuropathology and Experimental Neurology* 65(4): 305-18.
Luissint AC, Artus C, Glacial F, Ganeshamoorthy K, Couraud PO. (2012). Tight junctions at the blood brain barrier: physiological architecture and disease-associated dysregulation. *Fluids and Barriers of the CNS* 9(1): 23.
Lund H, Krakauer M, Skimminge A, Sellebjerg F, Garde E, *et al*. (2013). Blood-brain barrier permeability of normal appearing white matter in relapsing-remitting multiple sclerosis. *PLoS One* 8(2): e56375.
Ma YS, Wu SB, Lee WY, Cheng JS, Wei YH. (2009). Response to the increase of oxidative stress and mutation of mitochondrial DNA in aging. *Biochimica et Biophysica Acta* 1790(10): 1021-9.
Madeddu R, Farace C, Tolu P, Solinas G, Asara Y, *et al*. (2013). Cytoskeletal proteins in the cerebrospinal fluid as biomarker of multiple sclerosis. *Neurological Sciences* 34(2): 181-6.
Mahad D, Lassmann H, Turnbull D. (2008). Review: Mitochondria and disease progression in multiple sclerosis. *Neuropathology and Applied Neurobiology* 34(6): 577-89.
Mahad DJ, Ziabreva I, Campbell G, Lax N, White K, *et al*. (2009). Mitochondrial changes within axons in multiple sclerosis. *Brain* 132(5): 1161-74.
Mahmood T, Yang PC. (2012). Western blot: technique, theory, and trouble shooting. *North American Journal of Medical Sciences* 4(9): 429-34.
Mahon BD, Gordon SA, Cruz J, Cosman F, Cantorna MT. (2003). Cytokine profile in patients with multiple sclerosis following vitamin D supplementation. *J Neuroimmunol* 134(1-2): 128-32.
Mainini V, Bovo G, Chinello C, Gianazza E, Grasso M, *et al*. (2013). Detection of high molecular weight proteins by MALDI imaging mass spectrometry. *Molecular BioSystems* 9(6): 1101-7.
Majava V, Polverini E, Mazzini A, Nanekar R, Knoll W, *et al*. (2010). Structural and functional characterization of human peripheral nervous system myelin protein P2. *PLoS One* 5(4): e10300.
Makkink-Nombrado SV, Baak JP, Schuurmans L, Theeuwes JW, van der Aa. (1995). Quantitative immunohistochemistry using the CAS 200/486 image analysis system in invasive breast carcinoma: a reproducibilty study. *Anal Cell Pathol.* 8(3):227-245.
Malmestrom C, Haghighi S, Rosengren L, Andersen O, Lycke J. (2003). Neurofilament light protein and glial fibrillary acidic protein as biological markers in MS. *Neurology* 61(12): 1720-5.
Maragakis NJ, Dietrich J, Wong V, Xue H, Mayer-Proschel M, *et al*. (2004a). Glutamate transporter expression and function in human glial progenitors. *Glia* 45(2): 133-43.
Maragakis NJ, Dykes-Hoberg M, Rothstein JD. (2004b). Altered expression of the glutamate transporter EAAT2b in neurological disease. *Annals of Neurology* 55(4): 469-77.
Martinet W, Abbeloos V, Van Acker N, De Meyer GR, Herman AG, Kockx MM. (2004). Western blot analysis of a limited number of cells: a valuable adjunct to proteome analysis of paraffin wax-embedded, alcohol-fixed tissue after laser capture microdissection. *The Journal of Pathology* 202(3): 382-8.
Marz P, Heese K, Dimitriades-Schmutz B, Rose-John S, Otten U. (1999). Role of interleukin-6 and soluble IL-6 receptor in region-specific induction of astrocytic differentiation and neurotrophin expression. *Glia* 26: 191-200.

Mashayekhi F, Hadavi M, Vaziri HR, Naji M. (2010). Increased acidic fibroblast growth factor concentrations in the serum and cerebrospinal fluid of patients with Alzheimer's disease. *Journal of Clinical Neuroscience* 17(3): 357-9.

Mason JL, Suzuki K, Chaplin DD, Matsushima GK. (2001). Interleukin-1beta promotes repair of the CNS. *The Journal of Neuroscience* 21: 7046-52.

Matarese G, Di Giacomo A, Sanna V, Lord GM, Howard JK, *et al*. (2001a.) Requirement for leptin in the induction and progression of autoimmune encephalomyelitis. *Journal of Immunology* 166(10): 5909-16.

Matarese G, Sanna V, Di Giacomo A, Lord GM, Howard JK, *et al*. (2001b). Leptin potentiates experimental autoimmune encephalomyelitis in SJL female mice and confers susceptibility to males. *European Journal of Immunology* 31(5): 1324-32.

Matejuk A, Dwyer J, Zamora A, Vandenbark AA, Offner H. (2002). Evaluation of the effects of 17beta-estradiol (17beta-e2) on gene expression in experimental autoimmune encephalomyelitis using DNA microarray. *Endocrinology* 143(1): 313-9.

Matejuk A, Hopke C, Dwyer J, Subramanian S, Jones RE, *et al*. (2003). CNS gene expression pattern associated with spontaneous experimental autoimmune encephalomyelitis. *J Neurosci Res* 73(5): 667-78.

Matsumoto T, Imagama S, Hirano K, Ohgomori T, Natori T, *et al*. (2012). CD44 expression in astrocytes and microglia is associated with ALS progression in. *Neuroscience Letters* 520(1): 115-20.

Mattsson N, Andreasson U, Persson S, Carrillo MC, Collins S, *et al*. (2013). CSF biomarker variability in the Alzheimer's Association quality control program. *Alzheimer's & Dementia* 9(3): 251-61.

Matute C, Sanchez-Gomez MV, Martinez-Millan L, Miledi R. (1997). Glutamate receptor-mediated toxicity in optic nerve oligodendrocytes. *Proceedings of the National Academy of Sciences of the United States of America* 94(16): 8830-5.

Matute C. (2006). Oligodendrocyte NMDA receptors: a novel thereputic target. *Trends Mol Med* 12:289-292.

Mazurek N, Frisk AL, Beekman JM, Hartwig A, Meyer K. (2013). Comparison of progestin transcriptional profiles in rat mammary gland using Laser Capture Microdissection and whole tissue-sampling. *Experimental and Toxicologic Pathology* 65(7-8): 949-960.

McDonald JW, Althomsons SP, Hyrc KL, Choi DW, Goldberg MP. (1998). Oligodendrocytes from forebrain are highly vulnerable to AMPA/kainate receptor-mediated excitotoxicity. *Nature Medicine* 4(3): 291-7.

McFarland HF, Martin R. (2007). Multiple sclerosis: a complicated picture of autoimmunity. *Nature Immunology* 8(9): 913-9.

McQuaid S, Cunnea P, McMahon J, Fitzgerald U. (2009). The effects of blood-brain barrier disruption on glial cell function in multiple sclerosis. *Biochemical Society Transactions* 37(1): 329-31.

McRae BL, Kennedy MK, Tan LJ, Dal Canto MC, Picha KS, Miller SD. (1992). Induction of active and adoptive relapsing experimental autoimmune encephalomyelitis (EAE) using an encephalitogenic epitope of proteolipid protein. *J Neuroimmunol* 38(3): 229-40.

Mecha M, Carrillo-Salinas FJ, Mestre L, Feliu A, Guaza C. (2013). Viral models of multiple sclerosis: neurodegeneration and demyelination in mice infected with Theiler's virus. *Progress in Neurobiology* 101-102: 46-64.

Mehta A, Prabhakar M, Kumar P, Deshmukh R, Sharma PL. (2013). Excitotoxicity: bridge to various triggers in neurodegenerative disorders. *European Journal of Pharmacology* 698(1-3): 6-18.

Melief J, Schuurman KG, van de Garde MD, Smolders J, van Eijk M, *et al*. (2013). Microglia in normal appearing white matter of multiple sclerosis are alerted but immunosuppressed. *Glia* 61(11): 1848-61.
Mercer LD, Kelly BL, Horne MK, Beart PM. (2005). Dietary polyphenols protect dopamine neurons from oxidative insults and apoptosis: investigations in primary rat mesencephalic cultures. *Biochemical Pharmacology* 69(2): 339-45.
Messersmith DJ, Murtie JC, Le TQ, Frost EE, Armstrong RC. (2000). Fibroblast growth factor 2 (FGF2) and FGF receptor expression in an experimental demyelinating disease with extensive remyelination. *J Neurosci Res* 62: 241-56.
Mestas J, Hughes CC. (2004). Of mice and not men: differences between mouse and human immunology. *Journal of Immunology* 172(5): 2731-8.
Michel C, Desdouets C, Sacre-Salem B, Gautier JC, Roberts R, Boitier E. (2003). Liver gene expression profiles of rats treated with clofibric acid: comparison of whole liver and laser capture microdissected liver. *The American Journal of Pathology* 163(6): 2191-9.
Michetti F, Massaro A, Murazio M. (1979). The nervous system-specific S-100 antigen in cerebrospinal fluid of multiple sclerosis patients. *Neuroscience Letters* 11(2): 171-5.
Migheli A, Cordera S, Bendotti C, Atzori C, Piva R, Schiffer D. (1999). S-100beta protein is upregulated in astrocytes and motor neurons in the spinal cord of patients with amyotrophic lateral sclerosis. *Neuroscience Letters* 261(1-2): 25-8.
Mikesh LM, Aramadhaka LR, Moskaluk C, Zigrino P, Mauch C, Fox JW. (2013). Proteomic anatomy of human skin. *Journal of Proteomics* 84: 190-200.
Mikkat S, Lorenz P, Scharf C, Yu X, Glocker MO, Ibrahim SM. (2010). MS characterization of qualitative protein polymorphisms in the spinal cords of inbred mouse strains. *Proteomics* 10(5): 1050-62.
Mikkelsen HB, Larsen, JO, Froh P, Nguyen TH. (2011). Quantitative assessment of macrophages in the muscularis externa of mouse intestines. *The Anatomical Record* 294:1557-1565.
Miljkovic D, Timotijevic G, Stojkovic MM. (2011). Astrocytes in the tempest of multiple sclerosis. *FEBS Letters* 585(23): 3781-3788.
Miller DH, Thompson AJ, Filippi M. (2003). Magnetic resonance studies of abnormalities in the normal appearing white matter and grey matter in multiple sclerosis. *J Neurol* 250(12): 1407-19.
Miller E. (2012). Multiple sclerosis. *Advances in Experimental Medicine and Biology* 724: 222-38.
Miller E, Wachowicz B, Majsterek I. (2013). Advances in Antioxidative Therapy of Multiple Sclerosis. *Current Medicinal Chemistry* 20(37): 4720-30.
Mills E, Dong XP, Wang F, Xu H. (2010). Mechanisms of brain iron transport: insight into neurodegeneration and CNS disorders. *Future Medicinal Chemistry* 2(1): 51-64.
Milo R, Kahana E. (2010). Multiple sclerosis: Geoepidemiology, genetics and the environment. *Autoimmunity Reviews* 9(5): A387-A94.
Minagar A, Alexander JS. (2003). Blood-brain barrier disruption in multiple sclerosis. *Multiple Sclerosis* 9(6): 540-9.
Minghetti L. (2004). Cyclooxygenase-2 (COX-2) in inflammatory and degenerative brain diseases. *Journal of Neuropathology and Experimental Neurology* 63(9): 901-10.
Missler U, Wandinger KP, Wiesmann M, Kaps M, Wessel K. (1997). Acute exacerbation of multiple sclerosis increases plasma levels of S-100 protein. *Acta Neurologica Scandinavica* 96(3): 142-4.

Mistry N, Tallantyre EC, Dixon JE, Galazis N, Jaspan T, *et al*. (2011). Focal multiple sclerosis lesions abound in 'normal appearing white matter'. *Multiple Sclerosis* 17(11): 1313-23.
Mitosek-Szewczyk K, Sulkowski G, Stelmasiak Z, Struzynska L. (2008). Expression of glutamate transporters GLT-1 and GLAST in different regions of rat brain during the course of experimental autoimmune encephalomyelitis. *Neuroscience* 155(1): 45-52.
Mix E, Ibrahim S, Pahnke J, Koczan D, Sina C, *et al*. (2004). Gene-expression profiling of the early stages of MOG-induced EAE proves EAE-resistance as an active process. *J Neuroimmunol* 151(1-2): 158-70.
Mix E, Ibrahim SM, Pahnke J, Glass A, Mazon-Pelaez I, *et al*. (2006). 3-Hydroxy-3-methylglutaryl coenzyme A reductase inhibitor Atorvastatin mediated effects depend on the activation status of target cells in PLP-EAE. *Journal of Autoimmunity* 27(4): 251-65.
Mojsilovic-Petrovic J, Nesic M, Pen A, Zhang W, Stanimirovic D. (2004). Development of rapid staining protocols for laser-capture microdissection of brain vessels from human and rat coupled to gene expression analyses. *J Neurosci Methods* 133(1-2): 39-48.
Moore CS, Abdullah SL, Brown A, Arulpragasam A, Crocker SJ. (2011). How factors secreted from astrocytes impact myelin repair. *J Neurosci Res* 89(1): 13-21.
Moos T. (2002). Brain iron homeostasis. *Danish Medical Bulletin* 49(4): 279-301.
Moos T, Morgan EH. (1998). Evidence for low molecular weight, non-transferrin-bound iron in rat brain and cerebrospinal fluid. *J Neurosci Res* 54(4): 486-94.
Moos T, Morgan EH. (2004). The significance of the mutated divalent metal transporter (DMT1) on iron transport into the Belgrade rat brain. *Journal of Neurochemistry* 88(1): 233-45.
Moos T, Rosengren Nielsen T, Skjorringe T, Morgan EH. (2007). Iron trafficking inside the brain. *Journal of Neurochemistry* 103(5): 1730-40.
Moos T, Skjoerringe T, Gosk S, Morgan EH. (2006). Brain capillary endothelial cells mediate iron transport into the brain by segregating iron from transferrin without the involvement of divalent metal transporter 1. *Journal of Neurochemistry* 98(6): 1946-58.
Morelli A, Ravera S, Calzia D, Panfoli I. (2012). Impairment of heme synthesis in myelin as potential trigger of multiple sclerosis. *Medical Hypotheses* 78(6): 707-10.
Mouledous L, Hunt S, Harcourt R, Harry J, Williams KL, Gutstein HB. (2003a). Navigated laser capture microdissection as an alternative to direct histological staining for proteomic analysis of brain samples. *Proteomics* 3(5): 610-5.
Mouledous L, Hunt S, Harcourt R, Harry JL, Williams KL, Gutstein HB. (2002). Lack of compatibility of histological staining methods with proteomic analysis of laser-capture microdissected brain samples. *Journal of Biomolecular Techniques* 13(4): 258-64.
Mouledous L, Hunt S, Harcourt R, Harry JL, Williams KL, Gutstein HB. (2003b). Proteomic analysis of immunostained, laser-capture microdissected brain samples. *Electrophoresis* 24(1-2): 296-302.
Mu Y, Chen Y, Zhang G, Zhan X, Li Y, *et al*. (2013). Identification of stromal differentially expressed proteins in the colon carcinoma by quantitative proteomics. *Electrophoresis* 34(11): 1679-92.
Munger KL. (2013). Childhood obesity is a risk factor for multiple sclerosis. *Multiple Sclerosis* 19(13): 1800.
Munger KL, Chitnis T, Ascherio A. (2009). Body size and risk of MS in two cohorts of US women. *Neurology* 73(19): 1543-50.

Munro KM, Perreau VM. (2009). Current and future applications of transcriptomics for discovery in CNS disease and injury. *Neurosignals* 17(4): 311-27.
Murray GI. (2007). An overview of laser microdissection technologies *Acta Histochem*, 109: 171-6.
Muscoli C, Visalli V, Colica C, Nistico R, Palma E, *et al*. (2005). The effect of inflammatory stimuli on NMDA-related activation of glutamine synthase in human cultured astroglial cells. *Neuroscience Letters* 373(3): 184-8.
Mycko MP, Brosnan CF, Raine CS, Fendler W, Selmaj KW. (2012). Transcriptional profiling of microdissected areas of active multiple sclerosis lesions reveals activation of heat shock protein genes. *J Neurosci Res* 90(10): 1941-8.
Mycko MP, Papoian R, Boschert U, Raine CS, Selmaj KW. (2003). cDNA microarray analysis in multiple sclerosis lesions: detection of genes associated with disease activity. *Brain* 126(5): 1048-57.
Mycko MP, Papoian R, Boschert U, Raine CS, Selmaj KW. (2004). Microarray gene expression profiling of chronic active and inactive lesions in multiple sclerosis. *Clinical Neurology & Neurosurgery* 106(3): 223-9.
Naert G, Rivest S. (2011). The role of microglial cell subsets in Alzheimer's disease. *Curr Alzheimer Res* 8: 151-5.
Nair A, Frederick TJ, Miller SD. (2008). Astrocytes in multiple sclerosis: a product of their environment. *Cellular & Molecular Life Sciences* 65(17): 2702-20.
Naito S, Namerow N, Mickey MR, Terasaki PI. (1972). Multiple sclerosis: association with HL-A3. *Tissue Antigens* 2(1): 1-4.
Nanitsos EK, Nguyen KT, St'astny F, Balcar VJ. (2005). Glutamatergic hypothesis of schizophrenia: involvement of Na+/K+-dependent glutamate transport. *Journal of Biomedical Science* 12(6): 975-84.
Nash B, Ioannidou K, Barnett SC. (2011a). Astrocyte phenotypes and their relationship to myelination. *Journal of Anatomy* 219(1): 44-52.
Nash B, Thomson CE, Linington C, Arthur AT, McClure JD, *et al*. (2011b). Functional duality of astrocytes in myelination. *The Journal of Neuroscience* 31(37): 13028-38.
Navarrete-Talloni MJ, Kalkuhl A, Deschl U, Ulrich R, Kummerfeld M, *et al*. (2010). Transient peripheral immune response and central nervous system leaky compartmentalization in a viral model for multiple sclerosis. *Brain Pathology* 20(5): 890-901.
Nawshad A, LaGamba D, Olsen BR, Hay ED. (2004). Laser capture microdissection (LCM) for analysis of gene expression in specific tissues during embryonic epithelial-mesenchymal transformation. *Developmental Dynamics* 230(3): 529-34.
Nedergaard M, Ransom B, Goldman SA. (2003). New roles for astrocytes: redefining the functional architecture of the brain. *Trends in Neurosciences* 26(10): 523-30.
Nessler S, Bruck W. (2010). Advances in multiple sclerosis research in 2009. *J Neurol* 257(9): 1590-3.
Neumann H, Medana IM, Bauer J, Lassmann H. (2002). Cytotoxic T lymphocytes in autoimmune and degenerative CNS diseases. *Trends Neurosci* 25(6): 313-9.
Newcombe J, Uddin A, Dove R, Patel B, Turski L, *et al*. (2008). Glutamate receptor expression in multiple sclerosis lesions. *Brain Pathology* 18(1): 52-61.
Neymeyer V, Tephly TR, Miller MW. (1997). Folate and 10-formyltetrahydrofolate dehydrogenase (FDH) expression in the central nervous system of the mature rat *Brain Res* 766: 195-204.
Nicot A, Kurnellas M, Elkabes S. (2005). Temporal pattern of plasma membrane calcium ATPase 2 expression in the spinal cord correlates with the course of

clinical symptoms in two rodent models of autoimmune encephalomyelitis. *The European Journal of Neuroscience* 21(10): 2660-70.
Nicot A, Ratnakar PV, Ron Y, Chen CC, Elkabes S. (2003). Regulation of gene expression in experimental autoimmune encephalomyelitis indicates early neuronal dysfunction. *Brain* 126(2): 398-412.
Nijveldt RJ, van Nood E, van Hoorn DE, Boelens PG, van Norren K, van Leeuwen PA. (2001). Flavonoids: a review of probable mechanisms of action and potential applications. *The American Journal of Clinical Nutrition* 74(4): 418-25.
Nikcevich KM, Gordon KB, Tan L, Hurst SD, Kroepfl JF, *et al*. (1997). IFN-gamma-activated primary murine astrocytes express B7 costimulatory molecules and prime naive antigen-specific T cells. *Journal of Immunology* 158(2): 614-21.
Nimmerjahn A, Kirchhoff F, Helmchen F. (2005). Resting microglial cells are highly dynamic surveillants of brain parenchyma in vivo. *Science* 308(5726): 1314-8.
Nishie M, Mori F, Ogawa M, Sannohe S, Tanno K, *et al*. (2004). Multinucleated astrocytes in old demyelinated plaques in a patient with multiple sclerosis. *Neuropathology* 24(3): 248-53.
Norgren N, Sundstrom P, Svenningsson A, Rosengren L, Stigbrand T, Gunnarsson M. (2004). Neurofilament and glial fibrillary acidic protein in multiple sclerosis. *Neurology* 63(9): 1586-90.
O'Callaghan JP, Sriram K. (2005). Glial fibrillary acidic protein and related glial proteins as biomarkers of neurotoxicity. *Expert Opinion on Drug Safety* 4(3): 433-42.
O'Connor KC, Appel H, Bregoli L, Call ME, Catz I, *et al*. (2005). Antibodies from inflamed central nervous system tissue recognize myelin oligodendrocyte glycoprotein. *Journal of Immunology* 175(3): 1974-82.
Odoardi F, Sie C, Streyl K, Ulaganathan VK, Schlager C, *et al*. (2012). T cells become licensed in the lung to enter the central nervous system. *Nature* 488(7413): 675-9.
Okuda Y, Okuda M, Bernard CC. (2002). The suppression of T cell apoptosis influences the severity of disease during the chronic phase but not the recovery from the acute phase of experimental autoimmune encephalomyelitis in mice. *J Neuroimmunol* 131(1-2): 115-25.
Olechowski CJ, Parmar A, Miller B, Stephan J, Tenorio G, *et al*. (2010). A diminished response to formalin stimulation reveals a role for the glutamate transporters in the altered pain sensitivity of mice with experimental autoimmune encephalomyelitis (EAE). *Pain* 149(3): 565-72.
Ordway GA, Szebeni A, Duffourc MM, Dessus-Babus S, Szebeni K. (2009). Gene expression analyses of neurons, astrocytes, and oligodendrocytes isolated by laser capture microdissection from human brain: detrimental effects of laboratory humidity. *J Neurosci Res* 87(11): 2430-8.
Orino K, Lehman L, Tsuji Y, Ayaki H, Torti SV, Torti FM. (2001). Ferritin and the response to oxidative stress. *The Biochemical Journal* 357(1): 241-7.
Ortiz GG, Pacheco-Moises FP, Bitzer-Quintero OK, Ramirez-Anguiano AC, Flores-Alvarado LJ, *et al* (2013) Immunology and oxidative stress in multiple sclerosis: Clinical and basic approach. *Clinical and Developmental Immunology* 2013:1-14.
Padovani-Claudio DA, Liu L, Ransohoff RM, Miller RH. (2006). Alterations in the oligodendrocyte lineage, myelin, and white matter in adult mice lacking the chemokine receptor CXCR2. *Glia* 54(5): 471-83.
Paintlia AS, Paintlia MK, Singh AK, Stanislaus R, Gilg AG, *et al*. (2004). Regulation of gene expression associated with acute experimental autoimmune encephalomyelitis by Lovastatin. *J Neurosci Res* 77(1): 63-81.

Pampliega O, Domercq M, Villoslada P, Sepulcre J, Rodriguez-Antiguedad A, Matute C. (2008). Association of an EAAT2 polymorphism with higher glutamate concentration in relapsing multiple sclerosis. *J Neuroimmunol* 195(1-2): 194-8.

Papanikolaou G, Pantopoulos K. (2005). Iron metabolism and toxicity. *Toxicology and Applied Pharmacology* 202(2): 199-211.

Parakalan R, Jiang B, Nimmi B, Janani M, Jayapal M, *et al*. (2012). Transcriptome analysis of amoeboid and ramified microglia isolated from the corpus callosum of rat brain. *BMC Neuroscience* 13: 64.

Pareek TK, Belkadi A, Kesavapany S, Zaremba A, Loh SL, *et al*. (2011). Triterpenoid modulation of IL-17 and Nrf-2 expression ameliorates neuroinflammation and promotes remyelination in autoimmune encephalomyelitis. *Scientific Reports* 1: 201.

Patel AJ, Hunt A, Kiss J. (1989). Neonatal thyroid deficiency has differential effects on cell specific markers for astrocytes and oligodendrocytes in the rat brain *Neurochem Int* 15: 239-48.

Patel V, Hood BL, Molinolo AA, Lee NH, Conrads TP, *et al*. (2008). Proteomic analysis of laser-captured paraffin-embedded tissues: a molecular portrait of head and neck cancer progression. *Clinical Cancer Research* 14(4): 1002-14.

Pavlidis P, Li Q, Noble WS. (2003). The effect of replication on gene expression microarray experiments. *Bioinformatics* 19(13): 1620-7.

Pedersen MO, Jensen R, Pedersen DS, Skjolding AD, Hempel C, *et al*. (2009). Metallothionein-I+II in neuroprotection. *BioFactors* 35(4): 315-25.

Peferoen L, Kipp M, van der Valk P, van Noort JM, Amor S. (2013). Review series on immune responses in neurodegenerative diseases: Oligodendrocyte-microglia cross-talk in the CNS. *Immunology* (Accepted Article) doi: 10.1111/imm.12163.

Penkowa M. (2006). Metallothioneins are multipurpose neuroprotectants during brain pathology. *The FEBS Journal* 273(9): 1857-70.

Penkowa M, Caceres M, Borup R, Nielsen FC, Poulsen CB, *et al*. (2006). Novel roles for metallothionein-I + II (MT-I + II) in defense responses, neurogenesis, and tissue restoration after traumatic brain injury: insights from global gene expression profiling in wild-type and MT-I + II knockout mice. *J Neurosci Res* 84(7): 1452-74.

Penkowa M, Camats J, Hadberg H, Quintana A, Rojas S, *et al*. (2003a). Astrocyte-targeted expression of interleukin-6 protects the central nervous system during neuroglial degeneration induced by 6-aminonicotinamide. *J Neurosci Res* 73(4): 481-96.

Penkowa M, Espejo C, Martinez-Caceres EM, Montalban X, Hidalgo J. (2003b). Increased demyelination and axonal damage in metallothionein I+II-deficient mice during experimental autoimmune encephalomyelitis. *Cellular and Molecular Life Sciences* 60(1): 185-97.

Penkowa M, Espejo C, Martinez-Caceres EM, Poulsen CB, Montalban X, Hidalgo J. (2001a). Altered inflammatory response and increased neurodegeneration in metallothionein I+II deficient mice during experimental autoimmune encephalomyelitis. *J Neuroimmunol* 119(2): 248-60.

Penkowa M, Espejo C, Ortega-Aznar A, Hidalgo J, Montalban X, Martinez Caceres EM. (2003c). Metallothionein expression in the central nervous system of multiple sclerosis patients. *Cellular and Molecular Life Sciences* 60(6): 1258-66.

Penkowa M, Florit S, Giralt M, Quintana A, Molinero A, *et al*. (2005). Metallothionein reduces central nervous system inflammation, neurodegeneration, and cell death following kainic acid-induced epileptic seizures. *J Neurosci Res* 79(4): 522-34.

Penkowa M, Giralt M, Thomsen PS, Carrasco J, Hidalgo J. (2001b). Zinc or copper deficiency-induced impaired inflammatory response to brain trauma may be

caused by the concomitant metallothionein changes. *Journal of Neurotrauma* 18(4): 447-63.
Penkowa M, Hidalgo J. (2000). Metallothionein I+II expression and their role in experimental autoimmune encephalomyelitis. *Glia* 32(3): 247-63.
Penkowa M, Hidalgo J. (2001). Metallothionein treatment reduces proinflammatory cytokines IL-6 and TNF-alpha and apoptotic cell death during experimental autoimmune encephalomyelitis (EAE). *Exp Neurol* 170(1): 1-14.
Penkowa M, Hidalgo J. (2003). Treatment with metallothionein prevents demyelination and axonal damage and increases oligodendrocyte precursors and tissue repair during experimental autoimmune encephalomyelitis. *J Neurosci Res* 72(5): 574-86.
Perea G, Navarrete M, Araque A. (2009). Tripartite synapses: astrocytes process and control synaptic information. *Trends Neurosci* 32: 421-31.
Perez CA, Tong Y, Guo M. (2008). Iron Chelators as Potential Therapeutic Agents for Parkinson's Disease. *Current Bioactive Compounds* 4(3): 150-58.
Persidsky Y, Ramirez SH, Haorah J, Kanmogne GD. (2006). Blood-brain barrier: structural components and function under physiologic and pathologic conditions. *Journal of Neuroimmune Pharmacology* 1(3): 223-36.
Peskind ER, Griffin WS, Akama KT, Raskind MA, Van Eldik LJ. (2001). Cerebrospinal fluid S100B is elevated in the earlier stages of Alzheimer's disease. *Neurochem Int* 39(5-6): 409-13.
Petzold A, Baker D, Pryce G, Keir G, Thompson EJ, Giovannoni G. (2003a). Quantification of neurodegeneration by measurement of brain-specific proteins. *J Neuroimmunol* 138(1-2): 45-8.
Petzold A, Brassat D, Mas P, Rejdak K, Keir G, *et al*. (2004). Treatment response in relation to inflammatory and axonal surrogate marker in multiple sclerosis. *Multiple Sclerosis* 10(3): 281-3.
Petzold A, Eikelenboom MJ, Gveric D, Keir G, Chapman M, *et al*. (2002). Markers for different glial cell responses in multiple sclerosis: clinical and pathological correlations. *Brain* 125(7): 1462-73.
Petzold A, Jenkins R, Watt HC, Green AJ, Thompson EJ, *et al*. (2003b). Cerebrospinal fluid S100B correlates with brain atrophy in Alzheimer's disease. *Neuroscience Letters* 336(3): 167-70.
Pfaffl MW, Horgan GW, Dempfle L. (2002). Relative expression software tool (REST) for group-wise comparison and statistical analysis of relative expression results in real-time PCR. *Nucleic Acids Research* 30(9): e36.
Pfrieger FW, Slezak M. (2012). Genetic approaches to study glial cells in the rodent brain. *Glia* 60(5): 681-701.
Pieragostino D, Petrucci F, Del Boccio P, Mantini D, Lugaresi A, *et al*. (2010). Pre-analytical factors in clinical proteomics investigations: impact of ex vivo protein modifications for multiple sclerosis biomarker discovery. *Journal of Proteomics* 73: 579-92.
Pierrot-Deseilligny C. (2009). Clinical implications of a possible role of vitamin D in multiple sclerosis. *J Neurol* 256(9): 1468-79.
Pietersen CY, Lim MP, Woo TU. (2009). Obtaining high quality RNA from single cell populations in human postmortem brain tissue. *Journal of Visualized Experiments (30): 1-9.*
Ponta H, Sherman L, Herrlich PA. (2003). CD44: from adhesion molecules to signalling regulators. *Nature Reviews. Molecular Cell Biology* 4(1): 33-45.
Popescu BF, Lucchinetti CF. (2012). Meningeal and cortical grey matter pathology in multiple sclerosis. *BMC Neurology* 12: 11.

Pozhitkov AE, Boube I, Brouwer MH, Noble PA. (2010). Beyond Affymetrix arrays: expanding the set of known hybridization isotherms and observing pre-wash signal intensities. *Nucleic acids research* 38(5): e28.

Prada FA, Quesada A, Dorado ME, Chmielewski C, Prada C. (1998). Glutamine synthetase (GS) activity and spatial and temporal patterns of GS expression in the developing chick retina: relationship with synaptogenesis in the outer plexiform layer. *Glia* 22: 221-36.

Qian ZM, Liao QK, To Y, Ke Y, Tsoi YK, *et al*. (2000). Transferrin-bound and transferrin free iron uptake by cultured rat astrocytes. *Cellular and Molecular Biology* 46(3): 541-8.

Qian ZM, Shen X. (2001). Brain iron transport and neurodegeneration. *Trends Mol Med* 7(3): 103-8.

Qian ZM, To Y, Tang PL, Feng YM. (1999). Transferrin receptors on the plasma membrane of cultured rat astrocytes. *Experimental Brain Research.* 129(3): 473-6.

Rajalahti T, Kroksveen AC, Arneberg R, Berven FS, Vedeler CA, *et al*. (2010). A multivariate approach to reveal biomarker signatures for disease classification: application to mass spectral profiles of cerebrospinal fluid from patients with multiple sclerosis. *J Proteome Res* 9(7): 3608-20.

Ramaglia V, Hughes TR, Donev RM, Ruseva MM, Wu X, *et al.* (2012). C3-dependent mechanism of microglial priming relevant to multiple sclerosis. *Proceedings of the National Academy of Sciences of the United States of America* 109(3): 965-70.

Ramagopalan SV, Knight JC, Ebers GC. 2009. Multiple sclerosis and the major histocompatibility complex. *Current Opinion In Neurology* 22(3): 219-25.

Ramagopalan SV, Lee JD, Yee IM, Guimond C, Traboulsee AL, *et al*. (2013). Association of smoking with risk of multiple sclerosis: a population-based study. *J Neurol* 260(7): 1778-81.

Ramanathan M, Weinstock-Guttman B, Nguyen LT, Badgett D, Miller C, *et al*. (2001). In vivo gene expression revealed by cDNA arrays: the pattern in relapsing-remitting multiple sclerosis patients compared with normal subjects. *J Neuroimmunol* 116(2): 213-9.

Ramos P, Santos A, Pinto NR, Mendes R, Magalhaes T, Almeida A. (2013). Iron levels in the human brain: A post-mortem study of anatomical region differences and age-related changes. *Journal of Trace Elements in Medicine and Biology* 28(1): 13-7.

Ratzer R, Sondergaard H, Christensen JR, Bornsen L, Borup R, *et al*. (2013). Gene expression analysis of relapsing-remitting, primary progressive and secondary progressive multiple sclerosis. *Multiple Sclerosis* 19(14): 1841-8.

Raven EP, Lu PH, Tishler TA, Heydari P, Bartzokis G. (2013). Increased iron levels and decreased tissue integrity in hippocampus of Alzheimer's disease detected in vivo with magnetic resonance imaging. *Journal of Alzheimer's Disease* 37(1): 127-36.

Regan MR, Huang YH, Kim YS, Dykes-Hoberg MI, Jin L, *et al*. (2007). Variations in promoter activity reveal a differential expression and physiology of glutamate transporters by glia in the developing and mature CNS. *The Journal of Neuroscience* 27(25): 6607-19.

Regan RF, Kumar N, Gao F, Guo Y. (2002). Ferritin induction protects cortical astrocytes from heme-mediated oxidative injury. *Neuroscience* 113(4): 985-94.

Rejdak K, Petzold A, Kocki T, Kurzepa J, Grieb P, *et al*. (2007). Astrocytic activation in relation to inflammatory markers during clinical exacerbation of relapsing-remitting multiple sclerosis. *Journal of Neural Transmission* 114(8): 1011-5.

Ren ZP, Hedrum A, Ponten F, Nister M, Ahmadian A, *et al*. (1996). Human epidermal cancer and accompanying precursors have identical p53 mutations different from p53 mutations in adjacent areas of clonally expanded non-neoplastic keratinocytes. *Oncogene* 12(4): 765-73.

Reuss B, von Bohlen und Halbach O. (2003). Fibroblast growth factors and their receptors in the central nervous system. *Cell and Tissue Research* 313(2): 139-57.

Reynolds R, Roncaroli F, Nicholas R, Radotra B, Gveric D, Howell O. (2011). The neuropathological basis of clinical progression in multiple sclerosis. *Acta Neuropathol* 122(2): 155-70.

Reyzer ML, Caprioli RM. (2007). MALDI-MS-based imaging of small molecules and proteins in tissues. *Current Opinion in Chemical Biology* 11: 29-35.

Ridet JL, Malhotra SK, Privat A, Gage FH. (1997). Reactive astrocytes: cellular and molecular cues to biological function. *Trends Neurosci* 20: 570-7.

Rivers TM, Sprunt DH, Berry GP. (1933). Observations on Attempts to Produce Acute Disseminated Encephalomyelitis in Monkeys. *The Journal of experimental Medicine* 58(1): 39-53.

Robinson SR. (2001). Changes in the cellular distribution of glutamine synthetase in Alzheimer's disease. *J Neurosci Res* 66(5): 972-80.

Rodriguez AS, Espina BH, Espina V, Liotta LA. (2008a). Automated laser capture microdissection for tissue proteomics. *Methods in Molecular Biology* 441: 71-90.

Rodriguez FJ, Giannini C, Asmann YW, Sharma MK, Perry A, *et al*. (2008b). Gene expression profiling of NF-1-associated and sporadic pilocytic astrocytoma identifies aldehyde dehydrogenase 1 family member L1 (ALDH1L1) as an underexpressed candidate biomarker in aggressive subtypes. *Journal of Neuropathology and Experimental Neurology* 67(12): 1194-204.

Rohner TC, Staab D, Stoeckli M. (2005). MALDI mass spectrometric imaging of biological tissue sections. *Mechanisms of Ageing & Development* 126(1): 177-85.

Roscoe WA, Welsh ME, Carter DE, Karlik SJ. (2009). VEGF and angiogenesis in acute and chronic MOG((35-55)) peptide induced EAE. *J Neuroimmunol* 209: 6-15.

Rosenling T, Attali A, Luider TM, Bischoff R. (2011). The experimental autoimmune encephalomyelitis model for proteomic biomarker studies: from rat to human. *Clinica Chimica Acta* 412(11-12): 812-22.

Rossi L, Mazzitelli S, Arciello M, Capo CR, Rotilio G. (2008). Benefits from dietary polyphenols for brain aging and Alzheimer's disease. *Neurochemical research* 33(12): 2390-400.

Rothermundt M, Peters M, Prehn JH, Arolt V. (2003). S100B in brain damage and neurodegeneration. *Microscopy Research and Technique* 60(6): 614-32.

Rothstein JD, Dykes-Hoberg M, Pardo CA, Bristol LA, Jin L, *et al*. (1996). Knockout of glutamate transporters reveals a major role for astroglial transport in excitotoxicity and clearance of glutamate. *Neuron* 16: 675-86.

Rouault TA, Cooperman S. 2006. Brain iron metabolism. *Seminars in Pediatric Neurology* 13(3): 142-8.

Rubio N, Sanz-Rodriguez F. (2007). Induction of the CXCL1 (KC) chemokine in mouse astrocytes by infection with the murine encephalomyelitis virus of Theiler. *Virology* 358(1): 98-108.

Rus H, Cudrici C, Niculescu F, Shin ML. (2006). Complement activation in autoimmune demyelination: dual role in neuroinflammation and neuroprotection. *J Neuroimmunol* 180(1-2): 9-16.

Sadovnick AD. (2013). Differential effects of genetic susceptibility factors in males and females with multiple sclerosis. *Clinical Immunology* 149(2): 170-5.
Sadovnick AD, Baird PA, Ward RH. (1988). Multiple sclerosis: updated risks for relatives. *Am J Med Genet* 29(3): 533-41.
Salmaggi A, Gelati M, Dufour A, Corsini E, Pagano S, *et al*. (2002). Expression and modulation of IFN-gamma-inducible chemokines (IP-10, Mig, and I-TAC) in human brain endothelium and astrocytes: possible relevance for the immune invasion of the central nervous system and the pathogenesis of multiple sclerosis. *Journal of Interferon & Cytokine Research* 22(6): 631-40.
Salvador GA. (2010). Iron in neuronal function and dysfunction. *BioFactors* 36(2): 103-10.
Sanders ME, Dias EC, Xu BJ, Mobley JA, Billheimer D, *et al*. (2008). Differentiating proteomic biomarkers in breast cancer by laser capture microdissection and MALDI MS. *J Proteome Res* 7(4): 1500-7.
Sarchielli P, Di Filippo M, Ercolani MV, Chiasserini D, Mattioni A, *et al*. (2008). Fibroblast growth factor-2 levels are elevated in the cerebrospinal fluid of multiple sclerosis patients. *Neuroscience Letters* 435: 223-8.
Sarchielli P, Presciutti O, Pelliccioli GP, Tarducci R, Gobbi G, *et al*. (1999). Absolute quantification of brain metabolites by proton magnetic resonance spectroscopy in normal-appearing white matter of multiple sclerosis patients. *Brain* 122(3): 513-21.
Sathe K, Maetzler W, Lang JD, Mounsey RB, Fleckenstein C, *et al*. (2012). S100B is increased in Parkinson's disease and ablation protects against MPTP-induced toxicity through the RAGE and TNF-alpha pathway. *Brain* 135(11): 3336-47.
Satoh J, Tabunoki H, Nanri Y, Arima K, Yamamura T. (2006). Human astrocytes express 14-3-3 sigma in response to oxidative and DNA-damaging stresses. *Neurosci Res* 56(1): 61-72.
Sawada J, Kikuchi Y, Shibutani M, Mitsumori K, Inoue K, Kasahara T. (1994). Induction of metallothionein in astrocytes by cytokines and heavy metals. *Biological Signals* 3(3): 157-68.
Sayed BA, Walker ME, Brown MA. (2011). Cutting edge: mast cells regulate disease severity in a relapsing-remitting model of multiple sclerosis. *Journal of Immunology* 186(6): 3294-8.
Schaf DV, Tort AB, Fricke D, Schestatsky P, Portela LV, *et al*. (2005). S100B and NSE serum levels in patients with Parkinson's disease. *Parkinsonism & Related Disorders* 11(1): 39-43.
Schiffenbauer J, Johnson HM, Butfiloski EJ, Wegrzyn L, Soos JM. (1993). Staphylococcal enterotoxins can reactivate experimental allergic encephalomyelitis. *Proceedings of the National Academy of Sciences of the United States of America* 90(18): 8543-6.
Schutze K, Lahr G. (1998). Identification of expressed genes by laser-mediated manipulation of single cells. *Nature Biotechnology* 16(8): 737-42.
Scott HA, Gebhardt FM, Mitrovic AD, Vandenberg RJ, Dodd PR. (2011). Glutamate transporter variants reduce glutamate uptake in Alzheimer's disease. *Neurobiol Aging* 32(3): 553 e1-11.
Sen J, Belli A. (2007). S100B in neuropathologic states: the CRP of the brain? *J Neurosci Res* 85(7): 1373-80.
Sequeira A, Morgan L, Walsh DM, Cartagena PM, Choudary P, *et al*. (2012). Gene expression changes in the prefrontal cortex, anterior cingulate cortex and nucleus accumbens of mood disorders subjects that committed suicide. *PLoS One* 7(4): e35367.

Serrano-Pozo A, Gomez-Isla T, Growdon JH, Frosch MP, Hyman BT. (2013a). A phenotypic change but not proliferation underlies glial responses in Alzheimer disease. *The American Journal of Pathology* 182(6): 2332-44.

Serrano-Pozo A, Muzikansky A, Gomez-Isla T, Growdon JH, Betensky RA, *et al*. (2013b). Differential relationships of reactive astrocytes and microglia to fibrillar amyloid deposits in Alzheimer disease. *Journal of Neuropathology and Experimental Neurology* 72(6): 462-71.

Shamoto-Nagai M, Maruyama W, Yi H, Akao Y, Tribl F, *et al*. (2006). Neuromelanin induces oxidative stress in mitochondria through release of iron: mechanism behind the inhibition of 26S proteasome. *J Neural Transm* 113(5): 633-44.

Sherman LS, Struve JN, Rangwala R, Wallingford NM, Tuohy TM, Kuntz Ct. (2002). Hyaluronate-based extracellular matrix: keeping glia in their place. *Glia 38(2):* 93-102.

Shevchenko A, Loboda A, Shevchenko A, Ens W, Standing KG. (2000). MALDI quadrupole time-of-flight mass spectrometry: a powerful tool for proteomic research. *Analytical Chemistry* 72(9): 2132-41.

Shi SR, Liu C, Pootrakul L, Tang L, Young A, *et al*. (2008). Evaluation of the value of frozen tissue section used as "gold standard" for immunohistochemistry. *American Journal of Clinical Pathology* 129(3): 358-66.

Shi SR, Liu C, Taylor CR. (2007). Standardization of immunohistochemistry for formalin-fixed, paraffin-embedded tissue sections based on the antigen-retrieval technique: from experiments to hypothesis. *The Journal of Histochemistry and Cytochemistry* 55(2): 105-9.

Shi SR, Shi Y, Taylor CR. (2011). Antigen retrieval immunohistochemistry: review and future prospects in research and diagnosis over two decades. *The Journal of Histochemistry and Cytochemistry* 59(1): 13-32.

Shiihara T, Miyake T, Izumi S, Sugihara S, Watanabe M, *et al*. (2013). Serum and CSF biomarkers in acute pediatric neurological disorders. *Brain & Development* http://dx.doi.org/10.1016/j.braindev.2013.06.011.

Shin JW, Nguyen KT, Pow DV, Knight T, Buljan V, *et al*. (2009). Distribution of glutamate transporter GLAST in membranes of cultured astrocytes in the presence of glutamate transport substrates and ATP. *Neurochemical Research* 34(10): 1758-66.

Shivane AG, Chakrabarty A. (2007). Multiple sclerosis and demyelination. *Current Diagnostic Pathology* 13(3): 193-202.

Siddappa AJ, Rao RB, Wobken JD, Leibold EA, Connor JR, Georgieff MK. (2002). Developmental changes in the expression of iron regulatory proteins and iron transport proteins in the perinatal rat brain. *J Neurosci Res* 68(6): 761-75.

Simmons SB, Pierson ER, Lee SY, Goverman JM. (2013). Modeling the heterogeneity of multiple sclerosis in animals. *Trends In Immunology* 34(8): 410-22.

Simpson JE, Ince PG, Lace G, Forster G, Shaw PJ, *et al*. (2010). Astrocyte phenotype in relation to Alzheimer-type pathology in the ageing brain. *Neurobiology of Aging* 31(4): 578-90.

Simpson JE, Ince PG, Shaw PJ, Heath PR, Raman R, *et al*. (2011). Microarray analysis of the astrocyte transcriptome in the aging brain: relationship to Alzheimer's pathology and APOE genotype. *Neurobiol Aging* 32(10): 1795-807.

Skjorringe T, Moller LB, Moos T. (2012). Impairment of interrelated iron- and copper homeostatic mechanisms in brain contributes to the pathogenesis of neurodegenerative disorders. *Frontiers in Pharmacology* 3: 169.

Skold K, Svensson M, Nilsson A, Zhang X, Nydahl K, *et al*. (2006). Decreased striatal levels of PEP-19 following MPTP lesion in the mouse. *J Proteome Res* 5(2): 262-9.

Smolinska A, Posma JM, Blanchet L, Ampt KA, Attali A, *et al*. (2012). Simultaneous analysis of plasma and CSF by NMR and hierarchical models fusion. *Analytical and Bioanalytical Chemistry* 403(4): 947-59.
So PK, Hu B, Yao ZP. (2013). Mass spectrometry: towards in vivo analysis of biological systems. *Molecular BioSystems* 9(5): 915-29.
Sobel RA, Moore GW. (2008). Demyelinating Diseases. In, *Greenfield's Neuropathology*, 8th Ed, Hodder Arnold. London, pp1513-1607.
Sofroniew MV. (2009). Molecular dissection of reactive astrogliosis and glial scar formation. *Trends Neurosci* 32: 638-47.
Sofroniew MV, Vinters HV. (2010). Astrocytes: biology and pathology. *Acta Neuropathologica* 119(1): 7-35.
Song F, Bandara M, Deol H, Loeb JA, Benjamins J, Lisak RP. (2013). Complexity of trophic factor signaling in experimental autoimmune encephalomyelitis: Differential expression of neurotrophic and gliotrophic factors. *J Neuroimmunol* 262(1-2): 11-8.
Sorci G, Bianchi R, Riuzzi F, Tubaro C, Arcuri C, *et al*. (2010). S100B Protein, A Damage-Associated Molecular Pattern Protein in the Brain and Heart, and Beyond. *Cardiovascular Psychiatry and Neurology* 10: 1-13.
Sorci G, Riuzzi F, Arcuri C, Tubaro C, Bianchi R, *et al*. (2013). S100B protein in tissue development, repair and regeneration. *World Journal of Biological Chemistry* 4(1): 1-12.
Sospedra M, Martin R. (2005). Immunology of multiple sclerosis. *Annu Rev Immunol* 23: 683-747.
Spach KM, Pedersen LB, Nashold FE, Kayo T, Yandell BS, *et al*. (2004). Gene expression analysis suggests that 1,25-dihydroxyvitamin D3 reverses experimental autoimmune encephalomyelitis by stimulating inflammatory cell apoptosis. *Physiological Genomics* 18(2): 141-51.
Spinola M, Meyer P, Kammerer S, Falvella FS, Boettger MB, *et al*. (2006). Association of the PDCD5 locus with lung cancer risk and prognosis in smokers. *Journal of Clinical Oncology* 24(11): 1672-8.
Sriram S. (2011). Role of glial cells in innate immunity and their role in CNS demyelination. *J Neuroimmunol* 239: (13-20).
Sriram S, Steiner I. (2005). Experimental allergic encephalomyelitis: a misleading model of multiple sclerosis. *Annals of Neurology* 58(6): 939-45.
Stables MJ, Newson J, Ayoub SS, Brown J, Hyams CJ, Gilroy DW. (2010). Priming innate immune responses to infection by cyclooxygenase inhibition kills antibiotic-susceptible and -resistant bacteria. *Blood* 116(16): 2950-9.
Stadelmann C. (2011). Multiple sclerosis as a neurodegenerative disease: pathology, mechanisms and therapeutic implications. *Current Opinion in Neurology* 24(3): 224-9.
Stadelmann C, Kerschensteiner M, Misgeld T, Bruck W, Hohlfeld R, Lassmann H. (2002). BDNF and gp145trkB in multiple sclerosis brain lesions: neuroprotective interactions between immune and neuronal cells? *Brain* 125(1): 75-85.
Stan AD, Ghose S, Gao XM, Roberts RC, Lewis-Amezcua K, *et al*. (2006). Human postmortem tissue: what quality markers matter? *Brain Res* 1123(1): 1-11.
Stauber J, Lemaire R, Franck J, Bonnel D, Croix D, *et al*. (2008). MALDI imaging of formalin-fixed paraffin-embedded tissues: application to model animals of Parkinson disease for biomarker hunting. *J Proteome Res* 7(3): 969-78.
Steiner J, Bernstein HG, Bielau H, Berndt A, Brisch R, *et al*. (2007). Evidence for a wide extra-astrocytic distribution of S100B in human brain. *BMC Neuroscience* 8: 2.

Steiner J, Bogerts B, Schroeter ML, Bernstein HG. (2011). S100B protein in neurodegenerative disorders. *Clinical Chemistry and Laboratory Medicine* 49(3): 409-24.
Steinman L. (1999). Assessment of animal models for MS and demyelinating disease in the design of rational therapy. *Neuron* 24(3): 511-4.
Stoeckli M, Knochenmuss R, McCombie G, Mueller D, Rohner T, *et al*. (2006). MALDI MS imaging of amyloid. *Methods in Enzymology* 412: 94-106.
Stoeckli M, Staab D, Staufenbiel M, Wiederhold KH, Signor L. (2002). Molecular imaging of amyloid beta peptides in mouse brain sections using mass spectrometry. *Analytical Biochemistry* 311: 33-9.
Stojanovic IR, Kostic M, Ljubisavljevic S. (2014). The role of glutamate and its receptors in multiple sclerosis. *J Neural Transm* 15:1-11.
Stoop MP, Dekker LJ, Titulaer MK, Burgers PC, Sillevis Smitt PA, *et al*. (2008). Multiple sclerosis-related proteins identified in cerebrospinal fluid by advanced mass spectrometry. *Proteomics* 8(8): 1576-85.
Strand C, Enell J, Hedenfalk I, Ferno M. (2007). RNA quality in frozen breast cancer samples and the influence on gene expression analysis--a comparison of three evaluation methods using microcapillary electrophoresis traces. *BMC Molecular Biology* 8: 38.
Strohalm M, Kavan D, Novak P, Volny M, Havlicek V. (2010). mMass 3: a cross-platform software environment for precise analysis of mass spectrometric data. *Analytical Chemistry* 82(11): 4648-51.
Stromnes IM, Cerretti LM, Liggitt D, Harris RA, Goverman JM. (2008). Differential regulation of central nervous system autoimmunity by T(H)1 and T(H)17 cells. *Nature Medicine* 14(3): 337-42.
Struve J, Maher PC, Li YQ, Kinney S, Fehlings MG, *et al*. (2005). Disruption of the hyaluronan-based extracellular matrix in spinal cord promotes astrocyte proliferation. *Glia* 52(1): 16-24.
Stuve O, Youssef S, Slavin AJ, King CL, Patarroyo JC, *et al*. (2002). The role of the MHC class II transactivator in class II expression and antigen presentation by astrocytes and in susceptibility to central nervous system autoimmune disease. *Journal of Immunology* 169(12): 6720-32.
Stys PK, Zamponi GW, van Minnen J, Geurts JJ. (2012). Will the real multiple sclerosis please stand up? *Nature Reviews. Neuroscience* 13(7): 507-14.
Su K, Bourdette D, Forte M. (2013). Mitochondrial dysfunction and neurodegeneration in multiple sclerosis. *Frontiers in Physiology* 4: 169.
Su KG, Banker G, Bourdette D, Forte M. (2009). Axonal degeneration in multiple sclerosis: the mitochondrial hypothesis. *Current Neurology and Neuroscience Reports* 9(5): 411-7.
Suarez I, Bodega G, Fernandez B. (2002). Glutamine synthetase in brain: effect of ammonia. *Neurochem Int* 41(2-3): 123-42.
Sussmuth SD, Sperfeld AD, Hinz A, Brettschneider J, Endruhn S, *et al*. (2010). CSF glial markers correlate with survival in amyotrophic lateral sclerosis. *Neurology* 74(12): 982-7.
Swanson RA, Ying W, Kauppinen TM. (2004). Astrocyte influences on ischemic neuronal death. *Current Molecular Medicine* 4(2): 193-205.
Szalai AJ, Hu X, Adams JE, Barnum SR. (2007). Complement in experimental autoimmune encephalomyelitis revisited: C3 is required for development of maximal disease. *Molecular Immunology* 44(12): 3132-6.
Szolnoki Z, Kondacs A, Mandi Y, Somogyvari F. (2007). A cytoskeleton motor protein genetic variant may exert a protective effect on the occurrence of multiple

sclerosis: the janus face of the kinesin light-chain 1 56836CC genetic variant. *Neuromolecular Medicine* 9(4): 335-9.

Tajouri L, Mellick AS, Ashton KJ, Tannenberg AE, Nagra RM, *et al*. (2003). Quantitative and qualitative changes in gene expression patterns characterize the activity of plaques in multiple sclerosis. *Brain Research. Molecular Brain Research* 119: 170-83.

Takahashi K, Yoshino T, Hayashi K, Sonobe H, Ohtsuki Y. (1987). S-100 beta positive human T lymphocytes: their characteristics and behavior under normal and pathologic conditions. *Blood* 70(1): 214-20.

Takeda A, Takatsuka K, Sotogaku N, Oku N. (2002). Influence of iron-saturation of plasma transferrin in iron distribution in the brain. *Neurochem Int* 41(4): 223-8.

Tan L, Gordon KB, Mueller JP, Matis LA, Miller SD. (1998). Presentation of proteolipid protein epitopes and B7-1-dependent activation of encephalitogenic T cells by IFN-gamma-activated SJL/J astrocytes. *Journal of Immunology* 160(9): 4271-9.

Tangrea MA, Hanson JC, Bonner RF, Pohida TJ, Rodriguez-Canales J, Emmert-Buck MR. (2011). Immunoguided microdissection techniques. *Methods in Molecular Biology* 755: 57-66.

Tansey FA, Farooq M, Cammer W. (1991). Glutamine synthetase in oligodendrocytes and astrocytes: new biochemical and immunocytochemical evidence. *Journal of Neurochemistry* 56(1): 266-72.

Tanuma N, Sakuma H, Sasaki A, Matsumoto Y. (2006). Chemokine expression by astrocytes plays a role in microglia/macrophage activation and subsequent neurodegeneration in secondary progressive multiple sclerosis. *Acta Neuropathol* 112(2): 195-204.

Teunissen C, Menge T, Altintas A, Alvarez-Cermeno JC, Bertolotto A, *et al*. (2013). Consensus definitions and application guidelines for control groups in cerebrospinal fluid biomarker studies in multiple sclerosis. *Multiple Sclerosis* 19(13): 1802-9.

Thiel A, Heiss WD. (2011). Imaging of microglia activation in stroke. *Stroke 42:* 507-12.

Todorich B, Pasquini JM, Garcia CI, Paez PM, Connor JR. (2009). Oligodendrocytes and myelination: the role of iron. *Glia* 57(5): 467-78.

Todorich B, Zhang X, Slagle-Webb B, Seaman WE, Connor JR. (2008). Tim-2 is the receptor for H-ferritin on oligodendrocytes. *Journal of Neurochemistry* 107(6): 1495-505.

Tombini M, Squitti R, Cacciapaglia F, Ventriglia M, Assenza G, *et al*. (2013). Inflammation and iron metabolism in adult patients with epilepsy: Does a link exist? *Epilepsy Research* 107(3): 244-252.

Torkildsen O, Stansberg C, Angelskar SM, Kooi EJ, Geurts JJ, *et al*. (2010). Upregulation of immunoglobulin-related genes in cortical sections from multiple sclerosis patients. *Brain Pathology* 20(4): 720-9.

Torres-Munoz JE, Van Waveren C, Keegan MG, Bookman RJ, Petito CK. (2004). Gene expression profiles in microdissected neurons from human hippocampal subregions. *Brain Research. Molecular Brain Research* 127: 105-14.

Traboulsee A, Dehmeshki J, Peters KR, Griffin CM, Brex PA, *et al*. (2003). Disability in multiple sclerosis is related to normal appearing brain tissue MTR histogram abnormalities. *Multiple Sclerosis* 9(6): 566-73.

Trabzuni D, Ryten M, Walker R, Smith C, Imran S, *et al*. (2011). Quality control parameters on a large dataset of regionally dissected human control brains for whole genome expression studies. *Journal of Neurochemistry* 119(2): 275-82.

Trapp BD, Nave KA. (2008). Multiple sclerosis: an immune or neurodegenerative disorder? *Annual Review of Neuroscience* 31: 247-69.
Trapp BD, Peterson J, Ransohoff RM, Rudick R, Mork S, Bo L. (1998). Axonal transection in the lesions of multiple sclerosis. *The New England Journal of Medicine* 338(5): 278-85.
Trim PJ, Atkinson SJ, Princivalle AP, Marshall PS, West A, Clench MR. (2008). Matrix-assisted laser desorption/ionisation mass spectrometry imaging of lipids in rat brain tissue with integrated unsupervised and supervised multivariant statistical analysis. *Rapid Communications in Mass Spectrometry* 22(10): 1503-9.
Trim PJ, Djidja MC, Muharib T, Cole LM, Flinders B, *et al*. (2012). Instrumentation and software for mass spectrometry imaging--making the most of what you've got. *Journal of Proteomics* 75(16): 4931-40.
Tselis A. (2012). Epstein-Barr virus cause of multiple sclerosis. *Current Opinion in Rheumatology* 24(4): 424-8.
Tsukada N, Miyagi K, Matsuda M, Yanagisawa N, Yone K. (1991). Tumor necrosis factor and interleukin-1 in the CSF and sera of patients with multiple sclerosis. *J Neurol Sci* 104(2): 230-4.
Tsunoda I, Kuang LQ, Theil DJ, Fujinami RS. (2000). Antibody association with a novel model for primary progressive multiple sclerosis: induction of relapsing-remitting and progressive forms of EAE in H2s mouse strains. *Brain Pathology* 10(3): 402-18.
Tuohy VK, Lu Z, Sobel RA, Laursen RA, Lees MB. (1989). Identification of an encephalitogenic determinant of myelin proteolipid protein for SJL mice. *Journal of Immunology* 142(5): 1523-7.
Ulrich R, Kalkuhl A, Deschl U, Baumgartner W. (2010). Machine learning approach identifies new pathways associated with demyelination in a viral model of multiple sclerosis. *Journal of Cellular and Molecular Medicine* 14(1-2): 434-48.
Vallejo-Illarramendi A, Domercq M, Perez-Cerda F, Ravid R, Matute C. (2006). Increased expression and function of glutamate transporters in multiple sclerosis. *Neurobiol Dis* 21(1): 154-64.
van der Star BJ, Vogel DY, Kipp M, Puentes F, Baker D, Amor S. (2012). In vitro and in vivo models of multiple sclerosis. *CNS & Neurological Disorders Drug Targets* 11(5): 570-88.
van der Valk P, Amor S. (2009b). Preactive lesions in multiple sclerosis. *Current Opinion in Neurology* 22(3): 207-13.
Van Der Voorn P, Tekstra J, Beelen RH, Tensen CP, Van Der Valk P, De Groot CJ. (1999). Expression of MCP-1 by reactive astrocytes in demyelinating multiple sclerosis lesions. *The American Journal of Pathology* 154(1): 45-51.
van Horssen J, Witte ME, Ciccarelli O. (2012). The role of mitochondria in axonal degeneration and tissue repair in MS. *Multiple Sclerosis* 18(8): 1058-67.
van Noort JM, van den Elsen PJ, van Horssen J, Geurts JJ, van der Valk P, Amor S. (2011). Preactive multiple sclerosis lesions offer novel clues for neuroprotective therapeutic strategies. *CNS & Neurological Disorders Drug Targets* 10(l): 68-81.
van Rensburg SJ, Kotze MJ, van Toorn R. (2012). The conundrum of iron in multiple sclerosis--time for an individualised approach. *Metabolic Brain Disease* 27(3): 239-53.
Vandewoestyne M, Goossens K, Burvenich C, Van Soom A, Peelman L, Deforce D. (2013). Laser capture microdissection: Should an ultraviolet or infrared laser be used? *Analytical Biochemistry* 439(2): 88-98.

Vass K, Lassmann H. (1990). Intrathecal application of interferon gamma. Progressive appearance of MHC antigens within the rat nervous system. *The American Journal of Pathology* 137(4): 789-800.

Ventura R, Harris KM. (1999). Three-dimensional relationships between hippocampal synapses and astrocytes. *The Journal of Neuroscience* 19(16): 6897-906.

Vercellino M, Merola A, Piacentino C, Votta B, Capello E, *et al*. (2007). Altered glutamate reuptake in relapsing-remitting and secondary progressive multiple sclerosis cortex: correlation with microglia infiltration, demyelination, and neuronal and synaptic damage. *Journal of Neuropathology and Experimental Neurology* 66(8): 732-9.

Vergara D, Martignago R, Leporatti S, Bonsegna S, Maruccio G, *et al*. (2009). Biomechanical and proteomic analysis of INF- beta-treated astrocytes. *Nanotechnology* 20(45): 455106.

Verkhratsky A, Olabarria M, Noristani HN, Yeh CY, Rodriguez JJ. (2010). Astrocytes in Alzheimer's disease. *Neurotherapeutics 7:* 399-412.

Veto S, Acs P, Bauer J, Lassmann H, Berente Z, *et al*. (2010). Inhibiting poly(ADP-ribose) polymerase: a potential therapy against oligodendrocyte death. *Brain* 133: 822-34.

Villarreal A, Aviles Reyes RX, Angelo MF, Reines AG, Ramos AJ. (2011). S100B alters neuronal survival and dendrite extension via RAGE-mediated NF-kappaB signaling. *Journal of Neurochemistry* 117(2): 321-32.

Vogel H, Butcher EC, Picker LJ. (1992). H-CAM expression in the human nervous system: evidence for a role in diverse glial interactions. *Journal of Neurocytology* 21(5): 363-73.

Volterra A, Meldolesi J. (2005). Astrocytes, from brain glue to communication elements: the revolution continues. *Nature Reviews. Neuroscience* 6: 626-40.

Walch A, Rauser S, Deininger SO, Hofler H. (2008). MALDI imaging mass spectrometry for direct tissue analysis: a new frontier for molecular histology. *Histochem Cell Biol* 130(3): 421-34.

Waller R, Woodroofe MN, Francese S, Heath PR, Wharton SB, *et al*. (2012). Isolation of enriched glial populations from post-mortem human CNS material by immuno-laser capture microdissection. *J Neurosci Methods* 208(2): 108-13.

Walsh MJ, Tourtellotte WW, Roman J, Dreyer W. (1985). Immunoglobulin G, A, and M--clonal restriction in multiple sclerosis cerebrospinal fluid and serum--analysis by two-dimensional electrophoresis. *Clinical Immunology and Immunopathology* 35(3): 313-27.

Wang Q, Woltjer RL, Cimino PJ, Pan C, Montine KS, *et al*. (2005). Proteomic analysis of neurofibrillary tangles in Alzheimer disease identifies GAPDH as a detergent-insoluble paired helical filament tau binding protein. *FASEB Journal* 19(7): 869-71.

Wang S, Rosengren LE, Franlund M, Hamberger A, Haglid KG. (1999). Bcl-2 expression regulates cell sensitivity to S100beta-mediated apoptosis. *Brain Research. Molecular Brain Research* 70(1): 167-76.

Wang T, Liu B, Qin L, Wilson B, Hong JS. (2004). Protective effect of the SOD/catalase mimetic MnTMPyP on inflammation-mediated dopaminergic neurodegeneration in mesencephalic neuronal-glial cultures. *J Neuroimmunol* 147(1-2): 68-72.

Wang X, Michaelis EK. (2010). Selective neuronal vulnerability to oxidative stress in the brain. *Frontiers in Aging Neuroscience* 2: 12.

Wang XS, Simmons Z, Liu W, Boyer PJ, Connor JR. (2006). Differential expression of genes in amyotrophic lateral sclerosis revealed by profiling the post mortem cortex. *Amyotroph Lateral Scler* 7: 201-10.
Weis S, Llenos IC, Dulay JR, Elashoff M, Martinez-Murillo F, Miller CL. (2007). Quality control for microarray analysis of human brain samples: The impact of postmortem factors, RNA characteristics, and histopathology. *J Neurosci Methods* 165: 198-209.
Weissert R. (2013). The immune pathogenesis of multiple sclerosis. *Journal of Neuroimmune Pharmacology* 8(4): 857-66.
Wenzel RJ, Matter U, Schultheis L, Zenobi R. (2005). Analysis of megadalton ions using cryodetection MALDI time-of-flight mass spectrometry. *Analytical Chemistry* 77(14): 4329-37.
Werner P, Pitt D, Raine CS. (2001). Multiple sclerosis: altered glutamate homeostasis in lesions correlates with oligodendrocyte and axonal damage. *Annals of Neurology* 50(2): 169-80.
West AK, Hidalgo J, Eddins D, Levin ED, Aschner M. (2008). Metallothionein in the central nervous system: Roles in protection, regeneration and cognition. *Neurotoxicology* 29(3): 489-503.
Whitney LW, Becker KG, Tresser NJ, Caballero-Ramos CI, Munson PJ, *et al*. (1999). Analysis of gene expression in mutiple sclerosis lesions using cDNA microarrays. *Annals of Neurology* 46(3): 425-8.
Whitney LW, Ludwin SK, McFarland HF, Biddison WE. (2001). Microarray analysis of gene expression in multiple sclerosis and EAE identifies 5-lipoxygenase as a component of inflammatory lesions. *J Neuroimmunol* 121(1-2): 40-8.
Williams A, Piaton G, Lubetzki C. (2007). Astrocytes--friends or foes in multiple sclerosis? *Glia* 55(13): 1300-12.
Williams R, Buchheit CL, Berman NE, LeVine SM. (2012). Pathogenic implications of iron accumulation in multiple sclerosis. *Journal of Neurochemistry* 120(1): 7-25.
Williams R, Rohr AM, Wang WT, Choi IY, Lee P, *et al*. (2011). Iron deposition is independent of cellular inflammation in a cerebral model of multiple sclerosis. *BMC Neuroscience* 12: 59.
Wisztorski M, Croix D, Macagno E, Fournier I, Salzet M. (2008). Molecular MALDI imaging: an emerging technology for neuroscience studies. *Developmental Neurobiology* 68(6): 845-58.
Wojciak-Stothard B, Entwistle A, Garg R, Ridley AJ. (1998). Regulation of TNF-alpha-induced reorganization of the actin cytoskeleton and cell-cell junctions by Rho, Rac, and Cdc42 in human endothelial cells. *Journal of Cellular Physiology* 176(1): 150-65.
Wong GH, Bartlett PF, Clark-Lewis I, Battye F, Schrader JW. (1984). Inducible expression of H-2 and Ia antigens on brain cells. *Nature* 310(5979): 688-91.
Wortsman J, Matsuoka LY, Chen TC, Lu Z, Holick MF. (2000). Decreased bioavailability of vitamin D in obesity. *The American journal of clinical nutrition* 72(3): 690-3.
Wu LJ, Leenders AG, Cooperman S, Meyron-Holtz E, Smith S, *et al*. (2004). Expression of the iron transporter ferroportin in synaptic vesicles and the blood-brain barrier. *Brain Res* 1001(1-2): 108-17.
Xiong Z, O'Hanlon D, Becker LE, Roder J, MacDonald JF, Marks A. (2000). Enhanced calcium transients in glial cells in neonatal cerebellar cultures derived from S100B null mice. *Experimental Cell Research* 257(2): 281-9.
Xu BJ, Caprioli RM, Sanders ME, Jensen RA. (2002). Direct analysis of laser capture microdissected cells by MALDI mass spectrometry. *J Am Soc Mass Spectrom* 13(11): 1292-7.

Xu BJ, Li J, Beauchamp RD, Shyr Y, Li M, *et al*. (2009). Identification of early intestinal neoplasia protein biomarkers using laser capture microdissection and MALDI MS. *Molecular & Cellular Proteomics* 8(5): 936-45.
Xu L, Hu J, Zhao Y, Hu J, Xiao J, *et al*. (2012). PDCD5 interacts with p53 and functions as a positive regulator in the p53 pathway. *Apoptosis* 17(11): 1235-45.
Yamamoto H, Konno H, Yamamoto T, Ito K, Mizugaki M, Iwasaki Y. (1987). Glutamine synthetase of the human brain: purification and characterization. *Journal of Neurochemistry* 49(2): 603-9.
Yamashita S, Okada Y. 2005. Mechanisms of heat-induced antigen retrieval: analyses in vitro employing SDS-PAGE and immunohistochemistry. *The Journal of Histochemistry and Cytochemistry* 53(1): 13-21.
Yan SS, Wu ZY, Zhang HP, Furtado G, Chen X, *et al*. (2003). Suppression of experimental autoimmune encephalomyelitis by selective blockade of encephalitogenic T-cell infiltration of the central nervous system. *Nature Medicine* 9(3): 287-93.
Yang Y, Estrada EY, Thompson JF, Liu W, Rosenberg GA. (2007). Matrix metalloproteinase-mediated disruption of tight junction proteins in cerebral vessels is reversed by synthetic matrix metalloproteinase inhibitor in focal ischemia in rat. *Journal of Cerebral Blood Flow and Metabolism* 27(4): 697-709.
Yang Y, Vidensky S, Jin L, Jie C, Lorenzini I, *et al*. (2011). Molecular comparison of GLT1+ and ALDH1L1+ astrocytes in vivo in astroglial. *Glia* 59(2): 200-7.
Yang YH, Zhao M, Li WM, Lu YY, Chen YY, *et al*. (2006). Expression of programmed cell death 5 gene involves in regulation of apoptosis in gastric tumor cells. *Apoptosis* 11(6): 993-1001.
Yates JR, Ruse CI, Nakorchevsky A. (2009). Proteomics by mass spectrometry: approaches, advances, and applications. *Annual Review of Biomedical Engineering* 11: 49-79.
Yi JH, Hazell AS. (2006). Excitotoxic mechanisms and the role of astrocytic glutamate transporters in traumatic brain injury. *Neurochem Int* 48: 394-403.
Yukihira D, Miura D, Saito K, Takahashi K, Wariishi H. (2010). MALDI-MS-based high-throughput metabolite analysis for intracellular metabolic dynamics. *Analytical Chemistry* 82(10): 4278-82.
Zamanian JL, Xu L, Foo LC, Nouri N, Zhou L, *et al*. (2012). Genomic analysis of reactive astrogliosis. *The Journal of Neuroscience* 32(18): 6391-410.
Zeinstra E, Wilczak N, Streefland C, De Keyser J. (2000). Astrocytes in chronic active multiple sclerosis plaques express MHC class II molecules. *Neuroreport* 11(1): 89-91.
Zeis T, Graumann U, Reynolds R, Schaeren-Wiemers N. (2008). Normal-appearing white matter in multiple sclerosis is in a subtle balance between inflammation and neuroprotection. *Brain* 131: 288-303.
Zeltner L, Schittenhelm J, Mittelbronn M, Roser F, Tatagiba M, *et al*. (2007). The astrocytic response towards invasive meningiomas. *Neuropathology and Applied Neurobiology* 33: 163-8.
Zhang J, Zhang Y, Wang J, Cai P, Luo C, *et al*. (2010). Characterizing iron deposition in Parkinson's disease using susceptibility-weighted imaging: an in vivo MR study. *Brain Res* 1330: 124-30.
Zhang X, Xie W, Qu S, Pan T, Wang X, Le W. (2005). Neuroprotection by iron chelator against proteasome inhibitor-induced nigral degeneration. *Biochemical and Biophysical Research Communications* 333(2): 544-9.

Zhang Y, Taveggia C, Melendez-Vasquez C, Einheber S, Raine CS, *et al*. (2006). Interleukin-11 potentiates oligodendrocyte survival and maturation, and myelin formation. *The Journal of Neuroscience* 26(47): 12174-85.

Zhang Y, Zabad R, Wei X, Metz L, Hill M, Mitchell J. (2007). Deep grey matter "black T2" on 3 tesla magnetic resonance imaging correlates with disability in multiple sclerosis. *Multiple Sclerosis* 13(7): 880-3.

Zhao Y, Davis HW. (1998). Hydrogen peroxide-induced cytoskeletal rearrangement in cultured pulmonary endothelial cells. *Journal of Cellular Physiology* 174(3): 370-9.

Zhao Y, Rempe DA. (2010). Targeting astrocytes for stroke therapy. *Neurotherapeutics* 7: 439-51.

Zheng W, Monnot AD. (2012). Regulation of brain iron and copper homeostasis by brain barrier systems: implication in neurodegenerative diseases. *Pharmacology & Therapeutics* 133(2): 177-88.

Zhu D, Tan KS, Zhang X, Sun AY, Sun GY, Lee JC. (2005). Hydrogen peroxide alters membrane and cytoskeleton properties and increases intercellular connections in astrocytes. *Journal of Cell Science* 118(16): 3695-703.

Ziabreva I, Campbell G, Rist J, Zambonin J, Rorbach J, *et al*. (2010). Injury and differentiation following inhibition of mitochondrial respiratory chain complex IV in rat oligodendrocytes. *Glia* 58(15): 1827-37.

Ziats MN, Rennert OM. (2013). Identification of differentially expressed microRNAs across the developing human brain. *Molecular Psychiatry (Ahead of print).*

Zotova E, Holmes C, Johnston D, Neal JW, Nicoll JA, Boche D. (2011). Microglial alterations in human Alzheimer's disease following Abeta42 immunization. *Neuropathology and Applied Neurobiology* 37(5): 513-24.

Zuvich RL, McCauley JL, Pericak-Vance MA, Haines JL. (2009). Genetics and pathogenesis of multiple sclerosis. *Semin Immunol* 21: 328-33.

PUBLICATION

Journal of Neuroscience Methods 208 (2012) 108–113

Contents lists available at SciVerse ScienceDirect

Journal of Neuroscience Methods

journal homepage: www.elsevier.com/locate/jneumeth

Basic Neuroscience

Isolation of enriched glial populations from post-mortem human CNS material by immuno-laser capture microdissection

R. Waller[a,c], M.N. Woodroofe[c], S. Francese[c], P.R. Heath[a], S.B. Wharton[a], P.G. Ince[a], B. Sharrack[a,b,1], J.E. Simpson[a,*,1]

[a] Sheffield Institute for Translational Neuroscience, The University of Sheffield, UK
[b] Department of Neurology, Royal Hallamshire Hospital, Sheffield, UK
[c] Biomedical Research Centre, Sheffield Hallam University, UK

ARTICLE INFO

Article history:
Received 27 February 2012
Received in revised form 16 April 2012
Accepted 18 April 2012

Keywords:
Astrocyte
Oligodendrocyte
Microglia
RNA
Laser capture microdissection
Post-mortem human brain

ABSTRACT

Isolating individual populations of cells from post-mortem (PM) central nervous system (CNS) tissue for transcriptomic analysis will provide important insights into the pathogenesis of neurodegenerative diseases. To date, research on individual CNS cell populations has been hindered by the availability of suitable PM material, unreliable sample preparation and difficulties obtaining individual cell populations. In this paper we report how rapid immunohistochemistry combined with laser capture microdissection (immuno-LCM) enables the isolation of specific cell populations from PM CNS tissue, thereby enabling the RNA profile of these individual cell types to be investigated. Specifically, we detail methods for isolating enriched glial populations (astrocytes, oligodendrocytes and microglia) and confirm this cell enrichment by polymerase chain reaction (PCR). In addition, the study details the numbers of each glial population required to obtain 50 ng RNA, a suitable amount of starting material required to carry out microarray analysis that potentially may identify alterations of cell-specific genes and pathways associated with a range of neurodegenerative disorders.

1. Introduction

Defining changes in the transcriptome profile of individual cell populations within the central nervous system (CNS) is a key approach to identifying novel factors which contribute to pathology (Curran et al., 2000; Fend and Raffeld, 2000). To date, the majority of studies investigating altered gene expression in brain tissue have evaluated changes in a heterogeneic cell population derived from whole-tissue extracts (Bossers et al., 2009; Grunblatt et al., 2007; Murray, 2007; Wang et al., 2006). Genomic studies are impeded by limitations in obtaining high quality RNA from human post-mortem (PM) material due to a number of factors including: post-mortem delay, tissue pH and the agonal state of the patient prior to death (Weis et al., 2007). Furthermore, in most cases, patients die at the late stages of long standing disease which can skew the data recovered (Kinter et al., 2008). However, the functional data retrieved from human autopsy-derived material may be more relevant than results generated from cell or animal disease models, which do not entirely correlate to the human biological system and disease processes (Jucker, 2010). The few studies to date which have examined the genome of specific cell populations with respect to pathology have been impeded by technical difficulties in obtaining specific-cell enriched samples (Murray, 2007) and the unreliability of the protocols (Eltoum et al., 2002).

Laser capture microdissection (LCM) has revolutionalised the isolation of defined regions and specific cell populations from human tissue (Emmert-Buck et al., 1996). Using this approach in combination with histochemistry or immunohistochemistry (IHC) has become a valuable method for isolating individual cell-types from a complex heterogeneic population (Chu et al., 2009; Cunnea et al., 2010; Greene et al., 2010; Keeney and Bennett, 2010; Lawrie et al., 2001; Murray, 2007; Perez-Liz et al., 2008; Simpson et al., 2011). RNA extracted from LCM-isolated cells has previously been assessed by reverse transcription (RT) PCR analysis to examine the expression of candidate genes (Schutze and Lahr, 1998; Suarez-Quian et al., 1999). In contrast, microarray analysis allows the unbiased evaluation of the expression of the whole human genome, the transcriptome, at a given moment in time (Weis et al., 2007). Therefore, combining immuno-LCM with microarray technology has the potential to identify changes in the gene expression profile, which are associated with disease pathogenesis and increase understanding of the mechanisms involved.

Abbreviations: LCM, laser capture microdissection; RIN, RNA integrity number.

* Corresponding author at: Sheffield Institute for Translational Neuroscience, 385A Glossop Road, Sheffield S10 2HQ, UK. Tel.: +44 0114 222 2242; fax: +44 0114 222 2290.
E-mail address: julie.simpson@sheffield.ac.uk (J.E. Simpson).

[1] Joint senior authors.

0165-0270/$ – see front matter © 2012 Elsevier B.V. All rights reserved.
http://dx.doi.org/10.1016/j.jneumeth.2012.04.014

Glia, namely astrocytes, microglia and oligodendrocytes, play key roles within the CNS providing support and neuroprotection, and are capable of extensive signalling in response to specific stimuli, such as inflammation (Sobel and Moore, 2008). Astrocytes primarily provide neurotrophic support, maintain homeostasis by regulating the extracellular environment, and are components of the tripartite synapse (Fellin, 2009; Perea et al., 2009; Volterra and Meldolesi, 2005). Oligodendrocytes produce myelin which insulates axons and aids neurotransmission, while microglia form the basis of the immune system within the CNS (Sobel and Moore, 2008). Glia have been shown to contribute to the pathogenesis of a range of neurological disorders, including multiple sclerosis (Sriram, 2011), Alzheimer's disease (Naert and Rivest, 2011; Verkhratsky et al., 2010), Parkinson's disease (Halliday and Stevens, 2011), motor neurone disease (Lasiene and Yamanaka, 2011), Huntington's disease (Hsiao and Chern, 2010), and stroke (Thiel and Heiss, 2011; Zhao and Rempe, 2010). Therefore, the ability to isolate an enriched population of specific glial cells from PM CNS tissue at various stages of disease pathology will enable characterisation of their transcriptome, and aid in the discovery of novel mechanisms that contribute to disease progression. The current paper provides a detailed methodological approach to isolate enriched glial cell populations from frozen PM CNS tissue by combining rapid immunostaining with LCM, and details the approximate number of glia required to provide adequate mRNA for use in downstream applications, including microarray analysis.

2. Materials and methods

2.1. Human CNS tissue

Snap-frozen CNS tissue blocks from 6 cases were obtained from UK Multiple Sclerosis Society Tissue Bank (MREC/02/2/39) and the Medical Research Centre Cognitive Function and Ageing Neuropathology Study (CFANS) cohort, as shown in Table 1. In order to assess the initial RNA quality of the tissue, the starting RNA integrity number (RIN) of the tissue block was assessed using a previously reported method (Bahn et al., 2001). The RIN algorithm has been designed to provide unambiguous assessment of RNA integrity based on a numbering system from 1 to 10, with 1 being the most degraded profile and 10 being the most intact. One section (7 μm) was collected in a sterile Eppendorf tube and the RNA extracted using the standard Trizol method (Invitrogen, UK). The quantity of RNA from each sample was analysed using a NanoDrop 1000 spectrophotometer (Thermoscientific, UK) and the quality of RNA assessed on a 2100 bioanalyzer (Agilent, Palo Alto, CA, USA). Only samples with limited ribosomal degradation were taken forward for immuno-LCM.

2.2. Rapid immunohistochemistry (IHC) for use in LCM

Sections (7 μm) were collected onto uncharged, sterile glass slides and warmed to room temperature (RT) for 30 s. The sections were fixed in ice-cold acetone for 3 min and immunostained using the following modified rapid avidin/biotinylated enzyme complex (ABC) staining method (Vector Laboratories, UK). The protocol was carried out at room temperature (RT), using sterile solutions made with diethylpyrocarbonate (DEPC)-treated water and under RNase-free conditions. Sections were blocked in the relevant normal serum (2%) for 3 min, incubated with a specific cell phenotype marker antibody diluted in blocking serum (as shown in Table 2) for 3 min, and rinsed briefly with tris-buffered saline (TBS). Following a 3 min incubation with 5% biotinylated secondary antibody, the sections were rinsed with TBS, incubated with 4% horse-radish peroxidase conjugated ABC for 3 min, and washed briefly with TBS. Antibody staining was visualised with 4,4′-diaminodenzidine tetrahydrochloride (DAB; Vector Laboratories, UK) for 3 min. The sections were dehydrated in a graded series of alcohol (70%, 95%, 100%, 100% for 15 s each), cleared in xylene (15 s) and left to air dry in an air flow hood for 60 min prior to LCM.

2.3. Laser capture microdissection (LCM)

LCM was performed using a PixCell II laser-capture microdissection system (Arcturus Engineering, Mountain View, CA, USA) and CapSure Macro caps (Arcturus Engineering, Mountain View, CA). The air dried, immunostained section was overlaid with a thermoplastic film mounted on a transparent cap. An infrared laser was fired causing the film to melt and adhere to the cells of interest. The LCM system was set to the following parameters: 7.5 μm spot size and 40 mW power. Immunopositive cells were selected for capture using a 20× objective. After microdissection, the film was removed from the cap using sterile tweezers and transferred to a sterile 0.5 ml Eppendorf tube for RNA extraction.

2.4. RNA extraction and reverse transcriptase PCR analysis of enriched glial cell populations

Total RNA was isolated from laser captured microdissected cells using the PicoPure RNA isolation kit (Arcturus BioScience, UK), following the manufacturer's protocol. The quantity and quality of the RNA were determined using the NanoDrop 1000 spectrophotometer (Thermoscientific, UK) and 2100 Bioanalyzer, RNA 6000 Pico LabChip, respectively (Agilent, Palo Alto, CA, USA). All RNA samples were stored under sterile conditions at −80 °C for future analysis.

cDNA was synthesised using qScript cDNA mix/supermix (QUANTA, UK), following the manufacturer's protocol. Gene-specific primers were obtained from commercially available sources, or designed based on published sequences (Table 3). PCR was performed using 50 ng cDNA, 5× firepol green PCR mastermix (Solis Biodyne, UK) and optimised concentrations of forward and reverse primers (Table 3) in a total volume of 20 μl. Following denaturation at 95 °C for 10 min the products were amplified (GFAP, CD68: 40 cycles at 95 °C for 15 s, 60 °C for 60 s and then 72 °C for 15 min) (OLIG2: 35 cycles at 95 °C for 60 s, 60 °C for 45 s and 72 °C

Table 1
Details of cases used in this study.

Case	Age	Sex	pH	PMI (h)	RIN pre-LCM	RIN post-LCM	Cause of death
1[a]	101	F	5.9	18	6.3	5.2	Urinary tract infection
2[b]	77	F	6.6	9	5.2	3.5	Lung infection
3[b]	78	F	7.2	5	5.1	3.5	Metastatic carcinoma
4[b]	72	F	n/a	8	4.0	2.2	Bronchopneumonia
5[b]	86	F	6.6	11	4.0	2.2	Bronchopneumonia
6[b]	46	M	n/a	7	4.4	3.0	Bronchopneumonia

n/a: data not available.
[a] Case obtained from MRC-CFANS.
[b] Case obtained from MS Society Tissue Bank.

Table 2
Primary antibodies used to identify specific glial populations.

Antibody	Isotype	Specificity	Supplier	Dilution[a]
Glial fibrillary acidic protein (GFAP) (Reske-Nielsen et al., 1987)	Rabbit IgG	Astrocyte	DAKO	1:50
CD68 (Aoki et al., 1999)	Mouse IgG1	Microglia	DAKO	1:10
Oligodendrocyte-specific protein (OSP) (Simard et al., 2010)	Rabbit IgG	Oligodendrocyte	AbCam	1:25

[a] Primary antibody was diluted in 2% blocking serum.

Table 3
Primer sequence.

Gene	Primer sequence	Product size	Reference/source
GFAP	F: GCAGAAGCTCCAGGATGAAAC R: TCCACATGGACCTGCTGTC	213 bp	R&D Systems, UK
CD68	F: CGAGCATCATTCTTTCACCAGCT R: ATGAGAGGCAGCAAGATGGACC	135 bp	Cambridge Bioscience, UK
OLIG2	F: CCCTGAGGCTTTTCGGAGCG R: GCGGCTGTTGATCTTAGACGC	474 bp	Lin et al. (2005)
NFL	F: GGCTCTCAGTGTATTGGCTTCTGT R: AACCCAGCTCTAGTAAGCAGAAATG	84 bp	Designed in house

F, forward; R, reverse.

for 60 s, followed by 72 °C for 15 min). PCR products were visualised on a 3% agarose gel stained with ethidium bromide.

3. Results

3.1. Laser microdissection enables the isolation of specific glial populations

Rapid immunohistochemistry enabled the identification of specific populations of glia, as shown in Fig. 1. Astrocytes were identified by GFAP immunoreactivity with positive cells presenting in a typical stellate morphology associated with astrocyte cell bodies and their extended processes (Fig. 1A). Oligodendrocyte spherical cell bodies displayed intense OSP immunoreactivity (Fig. 1B) and resting microglia identified by CD68 were highly branched (ramified) in appearance (Fig. 1C). The immunopositive cells were isolated by LCM, as shown in Fig. 2.

3.2. Effect of immuno-LCM on RNA quality

Initial assessment of RNA quality pre-LCM indicated that 46% of tissue blocks (6/13) had a RIN greater than 4. These 6 cases were taken forward for further investigation and had a mean pre-LCM RIN of 4.8 (range 4–6.3), as shown in Table 1. Following LCM, the RIN decreased by 1.5 (range 1.1–1.8), but remained of sufficient quality for downstream applications, as shown in Fig. 3. Approximately 1000 astrocytes, 1000 microglia and 1500 oligodendrocytes were microdissected to obtain 50 ng total RNA.

3.3. Isolation of enriched glial cell populations

RNA isolated from GFAP$^+$ cells had high levels of GFAP transcripts but lower levels of CD68 and OLIG2 transcripts, confirming that the extracted RNA represented an enriched astrocyte population (Fig. 4). Similarly, RNA isolated from OSP$^+$ cells demonstrated high levels of OLIG2 transcript and lower levels of CD68 and GFAP transcripts (Fig. 4). Furthermore, RNA isolated from CD68$^+$ cells contained high levels of CD68 transcript and lower levels of the GFAP and OLIG2 transcripts, indicating that the extracted RNA represented an enriched microglial population. Low levels of GFAP transcripts were detected in the microglial and oligodendrocyte samples, and low levels of neurofilament light (NFL) transcripts were detected in the astrocyte samples (not shown), reflecting their proximity to astrocytes and axons, respectively.

4. Discussion

In this paper we demonstrate that immuno-LCM allows the recovery of high quality mRNA from specific glial cell populations isolated from human PM CNS tissue. This extracted RNA has the potential to be used in a variety of downstream genomic applications, including microarray analysis. This approach would enable

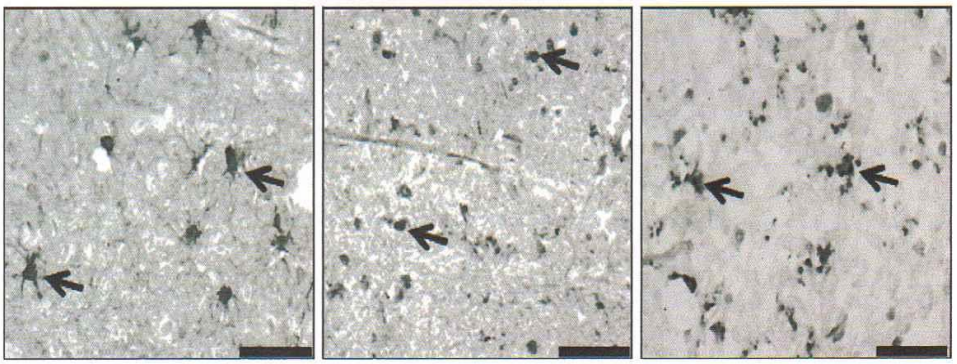

Fig. 1. Rapid immunohistochemical detection of glia cells. (A) Glial fibrillary acidic protein (GFAP) immunohistochemistry (IHC) was used to identify astrocytes, (B) OSP to identify oligodendrocytes, and (C) CD68 to visualise microglia. Examples of immunopositive cells are indicated by the arrows. Scale bar represents 50 μm.

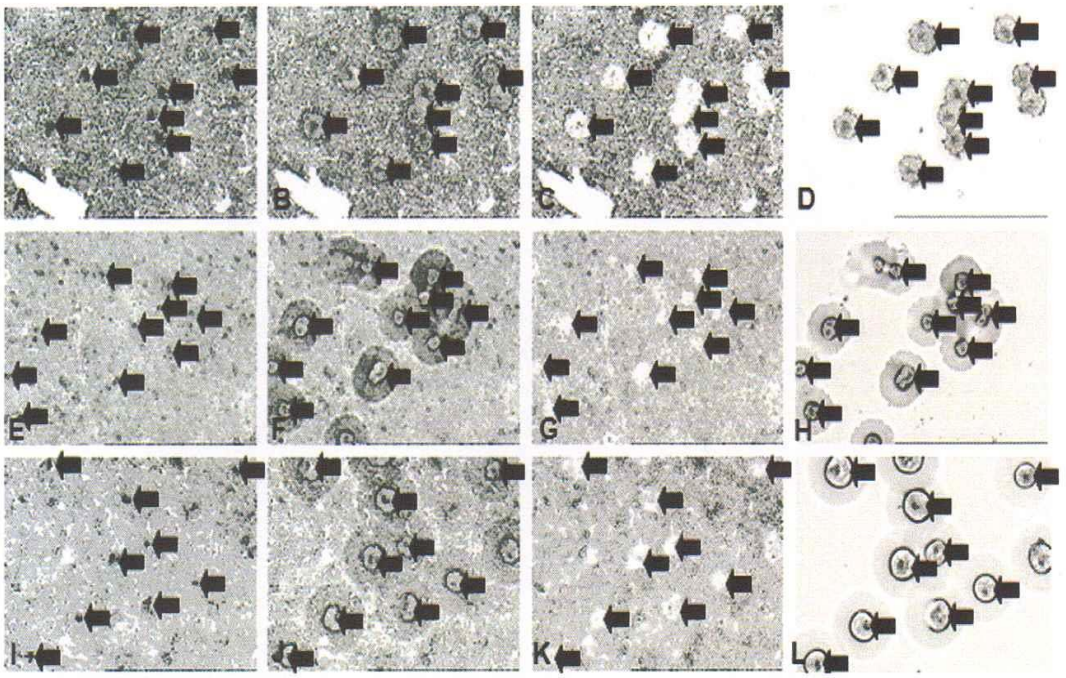

Fig. 2. Laser capture microdissection of (A–D) GFAP$^+$ astrocytes, (E–H) OSP$^+$ oligodendrocytes, and (I–L) CD68$^+$ microglia from frozen post-mortem human brain tissue. Immuno-positive cells were isolated using a PixCell II laser-capture microdissection system. The laser activated the transfer film on a cap placed on the tissue sample, fusing the film with the underlying cell, as indicated by the arrows (B, F, and J). The film was lifted off leaving unwanted cells behind (C, G, and K). The isolated cells were attached to the film, ready for RNA extraction (D, H, and L).

the investigation of the glial transcriptome to aid in identifying specific functional pathways, genes and potential biological markers associated with a variety of CNS pathologies.

Although an immuno-LCM enriched isolated cell population is not entirely homogenous, the samples obtained are highly-enriched for the specific cell-type of interest, as confirmed in this study by RT-PCR. Post-LCM, extracted RNA from frozen material is inevitably slightly degraded compared to pre-LCM, but still remains of sufficiently high quality for subsequent transcriptomic analysis as previously shown by our group (Simpson et al., 2011). Furthermore, a recent study has shown that microarray analysis of RNA extracted from post-mortem CNS tissue can give reliable results over a wide range of RIN numbers (RIN 1–8.5) (Trabzuni et al., 2011). The use of RIN values is currently accepted as the best measure of the quality of material for genetic studies, but its relevance is not absolute in terms of the outcome of downstream experiments (Koppelkamm et al., 2011; Stan et al., 2006). The ability to isolate enriched cell populations from human PM CNS material is crucial to fully understand their role/function in a variety of neurodegenerative disorders. This procedure enables valuable information to be obtained from PM material, which may be a more relevant approach than studying cell lines and animal models of disease alone as, although valuable, are not a true reflection of human disease pathogenesis (Jucker, 2010). Furthermore, analysing a sample enriched for one cell type over a heterogeneous cell population is advantageous as it aids understanding of the role of that specific

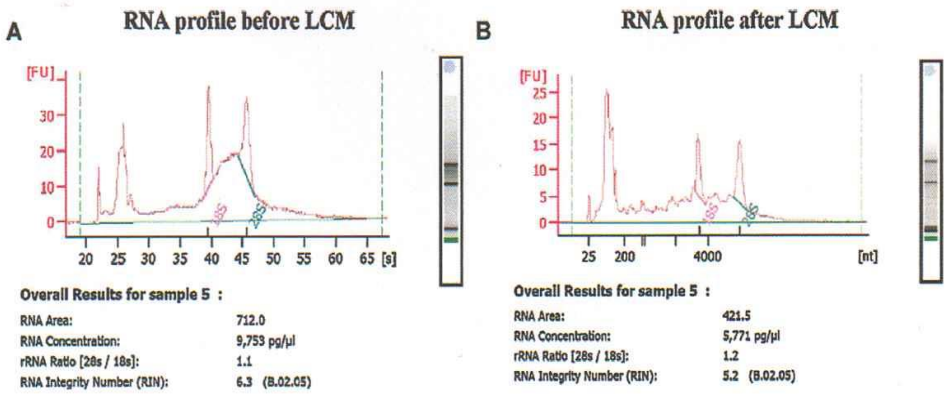

Fig. 3. Laser capture microdissection of immuno-positive cells from post-mortem CNS is associated with a decrease in the RNA integrity number. (A) The RIN value of 6.3 pre-LCM, decreases to (B) RIN 5.2, post-LCM. As degradation proceeds there is a decrease in the 28S and then 18S ribosomal peaks leading to a fall in the 28S to 18S ratio and an increase in the baseline signal between the two ribosomal peaks and the lower marker.

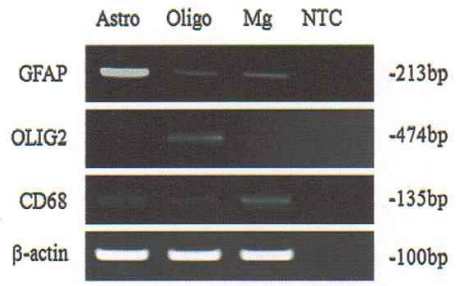

Key: Astro, astrocytes; Oligo, oligodendrocytes; Mg, microglia; NTC, no template control; GFAP, glial fibrillary acidic protein

Fig. 4. RT-PCR analysis of glial transcripts in cells isolated by immuno-LCM. GFAP$^+$ astrocytes are associated with high levels of GFAP and low levels of OLIG2 and CD68 transcripts. OSP$^+$ oligodendrocytes are associated with high levels of OLIG2 and low levels of GFAP and CD68 transcripts. CD68$^+$ microglia are associated with high levels of CD68 and low levels of GFAP and OLIG2 transcripts.

cell type, rather than an overview of a heterogeneic cell population which could mask valuable data and prove difficult in associating a pathogenic function to specific cell types.

The technique of isolating glial cells via immuno-LCM and extracting high quality mRNA has the potential to be used in a variety of downstream applications, including gene expression analysis and q(RT PCR) (Fink et al., 1998; Goldsworthy et al., 1999). The first study to implement LCM with microarray analysis investigated the gene expression of large and small neurones in the dorsal root ganglia of rats (Luo et al., 1999). Subsequent microarray studies employed histologically guided LCM isolation of specific cells from CNS material (Chu et al., 2009; Pietersen et al., 2009; Torres-Munoz et al., 2004), and more recently immuno-LCM isolated cells (Cunnea et al., 2010; Simpson et al., 2011). By accessing frozen human PM material, enriched populations of specific cells of interest can be isolated from this valuable resource using immuno-LCM, and a subsequent, detailed transcriptomic analysis performed to identify specific genes, which may have a crucial role in disease pathogenesis. Furthermore, complementary proteomic research may provide confirmation of whether genes and functional pathways identified in the transcriptome analysis are translated into proteins which contribute to pathology. For example, peptide profiling of immuno-LCM isolated cells can be carried out with the implementation of matrix assisted laser desorption ionisation mass spectrometry (MALDI-MS). This has been previously performed on invasive mammary carcinoma and control human breast epithelium cells (Sanders et al., 2008; Xu et al., 2002) and also in lung cancer where squamous cell carcinoma cells were identified through MALDI-MS (Bhattacharya et al., 2003) and could potentially be applied to immuno-LCM isolated CNS cell populations.

However, it should be recognised that not all PM material is suitable for this technique. The RNA quality of PM CNS material has been shown to be affected by the agonal state of the patient prior to death; studies have shown that prolonged hypoxia can result in reduced mRNA and protein stability (Harrison et al., 1991, 1995; Kingsbury et al., 1995). Furthermore, it has been proposed that brain pH can influence the RNA integrity of samples, as a brain pH of less than 6.0 has been identified as having reduced intact RNA (Kingsbury et al., 1995). Also, the brief freeze–thaw process required when sectioning tissue for immuno-LCM may contribute to a loss in RNA quality. PM material is generally at the end stage of disease, a factor that must be considered when interpreting immuno-LCM-derived genomic data. Formalin fixed, paraffin embedded material (FFPE) is commonly used for detailed histological characterisation, due to its better tissue morphology, ease of use and storage. To date, methods of extracting usable mRNA for microarray analysis from archived FFPE tissue are still in the developmental phase but could be of potential benefit in investigating the genomic and proteomics of well characterised cases in the future. However, despite the limitations of using immuno-LCM on frozen PM CNS material, as long as these factors are duly recognised and acknowledged, this technology will significantly contribute to defining the role of specific glial populations with respect to CNS pathology.

5. Conclusions

In summary, we have demonstrated the detailed methodology required for the isolation of enriched populations of GFAP$^+$ astrocytes, OSP$^+$ oligodendrocytes and CD68$^+$ microglia from frozen PM human CNS tissue using immuno-LCM. This paper fully acknowledges the problems associated with using human PM material, but recognises the potential benefits of using this valuable resource to gain a better understanding of disease pathogenesis. Furthermore, this paper reports the number of glia required to achieve a suitable amount of starting material (50 ng), an amount that we have previously shown to be sufficient for the amplification process prior to microarray analysis (Simpson et al., 2011). Potentially, transcriptomic investigation of immuno-LCM enriched cell populations may clarify their role in disease pathogenesis and identify relevant biological markers of disease.

Acknowledgements

Tissue samples and associated clinical and neuropathological data were supplied by the UK Multiple Sclerosis Tissue Bank, funded by the Multiple Sclerosis Society of Great Britain and Northern Ireland, registered charity 207495. The Cognitive Function and Ageing Neuropathology Study is funded by the Medical Research Council, UK. We are grateful to the respondents, their families, and their carers for agreement to participate in the brain donation programme. This work was supported by Biogen Idec.

References

Aoki T, Kobayashi K, Isaki K. Microglial and astrocytic change in brains of Creutzfeldt–Jakob disease: an immunocytochemical and quantitative study. Clin Neuropathol 1999;18:51–60.
Bahn S, Augood SJ, Ryan M, Standaert DG, Starkey M, Emson PC. Gene expression profiling in the post-mortem human brain—no cause for dismay. J Chem Neuroanat 2001:79–94.
Bhattacharya SH, Gal AA, Murray KK. Laser capture microdissection MALDI for direct analysis of archival tissue. J Proteome Res 2003;2:95–8.
Bossers K, Meerhoff G, Balesar R, van Dongen JW, Kruse CG, Swaab DF, et al. Analysis of gene expression in Parkinson's disease: possible involvement of neurotrophic support and axon guidance in dopaminergic cell death. Brain Pathol 2009:91–107.
Chu TT, Liu Y, Kemether E. Thalamic transcriptome screening in three psychiatric states. J Hum Genet 2009:665–75.
Cunnea P, McMahon J, O'Connell E, Mashayekhi K, Fitzgerald U, McQuaid S. Gene expression analysis of the microvascular compartment in multiple sclerosis using laser microdissected blood vessels. Acta Neuropathol (Berl) 2010;119:601–15.
Curran S, McKay JA, McLeod HL, Murray GI. Laser capture microscopy. Mol Pathol 2000;53:64–8.
Eltoum IA, Siegal GP, Frost AR. Microdissection of histologic sections: past, present, and future. Adv Anat Pathol 2002;9:316–22.
Emmert-Buck MR, Bonner RF, Smith PD, Chuaqui RF, Zhuang Z, Goldstein SR, et al. Laser capture microdissection. Science 1996;274:998–1001.
Fellin T. Communication between neurons and astrocytes: relevance to the modulation of synaptic and network activity. J Neurochem 2009:533–44.
Fend F, Raffeld M. Laser capture microdissection in pathology. J Clin Pathol 2000;53:666–72.
Fink L, Seeger W, Ermert L, Hanze J, Stahl U, Grimminger F, et al. Real-time quantitative RT-PCR after laser-assisted cell picking. Nat Med 1998;4:1329–33.
Goldsworthy SM, Stockton PS, Trempus CS, Foley JF, Maronpot RR. Effects of fixation on RNA extraction and amplification from laser capture microdissected tissue. Mol Carcinog 1999:86–91.
Greene JG, Dingledine R, Greenamyre JT. Neuron-selective changes in RNA transcripts related to energy metabolism in toxic models of parkinsonism in rodents. Neurobiol Dis 2010:476–81.

Grunblatt E, Zander N, Bartl J, Jie L, Monoranu CM, Arzberger T, et al. Comparison analysis of gene expression patterns between sporadic Alzheimer's and Parkinson's disease. J Alzheimers Dis 2007;12:291–311.
Halliday GM, Stevens CH. Glia: initiators and progressors of pathology in Parkinson's disease. Mov Disord 2011;26:6–17.
Harrison PJ, Heath PR, Eastwood SL, Burnet PW, McDonald B, Pearson RC. The relative importance of premortem acidosis and postmortem interval for human brain gene expression studies: selective mRNA vulnerability and comparison with their encoded proteins. Neurosci Lett 1995:151–4.
Harrison PJ, Procter AW, Barton AJ, Lowe SL, Najlerahim A, Bertolucci PH, et al. Terminal coma affects messenger RNA detection in post mortem human temporal cortex. Brain Res Mol Brain Res 1991;9:161–4.
Hsiao HY, Chern Y. Targeting glial cells to elucidate the pathogenesis of Huntington's disease. Mol Neurobiol 2010;41:248–55.
Jucker M. The benefits and limitations of animal models for translational research in neurodegenerative diseases. Nat Med 2010:1210–4.
Keeney PM, Bennett Jr JP. ALS spinal neurons show varied and reduced mtDNA gene copy numbers and increased mtDNA gene deletions. Mol Neurodegener 2010:21.
Kingsbury AE, Foster OJ, Nisbet AP, Cairns N, Bray L, Eve DJ, et al. Tissue pH as an indicator of mRNA preservation in human post-mortem brain. Brain Res Mol Brain Res 1995:311–8.
Kinter J, Zeis T, Schaeren-Wiemers N. RNA profiling of MS brain tissues. Int MS J 2008;15:51–8.
Koppelkamm A, Vennemann B, Lutz-Bonengel S, Fracasso T, Vennemann M. RNA integrity in post-mortem samples: influencing parameters and implications on RT-qPCR assays. Int J Legal Med 2011;125:573–80.
Lasiene J, Yamanaka K. Glial cells in amyotrophic lateral sclerosis. Neurol Res Int 2011;2011:718987.
Lawrie LC, Curran S, McLeod HL, Fothergill JE, Murray GI. Application of laser capture microdissection and proteomics in colon cancer. Mol Pathol 2001;54:253–8.
Lin YW, Deveney R, Barbara M, Iscove NN, Nimer SD, Slape C, et al. (BHLHB1), a bHLH transcription factor, contributes to leukemogenesis in concert with LMO1. Cancer Res 2005:7151–8.
Luo L, Salunga RC, Guo H, Bittner A, Joy KC, Galindo JE, et al. Gene expression profiles of laser-captured adjacent neuronal subtypes. Nat Med 1999;5:117–22.
Murray GI. An overview of laser microdissection technologies. Acta Histochem 2007:171–6.
Naert G, Rivest S. The role of microglial cell subsets in Alzheimer's disease. Curr Alzheimer Res 2011:151–5.
Perea G, Navarrete M, Araque A. Tripartite synapses: astrocytes process and control synaptic information. Trends Neurosci 2009:421–31.
Perez-Liz G, Del Valle L, Gentilella A, Croul S, Khalili K. Detection of JC virus DNA fragments but not proteins in normal brain tissue. Ann Neurol 2008;64:379–87.
Pietersen CY, Lim MP, Woo TU. Obtaining high quality RNA from single cell populations in human postmortem brain tissue. J Vis Exp 2009.
Reske-Nielsen E, Oster S, Reintoft I. Astrocytes in the prenatal central nervous system. From 5th to 28th week of gestation. An immunohistochemical study on paraffin-embedded material. Acta Pathol Microbiol Immunol Scand A 1987;95:339–46.
Sanders ME, Dias EC, Xu BJ, Mobley JA, Billheimer D, Roder H, et al. Differentiating proteomic biomarkers in breast cancer by laser capture microdissection and MALDI MS. J Proteome Res 2008;7:1500–7.
Schutze K, Lahr G. Identification of expressed genes by laser-mediated manipulation of single cells. Nat Biotechnol 1998;16:737–42.
Simard JM, Tsymbalyuk N, Tsymbalyuk O, Ivanova S, Yurovsky V, Gerzanich V. Glibenclamide is superior to decompressive craniectomy in a rat model of malignant stroke. Stroke 2010:531–7.
Simpson JE, Ince PG, Shaw PJ, Heath PR, Raman R, Garwood CJ, et al. Microarray analysis of the astrocyte transcriptome in the aging brain: relationship to Alzheimer's pathology and APOE genotype. Neurobiol Aging 2011 [Elsevier Inc.].
Sobel RA, Moore GW. Demyelinating diseases. 8th ed. London: Hodder Arnold; 2008.
Sriram S. Role of glial cells in innate immunity and their role in CNS demyelination. J Neuroimmunol A 2011:13–20 [Elsevier B.V.].
Stan AD, Ghose S, Gao XM, Roberts RC, Lewis-Amezcua K, Hatanpaa KJ, et al. Human postmortem tissue: what quality markers matter. Brain Res 2006;1123:1–11.
Suarez-Quian CA, Goldstein SR, Pohida T, Smith PD, Peterson JI, Wellner E, et al. Laser capture microdissection of single cells from complex tissues. Biotechniques 1999;26:328–35.
Thiel A, Heiss WD. Imaging of microglia activation in stroke. Stroke 2011:507–12.
Torres-Munoz JE, Van Waveren C, Keegan MG, Bookman RJ, Petito CK. Gene expression profiles in microdissected neurons from human hippocampal subregions. Brain Res Mol Brain Res 2004:105–14.
Trabzuni D, Ryten M, Walker R, Smith C, Imran S, Ramasamy A, et al. Quality control parameters on a large dataset of regionally dissected human control brains for whole genome expression studies. J Neurochem 2011;119:275–82.
Verkhratsky A, Olabarria M, Noristani HN, Yeh CY, Rodriguez JJ. Astrocytes in Alzheimer's disease. Neurotherapeutics 2010:399–412 [published by Elsevier Inc.].
Volterra A, Meldolesi J. Astrocytes, from brain glue to communication elements: the revolution continues. Nat Rev Neurosci 2005:626–40.
Wang XS, Simmons Z, Liu W, Boyer PJ, Connor JR. Differential expression of genes in amyotrophic lateral sclerosis revealed by profiling the post mortem cortex. Amyotroph Lateral Scler 2006:201–10.
Weis S, Llenos IC, Dulay JR, Elashoff M, Martinez-Murillo F, Miller CL. Quality control for microarray analysis of human brain samples: the impact of postmortem factors, RNA characteristics, and histopathology. J Neurosci Methods 2007:198–209.
Xu BJ, Caprioli RM, Sanders ME, Jensen RA. Direct analysis of laser capture microdissected cells by MALDI mass spectrometry. J Am Soc Mass Spectrom 2002;13:1292–7.
Zhao Y, Rempe DA. Targeting astrocytes for stroke therapy. Neurotherapeutics 2010:439–51 [published by Elsevier Inc.].